A-79-0073

SLL 79-132/OL
Vol. 2 cy 1

AFAPL-TR-78-51
Volume II

19980513 102

HIGH POWER MAGNETOHYDRODYNAMIC SYSTEM

D. W. SWALLOM
O. K. SONJU
D. E. MEADER
H. BECKER
MAXWELL LABORATORIES, INC.
200 WEST CUMMINGS PARK
WOBURN, MASSACHUSETTS 01801

RECEIVED
FEB 14 1979
BRI LIBRARY

JULY 1978

TECHNICAL REPORT AFAPL-TR-78-51, Volume II
Final Report May 1976 — June 1978

DTIC QUALITY INSPECTED 4

Approved for public release; distribution unlimited.

PLEASE RETURN TO:
BMD TECHNICAL INFORMATION CENTER
BALLISTIC MISSILE DEFENSE ORGANIZATION
7100 DEFENSE PENTAGON
WASHINGTON D.C. 20301-7100

AIR FORCE AERO PROPULSION LABORATORY
AIR FORCE WRIGHT AERONAUTICAL LABORATORIES
AIR FORCE SYSTEMS COMMAND
WRIGHT-PATTERSON AIR FORCE BASE, OHIO 45433

U3770

NOTICE

When Government drawings, specifications, or other data are used for any purpose other than in connection with a definitely related Government procurement operation, the United States Government thereby incurs no responsibility nor any obligation whatsoever; and the fact that the government may have formulated, furnished, or in any way supplied the said drawings, specifications, or other data, is not to be regarded by implication or otherwise as in any manner licensing the holder or any other person or corporation, or conveying any rights or permission to manufacture, use, or sell any patented invention that may in any way be related thereto.

This report has been reviewed by the Information Office, (ASD/OIP) and is releasable to the National Technical Information Service (NTIS). At NTIS, it will be available to the general public, including foreign nations.

This technical report has been reviewed and is approved for publication.

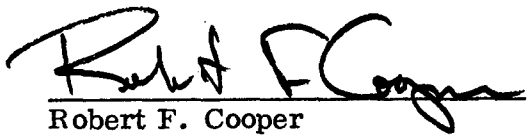

Robert F. Cooper
Program Manager

FOR THE COMMANDER

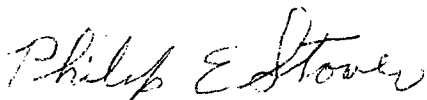

Philip E. Stover
Chief, High Power Branch

Copies of this report should not be returned unless return is required by security considerations, contractural obligations, or notice on a specific document.

AIR FORCE/56780/2 February 1979 — 250

Accession Number: 3770

Publication Date: Jul 01, 1978

Title: High Power Magnetohydrodynamic System

Personal Author: Swallom, D.W.; Sonju, O.K.; Meader, D.E.; Becker, H.

Corporate Author Or Publisher: Maxwell Laboratories Inc., 200 West Cummings Park, Woburn, MA 01801 Report Number: AFAPL-TR-78-51-Vol. II

Report Prepared for: Air Force Aero Propulsion Laboratory, Wright-Patterson AFB, OH 45433 Report Number Assigned by Contract Monitor: SLL 79-132/OL

Comments on Document: Archive, RRI, DEW

Descriptors, Keywords: Directed Energy Weapon DEW High Power Magnetohydrodynamic System Portable Supply Semiportable MHD Generator Fast Start Compact High Performance Flightweight Liquid Oxygen Hydrocarbon

Pages: 313

Cataloged Date: Sep 29, 1992

Contract Number: F33615-76-C-2104

Document Type: HC

Number of Copies In Library: 000001

Record ID: 24855

Source of Document: DEW

SECURITY CLASSIFICATION OF THIS PAGE *(When Data Entered)*

REPORT DOCUMENTATION PAGE		READ INSTRUCTIONS BEFORE COMPLETING FORM
1. REPORT NUMBER AFAPL-TR-78-51 Vol II	2. GOVT ACCESSION NO.	3. RECIPIENT'S CATALOG NUMBER
4. TITLE *(and Subtitle)* HIGH POWER MAGNETOHYDRODYNAMIC SYSTEM		5. TYPE OF REPORT & PERIOD COVERED Final Technical Report 17 May 76 -- 15 June 78 6. PERFORMING ORG. REPORT NUMBER
7. AUTHOR(s) D. W. Swallom, O. K. Sonju, D. E. Meader, H. Becker		8. CONTRACT OR GRANT NUMBER(s) F33615-76-C-2104
9. PERFORMING ORGANIZATION NAME AND ADDRESS Maxwell Laboratories, Inc. 200 West Cummings Park Woburn, Massachuetts 01801		10. PROGRAM ELEMENT, PROJECT, TASK AREA & WORK UNIT NUMBERS 31452636
11. CONTROLLING OFFICE NAME AND ADDRESS Air Force Aero Propulsion Laboratory (POD) Air Force Systems Command Wright-Patterson Air Force Base, Ohio 45433		12. REPORT DATE July 1978 13. NUMBER OF PAGES 313
14. MONITORING AGENCY NAME & ADDRESS*(if different from Controlling Office)*		15. SECURITY CLASS. *(of this report)* Unclassified 15a. DECLASSIFICATION/DOWNGRADING SCHEDULE

16. DISTRIBUTION STATEMENT *(of this Report)*

Approved for public release; distribution unlimited.

17. DISTRIBUTION STATEMENT *(of the abstract entered in Block 20, if different from Report)*

18. SUPPLEMENTARY NOTES - Major Subcontractors:

- Rocketdyne Division of Rockwell International - Combustor Subsystem and Development Testing Subcontractor.
- Magnetic Corporation of America - MHD Magnet Design Subcontractor.

19. KEY WORDS *(Continue on reverse side if necessary and identify by block number)*

Portable Power Supplies
Semi-Portable
MHD Generators
Fast Start Power Supplies
Compact MHD Generator
Burst Power Supplies
High Performance MHD Generator
Flightweight MHD

20. ABSTRACT *(Continue on reverse side if necessary and identify by block number)*

The technical effort discussed in this report covers Phase B of the High Power Magnetohydrodynamic System program, which is a multi-phase program to develop liquid oxygen/liquid hydrocarbon magnetohydrodynamic generators using cesium seed for high performance, portable power supply applications.

DD FORM 1 JAN 73 1473 EDITION OF 1 NOV 65 IS OBSOLETE

SECURITY CLASSIFICATION OF THIS PAGE *(When Data Entered)*

BLOCK 19 (Continued)

Lightweight Megawatt Power Supplies
Cesium Seeding of MHD Gases
JP-4 Fueled MHD
Filament Wound, Epoxy Coated Fiberglass
Portable High Power MHD Generators
Lightweight MHD
LOX/JP-4 Combustor System
Emulsified Fuel
Direct Energy Conversion Systems

BLOCK 20 (Continued)

During this phase a lightweight, high performance hot gas flow train using liquid oxygen and JP-4 was designed and component modeling completed. The magnetohydrodynamic channel/diffuser performance parameters which were used as the design criteria were an output power of 30 MWe, a specific energy extraction of 1.0 MJ/kg, and a specific power density of 200 MWe/m^3. To achieve these performance requirements, the required characteristic velocity efficiency of the combustion system was greater than 99%. During this program a limited amount of development testing was completed using a heat sink combustor and a diagnostics channel. These tests measured the combustor characteristic velocity efficiency and the gas electrical conductivity, as well as pressures, vibrations, and temperatures. The results of the development test program, which verified the design assumptions used to achieve the performance requirements, were a characteristic velocity efficiency of nearly 99% and a gas electrical conductivity at the magnetohydrodynamic channel inlet of 15 mhos/m.

FOREWORD

This final report was submitted by Maxwell Laboratories, Inc. under Contract No. F33615-76-C-2104. The effort was sponsored by the Air Force Aero Propulsion Laboratory, Air Force Systems Command, Wright-Patterson Air Force Base, Ohio, under Project 3145, Task 314526 and Work Unit 31452636 with Robert F. Cooper/AFAPL/POD as the Program Manager. Dr. Daniel W. Swallom and Dr. Otto K. Sonju of Maxwell Laboratories, Inc. were responsible for the technical work. The work discussed in this report was performed by Maxwell Laboratories, Inc., and two major subcontractors; Rocketdyne, A Division of Rockwell International and Magnetic Corporation of America.

The authors of this report appreciate the assistance given to them by the many individuals who contributed to the work performed on this report as well as the guidance given to them by USAF Program Manager, Robert F. Cooper, of the Air Force Aero Propulsion Laboratory.

This report was written and edited by the named authors of Maxwell Laboratories, Inc. Other individuals who participated in this work and contributed to the report include:

G. T. Heskey	Maxwell Laboratories, Inc.
R. V. Burry	Rockwell International
A. W. Huebner	Rockwell International
G. M. Suzuki	Rockwell International
J. M. Watkins	Rockwell International
D. D. Clarke	Rockwell International
R. J. Thome	Magnetic Corporation of America

Because of its length, this report is published in two volumes. The first contains Sections I through VI, Figures 1 through 155, Tables 1 through 46, References, and the List of Abbreviations. Volume II contains Sections VII through X, Appendices A through H, Figures 156 through 233 and C.1 through G.2, and Tables 47 through 79 and A.1 through H.1. The lists of References and Abbreviations are repeated.

TABLE OF CONTENTS (Continued)
(See Footnote*)

SECTION			PAGE
VII	DEVELOPMENT TEST ARTICLES		
	A.	Introduction	355*
	B.	Diagnostics Channel	355
		1. Introduction	355
		2. General Description	356
		3. Design Criteria	358
		4. Design Specifications	362
		5. Design Analysis	365
		6. Design Details	369
		7. Fabrication	375
		a. Introduction	375
		b. Fabrication Tooling	375
		c. Frame Array	379
		d. Case Fabrication	388
		e. Finishing Operations	396
		f. Cooling System Fabrication	403
		g. Final Tests and Measurements	404
	C.	Heat Sink Combustor	407
		1. Design	407
		a. Component Description	409
		b. Instrumentation	412
		c. Material	415
		d. Thermal Analysis	415
		e. Structural Analysis	418
		2. Fabrication	418
VIII	DEVELOPMENT TEST		
	A.	Introduction	423
	B.	Test Facility Description and Instrumentation	423
		1. Test Facility	423
		2. Instrumentation	429
	C.	Test Program Summary	431

NOTE: * As stated in the FOREWORD, this report consists of two Volumes. The page numbers, figure numbers, and table numbers are sequential through the two volumes.

Preceding Page Blank

TABLE OF CONTENTS (Continued)

SECTION			PAGE
(VIII)	D.	Test Results and Conclusions	441
		1. Summary of Results	441
		a. Ignition System Tests	441
		b. Sequence Development Tests	441
		c. Injector/Heat Sink Combustor Tests	442
		d. Diagnostics Channel Tests	442
		2. Ignition System	444
		a. Test Setup	444
		b. Test Description	451
		c. Conclusions	452
		3. Operational Sequence Development	456
		a. Test Setup	456
		b. Test Description	456
		c. Conclusions	460
		4. Injector Tests	463
		a. Test Setup	463
		b. Injector Test Description	463
		c. Combustor Performance	469
		d. Heat Transfer	469
		e. Combustor Stability	484
		f. Conclusions	498
		5. Diagnostics Channel Tests	499
		a. Introduction	499
		b. Test Setup	499
		c. Test Description - Combustor	500
		d. Test Description - Diagnostics Channel	503
		e. Results - Diagnostics Channel	503
		f. Conclusions	523
IX		AEDC TEST PROGRAM	
	A.	Introduction	525
	B.	Test Facility Description	525
	C.	Test Program Summary	527
	D.	Interface Control Summary	531
X		RELIABILITY AND MAINTAINABILITY ANALYSIS	
	A.	Introduction	533
	B.	Gas Generator Component Reliability	533
	C.	Feed Control System Reliability	534

SECTION			PAGE
(X)	D.	Gas Generator System Maintenance	536
		1. System Installation Inspection	536
		2. Post-Installation System Verification	536
		a. Leak/Functional Checkout	537
		b. Combustor Seal Checkout	537
		c. Injector Purge	537
		3. Pre-and Post-Operation Requirements	537
		a. Pre-Operation Requirements	537
		b. Post-Operation Maintenance	538
		4. Periodic Maintenance	539
		5. Corrective Maintenance and System Reverification	540
	E.	Channel/Diffuser and Manifolds	
		1. Electrode System	540
		2. Cooling System	542
		3. Gas Seals	542
		4. Channel/Diffuser Case	542
		5. Instrumentation and Electrical Components	542
		6. Requirements at Operating Site	547
		a. Installation Inspection	547
		b. Post-Installation System Verification	547
		c. Pre-Operation Requirements	548
		d. Post-Operation Maintenance	548
		e. Periodic and Corrective Maintenance	548
APPENDICES			
A		SAFETY AND HAZARD ANALYSIS	
		1. Introduction	549
		2. Combustor/Nozzle and Ancillary Preliminary Hazard Analysis	549
		a. Summary	549
		b. Potential Hazards	551
		c. Hazard Avoidance	552
		d. Format and Content	552
		3. Channel/Diffuser and Manifolds	555
		a. Areas to be Considered for the Channel/Diffuser and Manifolds	555
		b. Component Identification by Hazard Areas	566
		c. Hazard Analysis by Components	569

APPENDICES		PAGE
B	SUPPLEMENTARY SSFL TEST DATA	579
C	CHANNEL TOOLING AND MODELING	
	1. Introduction	585
	2. Channel/Diffuser Internal Contour	585
	3. Electrode Frames Modeling	586
	a. Current Collector Screen Attachment	586
	b. Prototype Perpendicular Frame Fabrication	589
	c. Prototype Diagonal Corner Fabrication	592
	d. Prototype Diagonal Frame Fabrication	592
	e. Cooling Tube Forming	598
	4. Composite Case	608
D	DYNAMIC ANALYSIS	
	1. Valve Contours	611
	2. Start Analysis	615
	3. Cutoff Analysis	616
E	NOZZLE DESIGN FOR IMPROVED FLOW FIELD UNIFORMITY	
	1. Introduction	621
	2. Discussion	621
F	INJECTOR TEST FAILURE DESCRIPTION	
	1. Introduction	625
	2. Recommendations	626
G	DATA ANALYSIS DESCRIPTION	
	1. Chamber Pressure	627
	2. Data Reduction - High Frequency	642
H	PLANNED FABRICATION PROCESS - DETAILED TASKS	643
	REFERENCES	651
	LIST OF ABBREVIATIONS, ACRONYMS, AND SYMBOLS	655

LIST OF ILLUSTRATIONS (Continued)
(Volume II)

FIGURE		PAGE
156	Diagnostics Channel Mounted to Solid Wall Combustor	357
157	Diagnostics Channel Instrumentation (Pressure, Acceleration, Conductivity)	360
158	Diagnostics Channel Instrumentation (Temperature)	361
159	Section View of Diagnostics Channel	372
160	Diagnostics Channel Design Overlay	373
161	Diagnostics Channel Electrodes	376
162	Diagnostics Channel Mandrel	378
163	Diagnostics Channel Electrode Fram	380
164	Partial Electrode Frame Assembly on Mandrel	383
165	Diagnostics Channel Mounted in Winding Fixture	385
166	Insulator Ceramic Emplacement	386
167	Completed Insulator Ceramic Emplacement	387
168	RTV Layer in Place	389
169	Filament Winding Operation	391
170	Partial Fiberglass Case Winding	393
171	Partial Fiberglass Case Winding	394
172	Completed Case Winding	395
173	Removal of Tube End Seals	397
174	Electrode Frame Cleaning	399
175	Electrode Ceramic Emplacement in Progress	401
176	Ceramic Void Region	402
177	Diagnostics Channel/Manifold Assembly	405
178	Completed Diagnostics Channel	406
179	Heat Sink Combustor Assembly	408
180	Heat Sink Combustor Sectioned	410

FIGURES		PAGE
181	Heat Sink Combustor Cooling Passages	411
182	Side Slot Redesign	413
183	Schematic of Bomb Port Locations	414
184	Heat Sink Temperature/Time Relationship	416
185	Heat Sink Coolant Water Flow Control	417
186	Heat Sink Temperature/Plug Thickness Relationship	419
187	Heat Sink Combustor Sections A & B	421
188	Combustor Hardware Installed	422
189	Bravo Test Stand	424
190	Installed Test Hardware	425
191	Fluid Supply System Schematic	426
192	Instrumentation Schematic	430
193	Combustor Characteristic Velocity Performance	443
194	ASI Hardware Installation	445
195	Gas Generator Test Schematic - Ignition Tests	446
196	ASI Start Sequence	447
197	ASI Shutdown Sequence	448
198	Instrumentation Schematic for Ignition Tests	450
199	ASI Injector Pressure Drop	453
200	Ignitor Operation, Test 033	455
201	Combustor Hardware Installation	457
202	MHD Combustor Start Transition	461
203	MHD Combustor Shutdown Transition	462
204	Injector Pressure Drop Summary	464
205	Hot Gas Side Heat Transfer Coefficient vs Distance from the Throat for the Hot Gas Generator	471
206	Hot Gas Side Heat Transfer Coefficient vs Distance from the Throat for the Hot Gas Generator	472

FIGURES		PAGE
207	Hot Gas Side Heat Transfer Coefficient vs Distance from the Throat for the Hot Gas Generator	473
208	Plug Outside Wall Temperature Rise Versus Time for the Gas Generator Heat Flux Meter in the Combustor Zone	475
209	Heat Rate vs Mixture Ratio for the Gas Generator	482
210	Heat Rate vs $Cs_2 CO_3$ Percentage for the Gas Generator	483
211	Top View of Original Acoustic Slot	485
212	Combustion Instability	486
213	Top View of Modified Acoustic Slot	488
214	Acoustic Slot Bandwidth	489
215	AMS Traces	494
216	Time-History Record for Test 038	495
217	Time-History Record for Test 004	496
218	Time-History Record for Test 005	497
219	Diagnostics Channel Instrumentation	501
220	Diagnostics Channel Installed for Testing	504
221	Diagnostics Channel Prior to Test	505
222	Diagnostics Channel After Testing	506
223	Gas Electrical Conductivity	509
224	Theoretical Electrical Conductivity	510
225	Axial Heat Flux Distribution	512
226	Axial Heat Flux Distribution	513
227	Comparison of Measured and Theoretical Heat Flux	515
228	Pressure Time-History Records	517
229	Vibration Time-History Records	518
230	AMS Pressure Traces	520

FIGURES		PAGE
231	AMS Vibration Traces	521
232	AEDC Test Facility	526
233	AEDC Test Program Logic	529
C.1	Electrode Screen Attachment	587
C.2	Electrode Frame	590
C.3	Short Mandrel Section	591
C.4	Electrode Frame Corner Geometry	593
C.5	Typical Diagonal Corner Detail	594
C.6	Model Diagonal Corners	595
C.7	Diagonal Electrode Frame Model	596
C.8	Prototype Diagonal Frame Mandrel	597
C.9	Diagonal Frame Cooling Tubes	599
C.10	Electrode Frame Corner Geometry	600
C.11	Grooves in Corner Blocks	601
C.12	Tube Corner Forming Tool	603
C.13	Tube Connection Forming Tool	604
C.14	Formed Connection Tubes	605
C.15	Straight Tube Flattening Die	606
C.16	Straight Tube Flattening Punch	607
C.17	Composite Case Model	609
D.1	Feed System Schematic	612
D.2	Curve of Flow vs Valve Position	613
D.3	Start and Cutoff for Nominal Test Flow Rate with 5% Seed Flow Rate	618
E.1	Truncated Ideal Bell Flow Field	622
E.2	Flow Field: Source Flow Nozzle	622
G.1	Combustor Static Pressure Profile	629
G.2	Gas Generator Theoretical Characteristic Velocity, 7% SPAN-80	632

LIST OF TABLES (Continued)
(Volume II)

TABLE		PAGE
47	Diagnostics Channel Instrumentation List	359
48	Diagnostics Channel Combustor Development Tests	363
49	Design Criteria for Diagnostics Channel	364
50	Design Specifications	366
51	High Power MHD Channel/Diffuser Frame Analysis for the Diagnostics Channel	367
52	High Power MHD Channel/Diffuser Case Analysis for the Diagnostics Channel	368
53	Thermal and Hydraulic Data for Diagnostics Channel	370
54	Fabrication Steps for Case Winding	392
55	Structural Summary - Heat Sink Combustor	420
56	Feed System Instrumentation List	432
57	Heat Sink Combustor Instrumentation List	434
58	Diagnostics Channel Instrumentation List	437
59	SSFL Test Summary	439
60	Ignition Test Instrumentation List	449
61	Ignitor Test Summary	454
62	Preliminary Results of Test 007 for the High Power MHD Gas Generator	477
63	Preliminary Results of Test 008 for the High Power MHD Gas Generator	478
64	Preliminary Results of Test 009 for the High Power MHD Gas Generator	479
65	Preliminary Results of Test 010 for the High Power MHD Gas Generator	480
66	Preliminary Results of Test 011 for the High Power MHD Gas Generator	481
67	Predicted Damping Coefficients	490
68	Steady-State PSD Summary (Amplitude of "spikes")	492
69	Steady-State AMS and Time History Summaries	493
70	Conductivity Test Results	508

LIST OF TABLES

TABLE		PAGE
71	Results of Test 008	516
72	AMS Trace Summary	522
73	30 MW Channel/Diffuser Test Plan at AEDC	530
74	Gas Generator System-Probability of Successful Operation	535
75	Electrode System RMA	541
76	Cooling System RMA	543
77	Gas Seals RMA	544
78	Channel and Diffuser Cases RMA	545
79	Instrumentation and Electrical RMA	546
A.1	Hazard Summary	550
A.2	Hazard Levels	554
A.3	Preliminary Hazard Analysis	556
B.1	Ignition System Development Test Data Summary	580
B.2	Gas Generator and Diagnostics Channel Development Test Data Summary	582
D.1	Maximum Predicted Start Transient Pressures vs Valve Plug Contour	614
D.2	Maximum Predicted Cutoff Valve Inlet Pressures vs Valve Plug Contour	614
D.3	Time to 90% Chamber Pressure as a Function of Valve Opening Time	617
D.4	Maximum LO_2 and Fuel Valve Inlet Pressures vs Valve Closing Time	617
G.1	30 MW MHD Data Reduction	633
G.2	Data Printout	638
H.1	Planned Fabrication Process/Detailed Tasks	644

SECTION VII

DEVELOPMENT TEST ARTICLES

A. INTRODUCTION

During the HPMS program, two components were fabricated for the development test program - a diagnostics channel and a heat sink combustor. The diagnostics channel was designed and fabricated by Maxwell Laboratories, Inc. while the heat sink combustor was designed and manufactured by Rocketdyne. The testing of these components was conducted at SSFL using the injector and ASI systems described in Section V and the seed system, feed system, and support structure discussed in Section VI.

The diagnostics channel was used to obtain design information on the plasma conductivity, heat flux, and wall static pressure, and to demonstrate the feasibility of the fabrication technique used for the construction of small MHD channels at the much higher flow rate of 30 kg/sec used in this program. The heat sink combustor, which was internally identical to the cooled wall combustor design, was used to obtain information on the injector performance, heat flux, static pressure profiles, and pressure oscillations that would have been difficult to obtain with a cooled wall combustor. The interface between the diagnostics channel and the heat sink combustor was identical to the interface between the cooled wall combustor and the high power MHD channel. Section B describes the design and fabrication of the diagnostics channel and Section C describes the design and manufacture of the heat sink combustor. The SSFL development test program and the tests results are described in Section VIII.

B. DIAGNOSTICS CHANNEL

1. Introduction

A diagnostics channel was fabricated for use in the SSFL development test program. The channel was designed for gas conductivity measurements; and hence, the electrode frames were oriented perpendicular to the gas flow direction. The channel construction was relatively simple and utilized fabrication techniques developed on previous efforts.[3,4] Instrumentation was

---

[3] O. K. Sonju, J. Teno, R. Kessler, L. Lontai, and D. E. Meader, "Status Report of the Design Study Analysis and the Design of a 10 MW Compace MHD Generator System," AFAPL-TR-74-47, Part II, June 1974.

[4] D. W. Swallom, O. K. Sonju, D. E. Meader, G. T. Heskey, "MHD Lightweight Channel Development", AFAPL-TR-78-41, 1978.

provided to ensure that satisfactory pressure, temperature and conductivity measurements were made. The requirements for the diagnostics channel were: (1) duplicate the nozzle/channel interface of the high power MHD channel; (2) allow for steady state operation; (3) permit a cycle life sufficient for the development test program with a reasonable margin of safety; (4) provide for instrumentation for measuring gas conductivity, wall heat flux, gas static pressure, channel vibrations, and electrode temperature distribution; and (5) demonstrate the feasibility of the lightweight construction technique for the high mass flow rate conditions. These requirements were satisfied by the diagnostics channel. The results of the development test program are described in Section VIII.

2. General Description

The diagnostics channel was a representation of the entrance region of the high power channel/diffuser. The only significant difference was the use of electrode frames which were oriented perpendicular to the gas flow direction instead of transition frames and frames at an angle to the gas flow direction. The electrode design was similar in cross section, and the case dimensions matched those of the high power channel/diffuser.

The diagnostics channel was bolted to the Rocketdyne combustor/nozzle with a structure capable of withstanding startup, steady state operation and shutdown. The short length of the diagnostics channel permitted the use of the cantilever arrangement shown in Figure 156. This arrangement provided maximum accessibility to the channel, and minimized the need for additional downstream support structure design and fabrication. Cantilevering the channel permitted drainage from the manifolds, if necessary, and provided for maximum ease of installation and removal of the channel on the test stand.

The inner contours of the combustor/nozzle and diagnostics channel were matched so that the axes were collinear. Three interface pins in the diagnostics channel and matching slots in the combustor/nozzle maintained this alignment while permitting relative transverse thermal expansion between the components at the interface plane. Axial contact was maintained by bolts in belleville springs. The bolt holes were oversized to avoid thermal restraint. The bellevilles permitted control of the interface preload. The total compression of the bellevilles was such that if there were any loads on the channel which tended to separate the channel from the nozzle, no release of gas through the interface O-ring would occur because the bellevilles would have been compressed flat and the bolts would have been fully effective as a stiff spring system before that would have happened. One of the purposes for the SSFL development tests was to demonstrate the structural performance of this system.

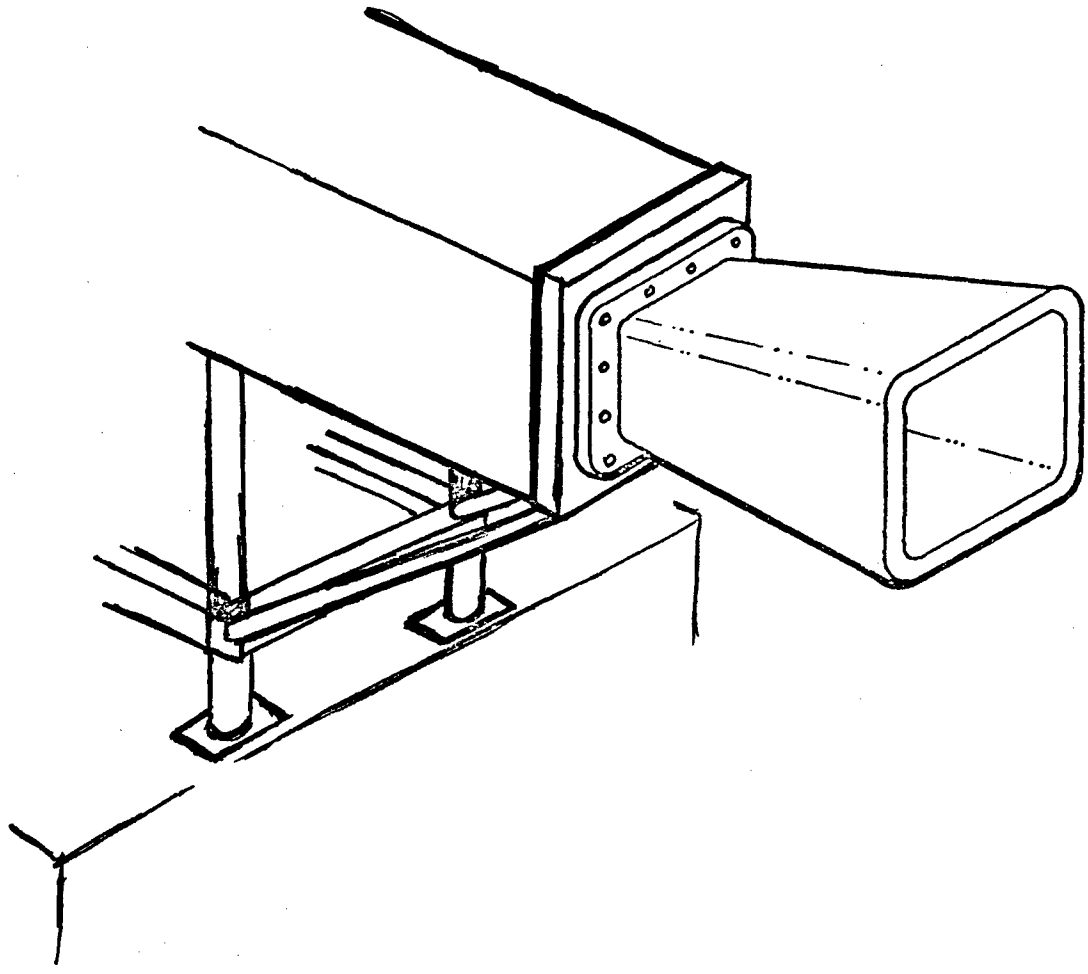

Figure 156. Diagnostics Channel Mounted to Solid Wall Combustor.

The diagnostics channel consisted of water cooled electrode frames which were oriented perpendicular to the flow axis. The electrode was constructed around the copper blocks comprising the electrode frame, and the cooling tube was attached to the outside of the copper frame. The inside or gas side of the copper block was formed into a single "U" shaped cup extending around the periphery of the electrode frame. Centered in the cup was an Inconel screen which had been brazed to the cup. The cups were filled with a castable stabilized zirconia ceramic. This electrode design provided an electrode capable of operating at a ceramic surface temperature of approximately 2000 K. SECTION IV provides a more complete description of the design features of the perpendicular electrode frames.

The channel was completed by assembling the electrode frames on the mandrel. After the electrodes were correctly spaced on the mandrel, the interelectrode gaps were filled with castable alumina. The winding of the outer shell with the epoxy-coated continuous filaments provided the outer case of the channel, which was the load carrying channel structural member. With this concept the load bearing member of the channel was at a relatively low temperature and provided the support for the high temperature electrode frames.

The diagnostics channel instrumentation was installed to record essential data used to establish the performance of the diagnostics channel. Table 47 provides a list of the diagnostics channel instrumentation for the SSFL development test program. The pressure, conductivity, and vibration instrumentation is shown schematically in Figure 157 while a schematic illustration of the temperature instrumentation is presented in Figure 158.

The pressure transducers, accelerometers, and water temperature thermocouples were installed during the channel installation at SSFL. The frame thermocouples and the voltage lugs were installed on the diagnostics channel during the channel fabrication. All test data was recorded by the SSFL test facility and processed by the data reduction program. These items are described more completely in Section VIII.

Subsequent sections of this chapter discuss the diagnostics channel design requirements and analysis and fabrication process. Additional design details are also presented in this subsection.

3. Design Criteria

The diagnostics channel was designed to simulate the entrance region of the high power MHD channel for 500 cycles of development testing at SSFL. A schematic view of the arrangement appears in Figure 156. The channel was bolted to the exit face of the combustor nozzle. The SSFL test facility provided the water to cool the channel and the supports for the water manifolds, which were bolted to the SSFL inlet and outlet piping.

TABLE 47. DIAGNOSTICS CHANNEL INSTRUMENTATION LIST

MEASUREMENT TYPE	DESCRIPTION	APPROXIMATE RANGE OF INTEREST	NUMBER OF MEASUREMENT LOCATIONS
Conductivity	Conductivity Circuit Differential Voltages	0 to 50 V	4 Differential Pairs
	Conductivity Circuit Current	0 to 50 A	1
Pressure	Channel Boundary Layer, Gas Static Pressure	1 to 5 atm	3
Temperature	Channel Wall	0 to 535 K	3
Temperature	Electrode Frames	0 to 815 K	3
Temperature	Cooling Water	0 to 535 K	6
Vibration	Channel/Structure	5 to 2000 Hz	5

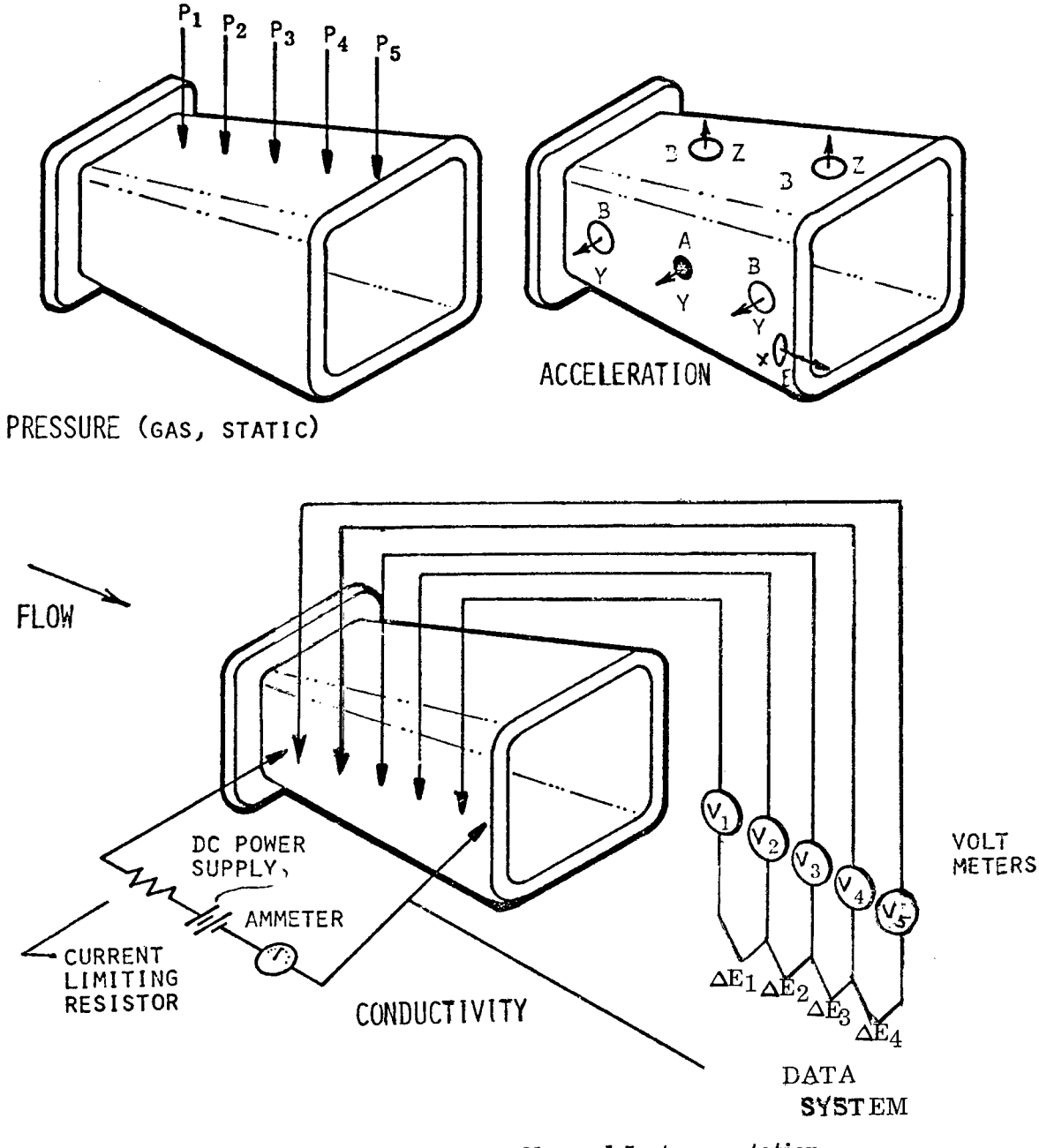

Figure 157. Diagnostics Channel Instrumentation (Pressure, Acceleration, Conductivity)

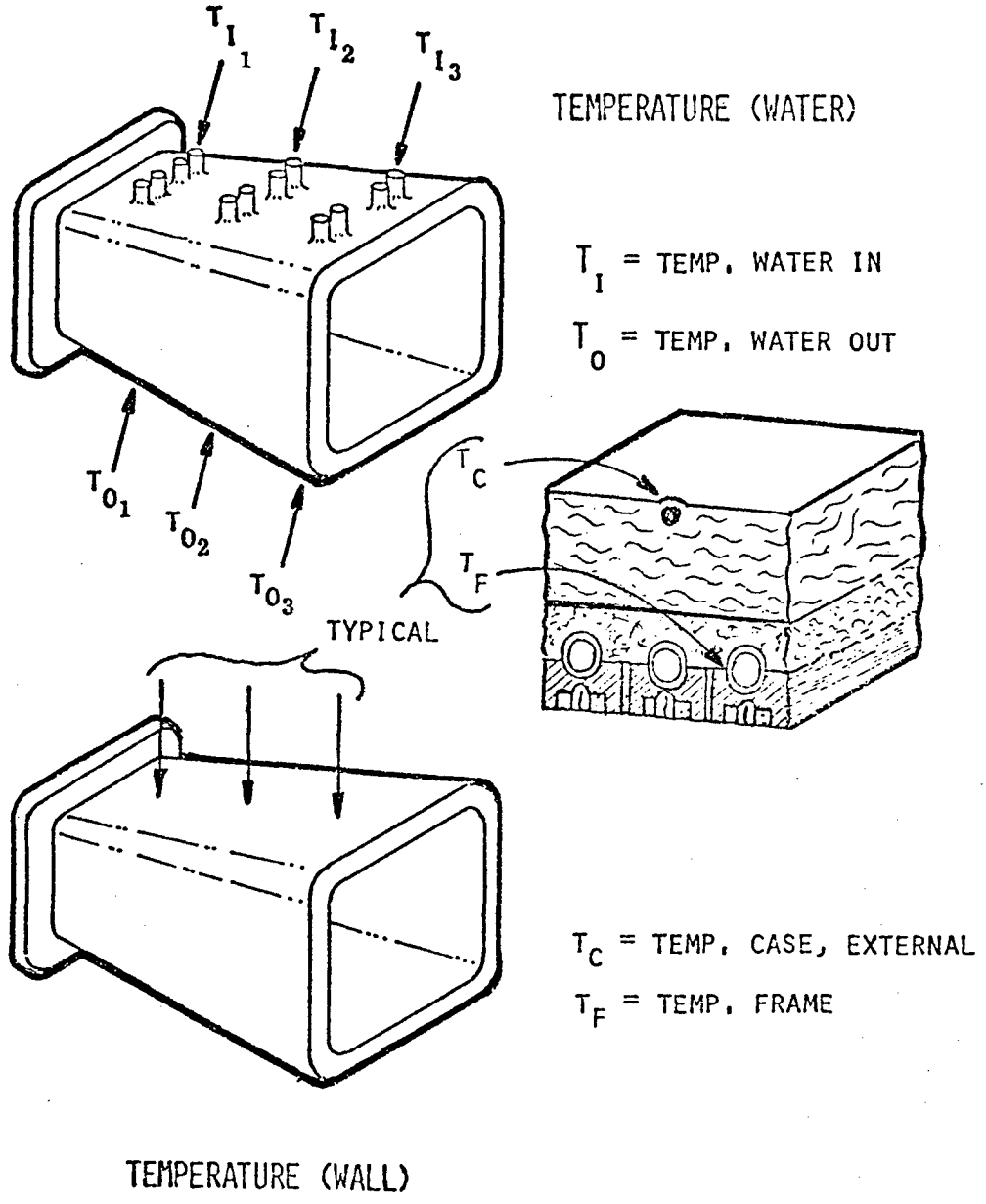

Figure 158. Diagnostics Channel Instrumentation (Temperature)

The main functions of the diagnostics channel during these tests were to provide an interface flange simulation for the combustor/nozzle and verification of the interface design for use on the high power MHD channel/diffuser, to obtain a measurement of electrical conductivity of the gas during the SSFL combustor development tests, and to acquire preliminary mechanical performance data to verify the lightweight, high power MHD channel/diffuser design. The test program during which the channel was tested is listed in Table 48. The diagnostics channel test objectives were: (1) nozzle/channel interface flange simulation for the cooled combustor/nozzle and the high power MHD channel/diffuser; (2) measurement of gas electrical conductivity during the SSFL development test program; and (3) acquisition of temperature, pressure, and vibration data to demonstrate the feasibility of design concept.

Design criteria for the diagnostics channel were established to ensure that all of the test objectives would be satisfied. Table 49 presents the design criteria for the diagnostics channel. A cantilever mount for the channel was selected to avoid the problems and complexities of a downstream support structure. A once through flow cooling system was utilized to reduce the cooling system complexity associated with flow restrictions and flow balancing.

4. Design Specifications

In order to meet the test objectives of the previous section and the design criteria listed in Table 49, the diagnostics channel was required to meet the same requirements as the entrance region of the high power MHD channel/diffuser. The high power MHD channel/diffuser design specifications and design analysis are presented in Section IV. The thermal and mechanical loadings for the diagnostics channel were equal to, or less than, those of the high power MHD channel/diffuser. Consequently, the factors of safety for the diagnostics channel were greater than or equal to those of the high power MHD channel/diffuser.

The entrance region of the high power MHD channel/diffuser had the shortest length electrode frames of any of the frames in the channel/diffuser. In the diagnostics channel these frames were all oriented normal to the channel axis. This change of orientation angle provided greater stiffness for the diagnostics channel frames than the high power MHD channel/diffuser upstream electrode frames where some of the frames were beginning to slope in the transition zone. However, the diagnostics channel case dimensions were approximately the same as the high power MHD channel/diffuser. Therefore, wall strength, stiffness, and natural frequency were greater for the diagnostics channel than they were for the high power MHD channel/diffuser.

TABLE 48. DIAGNOSTICS CHANNEL ROCKETDYNE COMBUSTOR DEVELOPMENT TESTS

Test No.	% Seed	P_c, atm	MR	Duration Sec	Test Objectives
006	Cs 5	30	3.34	2	Conductivity
007	Cs 10	30	3.34	2	Conductivity
008	Cs 5	30	3.00	2	Conductivity
009	Cs 5	30	3.34	2	Conductivity
010	Cs 10	30	3.00	2	Conductivity
011	Cs 10	30	3.00	2	Thermal

TABLE 49. DESIGN CRITERIA FOR DIAGNOSTICS CHANNEL

Thermal Cycles	500
Factor of Safety	
Based on Life (All Structural Components)	10
Based on Ultimate Strength (Case)	4
Breathing Deflection Limit	0.76 mm
Cooling System	Once Through Flow Pressurized Tank Fed
Heat Flux (Assumed Range)	
Inlet	~ 900 W/cm^2
Outlet	~ 600 W/cm^2
Mounting Configuration	Cantilevered from the Combustor/Nozzle Interface
Electrical Conditions (Nominal)	
Axial Current (Steady State)	40 A
Axial Electrode Field	2000 V/m

The limited flow capacity of the cooling water at the SSFL test facility required a water flow connection arrangement for the diagnostics channel which differed from the flow connections at the entrance region of the high power MHD channel/diffuser. The upstream frames of the diagnostics channel were cooled by feeding each of the cooling tubes in an electrode half-frame directly from the entrance manifold and also draining them directly to the outlet manifold. The downstream half-frame tubes were connected in series for each electrode.

The design specifications for the diagnostics channel are given in Table 50. These design specifications were similar to the specifications for the high power MHD channel/diffuser. However, the structural conditions for the diagnostics channel were less severe than those of the high power MHD channel/diffuser; hence, the analysis based on these specifications was conservative.

5. Design Analysis

The diagnostics channel consisted of an electrode frame array subsystem and a case subsystem. The frame array was the component that contained the cooling passages through which the cooling water flowed to control the temperature of the gas side wall material. The frame array also contained the electrode ceramic which provided the electrical current path. The filament-wound, fiberglass epoxy case held the frame array and protected it from vibrations and pulse loads while also providing the means of attaching the frame array to the combustor. The case sealed the channel against the possibility of gas leaks and provided electrical insulation.

The design analysis of the diagnostics channel has been based on the design specifications identified in Table 50. These criteria were primarily concerned with flow, temperature, and structural integrity. A primary factor related to the performance was the limitation of the wall deflections to 0.76 mm. Theoretical engineering investigations were conducted on all aspects of the design to ensure that the design criteria had been satisfied. This was accomplished by using the design and analysis approach utilized for the high power MHD channel/diffuser. Since the thermal and hydraulic conditions for the diagnostics channel and the MHD channel were identical and the structural conditions in the diagnostics channel were less severe than the high power MHD channel/diffuser, the design analysis for the high power MHD channel/diffuser described in Section IV, was used as the basis for the diagnostics channel design. Furthermore, the diagnostics channel was a simplified version of the entrance region of the full power system. As a result the factors of safety, which are summarized in Table 51 and Table 52 for the diagnostics channel, exceeded those for the high power MHD channel/diffuser.

TABLE 50. DESIGN SPECIFICATIONS

THERMAL	
Gas Face Frame Temperature	759 K
RTV Face Frame Temperature	366 K
Average Frame Temperature	562 K
Frame Temperature Gradient (Assumed Linear)	394 K
Case Inner Face Temperature (Assumed)	350 K
Case Outer Face Temperature (Assumed)	273 K
HYDRAULIC	
Coolant Passage Pressure	34 atm
Frame Pressure Drop	16 atm
Assumed Coolant Temperature (Frame Inlet)	290 K
Assumed Coolant Temperature (Frame Outlet) (Half-Frame/Frame)	320 K/350 K
Coolant Velocity (Half-Frame/Frame)	26 m/sec/19 m/sec
Coolant Flow Rate (Total)	44 liters/sec
STRUCTURAL	
Vibration Input	
Amplitude (Maximum)	4 g
Frequency	5 to 200 Hz
Channel Mass	63 kg
Channel Pressure	
Inlet	3 atm (Internal)
Inlet	1 atm (External)
Design ΔP	2 atm (Internal)
Thermal Cycles	500
Factor of Safety	
Based on Life	10
Based on Ultimate Strength	4
Wall Deflection	0.76 mm

Channel was bolted to the combustor/nozzle at the inlet with pins for collinearity of combustor and channel axes and with oversize bolt holes to avoid thermal stresses because of differences in radial movement of combustor and channel at the interface.

TABLE 51. HIGH POWER MHD CHANNEL/DIFFUSER FRAME ANALYSIS FOR THE DIAGNOSTICS CHANNEL

N = 1000

Loading	Applied Quantity	Allowable Quantity	Factor of Safety
3.5 atm (Channel Inlet)	$\epsilon = 3.0 \times 10^{-4}$		
Transverse	$\epsilon = 3.53 \times 10^{-3}$	$N = 7.1 \times 10^{4}$	71
Temperature Gradient, 389 K	$\epsilon_{TOT} = 3.83 \times 10^{-3}$		
Vibration $\Delta P = 0.19$ atm	$\Delta G = 2 \times 10^{-5}$ (0.5% increment)	$N = 6.6 \times 10^{4}$	66

NOTE: At 480 K and σ = 548 atm in CDA-102 copper, creep rate = 0.0012/1000 hr.

TABLE 52. HIGH POWER MHD CHANNEL/DIFFUSER CASE ANALYSIS FOR THE DIAGNOSTICS CHANNEL

N = 1000

Loading	Applied Quantity	Allowable Quantity	Factor of Safety
0.9 atm	δ = 0.39 mm	δ = 0.76 mm	2.0
(Channel Exit)	σ_P = 78 atm	σ = 817 atm $N > 10^6$	> 10
Thermal Shock (345 K)	σ_{TS} = 263 atm		
	$\sigma_P + \sigma_{TS}$ = 341 atm	$N > 10^6$	> 100
Restraint of Frame Growth	σ = 37 atm		
T = 420 K	$\sigma_P + \sigma_R$ = 115 atm	$N > 10^6$	> 100
Vibration			
Assume 25 g	$\Delta\sigma$ = 25 atm		
Longitudinal and Bending	σ_{TOT} = 140 atm	$N > 10^6$	> 100
(Equivalent to 0.23 atm)			

The channel design specifications in Table 50 summarize the parameters used to develop the structural integrity needed for survival. As was shown in this table, the cycle life requirement was assumed to be 500 cycles although only thirty-one runs were expected at SSFL. This provided some measure of survivability against possible unexpected load conditions provided that these loads were not catastrophic. The detailed design analysis for the structural as well as the thermal and hydraulic analysis is presented in Section IV and will not be repeated in this section.

The coolant requirements were minimized by the once-through flow paths of the half-frame and full frame electrode cooling loops. The flexible tubing which connected the half-frames and frames to the manifolds was shortened to a minimum length to minimize the pressure drop. Furthermore, the flow rate was kept as low as possible to minimize the pressure drop through the electrode frame cooling loops. The design summary of the cooling water flow and heat transfer analysis for two different axial locations is shown in Table 53. The flow analysis utilized the pressure drop data described in Section IV, which contains a figure showing the pressure drop for half-frame and frame cooling loops as a function of the water flow velocity.

The final design consideration was the survivability of the channel under vibratory inputs. The design condition of 4 g loading represented a general guide line for rocket motor testing. The channel could have survived much higher vibration levels, as is shown in Tables 51 & 52, which contain the summaries of applied and allowable quantities for the electrode frame array and the filament wound, fiberglass epoxy case of the high power MHD channel/diffuser. As shown in the Tables, factors of safety were large. The lowest value related to the ability of the frames to resist buckling. That factor also showed an appreciable level of safety. The case was the ultimate safety barrier for the channel. Table 52 shows a factor of safety of two based upon wall deflections. However, based upon stress level there was a factor of safety in excess of ten based upon static stress and a safety factor of 2000 based upon the design value of 500 thermal cycles.

6. Design Details

The design approach to the diagnostics channel was to use as many features as were possible that were common to the high power MHD channel/diffuser and the diagnostics channel. For instance, the MHD channel case winding pattern and thickness were used. Once-through parallel flow cooling was also utilized. Simplified construction features, such as circular cooling tubes, were also used.

TABLE 53. THERMAL AND HYDRAULIC DATA

DIAGNOSTICS CHANNEL

Heat Load	w/cm^2	905	750
Station X	cm	0	20
Heat Load per Frame	kW	76	70
H Required to Prevent Gas Side Overheating	w/cm^2K	13	8.4
V (Half-Frame/Frame)	m/sec	26/NA	NA/19
Cooling Flow per Half-Frame/Frame	liters/min	49/NA	NA/36
ΔP for V Half-Frame/Frame	atm	16/NA	NA/16
P Required to Prevent Boiling	atm	14	14
Required Pressure	atm	30	30
SSFL System Pressure	atm	40 atm	40 atm

NA = Not Applicable

The diagnostics channel was cantelivered from the exit face of the combustor/nozzle. This arrangement provided for maximum accessibility to the channel for attaching instrumentation leads and minimized the need for structure design and fabrication for a downstream support structure. This arrangement permited the removal of the diagnostics channel from the combustor face with a minimum of time and effort if this should be necessary.

The diagnostics channel test objectives served a dual diagnostic purpose: they permitted a measurement of the combustor performance as determined by the gas electrical conductivity and an evaluation of the channel mechanical performance. The mechanical performance information was required for the final design of the high power MHD channel/diffuser. If any modifications were indicated to optimize the performance of the high power MHD channel/diffuser, these would have become apparent during the SSFL development test program.

The design details of the diagnostics channel were similar to the design details presented in Section IV discussing the high power MHD channel/diffuser. These details will not be repeated in this Section. Figure 159 shows a cross section of the diagnostics channel including the case. The channel was constructed of forty identical, except for the frame width, electrode frames. Nineteen of the electrode frames in the inlet region had half-frame cooling loops while the downstream twenty-one frames had two half-frames connected in series to form the cooling loop. Frame anchor clips were provided to ensure the proper attachment of the electrode frames to the case.

The diagnostics channel was approximately 450 mm long with an inlet cross section of 181 mm x 197 mm and an exit cross section of 265 mm x 197 mm. The non-parallel walls diverged at an angle of 5.5 deg. Electrodes in the channel were of two types - ceramic and ceramic with Inconel screens. The ceramic or ceramic/screen electrode surface extended around the periphery of the electrode frame except for the corner regions. The electrode pitch was 11.3 mm with an insulator thickness of 1.8 mm.

A design overlay of the diagnostics channel system is shown in Figure 160. Some of the design features of the diagnostics channel are also shown. The inlet cooling manifold, item two, distributed the cooling water to 59 individual cooling loops, which consisted of 38 half-frame cooling loops and 21 full frame cooling loops. The half-frame cooling loop connectors are shown in the figure as item three. The barbed fittings, barb couplings, cooling tube elbows, manifold connectors, and the high pressure hose are shown as items five through ten, respectively. A transite exit shield, item eleven, was installed to act as a shield to protect the diagnostics channel and the cooling system from the thermal effects of the hot exhaust gas.

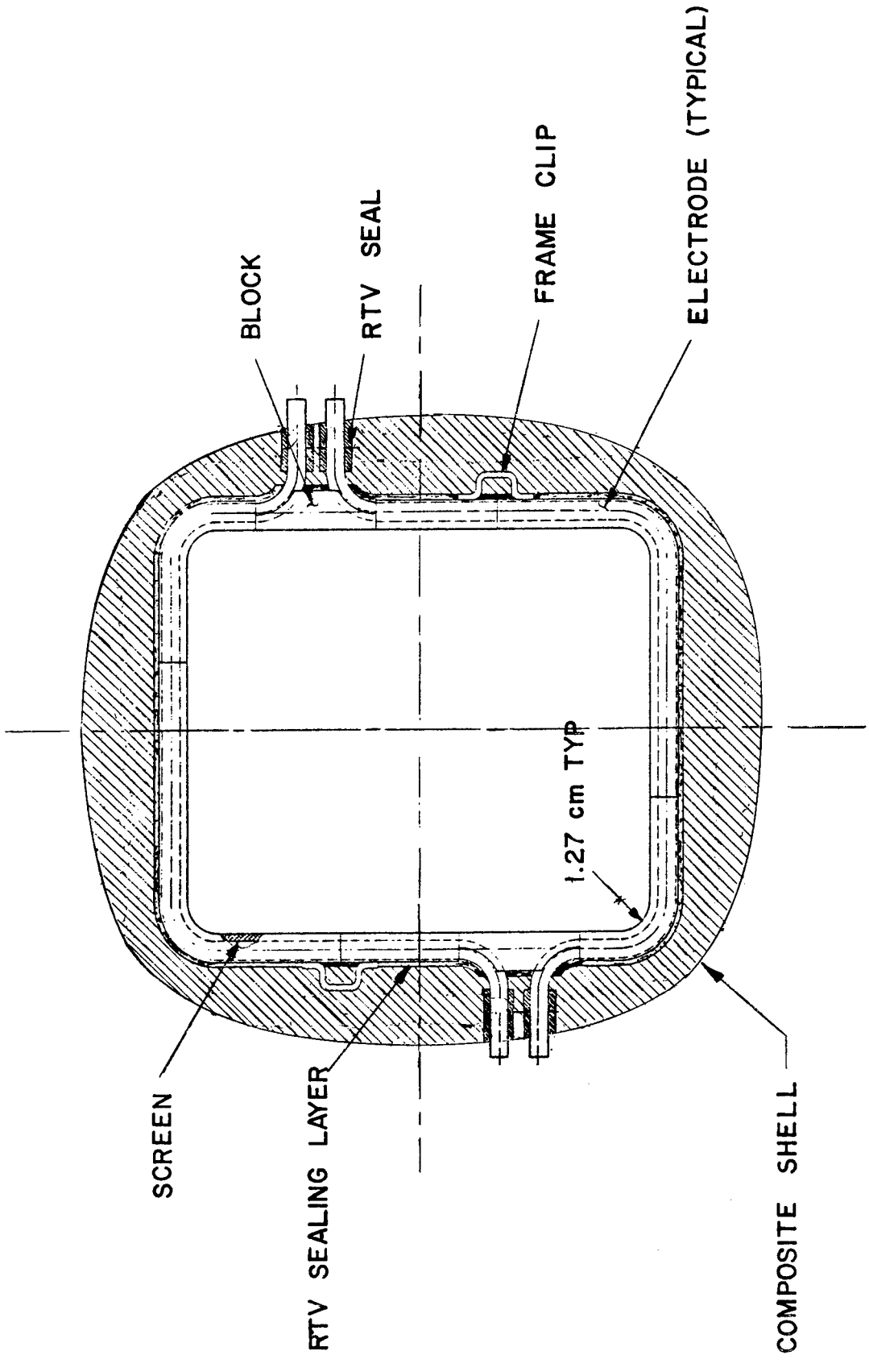

Figure 159. Section View of Diagnostics Channel.

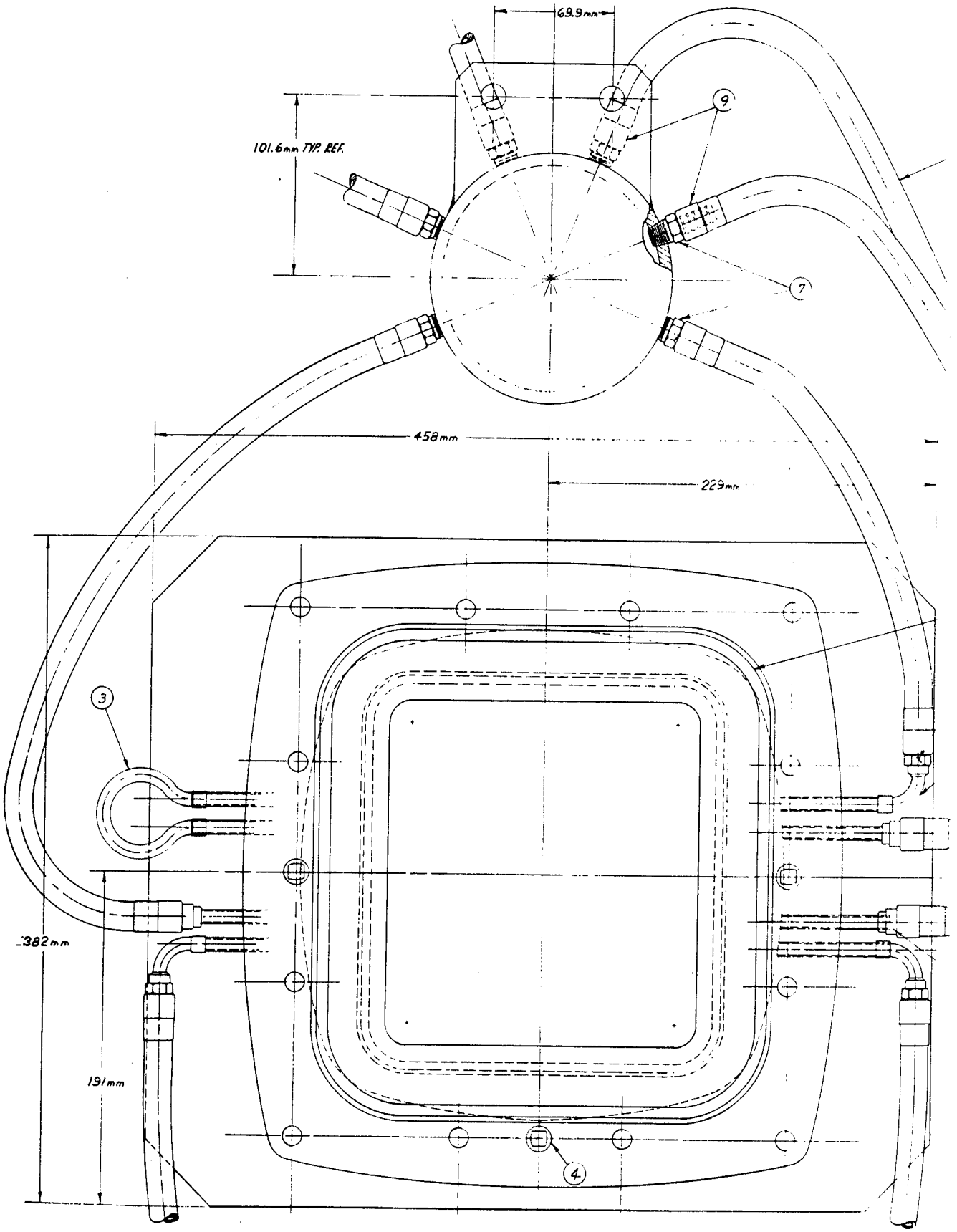

(1)

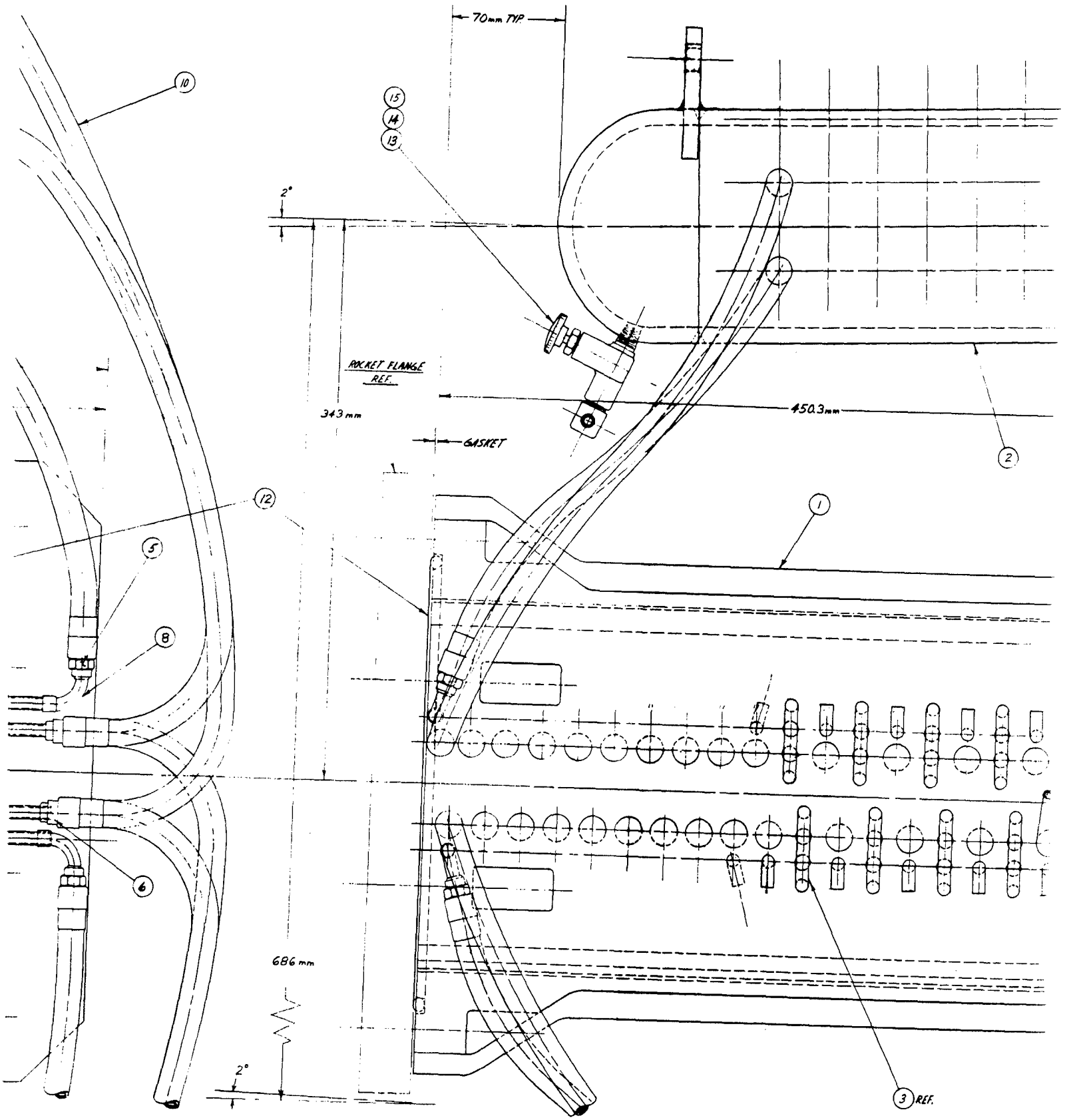
70mm TYP
10
15
14
13
2°
ROCKET FLANGE REF.
343 mm
450.3mm
GASKET
2
12
1
5
8
6
686 mm
2°
3 REF.

(2)

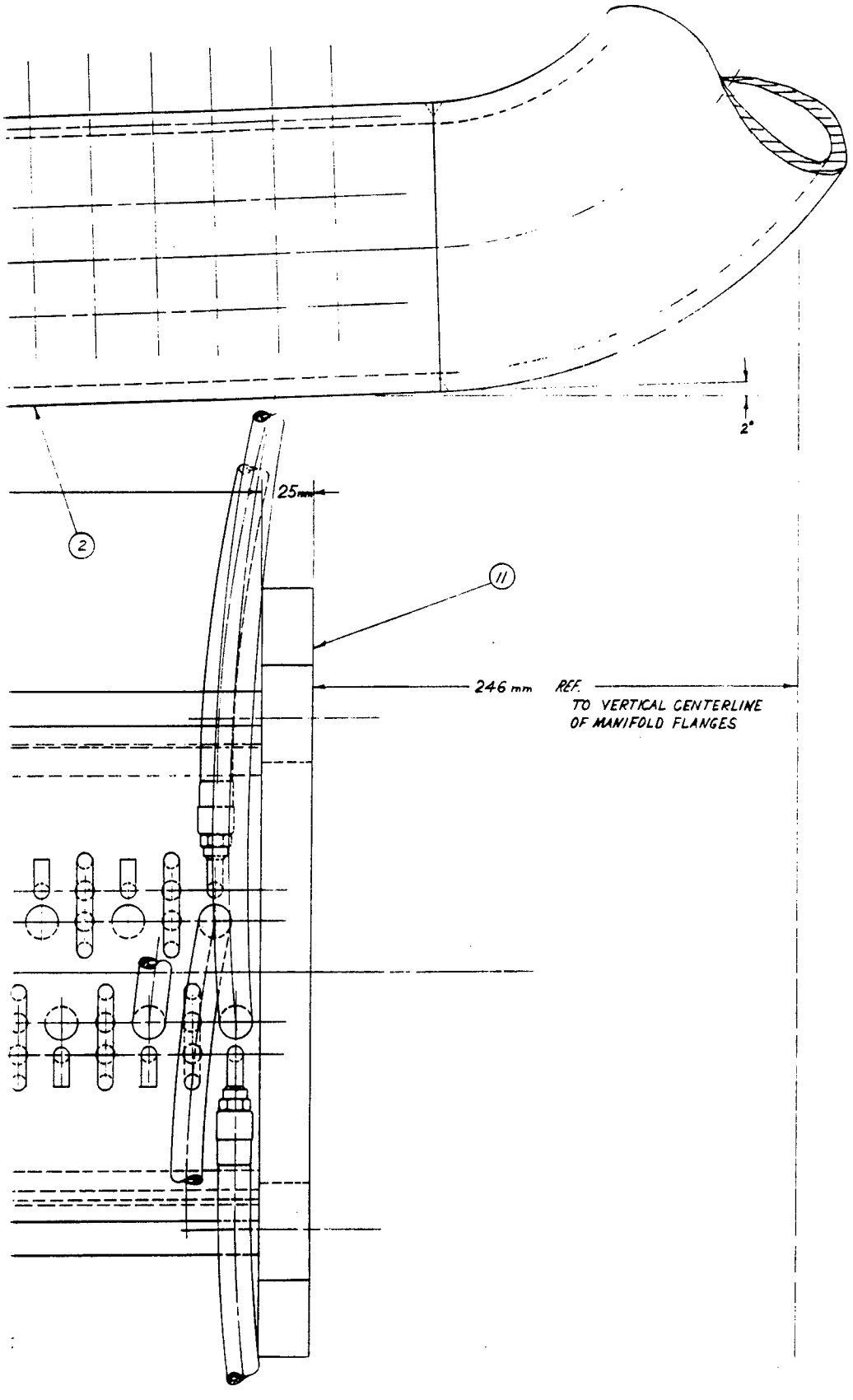

Figure 160. Diagnostics Channel Design Overlay.

In order to insure proper alignment of the combustor/nozzle flow axis with the diagnostics channel flow axis, the diagnostics channel was constructed with alignment pins. These were designed to fit into the alignment slots of the combustor nozzle. These pins are shown in Figure 160 as item four.

Typical electrode frame cross sections are shown in Figure 161 for both the ceramic and the ceramic with screen frames. To reduce the fabrication costs, the ceramic with screen frames were used for ten electrodes while the remaining thirty electrode frames were ceramic only. To provide electrode heat transfer data at different axial locations, the ten ceramic/screen electrode frames were used in two groups of five each starting with frame twenty and thirty-one, respectively.

7. Fabrication

a. Introduction

This section describes in detail the sequence of operations performed during the fabrication of the diagnostics channel. The problems encountered during the fabrication process are discussed as well as the method used to resolve the problem. Because of the importance of the tooling in the fabrication process, this item is discussed first, followed by the fabrication and assembly of the frame array on to the mandrel. Next, the case fabrication and finishing operation are discussed, and finally, the cooling system fabrication and the final tests and inspections. Throughout the fabrication many photos were taken to document progress. Where applicable, some of these photos are used to clarify the verbal descriptions of the tasks involved.

b. Fabrication Tooling

Mandrel. The utilization of a very accurate "form" or mandrel for building the diagnostics channel clearly made this mandrel the single, most valuable tool used in the entire building process. Some of the more important of the many functions of this tool included the following: (1) the establishment of the internal contour of the channel; (2) a "work station" for the frame fit-up, ceramic emplacement, hot gas barrier application, case winding and finishing operations; (3) a master gauge to establish the theoretical locations of the forty frames; (4) a means of supporting and rotating the channel in the winding fixture/oven during the curing of the case; and (5) an aid to the remanufacture and replacement of any given frame which has failed.

The mandrel was assembled from machined aluminum plates with trunnions fitted at each end for rotation in the winding fixture. To facilitate the removal of the mandrel at the end of the fabrication process, the plates were designed, once the trunnions and end plates were removed, to be independent of each other.

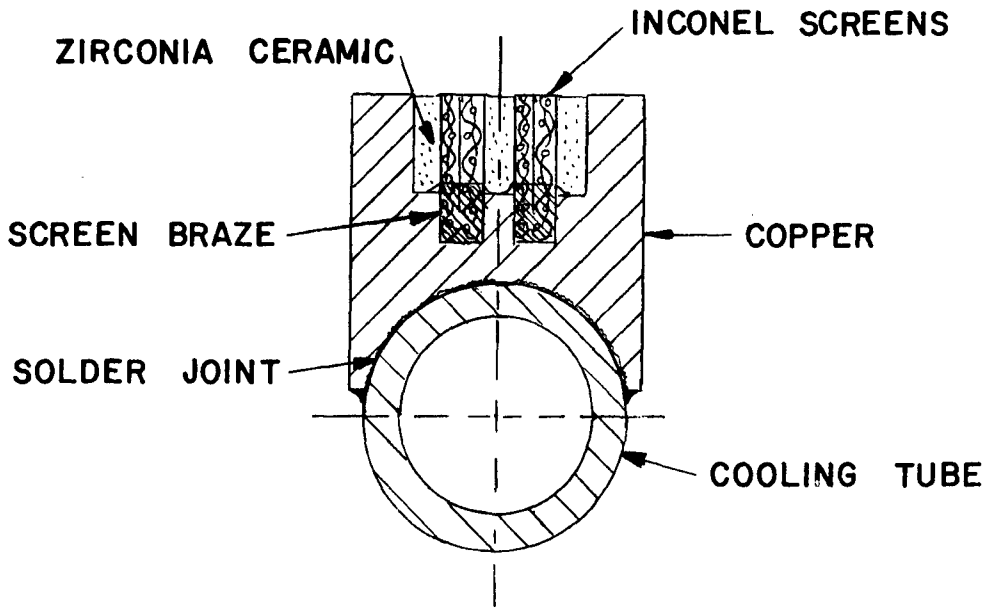

CERAMIC ELECTRODE WITH SCREENS

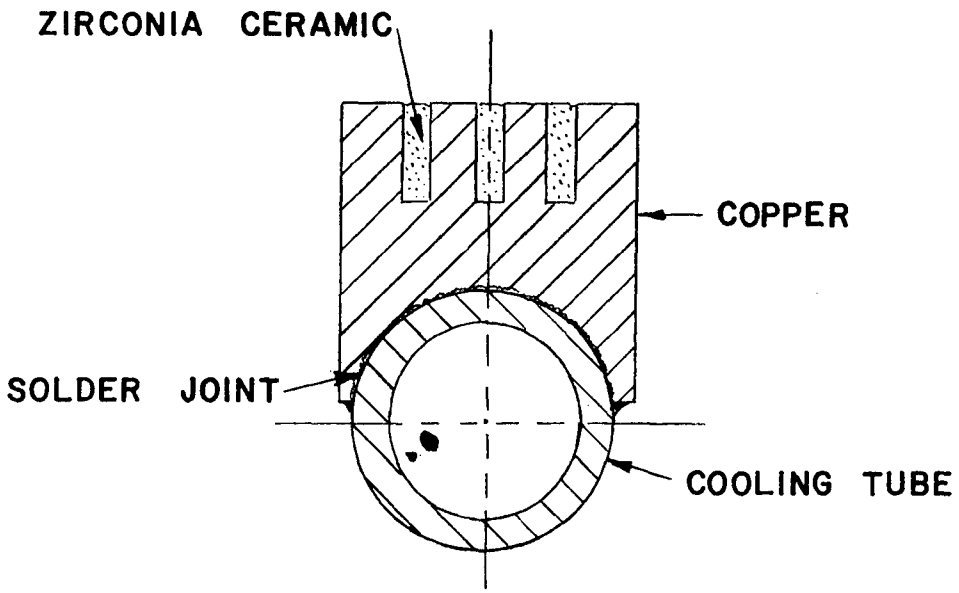

CERAMIC ELECTRODE WITHOUT SCREENS

Figure 161. Diagnostics Channel Electrodes.

In addition, the exterior of the plates was coated with a durable film of Teflon to act as a release agent.

In order to accomplish this, cast aluminum plates were carefully machined in accordance with the hot gas contour. The ends of the plates were drilled, reamed and/or threaded. The steel trunnions were then welded to the steel end plates. The end plates were drilled in accordance with the previously drilled holes. Next, the entire assembly was pinned and bolted together. No fasteners were used to join the side plates to themselves; only to the end plates. The flatness of the plates and the machining tolerances minimized the gaps along abutting surfaces of the side plates. A finish sanding completed the machining of the mandrel. Next, the mandrel contour was inspected for dimensional accuracy. Following some additional sanding to bring the entrance end of the mandrel into specification, the mandrel was then mounted vertically on a surface plate on the exit end.

To facilitate the assembly of the frame array, described later in this section, scribe marks were added to the mandrel. The scribe marks were required to be: (1) deep enough so that they were not hidden by the Teflon coating; (2) shallow enough so that they did not upset the smooth contour of the mandrel; and (3) located on the mandrel independently of any other scribe marks (i.e. non-accumulative positional tolerances). To accomplish this, the marks were applied using a 600 mm height gauge with a sharp nose scribe attachment. A scribe mark was located around the mandrel exterior at the theoretical position of the upstream face of each of the forty frames. Since each mark was located with respect to the surface plate, the tolerance on the location of each mark was constant and non-accumulative. A photograph of the completed mandrel is shown in Figure162.

Finally, the mandrel was sent out to be coated with a film of Teflon. Only the external surfaces of the side and end plates were treated. At this time two "winding flanges" were fabricated which were later assembled to the mandrel. The flanges were flat Teflon sheets backed by aluminum plates, which were attached to the mandrel end plates. These end plates "defined" the end faces of the channel. The epoxy coated roving was wound against them, but was not bonded to the Teflon. Following the successful dimensional inspection, the mandrel was carefully stored until needed.

Winding Fixture and Oven. Second in importance to the mandrel, the combination winding fixture and oven was used for a variety of efforts. The fixture consisted of a box made of steel angles and 9.5 mm thick Transite sheets. The box was made in two halves, which were readily separable. The lower half contained self-aligning ballbearings which supported the trunnions bolted to each end of the mandrel. This half also contained an electric motor with an infinitely

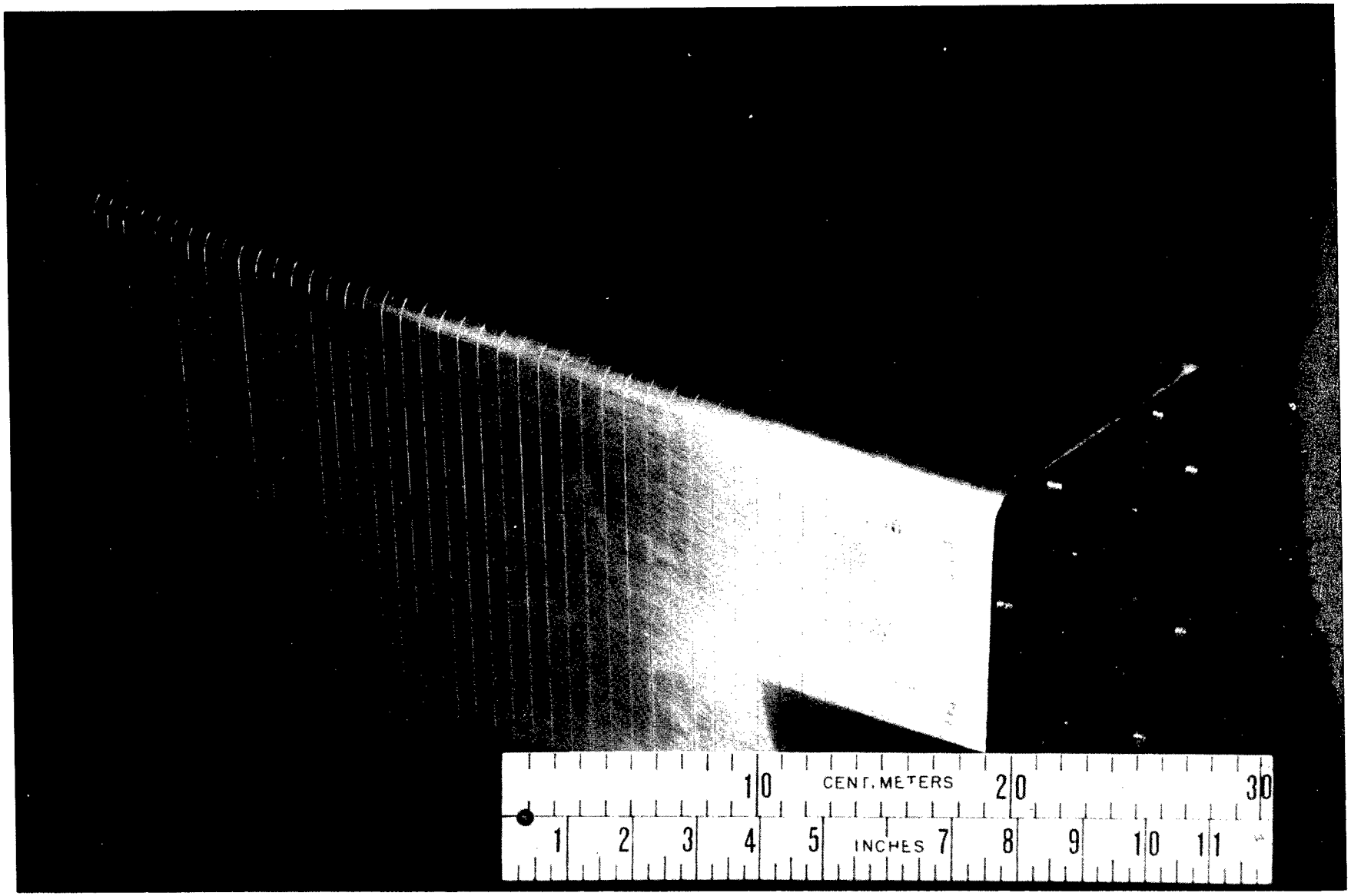

Figure 162. Diagnostics Channel Mandrel.

variable speed control and a reversing switch. A "V" belt and pulleys transmitted power to one of the mandrel trunnions. The upper half of the box contained several large strip heaters, a small blower, baffles, a light, two viewports and two thermocouples. A temperature controller connected to one of the thermocouples and to a relay which switched the heaters on and off provided a simple, reliable means to control oven temperature. The winding fixture was used as a work station for ceramic and silicone rubber implantation, a lathe for the filament winding of the case, and an oven for curing the ceramic and epoxy resin.

Epoxy Dispensing Mechanism and Layup Tools. A dispenser reservoir and mechanism was used to wet the roving and then remove the excess epoxy. The roving was manually guided as it passed over the rollers, and the rotation of the mandrel was also manually controlled. The roving tension was adjusted during the winding process to insure that the tension was always sufficient to provide a "tight" filament winding. The continuous rotation of the mandrel during the winding process minimized the amount of epoxy which dripped onto the base of the winding fixture. Other tools which were used included brushes to wet both the woven roving and fabric, and special serrated rollers to eliminate any air bubbles introduced by the winding and layup processes.

Interface Plates. A region of utmost concern was the alignment of the interior hot gas surfaces of the diagnostics channel and the combustor at installation. A step change in the cross sectional area at the nozzle/channel interface could seriously affect the flow uniformity and consequently, adversely affect the results of the SSFL development test program. To minimize the bore mismatch, two identical "interface templates" with the locating pin holes and two interior contour sides precision machined were fabricated for use in manufacturing the nozzle exit and the channel entrance. Locating holes for the clamping bolts were also provided. Each plate served to precisely locate the three alignment pins with respect to two selected adjacent hot gas surfaces.

During the fabrication, the templates were placed with the correct orientation on either the channel or combustor. After carefully aligning the two orthogonal legs of the triangle with the corresponding hot gas surfaces, the alignment pins and bolt holes were automatically located on the case.

c. Frame Array

The diagnostics channel consisted of forty electrode frames, which were oriented perpendicular to the gas flow direction. The frames were built up on the mandrel and then encased in a glass/epoxy resin case. A completed electrode frame is shown in Figure 163. This section describes the frame assembly from the machining to assembly onto the mandrel.

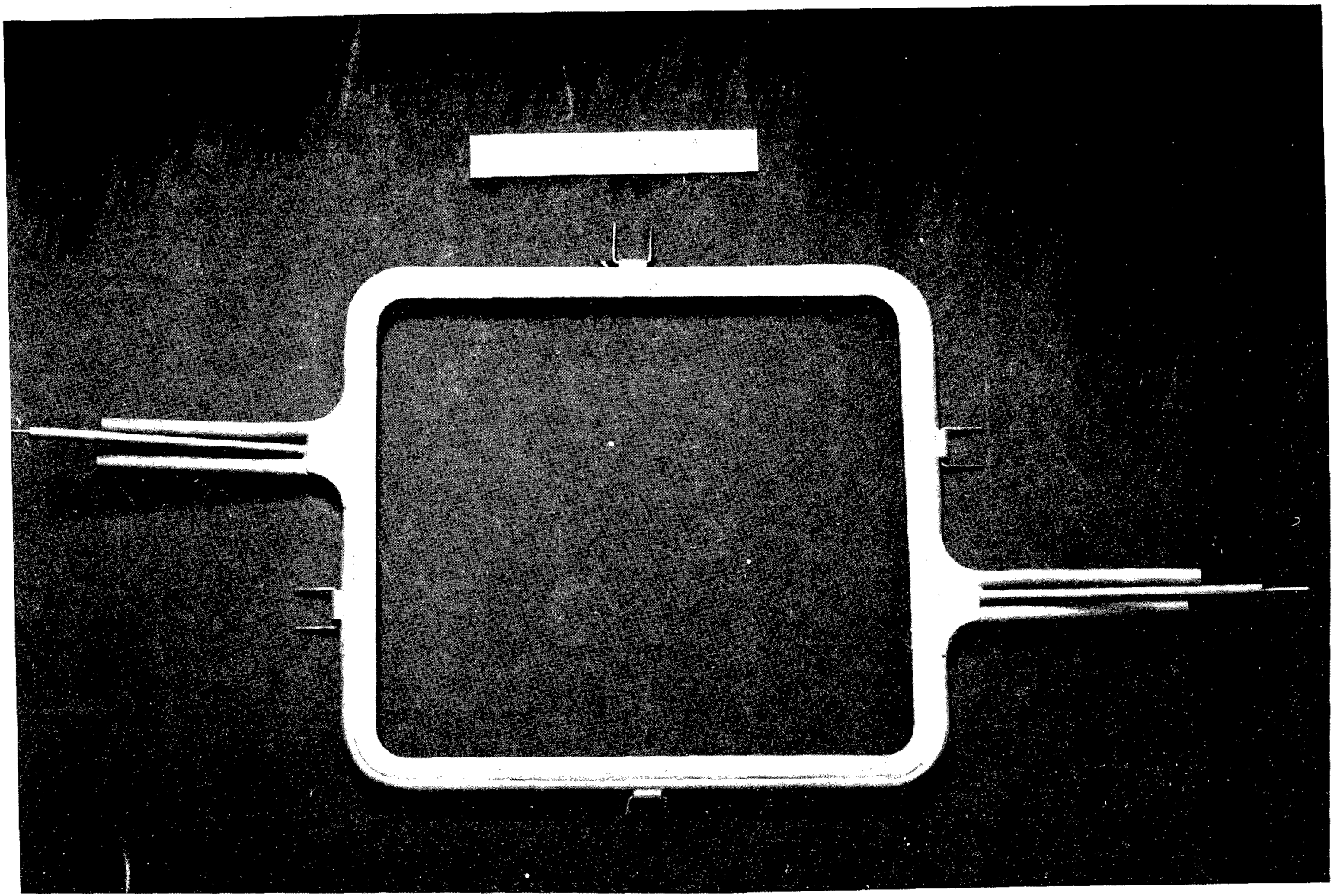

Figure 163. Diagnostics Channel Electrode Frame.

Component Machining. Each perpendicular frame consisted of four corner blocks, four rails which contained the current collector screens and grooves for the electrode ceramic, two tube spacer blocks which were located between the ends of the cooling tubes, and continuous cooling tubes that were attached to the outside of the frame. The screens were made from Inconel while all other metal components were copper.

The corner blocks, although difficult to visualize, were easy to machine once the set up had been completed. As described in Appendix C, the complex corner block geometry lended itself to conventional machining methods. There were only two different corner blocks in the channel - a "left-hand" block in the upper left and lower right corners, and a "right-hand" block on the upper right and lower left corners. The tube spacer blocks were machined from copper plate and did not pose any machining problems. Special cutters were fabricated to generate the required arcs. The frame anchor clips were made up from Be-Cu wire, and the pressure tap tubes from stainless steel tubing.

Cooling Tube Forming. The cooling tube formation was the most difficult part of the sequence because the basic requirement was to achieve intimate contact between the tube, rails, and tube spacer blocks without distorting the wall. (Appendix C-3 contains a more complete description of this process.) The cross section of the tube remained constant in the unform regions along the rails. After the basic frame had been brazed, the forming was done manually by using the frame itself as a die. The tubing was annealed following each bending operation to prevent the tubing from collapsing.

Brazing and Soldering. The brazing and soldering operations were probably the most important tasks of the entire fabrication process. For example, the special techniques described in Appendix C were developed to attach the Inconel screens to the rails since the common existing methods were unsatisfactory.

Following the attachment of the screens to 40 rails, the mandrel was set in a vertical position with the large end down, and the frame assembly was initiated. After a thorough cleaning of the components, four corner blocks for the largest frame were clamped in place using the scribe marks on the mandrel as a guide. The distance between the blocks were measured, and the appropriate rail was finished to the exact length required with space allowed for the braze thickness. At this point the rail was tack welded to the corner blocks. When all four rails were tacked, the interim assembly was removed from the mandrel and secured in a hold-down fixture. Next, all of the joints were torch brazed. The tube spacer blocks and pressure tap tubes were also added at this point.

The assembly was returned to the mandrel, checked, and adjusted if necessary. Shims were then added to guarantee 1.8 mm interframe gap. This process was repeated until all forty frames were assembled on the mandrel. Shims were added as necessary to position each frame to the appropriate scribe line. In addition, the gap between the frames and the mandrel was maintained below 0.25 mm. Figure 164 shows the partially complete assembly.

The next step was the attachment of the cooling tubes to the rails, corner blocks, and tube spacer blocks. To complete this step without upsetting the high and low temperature braze joints which were already completed, a low temperature solder was utilized. For each frame the tubes were first tack brazed in place, then the assembly was removed from the mandrel, and the tubes were thoroughly soldered to the frame using a high velocity torch. Finally, after placing the frame anchor brackets over a frame anchor clip, the brackets were soft soldered to the tube exteriors.

Water Flow Check. Of all the tests performed on the diagnostics channel during fabrication, none were more important than the water flow test. This test measured the pressure drop in each "half loop" at the water flow rate required to remove the nominal thermal load imposed on the channel by the hot plasma. This was done twice - after the final frame fit-up and after the case cure.

A very simple, yet reliable test apparatus to measure the pressure drop for a given water velocity was designed, fabricated, and checked out. During operation, the reservoir with a pressure gauge was filled with tap water at a pressure of ≈ 2 atm. The half-frame cooling path to be tested was connected between the high pressure water exhaust line and a pressure gauge. To this gauge a line which drained into the water collection container, was connected. The water reservoir was pressurized with nitrogen and using the timer, test runs of known duration were made, and the mass of water collected in the container during the test was determined. The mass flow rate of the water and the velocity of the water were calculated. This value was then compared to the velocity which theoretically would produce the required convective film coefficient. The system pressure drop was also measured and was subtracted from the pressure drop across the half-frame cooling path to yield the "half-frame cooling loop pressure drop." Using clamps to connect the lines to each path and a consistent sequence of operations, the water flow tests for each half-frame were completed and used to verify the cooling water requirement predictions for the channel.

Insulator Ceramic Emplacement. Following a thorough cleaning, drying and reinspection of the frames/mandrel assembly, the steel trunnions were attached to the mandrel end plates and the assembly was mounted in the winding

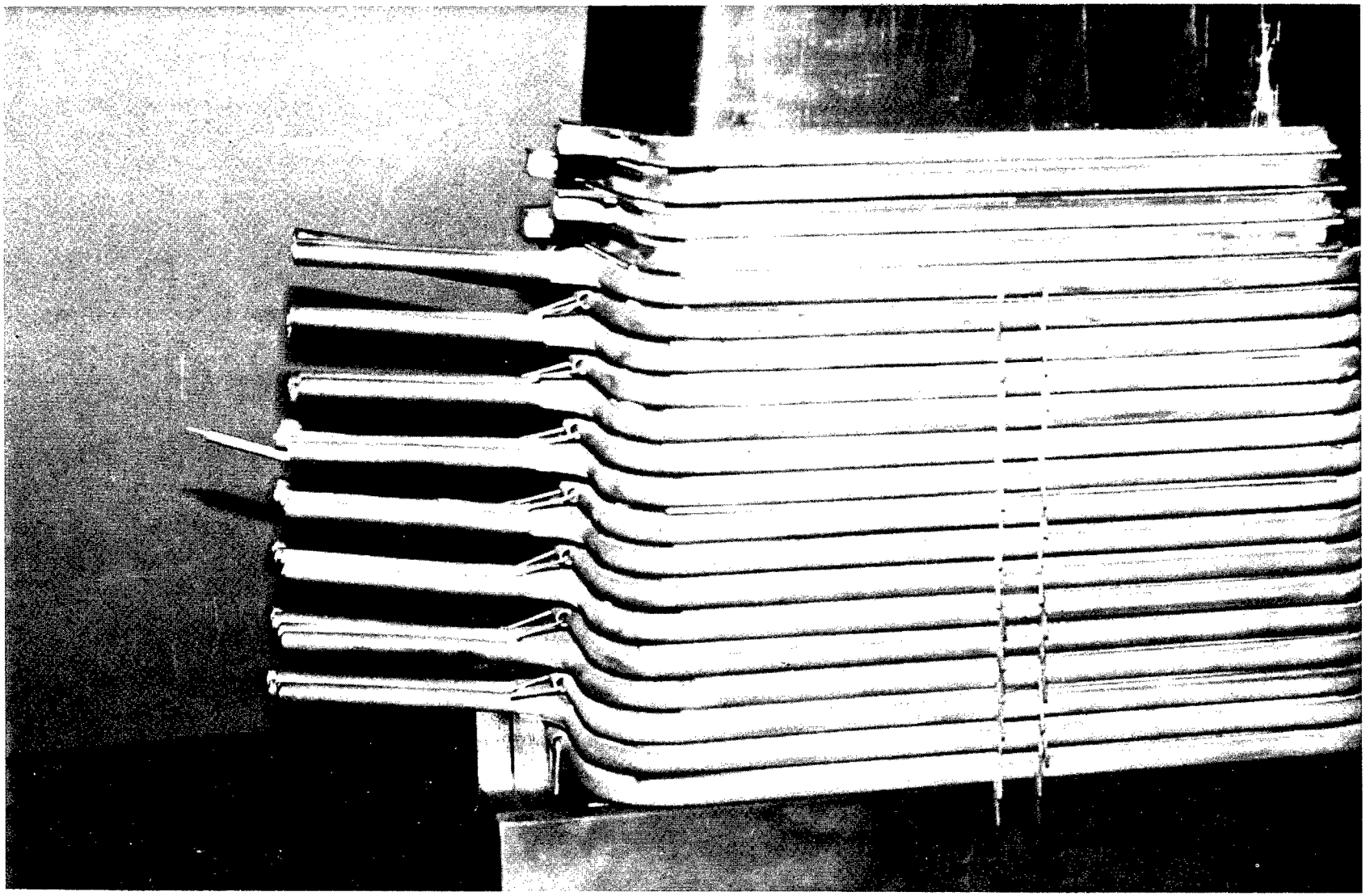

Figure 164. Partial Electrode Frame Assembly on Mandrel.

fixture. The alumina based insulator ceramic provided the electrical insulation between the adjacent frames of the channel. Ideally, the interframe gaps were filled from the mandrel surface to at least the top of the frame rails. This was done most effectively with the mandrel/frames assembly positioned horizontally in the winding fixture and oven assembly as shown in Figure 165.

The formulation and batch size selected for the insulator ceramic was: (1) 75 g of alumina powder; (2) 5.3 ml of water glass (calcium silicate); and (3) 10.6 ml of distilled water. Following the mixing of the water glass and water in a small graduated cylinder, the required mass of alumina was obtained and placed in a mixing container. Next, the binder liquid was added, and the mixture stirred into a uniform ceramic mixture with a small flat metal spatula.

Because of the wires and shims used to position and constrain the frames on the mandrel, the emplacement of the insulator ceramic was a multistep process. Working on the top side of the assembled channel, the accessible gaps were filled with ceramic using spatulas and air dried for about 20 min before rotating the channel and proceeding to the next side. Next,the assembly was baked for two hours at 330-355 K. After allowing the frames to cool, the shims and wires were removed, and the ceramic emplacement continued. Following a second bake and cool-down cycle, the gaps between the corners of the frames were filled, one at a time, with the corner being filled when it was positioned on the top. After the third bake/cool-down, the final repairs and touchups were made. A fourth bake completed the emplacement. Figure 166 shows the emplacement operation in progress. The fine nature and low viscosity of the insulator ceramic mixture precluded the need for vibratory de-aeration. Periodic rodding and tamping with the metal tools resulted in a dense, smooth ceramic.

The next step was to apply clear, non-self leveling room temperature vulcanizing (RTV) silicone rubber to all anchor brackets to position the anchor clips in a plane perpendicular to the hot gas surfaces. This placed the clips out of the way of future tasks. A half-hour was allowed for each side to set before rotating the mandrel. Finally, the mandrel and frames were baked in the oven for four hours at 355 K.

After the mandrel had cooled, the ceramic fill was resumed. Working again on one side at a time and then one corner at a time, all of the shims were removed, the gaps measured and recorded, and the alumina emplaced in the remaining gaps. Again, about 15-20 minutes was allowed before the mandrel was rotated. The assembly was again baked for four hours at 355 K. Figure 167 shows the diagnostics channel with all of the insulator ceramic emplaced.

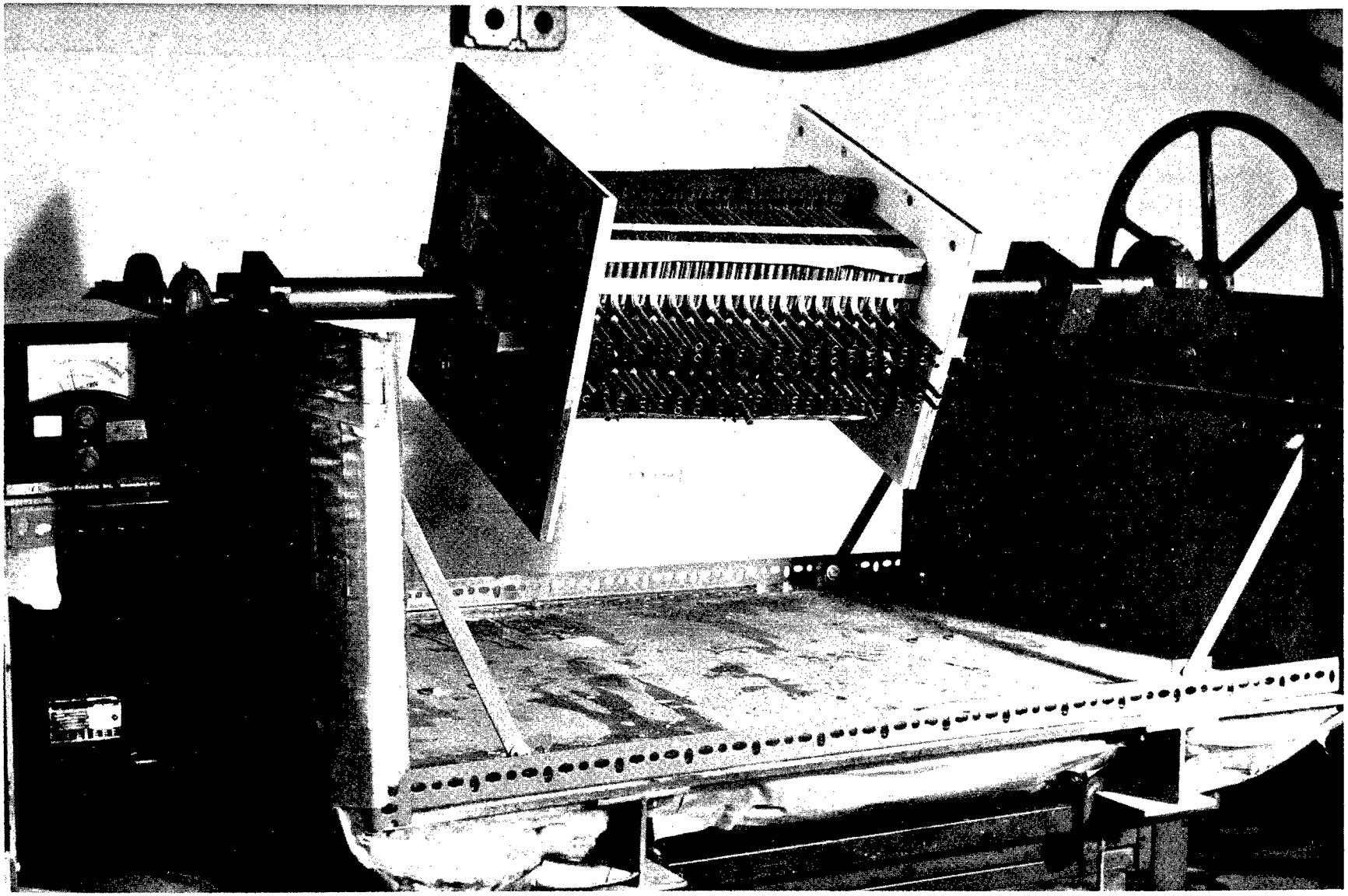

Figure 165. Diagnostics Channel Mounted in Winding Fixture.

Figure 166. Insulator Ceramic Emplacement.

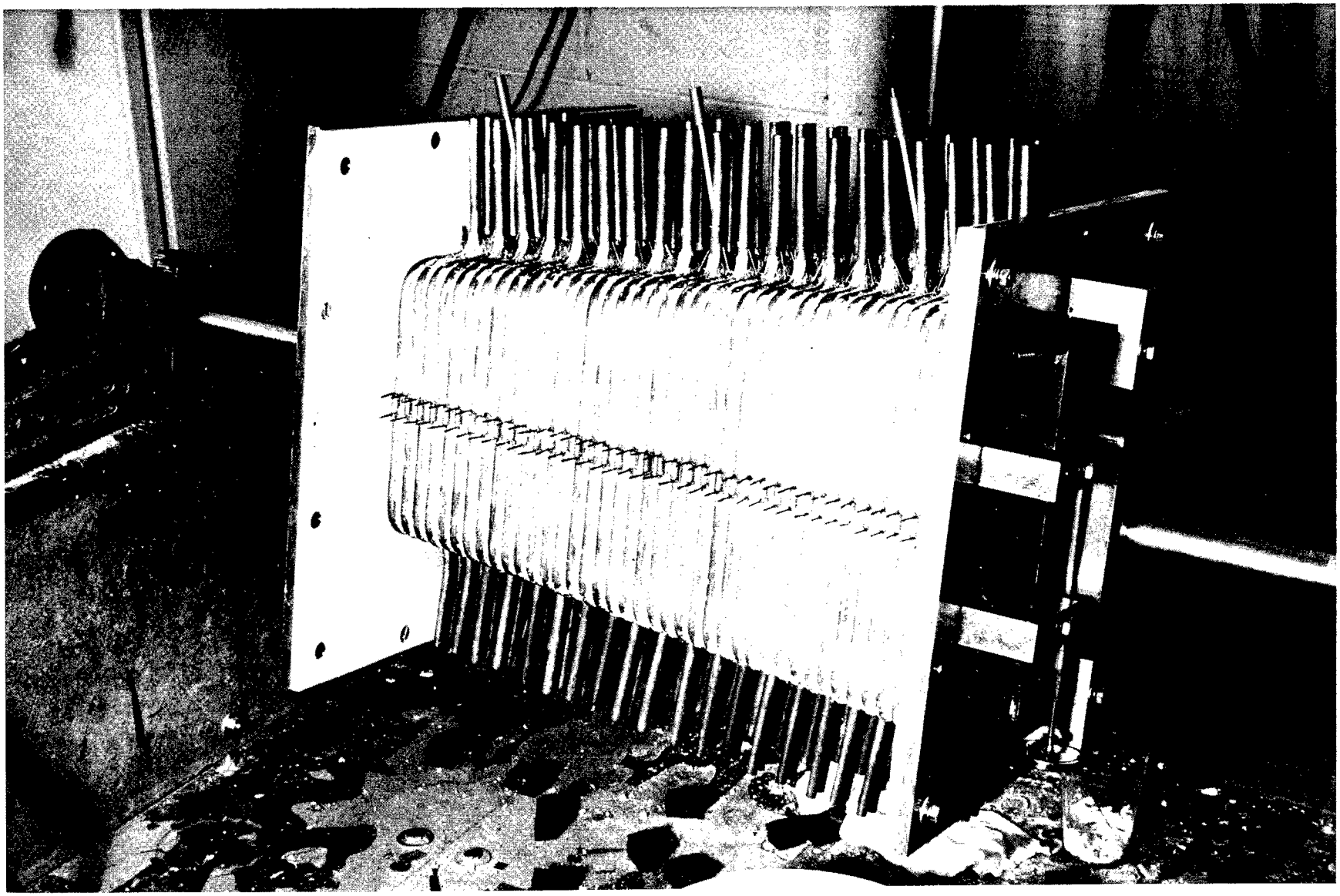

Figure 167. Completed Insulator Ceramic Emplacement.

Tube End Seals and the RTV Hot Gas Barrier. In order to prevent epoxy resin from entering the cooling tubes during the case winding, temporary tube end seals were fabricated and installed. These seals consisted of lengths of 7.8 o.d. x 1.5 mm wall silicone rubber tubing. Into one end of each piece of tubing a threaded plastic plug and a rubber slug were inserted. Mold release was applied to the entire assembly. The seals were then slipped over the end of all of the 160 cooling tubes. Similar but smaller seals were placed on each of the six pressure tap tubes.

At this time the three electrode frame temperature thermocouples were installed at frames #1, #20, and #30. For each thermocouple a 0.6 mm diameter hole was drilled at a 45 deg angle into each right side rail approximately 25 mm from the tube spacer block (towards the anchor) on the downstream face of the frame. The thermocouple was then inserted and the copper around the hole was staked. The wires were then carefully routed along the tubes and taped to the ends so that they did not interfere with future work.

The application of the RTV hot gas barrier was applied next. The mandrel was clamped so that the parallel sides were horizontal. White self-leveling RTV was applied manually to the spaces between the cooling tubes to a height of one-half the tube diameter. Heat lamps were used to semi-cure the RTV for four hours or until the RTV did not sag when the mandrel was rotated 45 deg in either direction. Next, the mandrel was rotated 180 deg to the other parallel side and the RTV application and semi-cure repeated. Then the mandrel was rotated 90 deg to a tapered side, and adjusted to provide a horizontal work surface. RTV was then applied to the tapered sides in the same manner as it was applied to the parallel sides.

Next, the second and final RTV fill was initiated. Enough rubber was applied to just cover the anchor brackets. The last step was to fill the corners with RTV. Corners were done one at a time, with a four hour semi-cure in between. Finally, the areas requiring touch-up were repaired as required. Excess RTV around the cooling tubes was cut away. A complete room temperature cure was then initiated. (See Figure 168.)

d. Case Fabrication

Interface Layer. The fabrication of the glass-epoxy "shell" or case began with the so called interface layer - i.e., a layer of cloth that bonded the case to the hot gas barrier.

Since one of the materials that easily bonded to cured RTV was uncured RTV, a single layer of 225 g fiberglass cloth was "semi-soaked" with RTV and applied to the hot gas barrier of the channel and cured for 24 hours. The

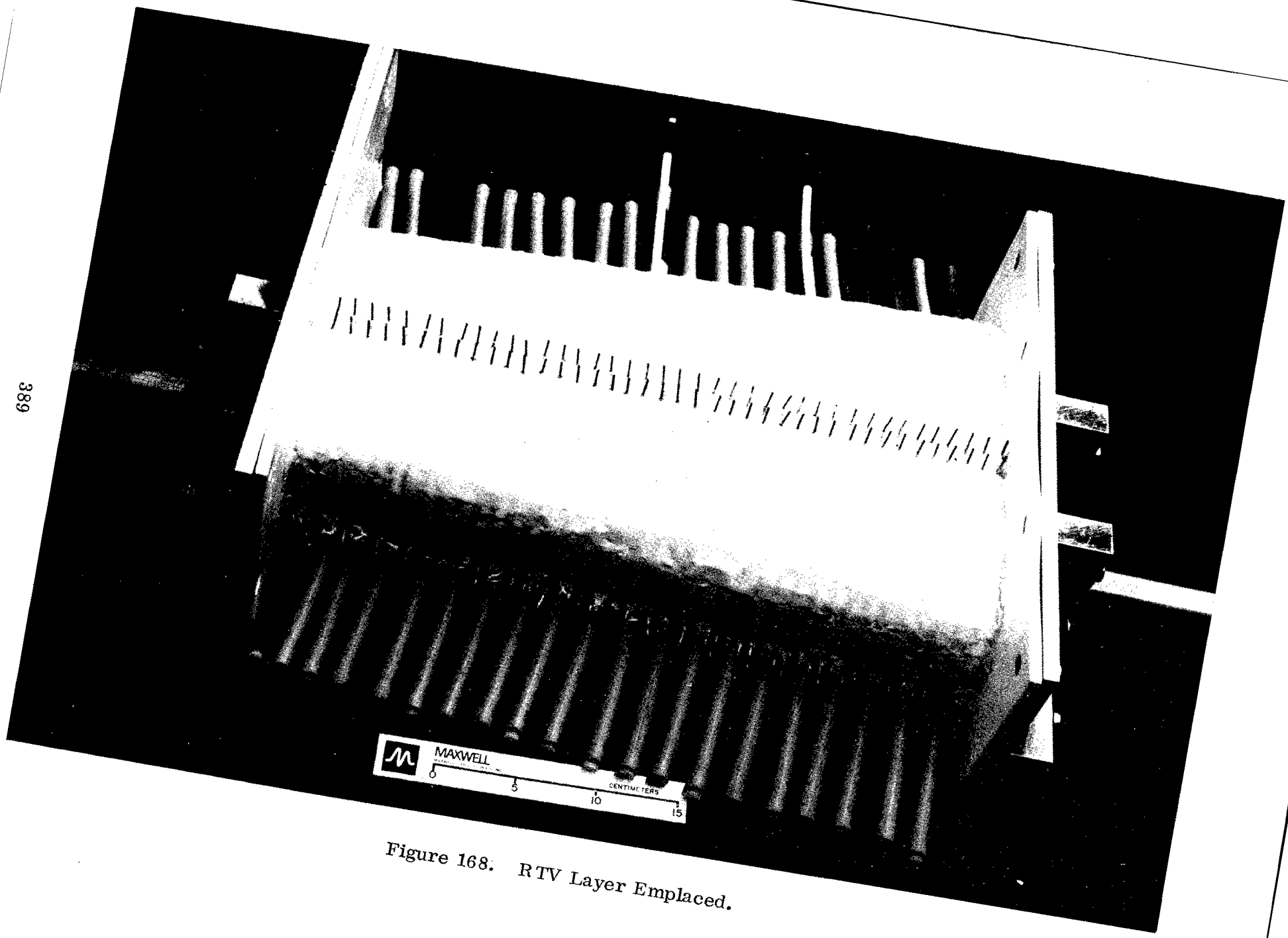

Figure 168. RTV Layer Emplaced.

principle utilized in this approach was that when the epoxy was applied to the dry portion of the cloth, a good bond would exist between the case and RTV with the cloth acting as an "interface."

Case Winding. Next, the task of winding the channel case was begun. Three forms of fiberglass were used: roving, woven roving, and cloth. The roving provided most of the case strength, the woven roving provided bulk to hasten case buildup, and the cloth was used as the interface layer and also for cosmetic purposes. The epoxy system consisted of a basic resin (100 parts by mass), an acid curing agent (100 parts by mass), and an acid curing accelerator (2 parts by mass). The epoxy was mixed and loaded into the dispenser mechanism. The roving was fed manually from the spool through the dispenser as shown by Figure 169. A manual foot switch controlled the rotation of the mandrel. During the winding process the case buildup was closely observed and air bubbles or entanglements were eliminated.

Table 54 summarizes the pattern used for building the case. (Note: Layer refers to a complete covering of the channel with glass in any form; course refers to roving strands wound along prescribed paths; 0 deg to 45 deg indicates the angle between the wound-on roving hank and the vertical plane; and serpentine refers to the routing of the roving in an "S" shaped pattern around adjacent tubes.) Figures 170 & 171 show the case winding process in various stages of completion.

Throughout the winding process, air bubbles in the epoxy were "pumped out" by periodically rolling the glass epoxy matrix with special serrated rollers. These tools were basic to the fiberglass/epoxy process and were the prime reason for the void-free case. The case thicknesses were recorded during the fabrication process. At the conclusion of the winding process, the following average case thicknesses were measured:

	Corners	Sides	Top and Bottom
Inlet End	41 mm	89 mm	59 mm
Outlet End	19 mm	38 mm	38 mm

Case Cure. To complete the case fabrication, the case was cured in the oven with the mandrel rotating constantly at approximately 7 rpm. The total cure time including warmup was 20 hours at 375 K. The temperatures were monitored throughout this period. Following the cure, the oven was opened and the channel allowed to cool to room temperature. The channel at this stage of fabrication is shown in Figure 172.

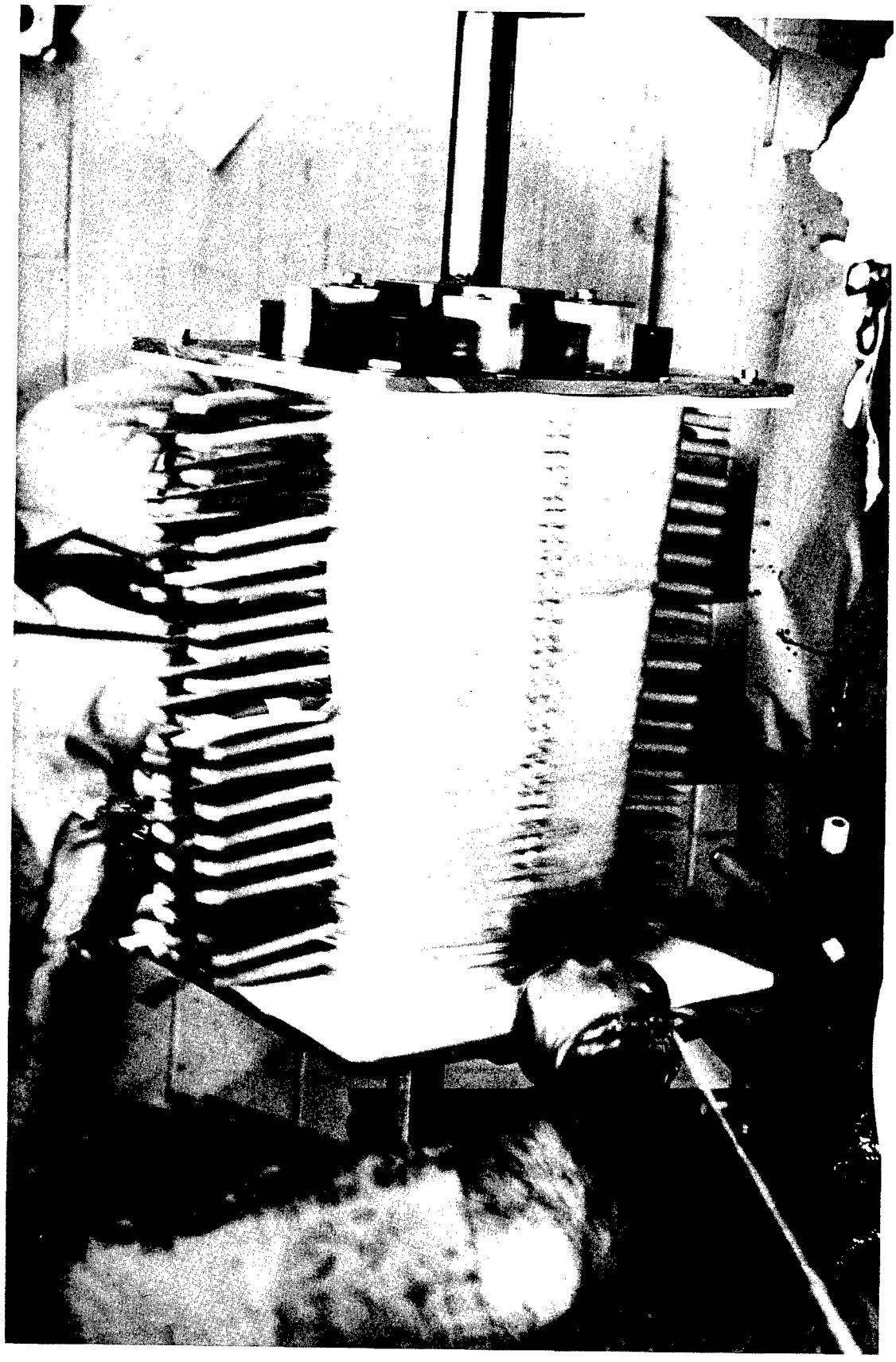

Figure 169. Filament Winding Operation.

TABLE 54. FABRICATION STEPS FOR CASE WINDING

1. Brushed on epoxy to remainder of dry cloth on the interface layer.
2. Starting at exit end, one course was wound to the inlet end. The roving was wound quite heavily on the inlet end to initiate the "cuff" buildup.
3. One layer, 0 deg, cloth.
4. One course (inlet to exit) of roving (3 hanks).
5. One layer, 0 deg, woven roving; measure case thickness; and repeat (2).
6. One layer, 0 deg, woven roving; and repeat (4).
7. One layer, 45 deg, cloth; and repeat (2).
8. One layer, 0 deg, cloth; and measure case thickness.
9. Roving, inlet end, frames #1 through #5, inlet towards outlet to inlet.
10. Same as (9), but frames #1 through #4.
11. Same as (9), but frames #1 through #3.
12. Same as (9), but frames #1 and #2.
13. Same as (9), but frame #1.
14. Three-inch wide cloth, 0 deg, frames #1 through #6; and repeat (9) through (14).
15. Roving, inlet to outlet.
16. One layer, 0 deg, cloth.
17. Built up area from frame #5 to #10 with roving.
18. One layer, 0 deg, matte; repeat (2); and measure case thickness.
19. Built up cuff with layer of matte, then layer of roving.
20. One layer, 0 deg, cloth; repeat (2) and (4); and measure case thickness.

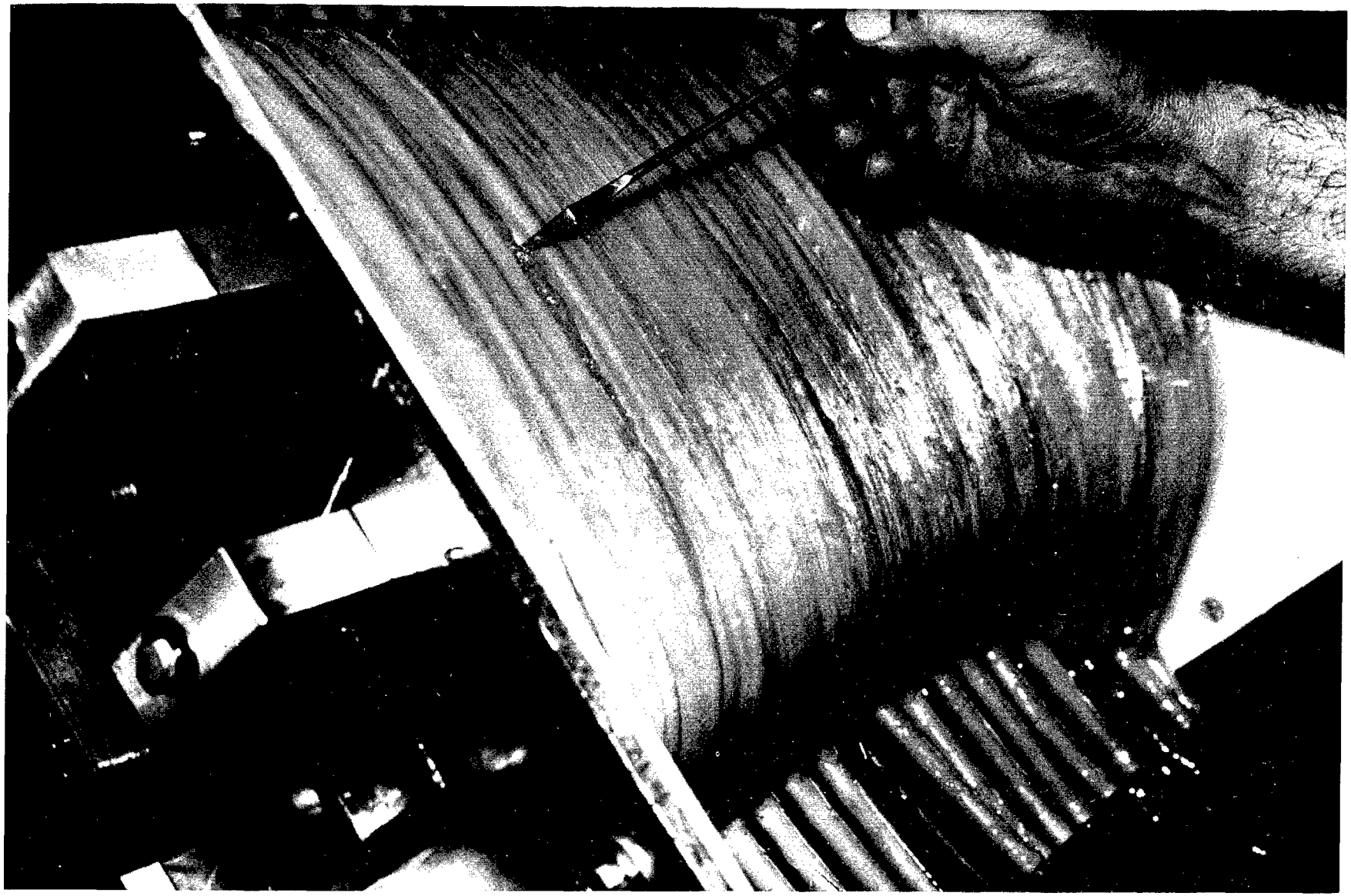

Figure 170. Partial Fiberglass Case Winding.

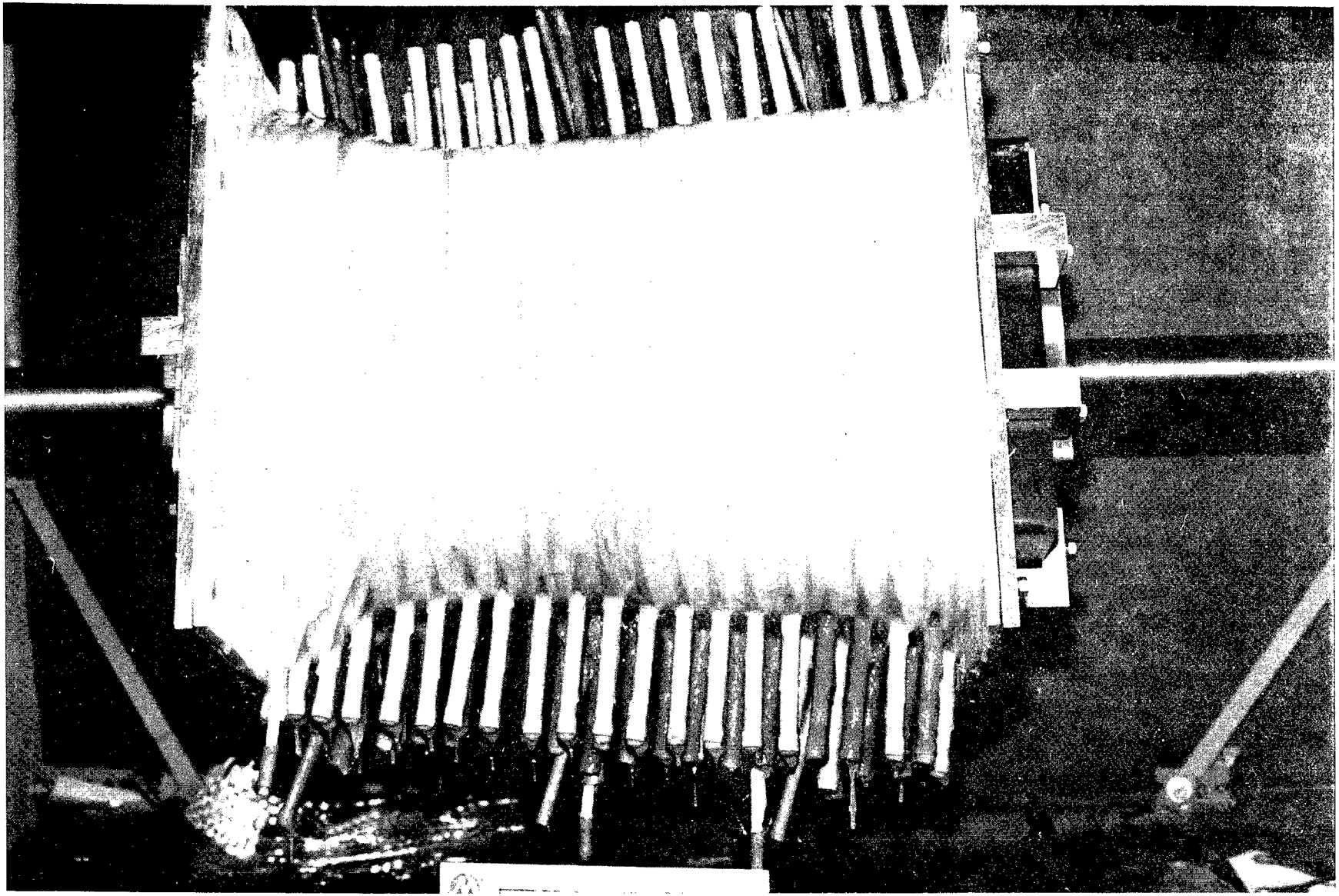

Figure 171. Partial Fiberglass Case Winding.

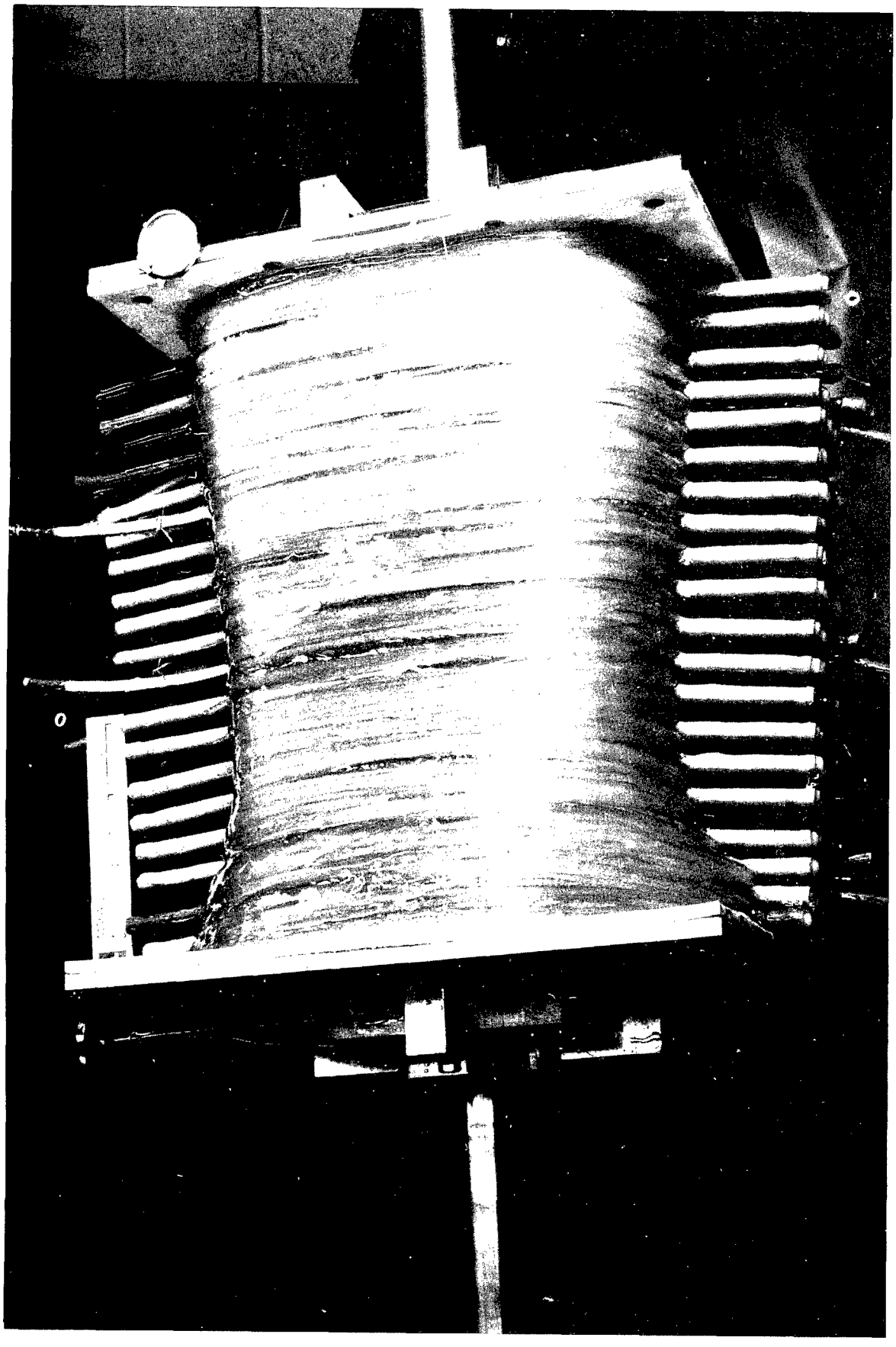

Figure 172. Completed Case Winding.

e. Finishing Operations

Initial Finishing Operations. After the case had cooled completely, several operations were performed prior to the machining of the case. All of the temporary tube end seals were removed as shown in Figure 173. After removing both of the winding flanges, all excess epoxy "flashing" was removed from around the tube cavities and both ends of the channel.

The channel/mandrel assembly was installed in a sandblasting chamber, and using a mini-sandblaster, each tube cavity was thoroughly abraded. This operation promoted a good bond between the case and the soon to be added RTV. Following a thorough cleaning, the assembly was reinstalled in the winding fixture with the cooling tube ends positioned vertically.

White, self-leveling RTV was cast into the cavities, one side at a time, to form a continuation of the hot gas barrier. At the same time minor blemishes and voids were repaired using an epoxy compatible with the one used in building the case. Both the RTV and epoxy were allowed to cure thoroughly.

Case Machining. The case machining work consisted primarily of: (1) facing off the inlet end of the channel; (b) milling the "O" ring groove in the inlet face; (3) drilling the eight bolt holes in the "cuff" of the channel; (4) drilling and boring the three alignment pin holes; (5) milling bolt head clearance cavities in the cuff; (6) drilling of heli-coil pilot holes in the exhaust face of the channel for the mounting of the heat shield; (7) fabrication of three alignment pins; and (8) attaching the cooling tube loops to the proper frame tubes.

During this machining the cooling tube for frame #1 was partially penetrated by a milling cutter in two places. While the penetration did not break through the tube, decreased cooling tube wall strength was a concern. Small copper slugs were fabricated and soldered to the tube over the damaged areas. Finally, the slug was encased in fast setting epoxy to increase the section modulus of the tube at the penetration points. The success of the repair was proven when the entire cooling system was pressurized. During this pressurization, a dial indicator was placed on the repair and no deflection occurred.

Mandrel Removal. Following the return of the channel from the machine shop, the machined areas were carefully inspected and photographed. The removal of the mandrel was the next step.

This task proved to be extremely difficult and was the most serious problem encountered during the channel fabrication. Initially, the mandrel end caps were easily removed. After one of the "constant width" mandrel sides had been moved inward away from the frames, an attempt was then made to tap out that side.

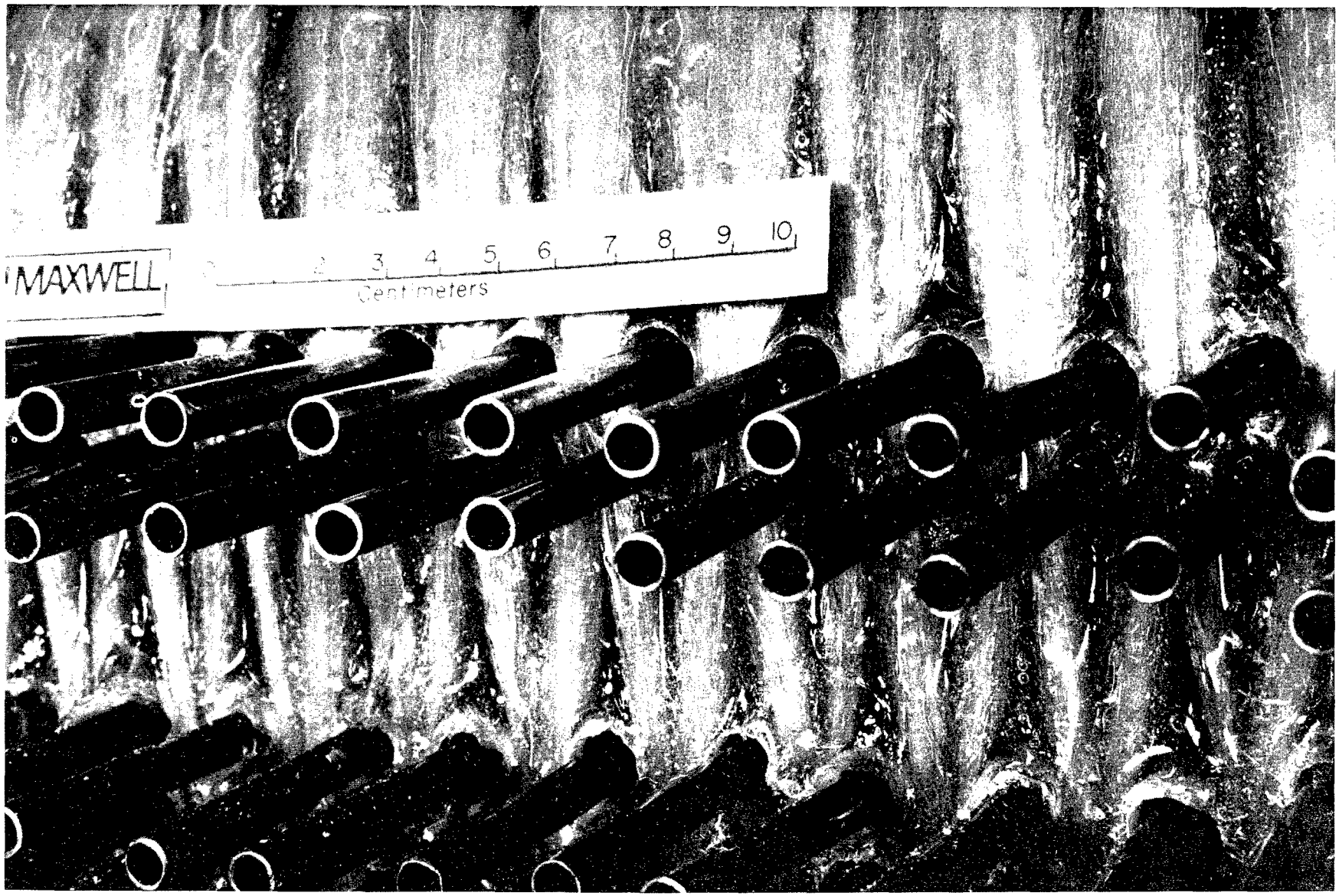

Figure 173. Removal of Tube End Seals.

However, the side would not move, and increased hammering only galled the aluminum. A relief on the tapered sides had been omitted. In addition, the "tapered sides" should have been sandwiched between the "constant width" sides rather than vice versa. To aid in the mandrel removal, dry ice was used to cool the mandrel section which was being removed. Although the section still had to be hammered out, the dry ice process worked. The frames were not damaged because the motion was between adjacent mandrel sides and not between the side and the frames. The second constant width side was more difficult to remove. Following several hours of chilling, this section still would not move, and galling became a problem. Finally, spreader bolts were used to gently expand the tapered side pieces, and after continued hammering, the section came out. The tapered sides were then easily removed. There was no apparent damage sustained during the mandrel removal process. Some voids were apparent in the ceramic. These were readily repaired. During the initial inspection, the alumina appeared very weak and brittle, easily scraped with a knife. Subsequent application of heat via heat lamps hardened the alumina. Apparently, while the outside of the ceramic had hardened, the unexposed surface against the mandrel had not.

Electrode Ceramic Emplacement. The zirconia based electrode ceramic served as a current conductor at high temperatures in the channel. This ceramic was emplaced between the copper fins and Inconel screens on all four sides of each frame. Ideally, the ceramic must also fill the screen interstices, providing mechanical strength and efficient heat transfer.

With the mandrel removed close inspection of the interior surface was made. This inspection showed that frame grooves required a thorough cleaning. Remnants of flux, stop-off, copper cleaner, etc., were clearly visible. Accordingly, all frame grooves and screens were sandblasted as shown in Figure 174. The alumina had hardened enough to tolerate the highly pressurized sand. This operation required more time than expected because of the small diameter of the sand stream and care required in abrading the copper. Some alumina was inadvertently sandblasted out, but repairs were easily made. Even though access to the frame grooves was better than anticipated, the total time to perform this task was much greater than expected.

The emplacement of the zirconia ceramic was the next operation. The following mixture was used: (1) 37 g of zirconia ceramic; (2) 6.5 g of zirconium diboride; and (3) 7.5 ml of zirconia bonding liquid.

The first two components were thoroughly dry mixed and then the liquid was slowly added. The solution was mixed until a mixture consistent in color and texture resulted. Modified plastic syringes were used to implant the ceramic into all the frame grooves. Entrapped air bubbles were eliminated by "rodding"

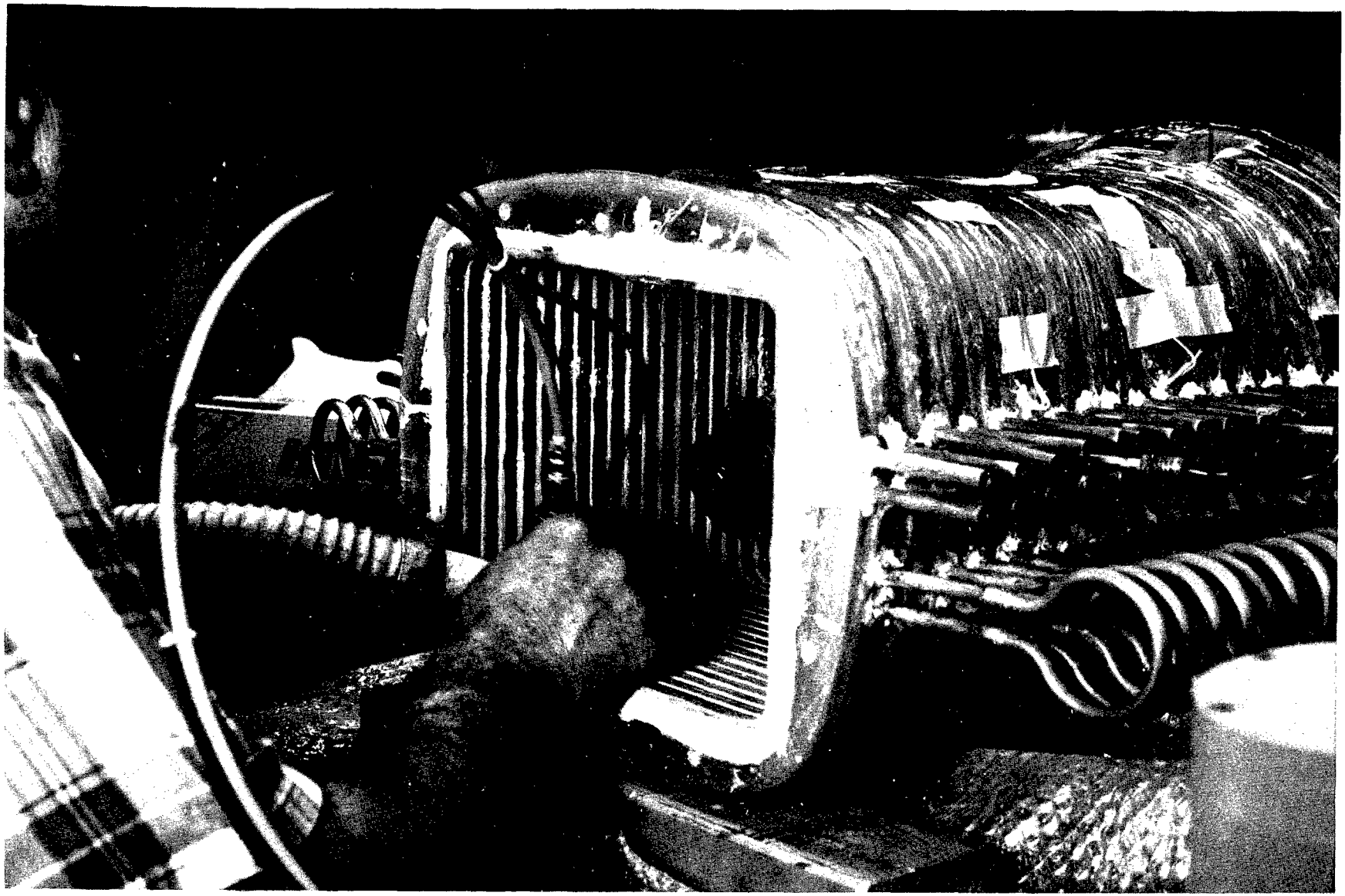

Figure 174. Electrode Frame Cleaning.

the zirconia with small metal spatulas. Figure 175 shows the ceramic emplacement in progress. To allow for shrinkage upon curing, the grooves were overfilled by about 0.4 to 0.8 mm with ceramic. All tools were cleaned in warm water after each fill. Each side of the channel was allowed to air dry 20 min before rotating the channel to the next side to be filled. A 0.6 mm diameter length of piano wire was placed inside each pressure tap to keep the holes free from ceramic. Finally, the ceramic was baked by placing the channel into a large floor oven in the vertical position for four hours at 360 K.

Final Finishing Operation. Once cooled, the channel was removed from the oven and carefully mounted horizontally. There were several high spots of zirconia which were removed to expose the copper fins and Inconel screens. Voids in both ceramics were readily repaired. The problem of voids, as shown in Figure 176, was far more pronounced in the alumina than the zirconia. Substantial effort was expended to patch, cure, and sand the ceramic. All ceramic powder was then removed. After this finishing operation, the final surface was quite smooth and void-free. The pressure tap holes were continually checked for obstructions.

Using a hand-held power grinder, a circular flat section approximately 25 mm in diameter was ground into the case exterior near frames #20 and #38, at the middle of the top and right sides. These flat sections were the locations of the piezoelectric accelerometers.

Next, the three alignment pins were installed. These were used to precisely align the inlet face of the channel with the exhaust face of the combustor nozzle. As previously mentioned, the holes for the pins were located using the interface plate. The channel was set in a vertical position resting on the outlet face. Using the interface plate as a guide, the pins were installed in the holes with quick setting epoxy. The epoxy was cured overnight at room temperature. The plate was carefully removed and the pins rechecked.

Heli-coil inserts were installed in the previously drilled pilot holes in the exit face of the channel for the purpose of mounting the Transite end shield. The end shield was then mounted to the channel, using non-self-leveling RTV as an in-place gasket. Three "dummy" pressure transducers for the three unused pressure taps and copper current taps were fabricated and installed. Three thermocouples were installed in one of the case corners at frames #3, #20, and #30. A small hole was drilled half way into the case and the thermocouple installed with quick setting epoxy. The sheathed leads were labeled and carefully taped to the case.

Figure 175. Electrode Ceramic Emplacement in Progress.

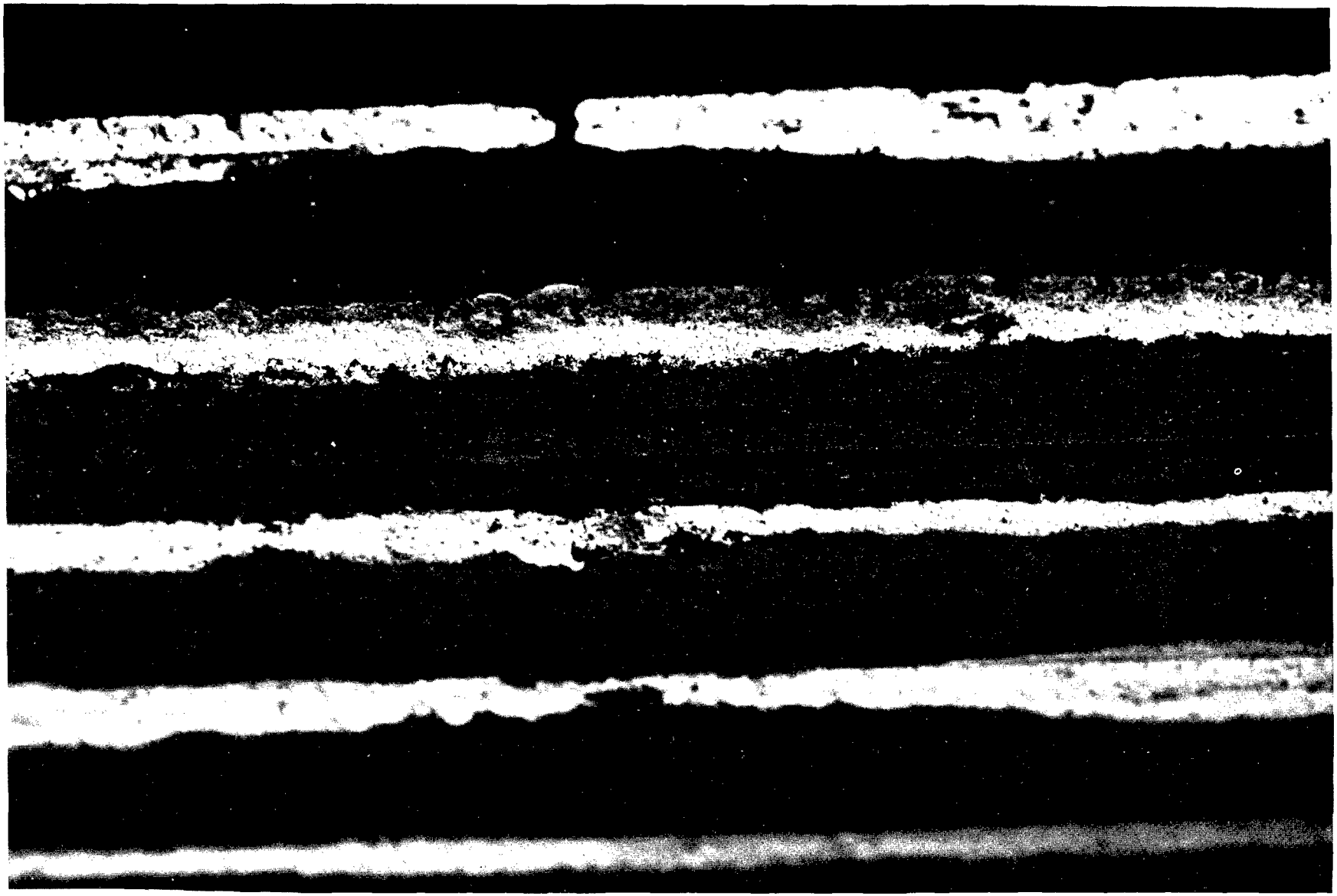

Figure 176. Ceramic Void Region.

f. Cooling System Fabrication

Manifolds. The inlet and outlet manifolds were fabricated from 125 mm diameter Schedule 40 steel pipe. On one end of each pipe, an end cap was welded in place. A 90 deg elbow and mounting flanges were welded on the other end. Sixty holes were drilled and tapped in each manifold to accommodate the cooling tube fittings. A drain valve was added to the bottom of the end cap in the inlet manifold. A support strap was added to the inlet manifold and provided a means of lifting the entire channel/manifold assembly at installation. Finally, both manifolds were primed with zinc chromate.

Cooling Tubes and Fittings. A very rugged flexible tubing with a polyamide core, a glass braid liner, and polyurethane jacket was used to connect the manifolds to the channel. The tubing required special barbed fittings with threaded ends for the manifolds and sweat-type ends for the frame cooling tubes. The interconnections between the frame "half-loops" in series were made by fabricating copper tube loops. These were soldered to the appropriate tubes at the same time the case was being machined.

Cooling Tubes Attachment. The cooling system for the diagnostics channel required careful design and production planning before being fabricated. The interconnection scheme and the soldering technique were the two areas of prime concern. Because of the high density of cooling tubes, fittings, and frame tube ends, the interconnection scheme, the soldering technique and the sequence of operations were extremely important. The cooling tube interconnection scheme with all inlets, outlets, elbows, loops, and transducers was determined for each frame. All flexible cooling tubes were precut, and sweat fittings were pretinned. Then, the polyamide core of the flexible tubing was expanded, the precut tubing was slipped over the barbed ends of the threaded and sweat type fittings, and the fittings were rotated to their approximate final orientation.

The fittings were then soldered to the frame tube ends. Asbestos sheets and moldable ceramic felt were used as heat shields along with a damp cloth to protect the flexible tubing and channel case from the soldering torch flame. This procedure provided adequate shielding of neighboring tubes and did not deform the polyamide inner core.

All flexible tube assemblies for both manifolds were installed. Six street "tees", used to mount the sheathed thermocouples which measure the outlet water temperature, were installed on the outlet manifold, positioned between the barbed fitting and the tapped hole in the manifold.

When the diagnostics channel finishing operations were completed, the channel was mounted with the manifolds on a wooden shipping cradle in a vertical position as shown in Figure 177. The cooling tubes from the manifolds were temporarily installed on the channel according to the predetermined scheme. Some changes were made in the tube lengths, elbow and straight fittings, etc. The actual tubing attachment, using a leak-proof solder joint, was next. After incorporating these hardware modifications the soldering operation began on the left side of the channel at the exit end and proceeded towards the inlet end, in a criss-cross fashion. Each joint was visually inspected for integrity and the routing of the tubes was inspected for neatness. At this time, a current tap was soldered to the tube end of each of the thirteen selected electrode frames. The completed channel is shown in Figure 178.

g. Final Tests and Measurements

Channel Vacuum Test. A vacuum test was performed on the diagnostics channel to check for internal leaks. Aluminum plates and RTV were used to seal off the ends of the channel. A clay-like molding compound was used to seal off the pressure taps. The pressure was cycled between near zero and atmospheric several times in order to seat the gaskets and seals. Then the pressure reduced to fifteen Torr, and the valve between the pump and channel was closed. The pressure held at fifteen Torr with no leaks present. The channel was determined to be free of leaks.

Channel Mass. The channel mass was measured just after the Transite heat shield was mounted but before the flexible tubes were attached. The mass was 63.2 kg.

Measurement of Channel Bore. Following the repair and touch up of the electrode ceramics, the height and width of the channel interior were measured at several points and compared to the nominal bore dimensions. The left and right sides of the channel were bowed outward slightly. One possible explanation of this phenomenon is that the frames expanded during the epoxy curing cycle. Upon cooling after gelation, all frames tried to return to their original position. The left and right sides, however, could not since they were rigidly "tied" to the case via the cooling tube ends. The top and bottom sides were not held rigidly in this manner.

To remedy the situation, additional alumina ceramic was applied in an attempt to build up these sides in the middle. The material was then cured and sanded to the correct level. The interface plate was reinstalled and used to gauge the build-up at frame #1. Finally, the interior dimensions at frame #1, #20, and #40 were obtained and recorded.

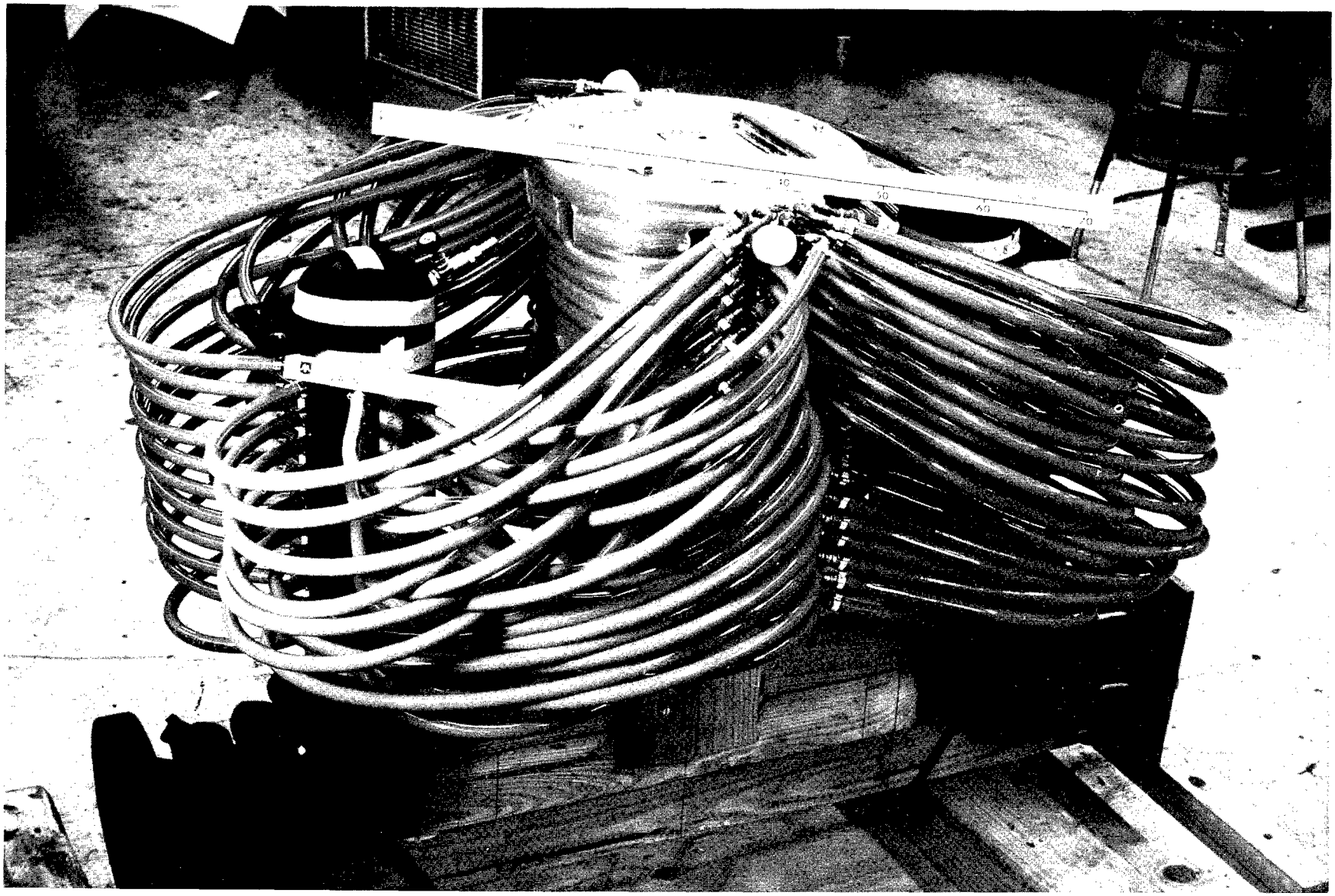

Figure 177. Diagnostics Channel/Manifold Assembly.

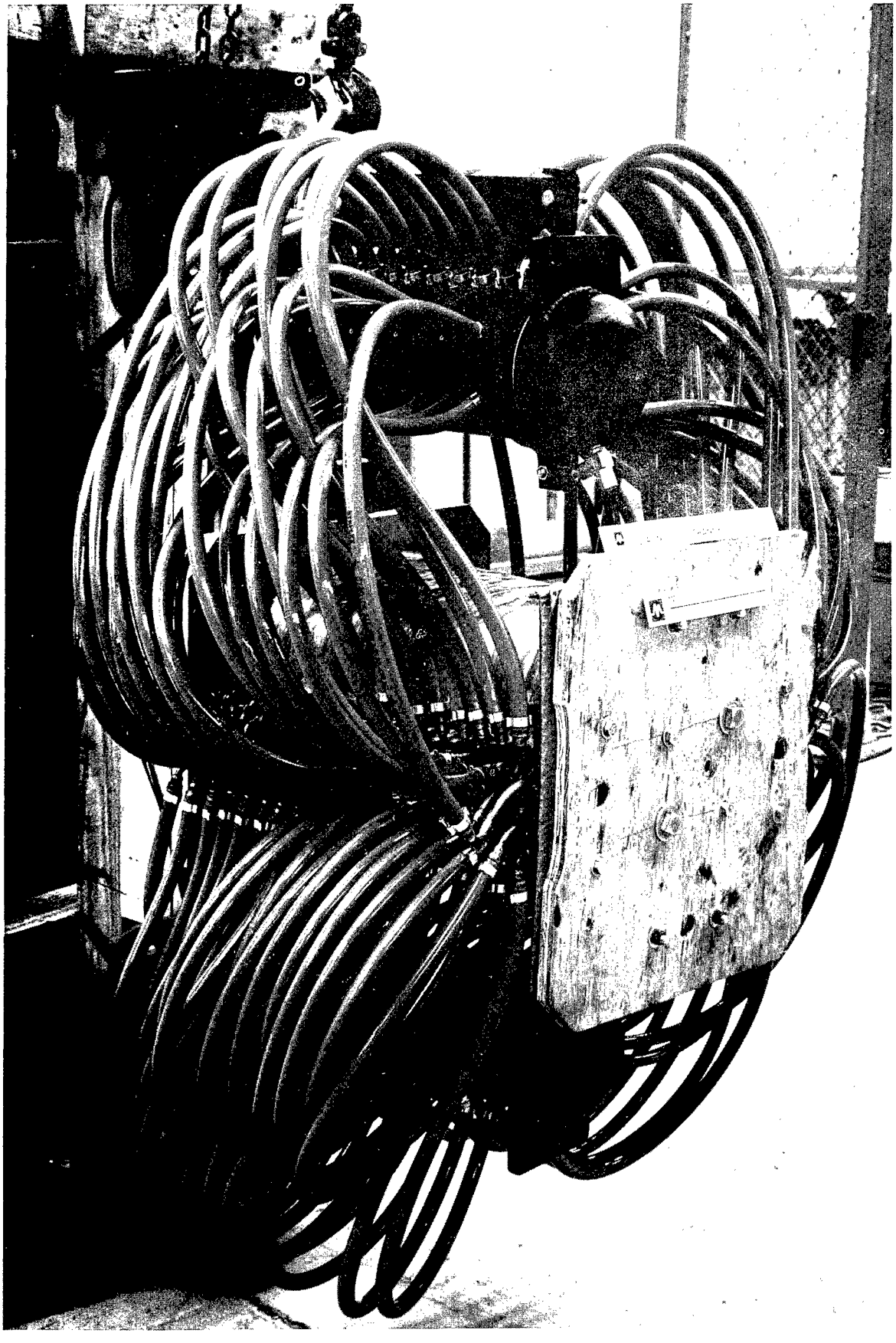

Figure 178. Completed Diagnostics Channel.

Cooling System Pressurization Test. The final and the most important test performed upon the channel/manifolds assembly was the pressurization of the entire cooling system. To conduct this test, aluminum plates and gaskets were bolted to the mounting flanges on the manifolds to seal off the cooling system. A high pressure bottle of nitrogen was fitted with a regulator and attached to the drain valve on the outlet manifold. Any unused holes in the manifolds were blocked with pipe plugs.

The regulator was set at 4.4 atm, and the valve was slowly opened. Since there were no leaks, the pressure slowly increased. At 16 atm, several leaks became apparent. Using a soapy water technique to detect these leaks, seven were located - two bad solder joints and five loose fittings. The system was depressureized. These joints were readily repaired, and the fittings were retightened and the cooling system repressurized. After repairing one additional leak at 30 atm, the pressure was increased to 35 atm. After several minutes at this pressure and with no leaks, the system was determined to be leak-tight.

This completed the successful fabrication of the diagnostics channel. At this point, the assembly and the spare parts and tools kit were carefully crated and shipped to Rocketdyne for the test program at SSFL (see Section VIII).

C. HEAT SINK COMBUSTOR

A heat sink combustor was designed and fabricated for use in development testing. This type of combustor could be fabricated relatively rapidly. This combined with the ease of instrumentation and sturdy construction made the combustor ideal for use in the early development testing.

The requirements for the heat sink combustor were: (1) duplicate the interior geometry of the cooled wall combustor and nozzle; (2) match the diagnostic channel interface; (3) provide an operating time of 2 to 3 sec; (4) provide a cyclic life sufficient for the development testing (~40 cycles); (5) provide instrumentation for heat flux, combustion performance, and combustion stability evaluations; and (6) diagnostics channel/nozzle interface temperature less than 533 K.

1. Design

The heat sink combustor assembly is illustrated along with the injector, acoustic slot spacer, and the igniters in Figure 179. The heat sink combustor was fabricated from solid oxygen-free high-conductivity (OHFC) copper and was approximately 91.9 cm in length. The combustor consisted of four sections which were designated (proceeding from the injector end) as: combustor Section A, combustor Section B, adapter, and nozzle. Selection of the multiple-section

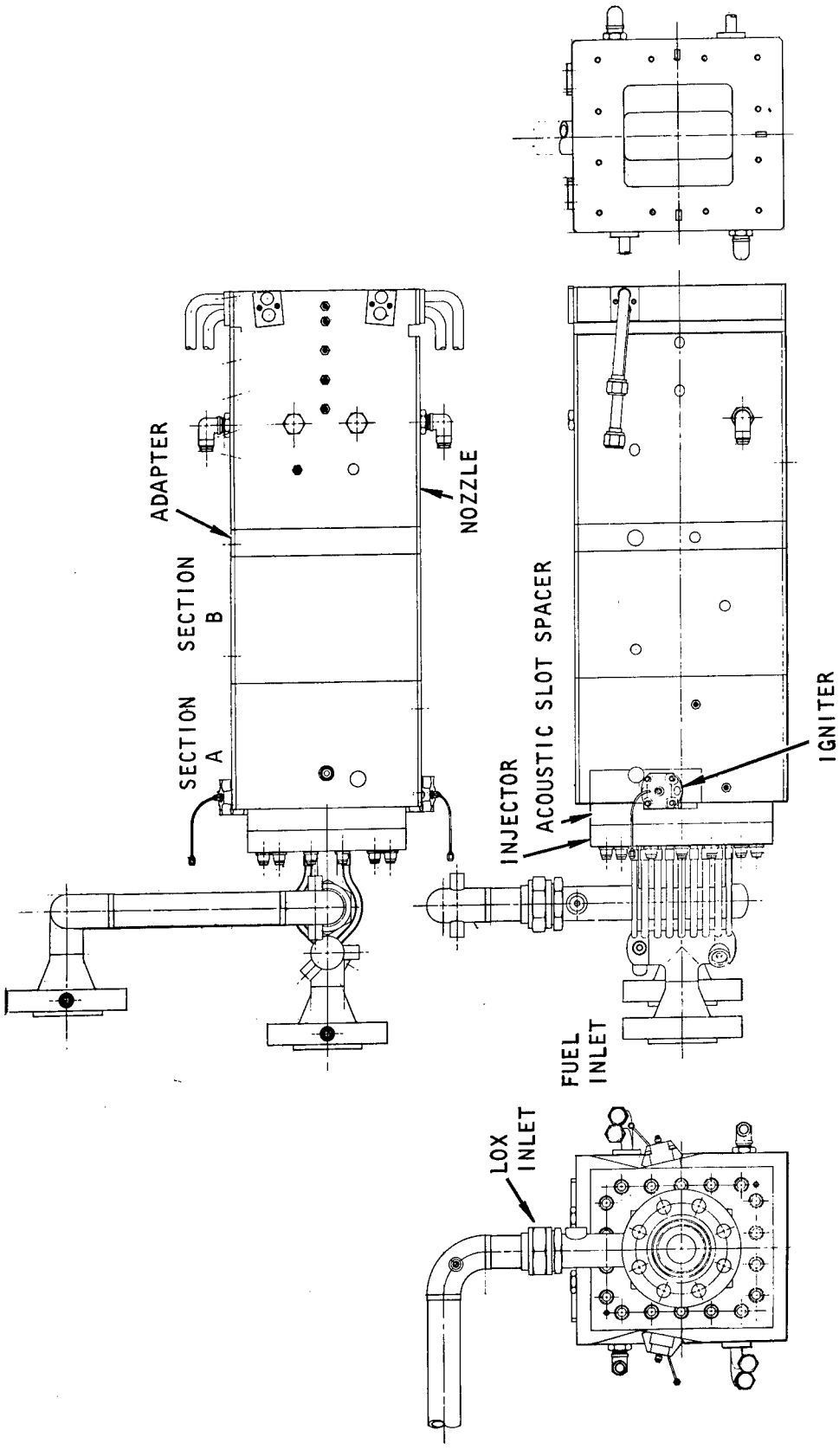

Figure 179 Heat Sink Combustor Assembly

design avoided the expense of large pieces of copper and provided the capability for varying combustor length. The sections were bolted together with eighteen stubs which were anchored in the nozzle section. The assembly formed a combustion section which was 68.6 cm long from injector to throat. Combustor Section B could be removed, resulting in a combustor length of 45.7 cm. The studs for the combustor were also used to secure the acoustic slot spacer and injector. The combustor was basically a heat sink type and could be operated only for 2 to 3 sec. The heat sink capability was augmented by water cooling in the throat and exit regions.

The combustor was structurally secured near the nozzle exit and supported along its entire length. This allowed the combustor to "grow" during operation without introducing loads into the channel. However, reactant manifold and valve mounting was designed to accommodate this growth. The combustor was mounted with the flat sides horizontal. This was identical to the arrangement that would be used in the power tests. Igniters were mounted on each vertical side, near the injector.

a. Component Description

The combustor design is illustrated in Figure 180. The internal geometry was designed to be identical to that of the cooled wall combustor. The nozzle section was 41.4 cm in length and 38.1 cm by 34.3cm in exterior cross section. Nozzle exit geometry was designed to match the entrance to the diagnostics channel. Twelve bolt holes were provided for attaching the diagnostics channel. Three slots were provided for locating pins. The seal for the interface was provided by the diagnostics channel The nozzle contour was identical to the cooled wall combustor described in Figure 77. The throat cross section was 8.48 cm by 19.7 cm, and the contraction region was 17.8 cm in length. This section mated with the adapter section. Alignment of the sections was assisted by the use of locating pins at each interface.

A slot was provided on the external surface near the exit. This slot matched a key on the support structure which secured the combustor under axial loads. The studs that held the combustor sections were secured in the nozzle section by the use of three helicoil inserts in each of the 18 holes.

The nozzle section was cooled at the throat and at the nozzle exit. The throat cooling was used to prevent material erosion under the high temperature gas. Two cooling passages were used at the exit to keep interface temperature below the maximum channel interface temperature of 533 K. Cooling passage geometry is illustrated in Figure 181. Deionized water was used as the coolant. Fittings for coolant line attachment were provided at the nozzle and exit.

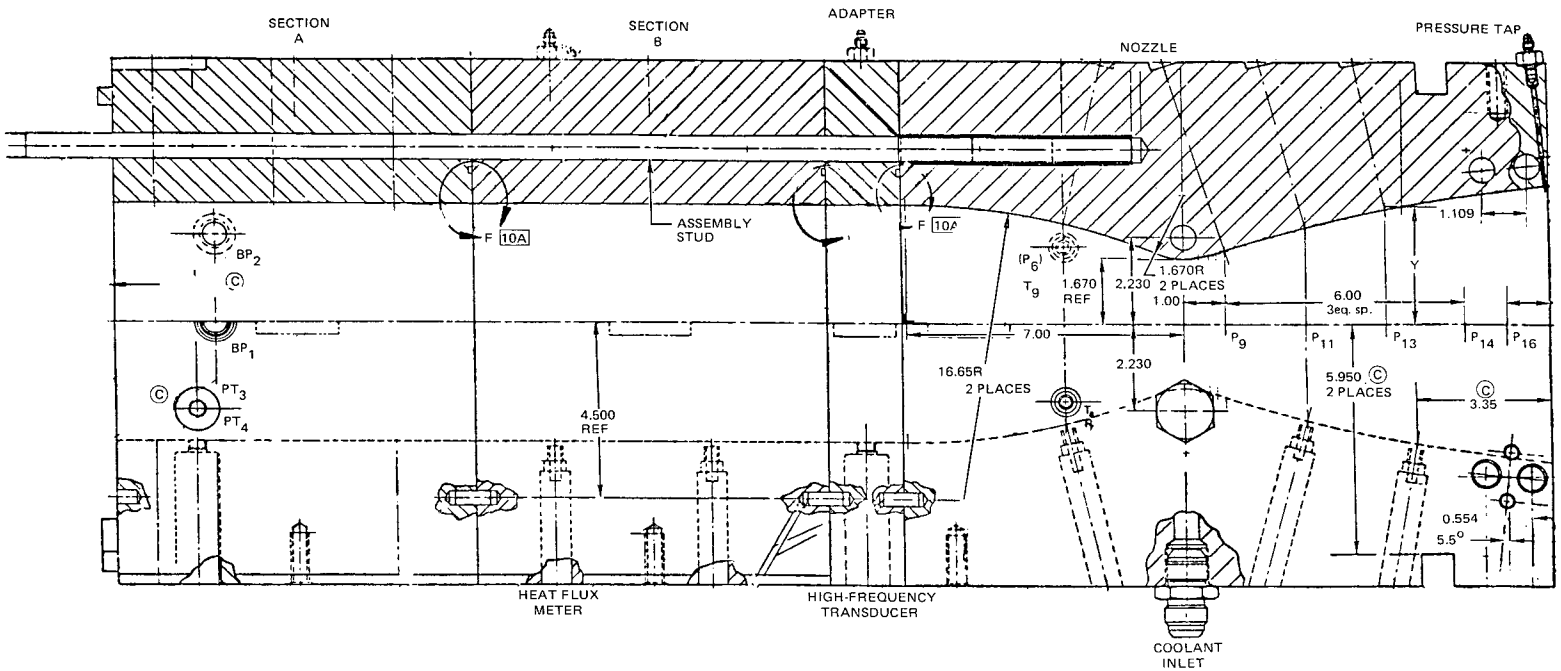

Figure 180. Heat Sink Combustor Sectioned

*This Is A Fabrication Drawing and Units are Not Metric

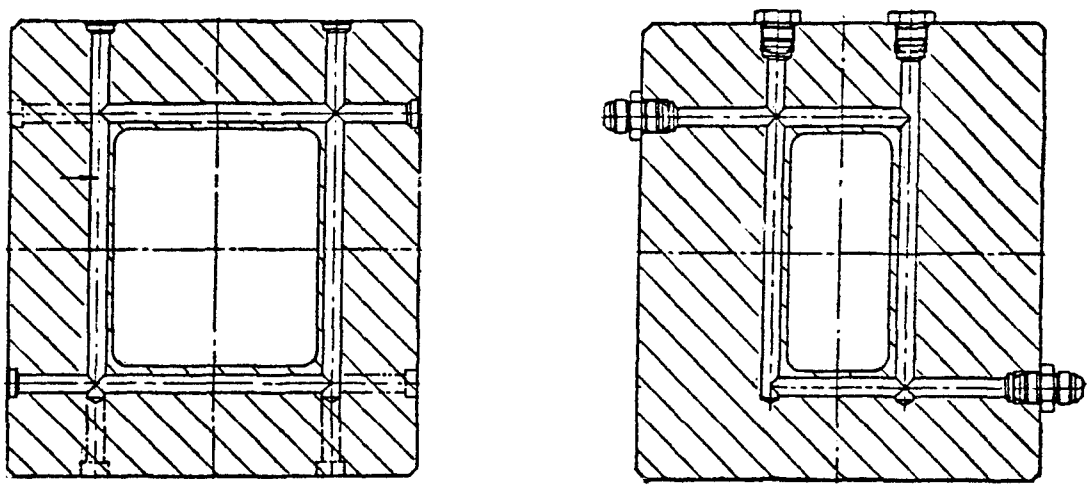

Figure 181. Heat Sink Combustor Cooling Passages

The adapter section was approximately 4.8 cm in length and provided for changing the corner radii from the nozzle section value of 1.28 cm to 0.64 cm. Use of this section avoided the need for a special large copper forging for the nozzle section. The interface between the transition section and the nozzle was sealed with O-rings.

Combustor Section B had a constant internal geometry with a cross section of 19.7 cm by 15.5 cm. The section was 22.9 cm in length and was a simple spacing section to provide the required combustor length. The wall thickness in this section was approximately 7.8 cm.

Combustor Section A was designed with internal geometry identical to Section B. However, following the combustion dynamic stability test, the Section A entrance corners on the side were beveled as illustrated in Figure 182. In conjunction with the acoustic slots, this beveling provided greater damping against combustion instability. In this section, provisions were made for the two igniter units. Openings for these units were located 3.2 cm from the combustor entrance on the vertical walls, slightly above the center. The openings were tilted downward at a angle of 0.21 rad to avoid potential accumulation of reactants in the igniter combustion chambers. The exterior of the combustor in this region was machined to allow mounting of the igniters. The igniters were bolted to the combustor.

Installation provisions were made for an electrically initiated bomb that was used to generate a pressure pulse during the dynamic stability tests. Two locations were provided near the injector end of this section. When the bombs were not used, these installations were plugged with copper inserts. Bomb port locations are illustrated in Figure 183. The bomb port locations were selected from the standpoint of: (1) placing the bomb in an axial plane (6 cm from the injector face) in which most of the combustion occurs; (2) placement of the bomb to favor no particular instability mode when the bomb was detonated; and (3) separation as far apart as practicable to prevent detonation of the second bomb by the detonation wave of the first bomb.

b. Instrumentation

Provisions were made for sixteen static wall pressure measurements, eleven heat flux measurements, and five high frequency pressure measurements. Wall pressure measurement locations ranged from 2.5 cm from the injector face to the nozzle exit. Both flat and contoured walls were instrumented. Heat flux "meters" were also located along the combustor axis. These meters consisted of a thermally isolated section of wall with a thermocouple. Four of the high frequency pressure transducer installations were located in Combustor Section A near the injector. The fifth location was in the adapter at the beginning of the convergence portion of the nozzle. The specific location of the measurements is summarized in Appendix G.

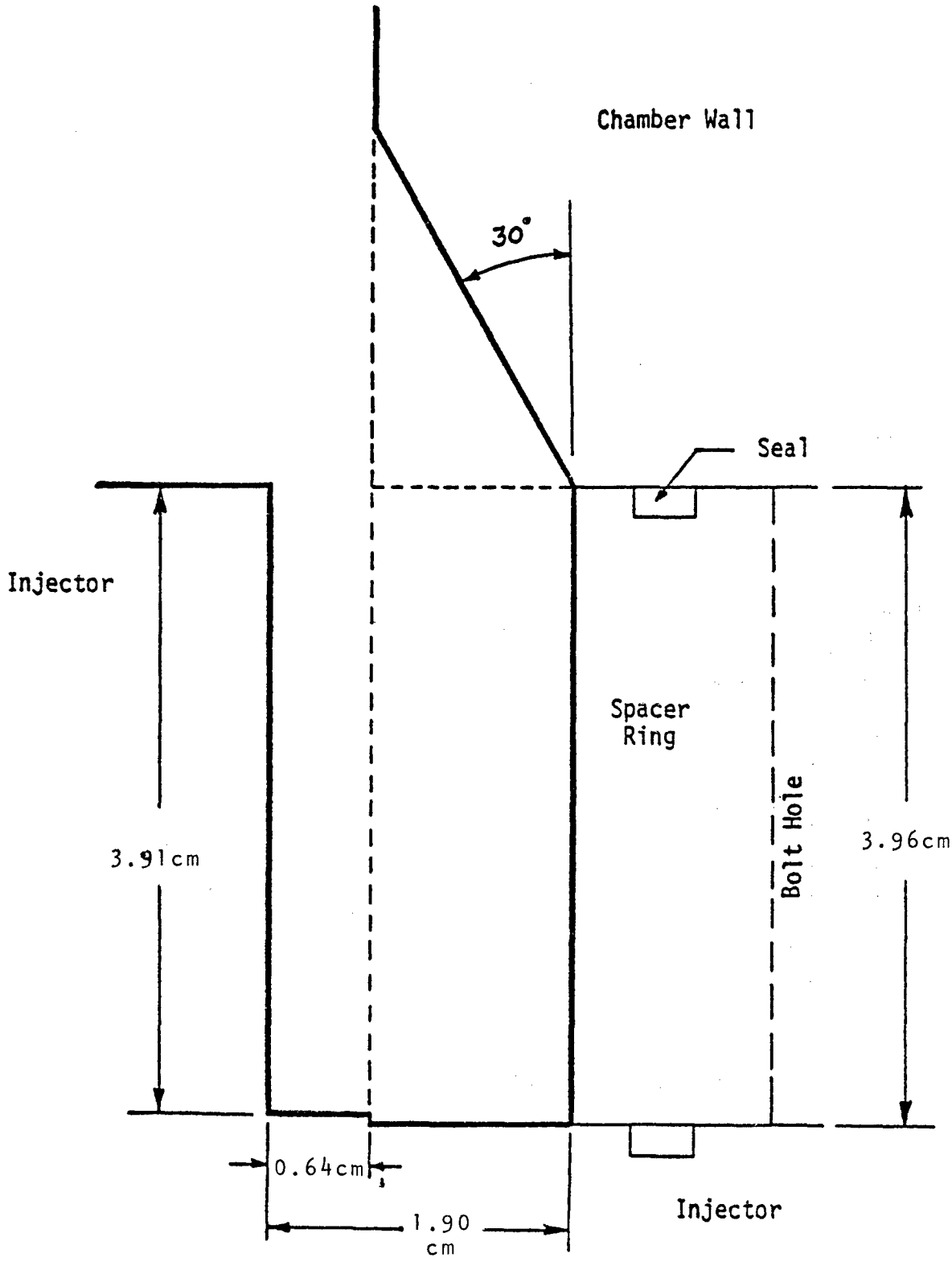

Figure 182. Side Slot Redesign.

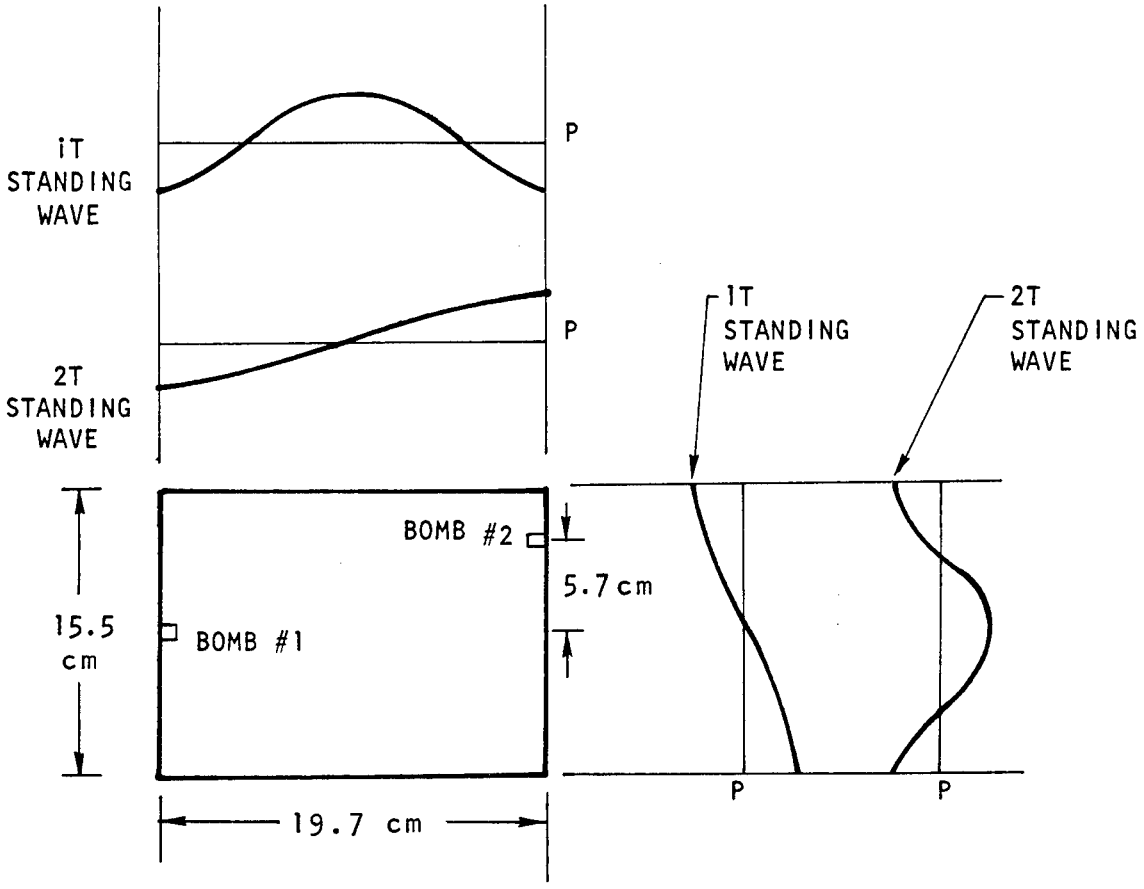

Figure 183. Schematic of Bomb Port Locations.

c. Material

The material used in the combustor was oxygen-free high conductivity (OFHC) copper. This material was selected based on its high conductivity and heat capacity, and its availability relative to the other copper alloys. This material was compatible with the combustion gases and had adequate strength and cycle life for the development test program.

d. Thermal Analysis

A transient thermal analysis was conducted for the heat sink combustor operating at nominal combustion pressure. Three areas were addressed: (1) solid wall sections; (2) heat flux meter section; and (3) water cooled sections. The thermal analysis was based on a throat heat flux of 1900 w/cm^2. This value was scaled using boundary layer relations to obtain values at other combustor locations.

Solid wall sections in the combustor were evaluated. A temperature trace versus time is presented in Figure 184. The inner surface temperatures were approximately 840 K after three sec of operation. In the analysis the full value of combustion pressure was assumed to be established at time zero. In actual operation the combined transient and steady-state operation could be about three and one-half seconds. The throat region was also analyzed, and the wall temperature at three seconds was found to be significantly in excess of values acceptable from a structural and durability standpoint. The nozzle exit region was analyzed, and an inner wall temperature of 840 K predicted after three seconds of operation. This was acceptable from structural considerations but was significantly higher than the 533 K value allowed at the combustor/channel interface. In both the throat and nozzle exit region, water cooling was necessary to augment the solid wall heat sink capacity.

The solid wall combustor was designed to have two water coolant passages at the nozzle exit and one coolant passage at the throat. The water flow rate requirement is shown in Figure 185. Two passages were used at the exit to reduce the two-dimensional flow of heat to the nozzle exit plane. The maximum gas side wall temperature in this region was 534 K which occurred at the exit lip at the 36 atm operating pressure. The temperature dropped rapidly from this point, and this design was considered acceptable. The water flow rate was calculated at 23.6 kg/sec and 12.7 kg/sec for the 36 and 30 atm operating conditions, respectively.

The calculated gas side wall temperature at the throat was 750 K. Flow rates of 6.4 and 4.5 kg/sec were required at the two operating conditions.

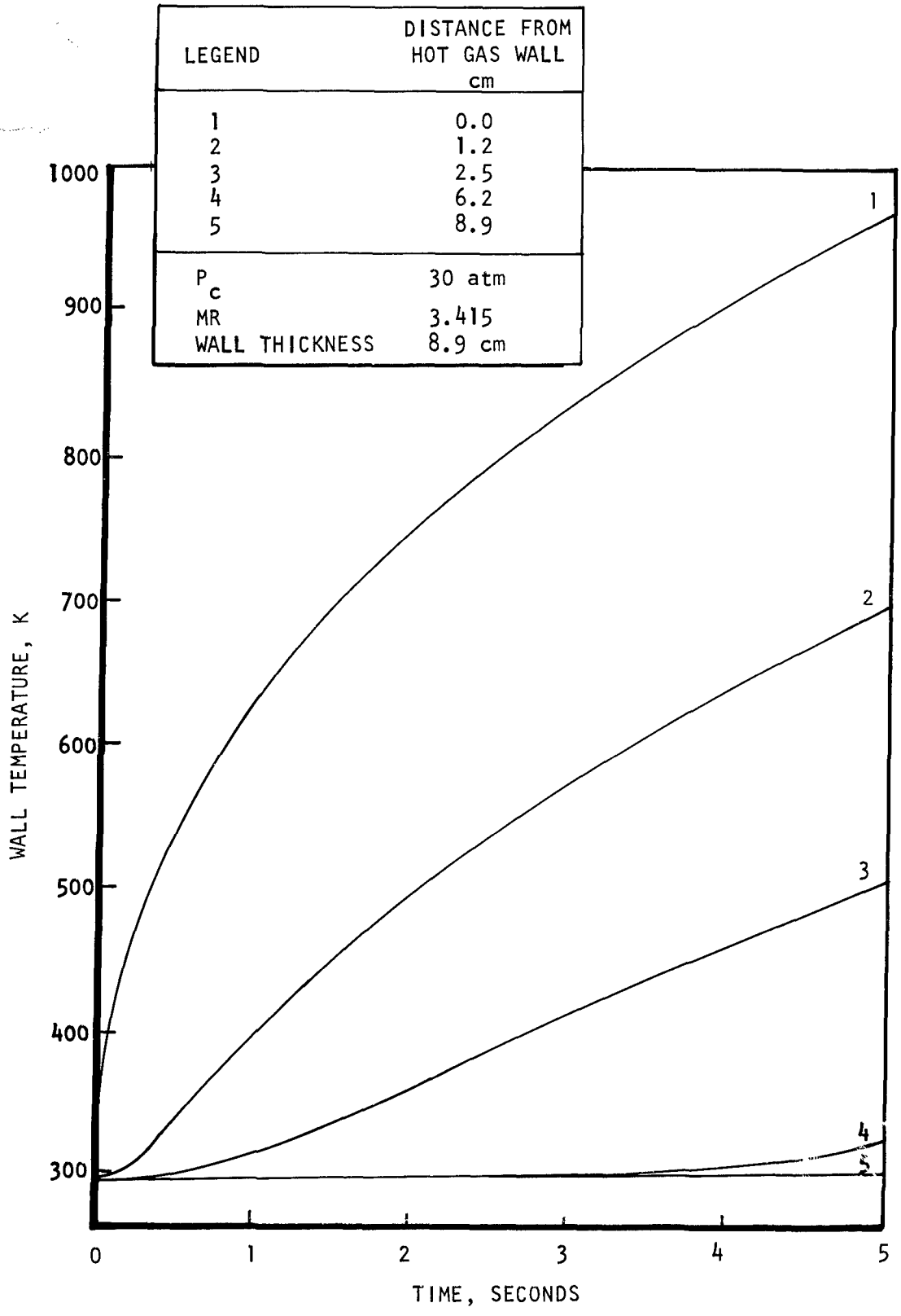

Figure 184 Heat Sink Temperature/Time Relationship

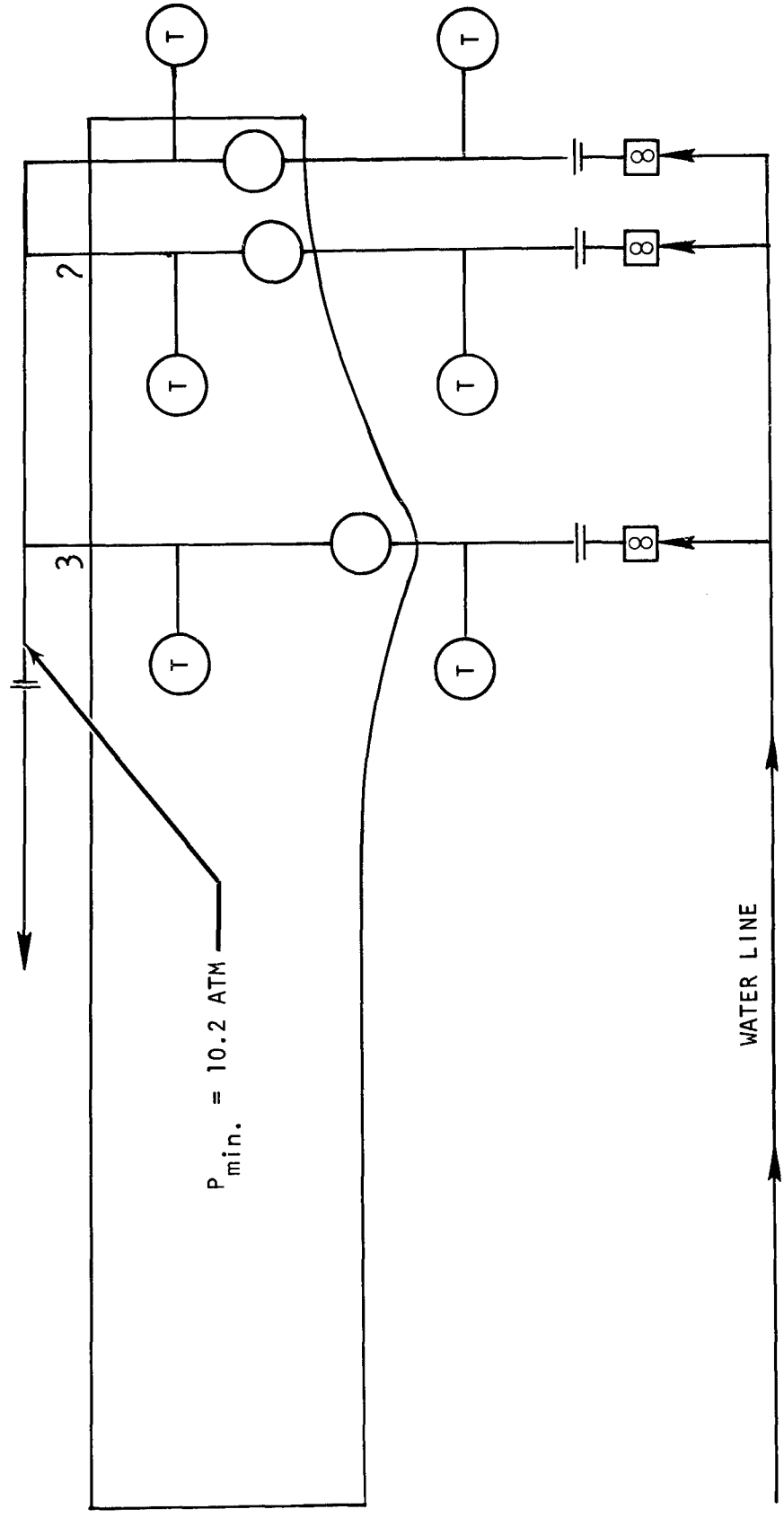

Figure 185 Heat Sink Coolant Water Flow Control

To maintain this temperature at the throat at a nucleate boiling condition, the static pressure of water must be at least 10 atm. Lower water pressure would cause the water flow rate requirement to increase. Therefore, an orifice was needed at the exit of the coolant passage. Since each coolant passage had a different flow rate, orifices were required at the inlet water line.

Thermal analysis of a heat flux meter was carried out for various calorimeter plug thicknesses. The hot- and cold-side wall temperatures are shown in Figure 186 as a function of plug thicknesses for 3- and 5-second firings. As shown, firings of longer than three seconds will cause high gas side-wall temperatures, resulting in a lowered life cycle capability. A 2.5 cm thick plug was chosen for the combustion zone and the nozzle area. In the convergent section the heat flux was higher than either the combustion zone or the nozzle and a 3.2 cm thick plug was chosen for this location of the combustor. The predicted response of these plugs was sufficient to provide accurate data for the determination of the heat flux and the gas side heat transfer coefficient.

e. Structural Analysis

Wall sections, heat flux meters, coolant passages, and structural support were analyzed. A summary of the wall and heat flux meter analysis is shown in Table 55.

2. Fabrication

The heat sink combustor was machined from four OFHC copper billets. Combustor Sections A and B are illustrated in Figure 187. To ensure proper mating of the diagnostics channel and the combustor, the nozzle exit bolt locations and location slots were machined using a template that was a duplicate of the diagnostics channel entrance template. Cooling water inlet and outlet fittings were fabricated and bolted to the combustor. The installed heat sink combustor is illustrated in Figure 188.

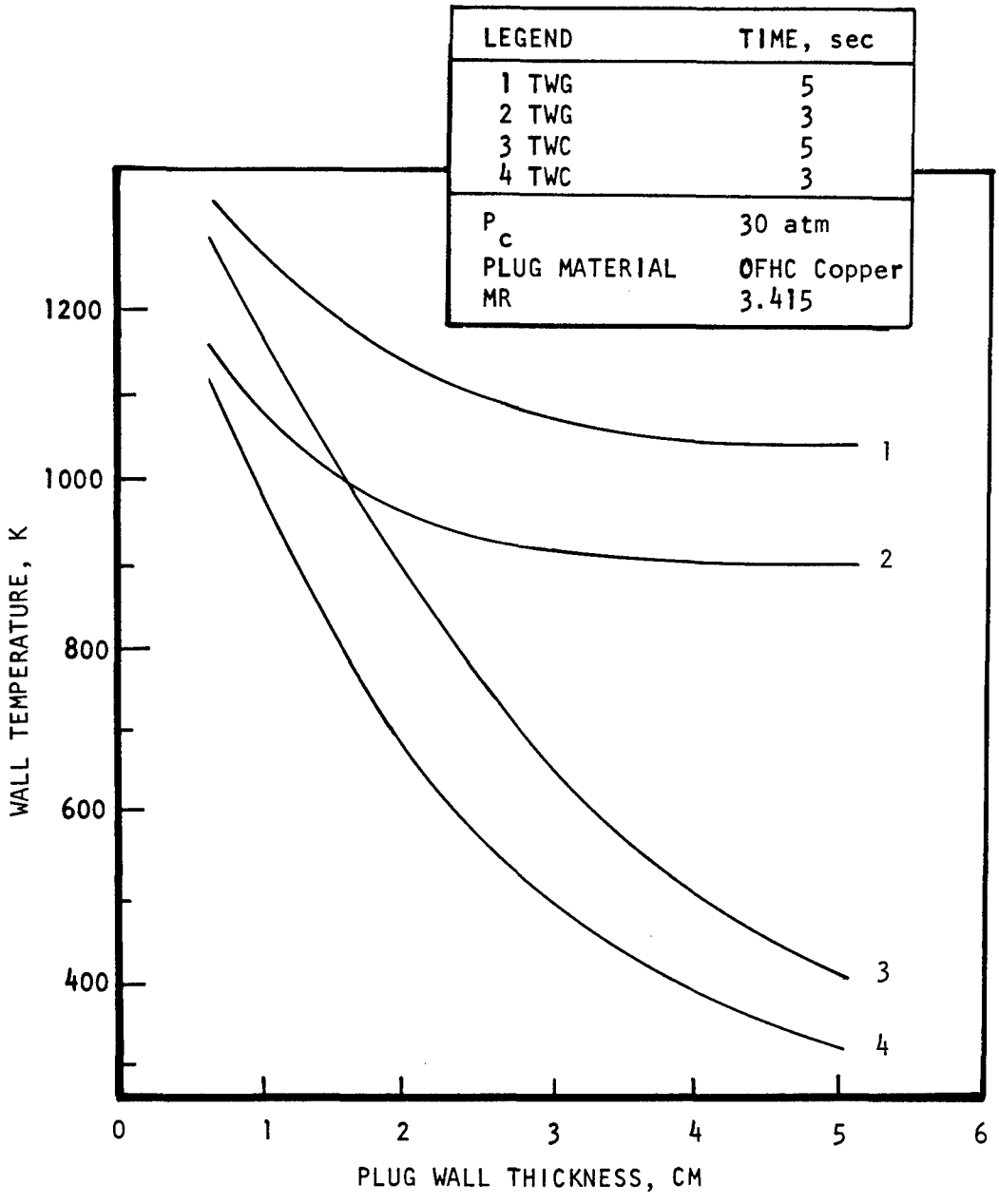

Figure 186. Heat Sink - Temperature/Plug Thickness Relationship.

TABLE 55. STRUCTURAL SUMMARY - HEAT SINK COMBUSTOR

Point	Combustor Wall	Heat Flux Meter
Material	OFHC	
Temperature, K	839	944
Safety Factor, yield	1.3	1.5
Safety Factor, Ultimate	3.3	3.8
Cycle Life	120	105
Safety Factor*	3	2.6

*Safety factors based on 40 complete thermal cycles.

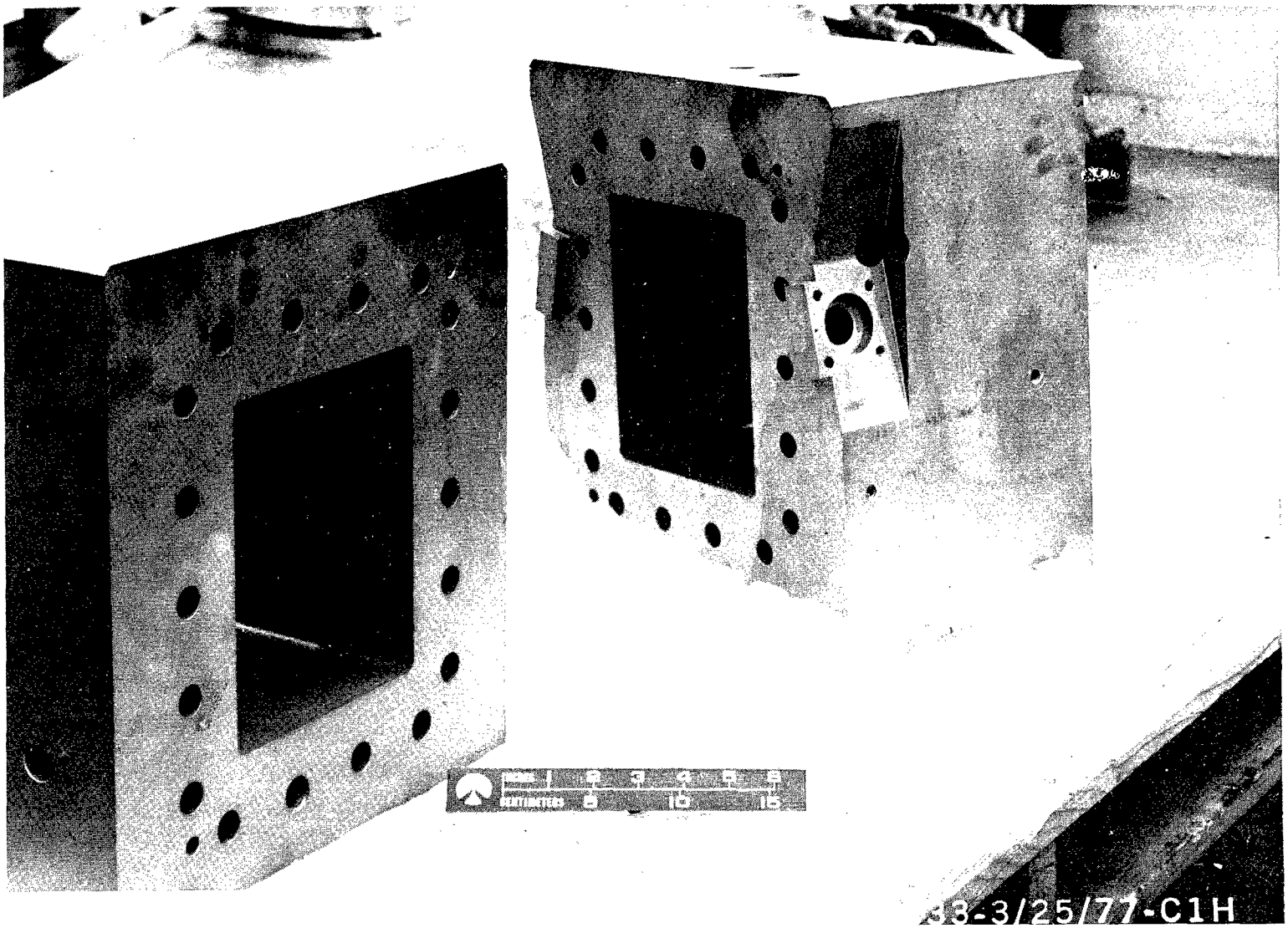

Figure 187. Heat Sink Combustor Sections A & B.

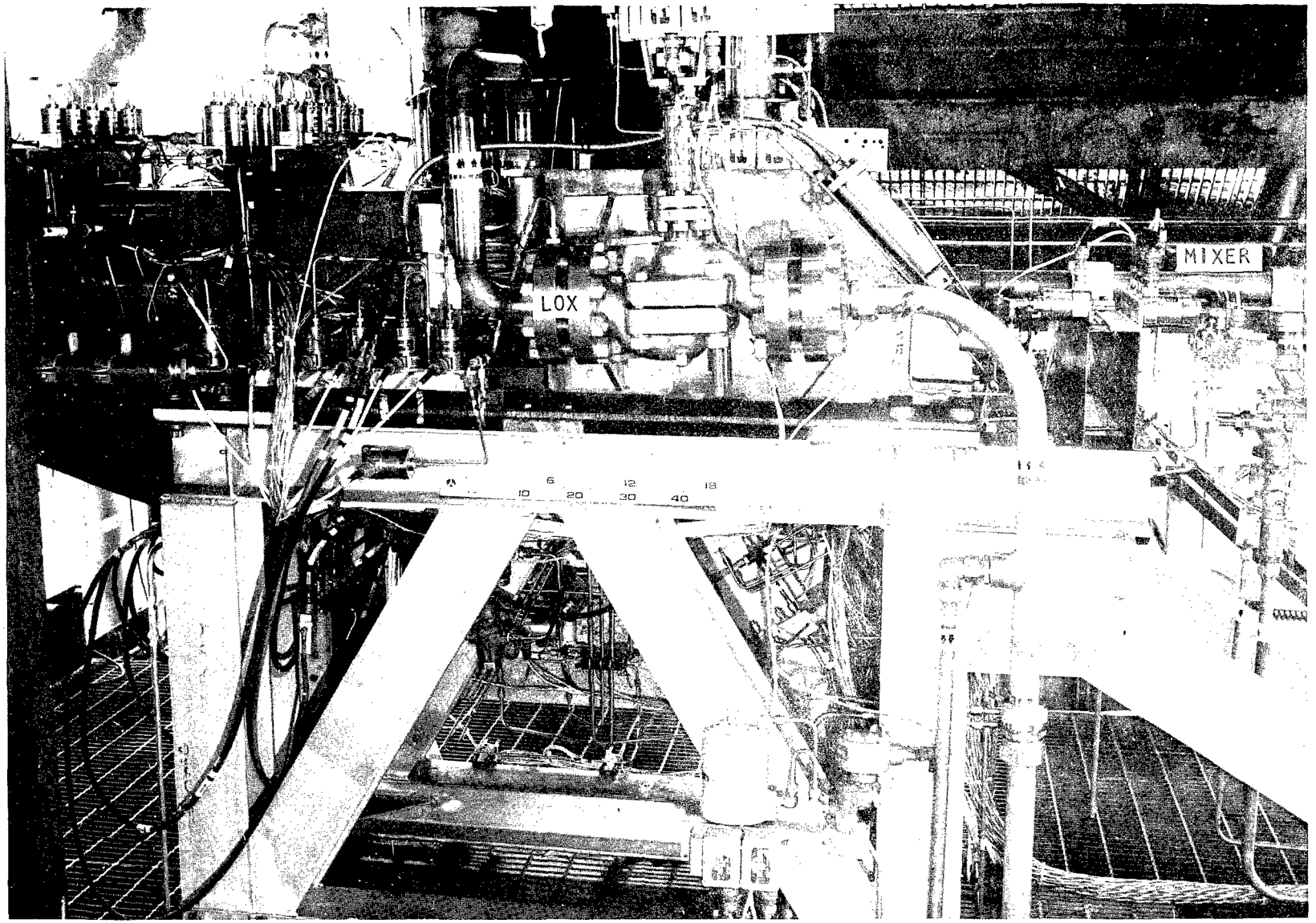

4LC31-6/21/77-S1 I

Figure 188. Combustor Hardware Installation

SECTION VIII

DEVELOPMENT TEST

A. INTRODUCTION

The gas generator system test program was conducted on test stand Bravo 1, at Rocketdyne's Santa Susana Field Laboratory (SSFL) (Figure 189) during the period from June 1977 through April 1978. The objective of the development test program was to check out, develop, and characterize the gas generator system and to demonstrate the operational capability to produce electrically conducting, hot gas at the design flow rates and temperatures. The gas generator system consisted of the ignition system, injector, seed mixer, and supply system and feed system for the hot gas flow train. A heat sink type development combustor was used in place of the cooled wall combustor. A diagnostics channel was used to determine the gas electrical conductivity and provide MHD channel design information. Facility systems were used for LO_2, fuel, purge, ignitor reactant, hydraulic and pneumatic supply. The design of the gas generator system was compatible with the Maxwell Laboratories high power MHD channel design, the Air Force Aero Propulsion Laboratory HPMS magnet at AEDC, and the AEDC test facility.

In the development test effort a series of component and system tests were conducted in a predetermined sequence to verify the design on a step-by-step basis before the complete MHD system was scheduled to be tested. The program logic used provided the minimum number of test variables per test and minimized the exposure of the hardware.

B. TEST FACILITY DESCRIPTION AND INSTRUMENTATION

The gas generator system used in development testing, shown in Figure 190, was primarily composed of components which would be used in the power extraction testing. These included the injector, seed mixer, seed supply system, ignition system, purge regulation system and reactant feed system. The developmental heat sink combustor was used in place of a cooled wall combustor. A portion of the support structure was also built to accommodate the hardware changes and instrumentation required in the development tests. For the last series of tests, a diagnostic channel was used to measure the gas conductivity.

1. Test Facility

A schematic for the gas generator system and the facility fluid supply system is presented in Figure 191. The gas generator system was identical to

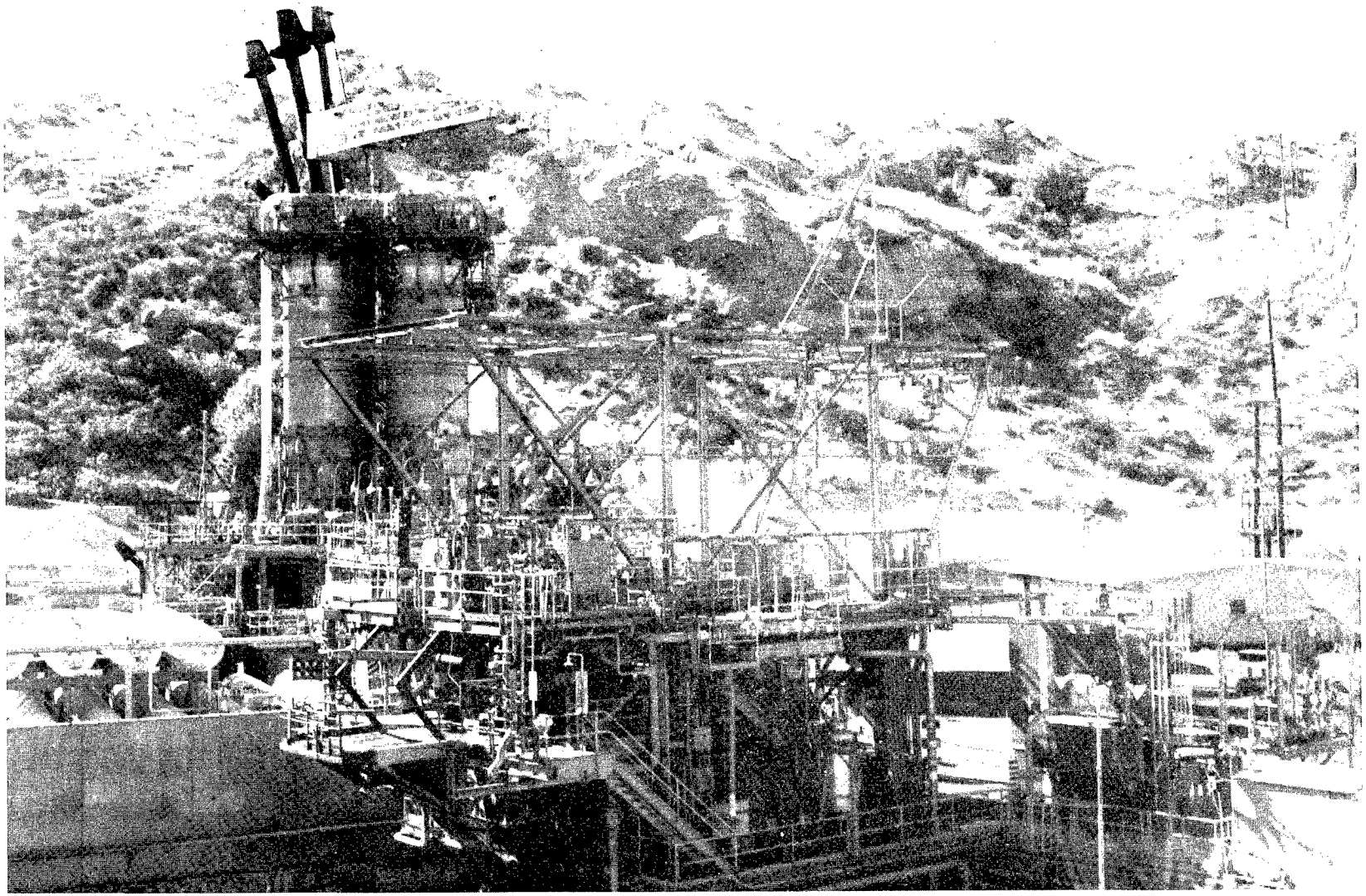

6DD31-9/18/75-S1C

Figure 189. Bravo Test Stand

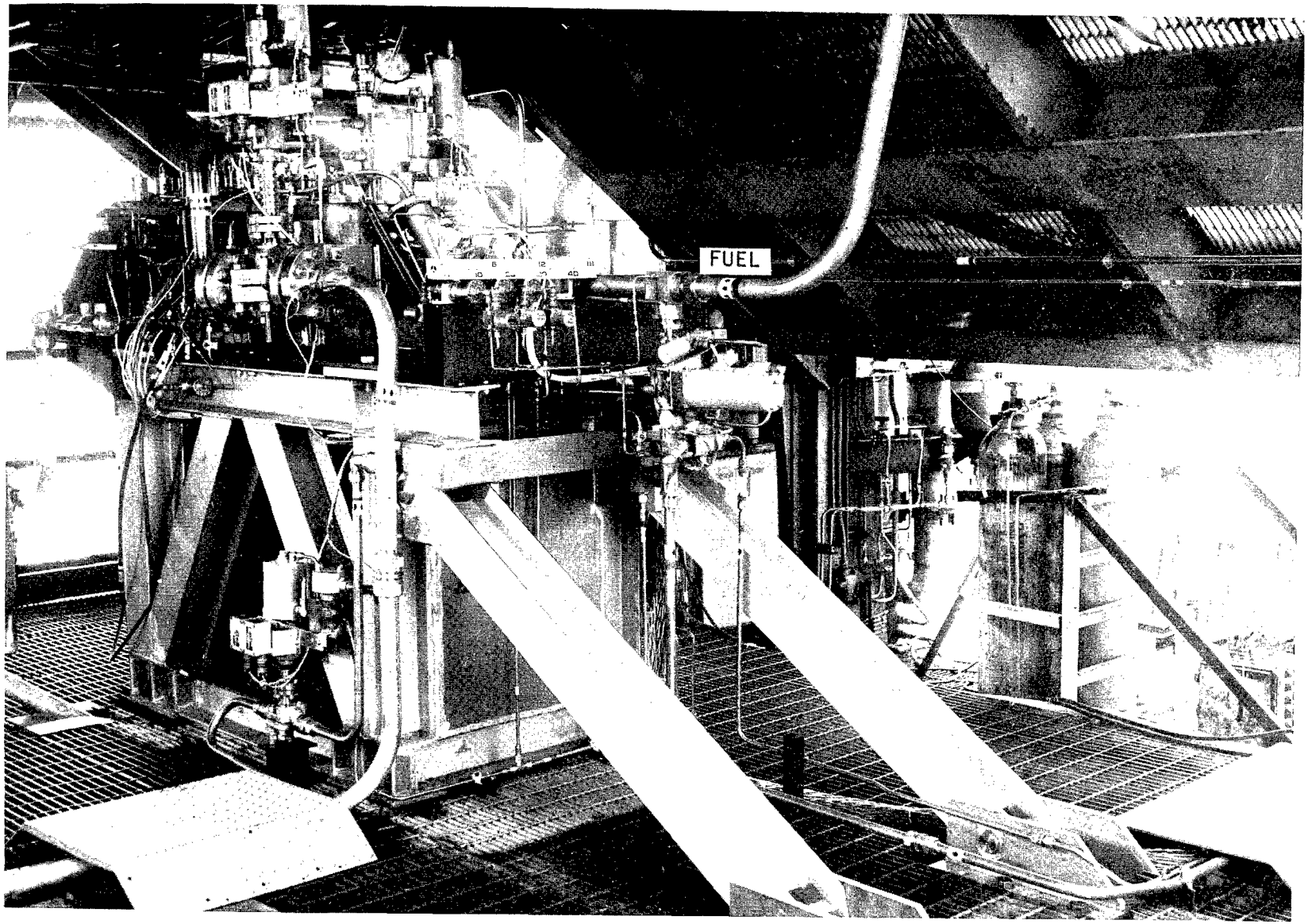

4LC31-6/21/77-S1H

Figure 190. Installed Test Hardware

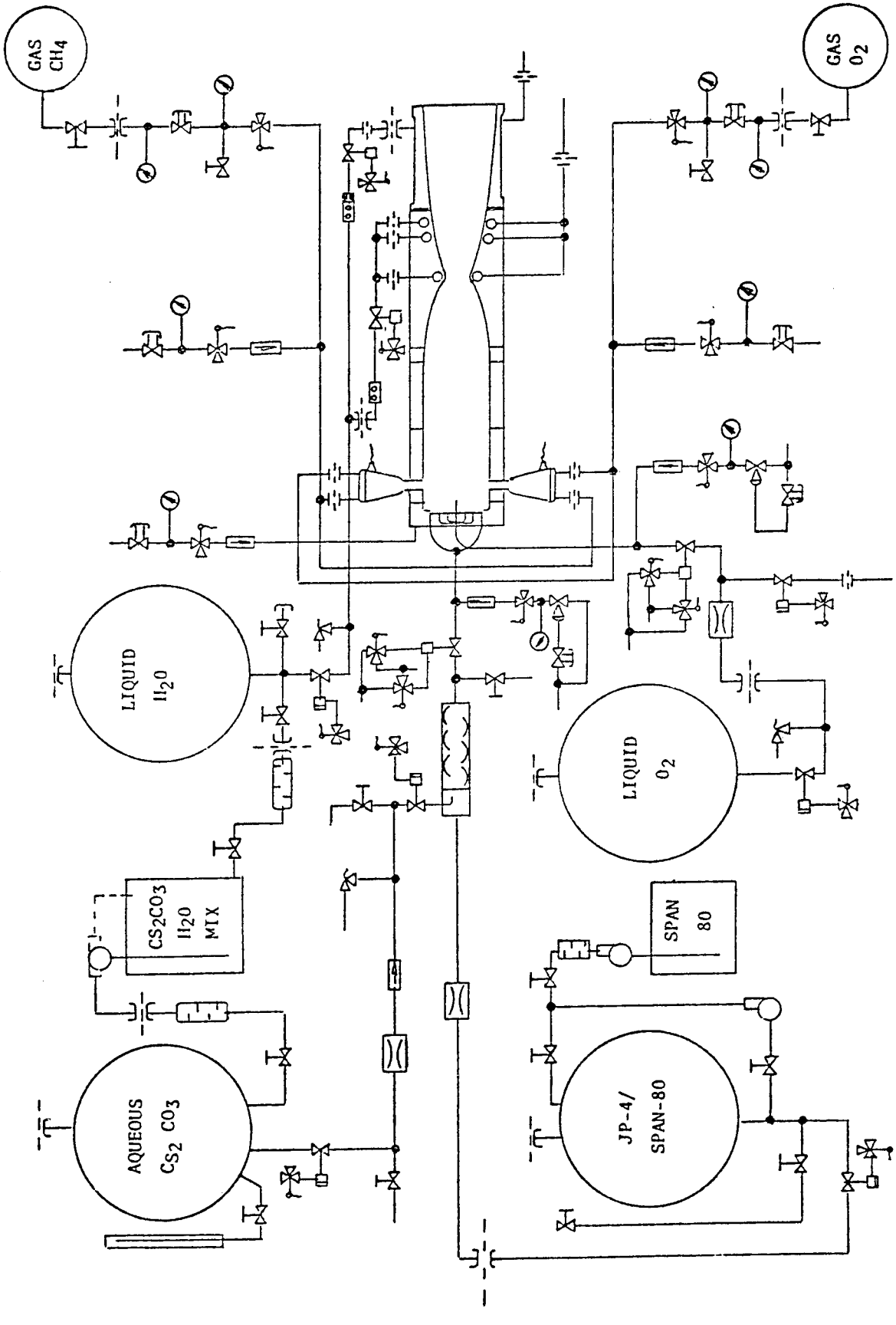

Figure 191. Fluid Supply System Schematic.

that described in Sections V and VI. Interfaces with the facility are indicated in Figure 189 and include: (1) fuel supply system; (2) SPAN-80 mixing system; (3) seed tank pressurant supply system; (4) cooling water system; (5) ignitor reactant supply system; (6) liquid oxygen supply system; (7) hydraulic power supply system; and (8) purge supply system. In addition to these items, the facility support systems provided instrumentation and recording, control sequencing, safety circuit monitoring, and electrical power.

The test facility was provided with a secondary control power supply in case a primary control power supply failure was realized. In addition, the gas generator system was designed for fail-safe shutdown in the case of a total control power failure.

The test facility consisted of a complete reactant feed system combined with the deliverable gas generator system. The reactant feed system delivered and controlled the flow of reactants to the combustor assembly and igniters. Three fluids were delivered to the combustor for main combustor operation: (1) liquid oxygen (LO_2); (2) JP-4 (aviation turbine fuel) with 7% SPAN-80 (a surfactant-sorbitan mono-oleate); and (3) a seed solution of 72% Cs_2CO_3 dissolved in water. The SPAN-80 was an emulsifier which was premixed with the JP-4 in the fuel tank. The seed was received in a powder form and premixed in the seed mixing tank prior to transfer through a filter system into the seed run tank. The LO_2 and JP-4/SPAN-80 were stored in facility tanks while the seed solution was stored in the seed system tank. These reactants were controlled by valves mounted on the support structure in the vicinity of the combustor assembly. The igniter reactants were gaseous oxygen and methane stored in "K" bottles. Gaseous nitrogen was used to purge the reactant lines at start and shutdown and was supplied from a facility source. Both the igniter and purge reactant were controlled through systems mounted on the igniter/purge panel. The igniter/purge panel, the reactant main valves, the mixer and the combustor assembly are mounted on the system support structure. The support was a two-piece structure mounting plate and truss assembly which was anchored to the test stand. The combustor fluid feed system, as illustrated in Figure 191 is described in the following paragraphs.

The LO_2 feed system was a five centimeter system rated for 137 atm and consisted of a LO_2 cavitating venturi, hydraulically controlled five centimeter main LO_2 valve, 2.5 cm LO_2 bleed valve, LO_2 bleed check valve, pressure relief valve, tank valve, 750 liter LO_2 run tank, and a pressurizing system.

The JP-4 feed system was also a five centimeter system rated for 137 atm and consisted of a flow control cavitating venturi, fuel and seed solution mixer, 1.3 cm fuel fleed hand valves, hydraulically controlled five centimeter main fuel valve, tank valve, tank recirculating system, a 11,350 liter run tank, and a pressurizing system.

The SPAN-80 supply system consisted of a stainless steel 210 liter commercial drum container and a commercial transfer pump used to feed the emulsifying agent to the JP-4 run tank.

The seed feed system was a 2.5 cm system rated for 137 atm and consisted of a seed solution mixing tank assembly, a 570 liter seed solution tank assembly, flow control cavitating venturi, seed solution feed assembly including pneumatically controlled 2.5 cm main seed valve, and seed bleed hand valves.

The ignition GO_2 feed system and the ignition methane feed system were identical 0.6 cm systems rated for 137 atm. The system consisted of a "K" bottle, pressure regulator, inlet and regulated pressure gauges, flow control orifices, solenoid operated shutoff valve, and a hand bleed valve. Each system supplied ignition gas to two augmented spark igniter assemblies.

The combustor coolant feed system was a five centimeter system rated for 137 atm and supplied demineralized (deionized) water to the combustor. The system consisted of a flow venturi, pneumatically controlled main coolant valve inlet pressure control orifices, a discharge pressure control orifice assembly, a tank valve and a 22,680 liter run tank with pressurizing and capabilities.

A diagnostics channel designed and fabricated by Maxwell Laboratories was supplied to Rocketdyne for the SSFL development test program. The channel was 45 cm long and was bolted and cantilevered from the exit flange of the combustor. The channel was cooled by water from the same source as the chamber coolant water and required a flow rate of approximately 50 kg/sec at 35 atm inlet pressure. A dc power supply and electrical cable were mounted in the power supply shed adjacent to the test stand and were used to supply current to the diagnostics channel during the tests.

The purge gas feed system was a GN_2 system rated for 137 atm. The system consisted of an inlet manifold including a 2.5 cm isolator check valve tapped off the area GN_2 bottle bank and five purge branches, namely, LO_2 injector manifold purge, fuel injector manifold purge, injector cavity purge, igniter GO_2 purge and igniter methane purge. Each purge branch included a pressure regulator, regulated pressure gauge, shutoff solenoid valve and a check valve for preventing contaminant reverse flow into the purge system.

The valve control pneumatic feed system was a regulated pressure GN_2 system to actuate the pneumatically controlled valves. The regulated GN_2 supply pressure of 11 atm will be required at the AEDC interface. The valve actuation speed will be individually controlled at the respective valve by orificing.

The valve control hydraulic feed system was a regulated pressure hydraulic system to actuate the hydraulically controlled valves; i.e., main LO_2 valve and main fuel valve, using regulated hydraulic supply pressures greater than 137 atm. Valve actuation speeds were controlled individually at the respective valve by orificing the inlet/outlet hydraulic lines.

The seed tank pressurizing gas feed system is a 2.5 cm high pressure GN_2 line connecting the seed tank pressurizing port with the area GN_2 supply system, regulated GN_2 supply pressures up to 137 atm were required.

The feed system was provided with pressure relief valves, bleed valves, vent valves, and drain valves to ensure safety and proper operation. The pressure relief valve prevented excessive pressure buildup within a closed system because of a pressure regulator malfunction, liquid vaporization or other causes. When a relief valve was actuated, the high pressure fluid was discharged until the pressure was reduced, and the valve was reseated. The bleed valve diverted the trapped gas pockets in the feed line to ensure that the line was fully primed up to the main valve. Both the gas and liquid were discharged under a low pressure until steady liquid flow was verified. The vent valve released pressurizing gases after the completion of a pressurization operation to return the feed system to the ambient pressure condition. After the system pressure was vented, the feed lines downstream of the source shutoff valves contained no pressure and were safe for service operation. The vent valves were actuated with cutoffs and also could be used to supplement the pressure relief valves for escess pressure release. The vented gases contained the vapor from the fluid being pressurized.

The bleed, vent, drain and relief discharge line were used to control flows of various fluids in the MHD hot gas flow train. The discharges were both in liquid and gaseous phases, and some were either high pressure, cryogenic temperature, high temperature, flammable and/or shock sensitive. Positive separation of LO_2 and GO_2 from JP-4 and methane was maintained.

2. Instrumentation

Instrumentation was provided to support the gas generator start and cutoff sequence, to protect the facility and test hardware from damage, and to obtain hardware performance information. An instrumentation schematic is presented in Figure 192.

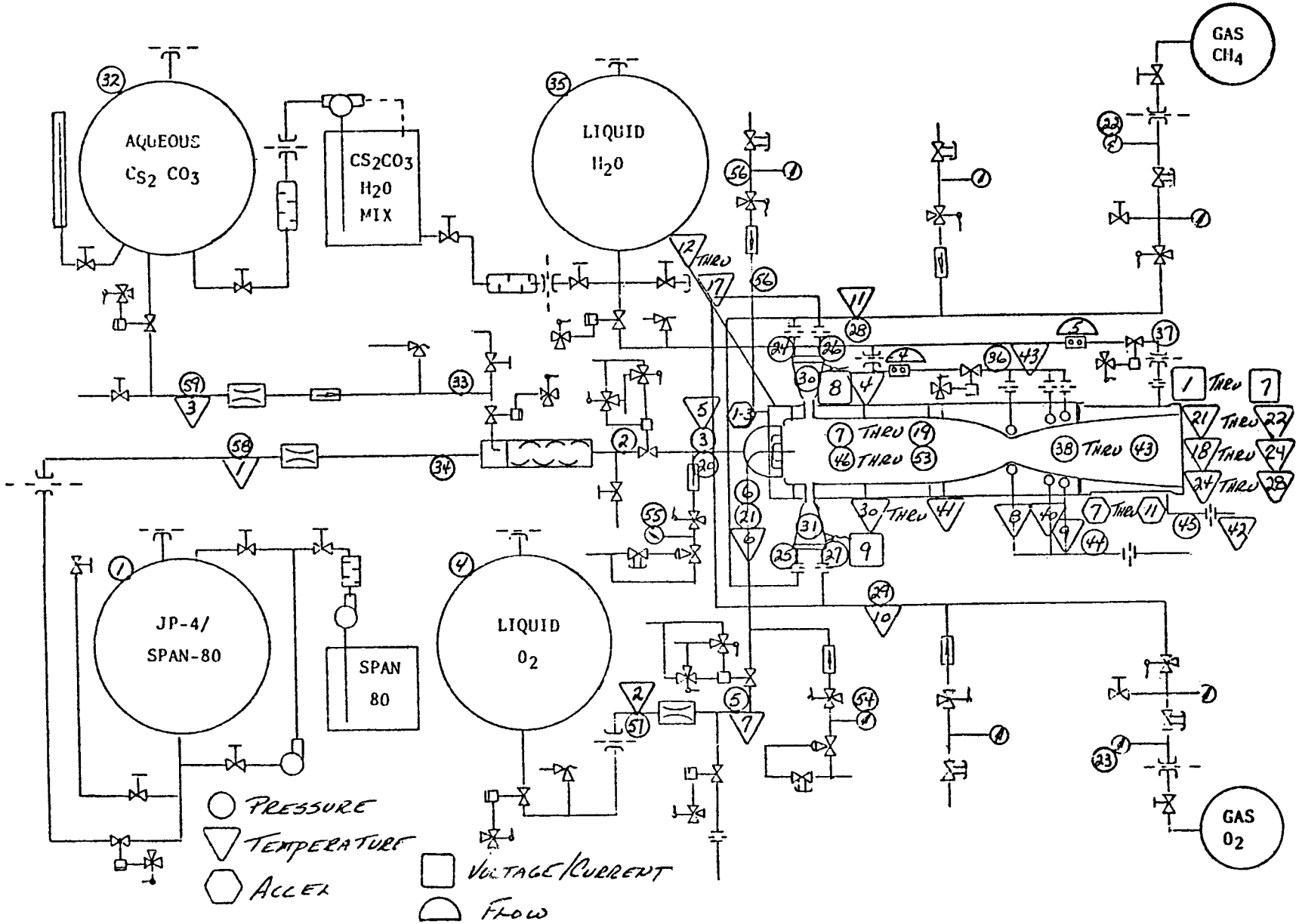

Figure 192. Instrumentation Schematics.

The feed system instrumentation is itemized in Table 56. The listed code numbers can be identified on the instrumentation schematic shown in Figure 192. These items listed were required to conduct the tests and establish the reactant systems were functioning properly.

The heat sink combustor was used throughout the test program and provided data to establish the characteristics of the combustor system prior to installation of the diagnostics channel. The instrumentation used to fulfill these requirements is itemized in Table 57. The listed code numbers can be identified on the instrumentation schematic presented in Figure 192. The instrumentation provided for full axial coverage of the combustor in both temperature and pressure. Three auxiliary cooling paths were provided in the combustor, and the individual instrumentation provided thermal data to predict local heat loads.

Instrumentation used during the diagnostics channel test series is presented in the following Table 58. The listed instrumentation was used to define the characteristics of the channel configuration and to prevent any impending damage that could have been incurred because of an abnormal condition. Not all the instrumentation listed was utilized on each test. In some cases different parameters were monitored to establish overall channel characteristics.

The steady-state data acquisition system consisted of a Beckman digital acquisition system supplemented with direct inking graphic recorders (DIGR's), oscillographs, and magnetic tape recorders. The method of recording the various instrumentation signals is indicated in Tables 56 to 58. The primary performance parameter signals were key-punched onto program control cards and inputted at the data processing area for computer processing to generate a program control tape. Data slice points were selected and the raw data tape computer processed to obtain a data tape containing only the selected data slice.

A data reduction program was used to convert instrumentation readings into useable units and for computing specific performance parameters. The equations used in the computation of performance parameters are listed in Appendix G.

C. TEST PROGRAM SUMMARY

The development test effort consisting of a total of 55 tests was completed on 7 April 1978. The tests are summarized in Table 59.

Thirty-one tests were conducted with the ignition system to evaluate the operating modes and assure reliable performance during main combustor operation.

TABLE 56. FEED SYSTEM INSTRUMENTATION LIST

PARAMETER	CALIBRATION RANGE	DIGITAL	DIGR	OSC	TAPE	PRECISION %	CODE NO.
Pressure	atm						
JP-4 Tank	0-137	X	X			0.5	1
JP-4 U/S Main Valve	0-137	X	X	X		0.5	2
JP-4 Injection	0-103	X	X	X		0.5	3
LO_2 Tank	0-137	X	X			0.5	4
LO_2 U/S Main Valve	0-103	X	X	X		0.5	5
LO_2 Injection	0-103	X	X	X		0.5	6
JP-4 Injection (High Freq)	0-69	X		X	X	10	20
LO_2 Injection (High Freq)	0-69				X	10	21
ASI Fuel Supply	0-205	X	X			0.5	22
ASI GO_2 Supply	0-205	X	X			0.5	23
ASI Fuel Injection #1	0-69	X		X		0.5	24
ASI Fuel Injection #2	0-69	X		X		0.5	25
ASI GO_2 Injection #1	0-69	X		X		0.5	26
ASI GO_2 Injection #2	0-69	X		X		0.5	27
ASI Fuel Venturi Inlet	0-137	X	X			0.5	28
ASI GO_2 Venturi Inlet	0-137	X	X			0.5	29
ASI Chamber #1	0-69	X	X	X		0.5	30
ASI Chamber #2	0-69	X	X	X		0.5	31
Seed Tank	0-137	X	X			0.5	32
Seed U/S Main Valve	0-137	X	X	X		0.5	33
Mixer Inlet	0-137	X				0.5	34
LO_2 System Purge	0-137	X	X			0.5	54
JP-4 System Purge	0-137	X	X			0.5	55
Acoustic Cavity Purge	0-137	X				0.5	56

TABLE 56. FEED SYSTEM INSTRUMENTATION LIST (Cont'd)

PARAMETER	CALIBRATION RANGE	DIGITAL	DIGR	OSC	TAPE	PRECISION %	CODE NO.
Pressure	atm						
LO_2 Venturi	0-137	X				0.5	57
JP-4 Venturi	0-137	X				0.5	58
Seed Venturi	0-137	X				0.5	59
Temperature	K						
JP-4 Venturi	275/340	X				5	1
LO_2 Venturi	310/90	X	X			1	2
Seed Venturi	275/340	X				5	3
JP-4 Injection	275/340	X				5	5
LO_2 Injection	310/90	X		X		1	6
LO_2 U/S Main Valve	310/90	X	X			1	7
ASI GO_2 Venturi Inlet	275/340	X				5	10
ASI Fuel Venturi Inlet	275/340	X				5	11
Acceleration	kHz						
Combustor Injector #1	0-10				X	10	1
Combustor Injector #2	0-10				X	10	2
Combustor Injector #3	0-10				X	10	3

TABLE 57. HEAT SINK COMBUSTOR INSTRUMENTATION LIST

PARAMETER	CALIBRATION RANGE	DIGITAL	DIGR	OSC	TAPE	PRECISION %	CODE NO.
Pressure	atm						
Chamber #1	0-69	X	X	X		0.5	7
Chamber #2	0-69	X				0.5	8
Chamber #3	0-69	X				0.5	9
Chamber #4	0-69	X	X	X		0.5	10
Chamber #5	0-69	X				0.5	11
Chamber #6	0-69	X				0.5	12
Chamber #7	0-69	X				0.5	13
Chamber #8	0-35	X				0.5	14
Chamber #9	0-35	X				0.5	46
Chamber #10	0-35	X				0.5	47
Chamber #11	0-35	X				0.5	48
Chamber #12	0-35	X				0.5	49
Chamber #13	0-35	X				0.5	50
Chamber #14	0-35	X				0.5	51
Chamber #15	0-35	X				0.5	52
Chamber #16	0-15	X				0.5	53
Chamber #18 (High Freq)	0-69	X		X	X	10	15
Chamber #19 (High Freq)	0-69	X		X	X	10	16
Chamber #20 (High Freq)	0-69	X		X	X	10	17
Chamber #21 (High Freq)	0-69	X		X	X	10	18
Chamber #22 (High Freq)	0-69	X		X	X	10	19
H_2O Tank	0-137	X	X			0.5	35
H_2O Combustor Inlet	0-69	X	X			0.5	36
H_2O Combustor Exit	0-35	X				0.5	44

TABLE 57. HEAT SINK COMBUSTOR INSTRUMENTATION LIST (Cont'd)

PARAMETER	CALIBRATION RANGE		DIGITAL	DIGR	OSC	TAPE	PRECISION %	CODE NO.
Temperature	K							
H_2O Flow Meter	275/340		X				5	4
H_2O Combustor Outlet #1	275/340		X	X			5	8
H_2O Combustor Outlet #2	275/340		X	X			5	40
H_2O Combustor Outlet #3	275/480		X	X			5	9
Injector Slot #1	275/1090		X				5	12
Injector Slot #2	275/1090		X				5	13
Injector Slot #3	275/1090		X				5	14
Injector Slot #4	275/1090		X				5	15
Injector Slot #5	275/1090		X				5	16
Injector Slot #6	275/1090		X				5	17
Chamber Wall #1	275/365		X				5	30
Chamber Wall #2	275/365		X				5	31
Chamber Wall #3	275/365		X				5	32
Chamber Wall #4	275/365		X				5	33
Chamber Wall #5	275/365		X				5	34
Chamber Wall #6	275/365		X				5	35
Chamber Wall #7	275/365		X				5	36
Chamber Wall #8	275/365		X				5	37
Chamber Wall #9	275/365		X				5	38
Chamber Wall #10	275/365		X				5	39
Chamber Wall #11	275/365		X				5	41
H_2O Combustor Inlet	275/340		X				5	43
Flows	liters/m	atm						
H_2O	1890	137	X	X	X		1	4

TABLE 57. HEAT SINK COMBUSTOR INSTRUMENTATION LIST (Cont'd)

PARAMETER	CALIBRATION RANGE	DIGITAL	DIGR	OSC	TAPE	PRECISION %	CODE NO.
Acceleration	kHz						
Combustor Injector #1	0-10				X	10	1
Combustor Injector #2	0-10				X	10	2
Combustor Injector #3	0-10				X	10	3

TABLE 58. DIAGNOSTICS CHANNEL INSTRUMENTATION LIST

PARAMETER	CALIBRATION RANGE	DIGITAL	DIGR	OSC	TAPE	PRECISION %	CODE NO.
Pressure	atm						
H_2O Tank	0-137	X	X			0.5	35
H_2O Test Channel Inlet	0-69	X	X			0.5	37
Test Channel Wall #1	0-7.8	X	X			0.5	38
Test Channel Wall #2	0-7.8	X	X			0.5	39
Test Channel Wall #3	0-7.8	X	X			0.5	40
Test Channel Wall #4	0-7.8	X				0.5	41
Test Channel Wall #5	0-7.8	X				0.5	42
Test Channel Wall #6	0-7.8	X				0.5	43
H_2O Channel Exit	0-35	X				0.5	45
Temperature	K						
H_2O Flow Meter	275/340	X				5	4
Channel Wall #1	275/530	X	X			5	18
Channel Wall #2	275/530	X				5	19
Channel Wall #3	275/530	X				5	20
Electrode Frames #1	275/810	X	X			5	21
Electrode Frames #2	275/810	X				5	22
Electrode Frames #3	275/810	X				5	23
H_2O Channel Out #1	275/530	X	X			5	24
H_2O Channel Out #2	275/530	X				5	25
H_2O Channel Out #3	275/530	X				5	26
H_2O Channel Out #4	275/530	X				5	27
H_2O Channel Out #5	275/530	X				5	28
H_2O Channel Out #6	275/530	X				5	29
H_2O Channel Man. Out	275/530	X	X			5	42

TABLE 58. DIAGNOSTICS CHANNEL INSTRUMENTATION LIST (Cont'd)

PARAMETER	CALIBRATION RANGE		DIGITAL	DIGR	OSC	TAPE	PRECISION %	CODE NO.
Flows	liters/m	atm						
H_2O Test Channel	3530	137	X	X	X		1	4
Acceleration	kHz							
Channel Structure #1	0-10					X	10	7
Channel Structure #2	0-10					X	10	8
Channel Structure #3	0-10					X	10	9
Channel Structure #4	0-10					X	10	10
Channel Structure #5	0-10					X	10	11
Voltage	V							
Channel #1	0-250		X					1
Channel #2	0-250		X					2
Channel #3	0-250		X					3
Channel #4	0-250		X					4
Channel #5	0-250		X					5
Power Supply	0-500		X					6
Current	A							
Conductivity	0-50		X					7
Exciter Voltage #1	0-10V			X	X			8
Exciter Voltage #2	0-10V			X	X			9

TABLE 59. SSFL TEST SUMMARY

Test Series	No. of Tests	Test Stand No. 632-	Objective	Pc Atm	Seed * %	Mixture Ratio	Comments
1	10	001 thru 010	Demonstrate Individual ASI Ignition	30	-	1.0	ASI Film Cooled
2	10	011 thru 020	Demonstrate Individual ASI Ignition No Coolant & Mixture Ratio Survey	30	-	0.7 to 1.3	Removed ASI Dump Coolant
3	7	021 thru 027	Demonstrate Dual ASI Ignition & Mixture Ratio Survey	30	-	0.7 to 1.3	Modified GO_2 Orifices & Flow Venturis
4	4	028 thru 031	Demonstrate Dual ASI Ignition With Complete Functional System	30	-	1.0	Installed Main Injector & Operated With All Purges Functioning
5	1	032	Demonstrate Main Combustor Ignition	-	-	-	Interpropellant Communication
6	1	033	Demonstrate LO_2 Priming, ASI Ignition & Sequence Check	-	-	-	First Complete Functional Check - No Fuel
7	4	034 thru 037	Demonstrate Main Ignition & Start Sequence	30	-	3.34	Short Test Durations to Define Start & Cutoff Modes
8	7	038 thru 044	Demonstrate Performance Nominal Pc 20%	24 to 36	-	2.4 to 3.4	Mixture Ratio & Pc Excursions
9	5	001 thru 005	Demonstrate Seeded Fuel Performance	30	5 to 10%	3.0 to 3.4	Mixture Ratio & Seed Ratio Excursions
10	6	006 thru 011	Demonstrate Diagnostics Channel Performance	24 & 30	5 to 10%	3.0 to 3.4	Conductivity Checks With Mixture & Seed Ratio

Footnote * Seed percentage is based on the mass flow of $Cs_2 CO_3$ as a percentage of the total mass flow.

Only the ignition system was active during these tests; the main stage reactant injection did not occur. In the course of these tests, three modifications were made to the initial design: (1) the dump-cooled ignitor tube was replaced with an uncooled tube to provide fuel flow control: (2) the ASI injector momentum ratio was modified; and (3) individual orifices were installed in the reactant lines to the individual ASI combustors. Following this, four dual ignitor tests were conducted in which consistent, stable ignition system operation occurred.

The initial combustor ignition test, #032, resulted in a catastrophic injector failure resulting from an interreactant communication in the injector manifold assembly. Subsequent failure analysis showed a gross print deviation by a contracted vendor during the early fabrication period, causing a structural failure when the injector was subjected to cryogenic oxygen and JP-4 at pressure. An account of this incident is presented in Appendix F.

After a delay, while a new injector was fabricated, the main combustor ignition series was initiated. Five tests were conducted during this phase to validate the start and cutoff sequence logic. Consistent operation was demonstrated. The shutdown sequence, however, resulted in carbon formation and on some occasions residual fuel in the combustor.

To eliminate this shutdown phenomena which would have been detrimental to the diagnostics channel operation, the shutdown sequence and purge modifications were continued into the next test series.

Having established the basic sequence logic, seven tests were conducted to demonstrate combustor performance at nominal chamber pressure and $\pm$ 20% of the nominal pressure. The test series successfully demonstrated operation at mixture ratios ranging from 2.4 to 3.4 and 24 to 36 atm of chamber pressure. During this series, the characteristic velocity efficiency was demonstrated to be 97.7%.

Having characterized the combustor without any seed, five tests were conducted with 4 to 10% Cs_2CO_3 seed as a fuel additive. During this test series the combustor performance was demonstrated at 3.0 to 3.4 mixture ratio with varying seed percentages. The overall combustor performance increased approximately 1% with the addition of the seed ranging from 98.5% with 5% seed to 98.7% with a 10% seed injection, a value several percent above that established on other LO_2/RP programs.

During this test series, the combustor dynamic stability was checked. Test #003 had an artificial pressure wave induced by the detonation of a 10 grain lead oxide bomb approximately 500 msec after the main chamber pressure

was obtained. Immediately, on detonation of the bomb, the combustor went unstable with vibration levels in excess of 200 g's peak-to-peak and severe pressure oscillations. Hardware damage was limited to the acoustic cavity spacer with minor burn damage to the injector and combustor.

After a thorough review of the stability test, a revised acoustic absorber cavity was designed. A cavity was tuned for the 2800 Hz first transverse mode that was triggered during the stability check, and a second cavity was tuned to increase damping at the 3570 Hz and 4800 Hz. Subsequent testing showed the combustor to function at an attenuated pressure and vibration oscillating levels.

The diagnostics channel was then installed for gas conductivity measurements. Six tests were successfully conducted and demonstrated channel performance at various seed and mixture ratio combinations. Measurements were taken to determine the gas electrical conductivity and to determine the heat load in the channel. The test matrix characterized the channel within the operational limits established for the combustor.

D. TEST RESULTS AND CONCLUSIONS

1. Summary of Results

The development tests performed to check out the ASI ignition system and the gas generator operation were conducted satisfactorily with normal development problems encountered during the test program. The test program summary is presented in Table 59 of the previous section.

a. Ignition System Tests

Thirty-one tests were conducted in this effort to characterize the ASI system and to demonstrate satisfactory single and dual ignition over a 0.7 to 1.3 mixture ratio range of 30 atm of pressure. The average ASI hot gas temperature for a mixture ratio of 1.0 was approximately 1230 K during the main combustor test series. The test series demonstrated characteristic velocity efficiencies of approximately 95% throughout the program. Normal design problems were encountered initially, but when solved, the reliability of the ASI's was excellent throughout the entire test series.

b. Sequence Development Tests

Six hot fire tests were conducted in characterizing the combustor operational start/shutdown logic. The first test of the series resulted in a catastrophic injector failure because of interreactant communication resulting from a fabrication machining error. The remaining tests defined the oxidizer and fuel priming times and system response times. Upon completion of this phase of testing the basic operational logic was defined.

c. Injector/Heat Sink Combustor Tests

Twelve hot fire tests were conducted during the characterizing of the combustor performance and functional operating limits. The results of this test series showed the combustor performance to be approximately 97.7% when operating at a no seed condition and 3 to 3.4 mixture ratio. As expected, when the mixture ratio dropped below 3.0, a fall-off in performance was realized. This is presented in Figure 193. With the addition of seed to the fuel at varying seed percentages the data showed the combustor characteristic velocity performance to increase. With 5% by mass $Cs_2 CO_3$ the combustor efficiency increased to approximately 98.5% and by using 10% by mass $Cs_2 CO_3$ increased the efficiency slightly to approximately 98.7%. A plot of this efficiency relationship with mixture ratio is presented in Figure 193.

The thermal data analyzed from this test series showed the combustor heat load to be sensitive to mixture ratio and seed percentages. The higher the ratio and seed percentage the higher the heat load. A thorough discussion of the test results and data is presented in a subsequent section. The results did show that if a combustor mixture ratio of approximately 3.0 and a seed percentage of less than 5% by mass $Cs_2 CO_3$ is utilized, the feasibility of regeneratively cooling a combustor with JP-4 is within the present defined test limits.

The combustor stability results realized during the test effort show the pressure oscillations to be well within the JANNAF requirements for unperturbed, stable operation.[2] On modifying the acoustic absorber as detailed in the discussion of stability, the pressure oscillations were decreased from 5% of chamber pressure to approximately 2.7%. This attenuation of the pressure oscillations resulted in more acceptable combustor operation for MHD applications.

d. Diagnostics Channel Tests

Six hot fire tests were conducted during this series demonstrating the compatibility of the channel with the combustor. During these tests considerable combustor data was realized. The tests were conducted over a range of mixture ratios 3.0 to 3.4 and seed percentages of 5 to 10%. AMS plots were made from the data and showed combustor parameters to be comparable to those realized on tests conducted without the channel. The gas electrical conductivity in the diagnostics channel was measured along with the heat load imposed on the diagnostics channel. Inlet gas conductivities ranged from 14 to 15 mhos/m for the various test conditions.

[2] "Combustion Stability Specifications and Verification Procedures for Liquid Propellant Rocket Engines," CPIA Publication 247, October 1973.

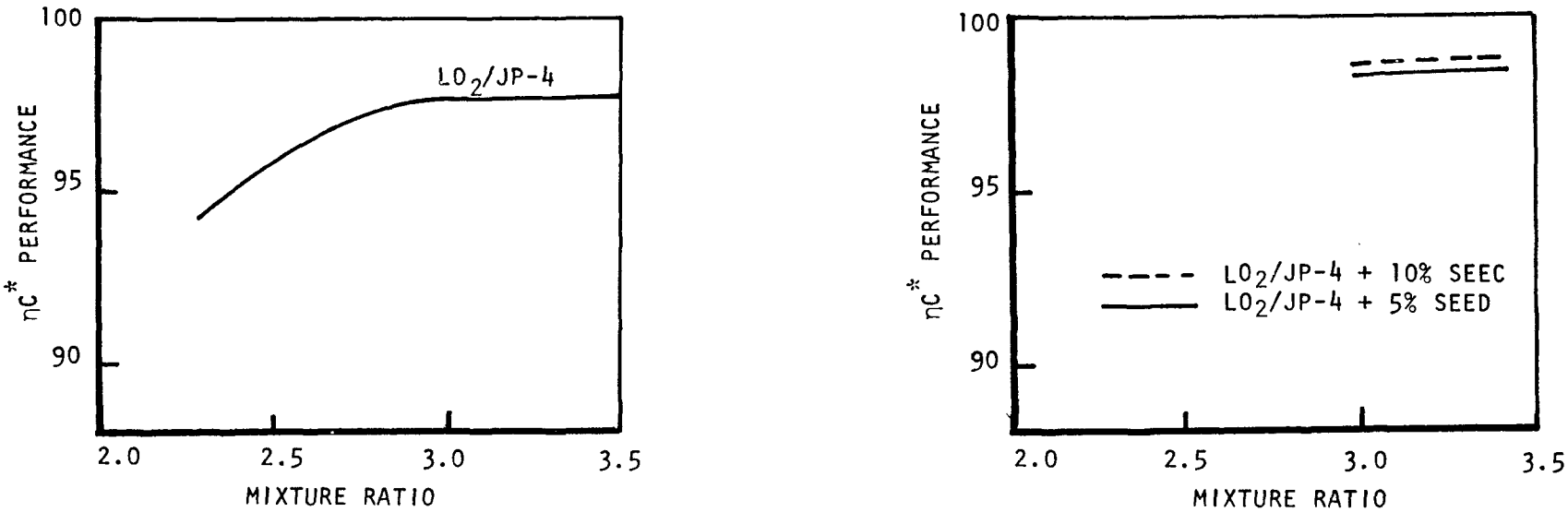

Figure 193. Combustor Characteristic Velocity Performance.

2. Ignition System

Ignition system tests were conducted with the objective to: (1) establish ASI ignition sequence; (2) verify repeatability of ignition sequence; (3) verify the absence of localized heating on the dummy injector and solid wall combustor; and (4) demonstrate ignition at various mixture ratios.

a. Test Setup

The test hardware used was as follows: (1) Augmented Spark Igniter assembly consisting of an exciter, cable, spark plug, cooled combustor liner, and uncooled combustor liner; (2) solid wall chamber (Sections A and B); and (3) dummy injector.

The hardware installation is shown in Figure 194. The basic gas generator installation was used. The feed system, consisting of the GO_2/GCH_4 supply, lines, valves and the purge, in conjunction with the control, instrumentation and data acquisition systems, was part of the gas generator system.

The ASI flow schematic is shown in Figure 195. The actual line and valve sizes are also indicated. The schematic shows the reactant and purge valves separated from the ASI for clarity. In practice, these valves were placed as close to the ASI as possible. The exciter location was dictated by the cable length as illustrated in Figure 194.

The igniter test operational requirements established early in the program were:

Chamber Pressure	-	30 atm
Oxygen Flow Rate	-	37 g/sec
Methane Flow Rate	-	37 g/sec
Oxygen Injection Pressure	-	35.4 atm
Methane Injection Pressure	-	35.0 atm
Mixture Ratio	-	1.0
Duration	-	1.0 sec

The ASI start/shutdown sequence used is illustrated schematically in Figures 196 and 197. The start and shutdown sequence shown is the optimized sequence used during the main combustor testing.

The instrumentation used for the ignition tests is shown in Table 60 and located in Figure 198. To expedite testing and minimize cost, the control room instrumentation was used and the digital requirements were not implemented until the final test series was conducted. After the ASI development effort was completed, the complete combustor hardware was installed. During this test effort under the simulated conditions, all data was documented.

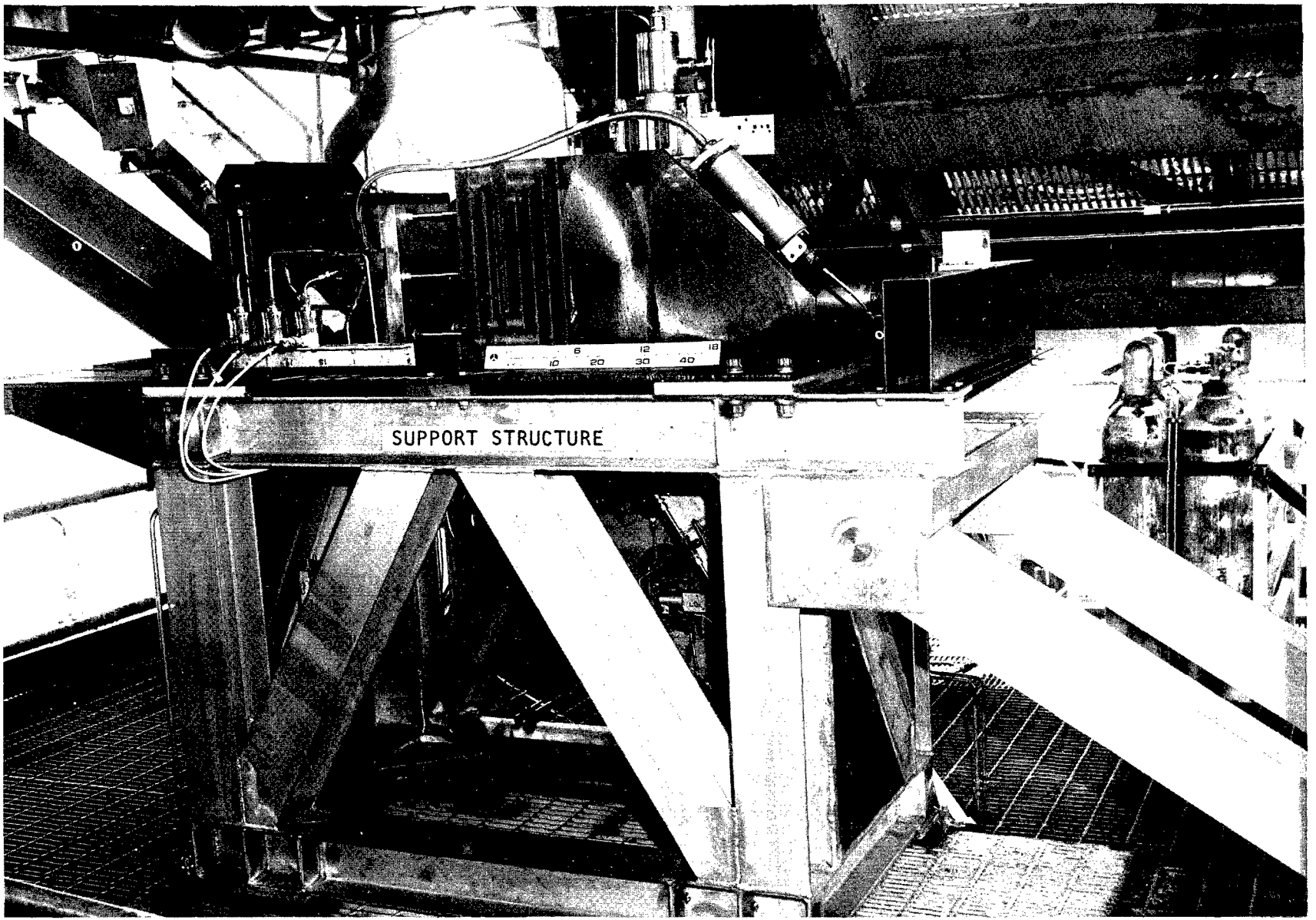

4LZ34-4/14/77-S1C

Figure 194 ASI Hardware Installation

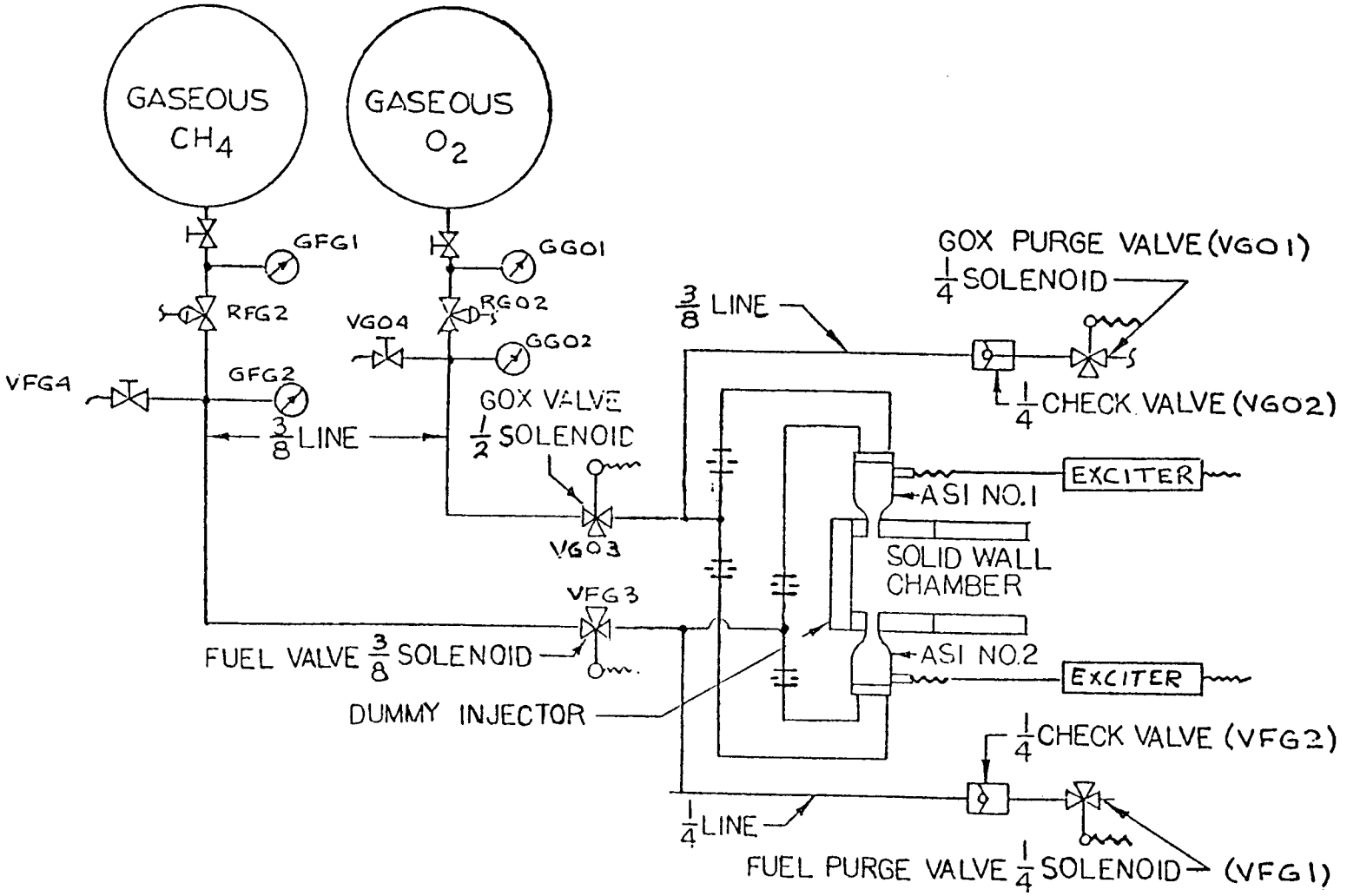

Figure 195. Gas Generator Test Schematic - Ignition Tests.

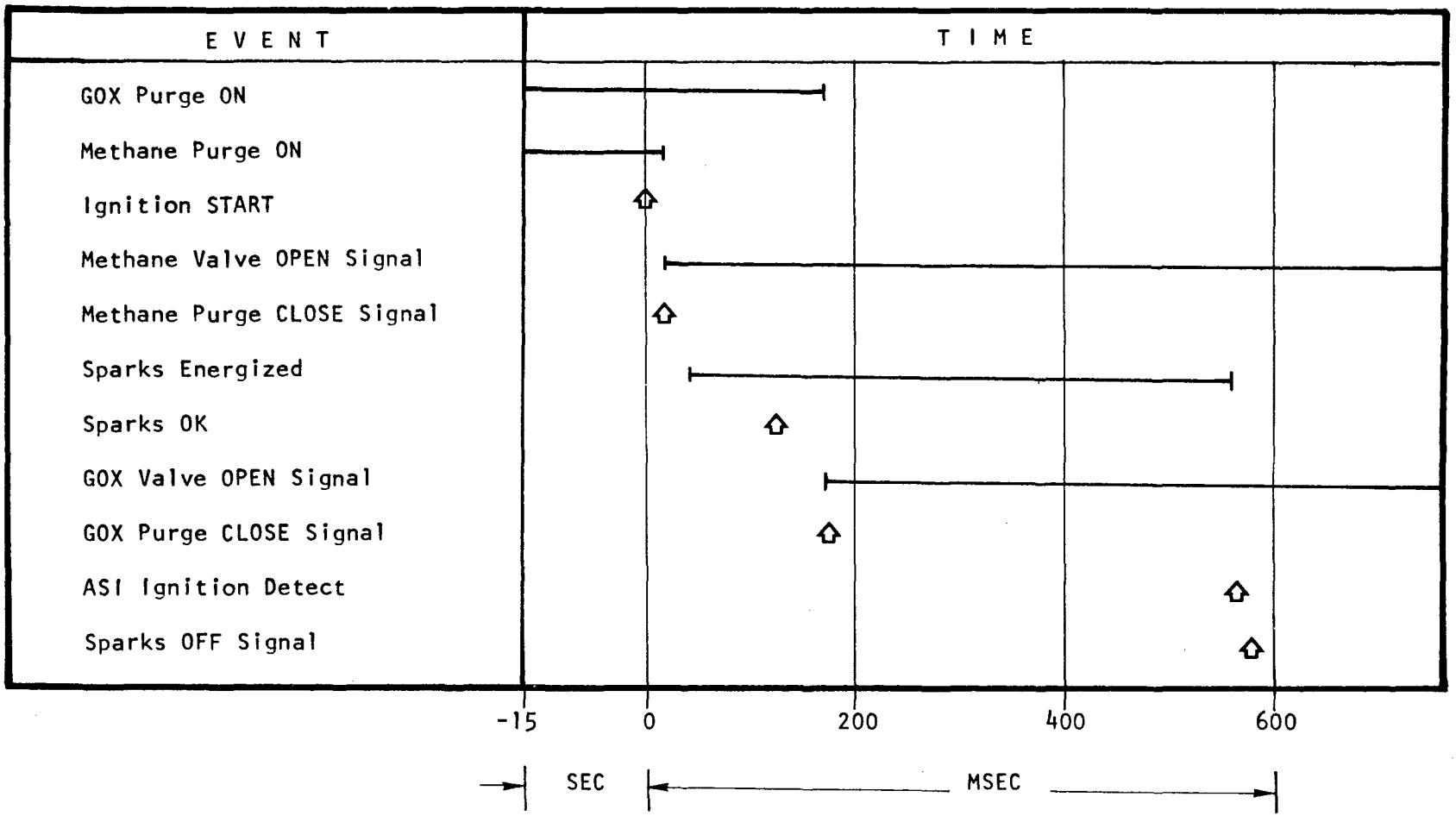

Figure 196. ASI Start Sequence.

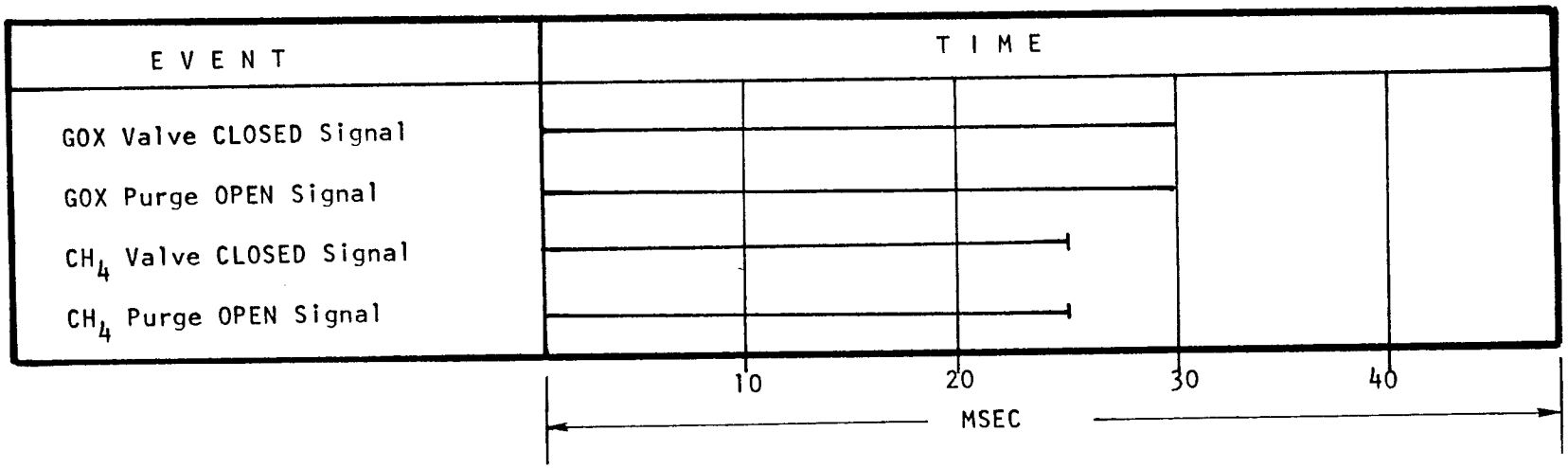

Figure 197. ASI Shutdown Sequence.

TABLE 60. IGNITION TEST INSTRUMENTATION LIST

PARAMETER	CALIBRATION RANGE	DIGITAL	DIGR	OSC	TAPE	PRECISION %	CODE NO.
Pressure	atm						
ASI Fuel Supply	0-205	X	X			0.5	1
ASI GO_2 Supply	0-205	X	X			0.5	2
ASI Fuel Injector #1	0-69	X	X	X		0.5	3
ASI Fuel Injector #2	0-69	X	X				4
ASI GO_2 Injector #1	0-69	X	X	X		0.5	5
ASI GO_2 Injector #2	0-69	X	X				6
ASI Fuel Venturi Inlet	0-69	X	X			0.5	7
ASI GO_2 Venturi Inlet	0-69	X	X			0.5	8
ASI Chamber #1	0-69	X	X	X		0.5	9
ASI Chamber #2	0-69	X	X	X		0.5	10
Combustor Chamber	0-6.9	X	X	X		0.5	11
Temperature	K						
ASI Fuel Venturi Inlet	170/340	X	X			5	12
ASI GO_2 Venturi Inlet	170/340	X	X			5	13
Combustor Chamber	275/1650		X			5	-
Signals	Vdc						
Sparks Energized #1	0-8	X		X			14
Sparks Energized #2	0-8	X		X			15
ASI Fuel Valve	28			X			16
ASI GO_2 Valve	28			X			17

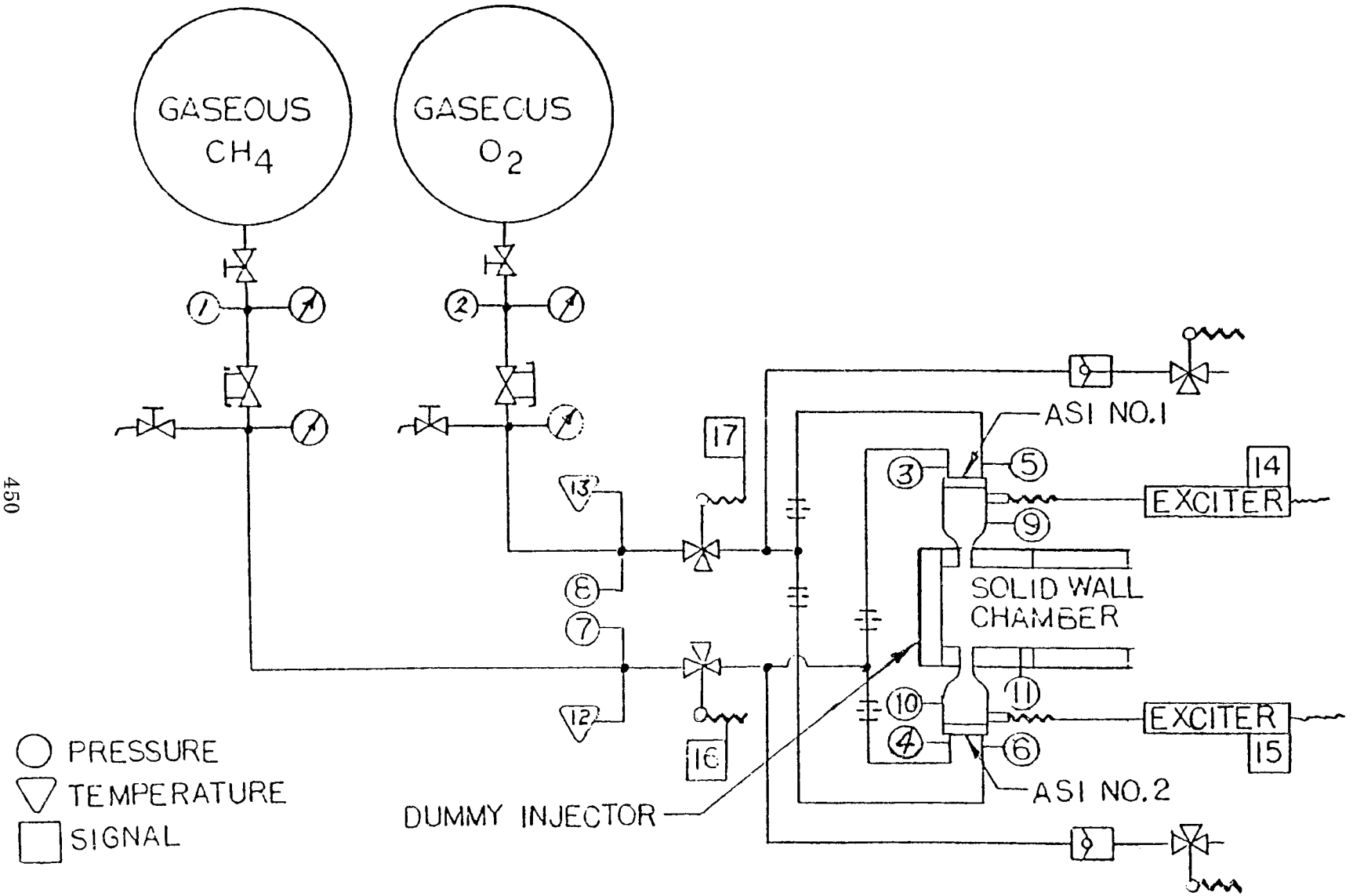

Figure 198. Instrumentation Schematic for Ignition Test.

The blueline and redline values used during the igniter test series were established after many tests were conducted. The ASI feasibility demonstration required numerous changes to be made to these values primarily to accommodate individual test requirements while establishing a workable start transition and main combustor ignition source. The blueline parameters assured an adequate reactant supply pressure was available for satisfactory operation, testing demonstrated a lower limit or minimum pressure that could be realized without jeopardizing the test. The redline and continue parameters established resulted in maintaining the igniter in a safe start/operating mode for the one second operational limit.

The one-second operational limit was a result of replacing the cooled ASI liner with an uncooled version. This change was made during the test effort to alleviate the requirement for a difficult balance circuit required by splitting the incoming fuel internally to the injector and coolant manifolds.

b. Test Description

During the igniter test evaluation, thirty-one test attempts were made. The last seven of these tests were conducted with the final hardware and facility configuration. A brief description of the tests is presented in the following paragraphs.

Tests 001 through 006 were conducted on 15 April 1977. Based on this checkout test series, several redline, blueline, and timer settings were modified.

On 19 April 1977, tests 007 and 008 were conducted. Test 007 resulted in single ignition of ASI #2 at a chamber pressure of 20.7 atm. A smooth ignition was demonstrated. For test 008, the feed system was switched to ASI #1 and no ignition was accomplished because of the low combustor fuel flow.

On 20 April 1977, tests 009 and 010 were conducted with both ASI units connected to the feed system. Based on the prior test results, a new fuel venturi was installed in the line to permit 150 g/sec methane flow at the design conditions.

On 22 April 1977, tests 011 through 013 were conducted. Prior to the test initiation, the dump coolant flow on both ASI's was terminated by the insertion of an "O" ring that restricted flow through the eight, 2.06 mm orifices. Again, the ASI's were independently tested.

After test 013, all subsequent testing was terminated until a thorough analysis of the ASI injector design was conducted. A redesign consisting of resizing the oxidizer orifices and eliminating the dump coolant was prepared. The hardware modifications were made and ASI testing was again initiated.

On 3 May 1977, tests 014 through 020 were conducted on the redesigned igniter. Based on this series of tests, the data showed that feeding two ASI's from one common sonic venturi created an abnormal flow distribution. An individual flow measuring device was installed in each ASI feed passage. Four sonic orifices were machined and inserted in their respective lines to control the reactant flow rate. These orifices were flow calibrated using GN_2 at their respective operating conditions.

On 4 May 1977, the ASI test program was again initiated. Tests 021 through 023 were conducted successfully. During this effort, only control room data was recorded. All of the previous problems appeared to solved. Therefore, after a visual inspection, several tests were conducted and documented. Tests 024 and 025 were conducted at nominal conditions. After this successful demonstration, ignition at two other mixture ratios was demonstrated. Similar ASI units in test at Rocketdyne have operated at mixture ratios far in excess of that demonstrated. With the completion of this test series, the objectives of the ASI test program were fulfilled. Subsequent to this ASI test activity, the injector hardware was installed and the systems characterized. On 21 June 1977, with all systems functional and all purges on, four additional ASI ignition tests were made, tests 028 through 031. The first test produced no ignition because of an interlock timer delay caused by a change in the electrical patch board. This was the first hot fire attempt using the complete injector series hardware and start sequence logic. Tests 029 through 031 were conducted successfully to demonstrate repeatedly the ASI ignition sequence and valve timings to be used for the forthcoming injector test series. All subsequent tests were conducted using the proven ASI's for ignition of the main combustor reactants.

Figure 199 illustrates the injector characterization results of the hot fire tests. Individual sonic orifices meter the flow, therefore, the variations shown in the pressure changes did not affect the ASI operation.

c. Conclusions

The ASI igniter test effort was successfully completed after several changes were incorporated in the ASI assembly hardware. Design changes were made in the oxidizer orifice size, the spark plug immersion depth and the film coolant. Thirty-one tests were conducted or attempted to complete the defined igniter test program. Of these test attempts, seven tests were conducted utilizing the final igniter and feed system design; all were successful. The ignition and start sequence used and defined as acceptable for the 30 MW MHD injector series were presented in the previous section. A test summary is presented in Table 61 and shows the individual test series and comments. Figure 200 illustrates ASI #1 chamber pressure profile; the fall-off in pressure was caused by low storage supply pressures.

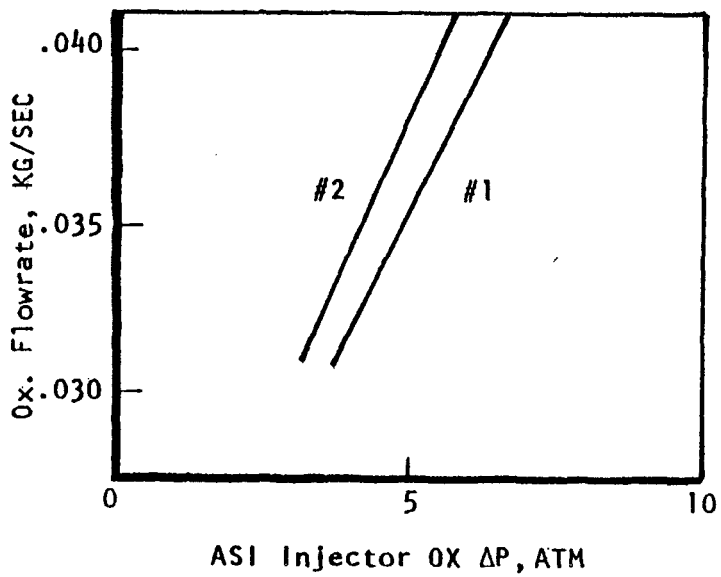

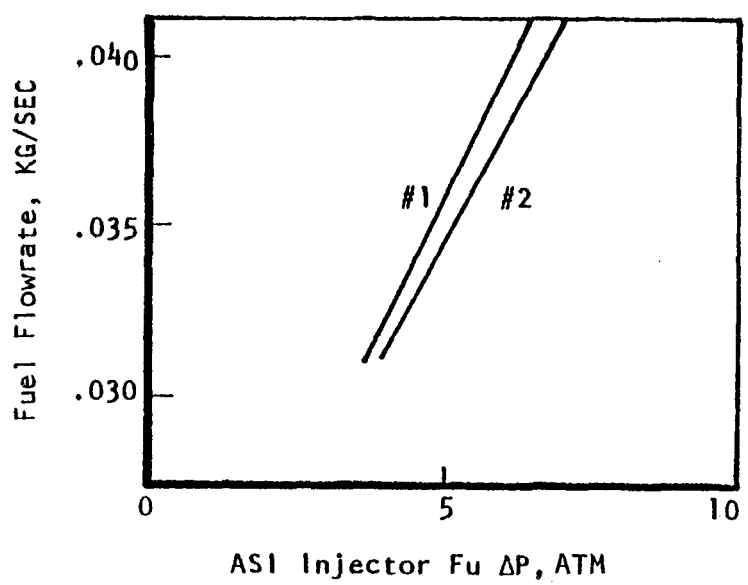

Figure 199. ASI Injector Pressure Drop.

TABLE 61. IGNITER TEST SUMMARY

Test Series	Number of Tests	Objective	Mixture Ratio	Comments
#1	10	Demo individual ASI ignition	1.0	ASI film cooled
#2	9	Demo individual ASI ignition no cooland and M/R survey	0.7-1.3	Eliminated ASI coolant
#3	7	Demo dual ignition and M/R survey	0.7-1.3	Modified injector orifices
#4	4	Demo dual ignition with functional hardware	1.0	Installed all hardware, new flow control devices and functional main combustor start simulation.

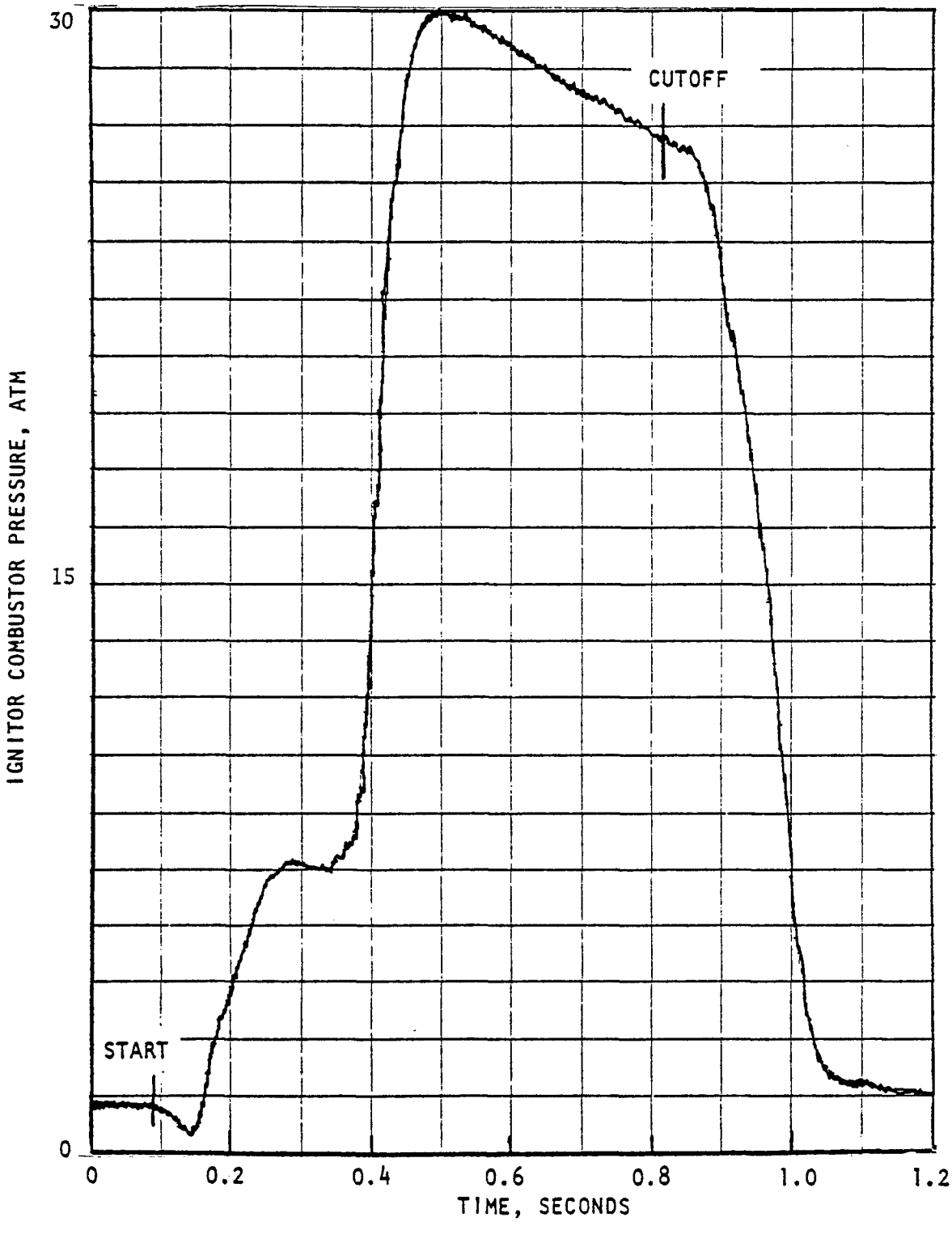

Figure 200. Igniter Test Summary.

3. Operational Sequence Development

Six tests were conducted to verify the operation sequence and to check out the gas generator components. These tests were all conducted at the nominal steady-state operating conditions. In the course of these tests four development problems were encountered and solved: (1) a new injector was fabricated to replace the injector destroyed on the initial test because of interreactant communication; (2) high frequency pressure transducer installation was revised to avoid mount leakage; (3) fuel contamination from the SPAN-80 was encountered and eliminated by system cleaning; and (4) carbon deposits in the combustor at shutdown were alleviated by sequence and purge modifications. At the conclusion of these tests a reliable start and shutdown sequence had been verified.

a. Test Setup

The hardware used for the operational sequence development test series is shown in Figure 201 and consisted of an augmented spark igniter assembly, solid wall combustor assembly, and injector. The feed system used consisted of the following items: (1) reactant supply; (2) fluid feed lines; (3) fluid feed valves; (4) check valves; (5) relief valves; (6) filters, (7) bleed and vent systems; and (8) miscellaneous fittings, etc. A schematic of these items and their respective location in the system is presented in Figure 191. The instrumentation used throughout the test series is identified in Figure 192. The code numbers can be correlated back to parameter identification by referring to Section VIII-B2.

b. Test Description

This initial series of tests established the combustor ignition and start sequence and provided a "hot-fire" checkout of the gas generator components. The start and cutoff sequence logic is illustrated in Figure 151. In these tests the sequence was implemented in steps until mainstage operation was achieved. Typical parameter values for the operational sequence are shown below.

Timing	Continue Signals	Redlines
T_1 = 1100 msec	P_1 = 11.2 atm	24.8 atm ≤ P (ASI) ≤ 41.1 atm
T_2 = 750 msec	P_2 = 24.8 atm	24.8 atm ≤ P (COMB) ≤ 41.1 atm
T_4 = 500 msec	P_3 = 14.6 atm	
T_6 = 2900 msec	P_4 = 24.8 atm	
T_m = 3800 msec	V = 100 g P-P for 50 msec	

These values were specifically defined in each test request and varied slightly depending on the test objectives.

During the operational sequence development test phase, six tests were conducted to define the combustor ignition characteristics and to develop a satisfactory start/cutoff operational logic. Additional testing after this development phase also contributed to the operational logic and sequence development.

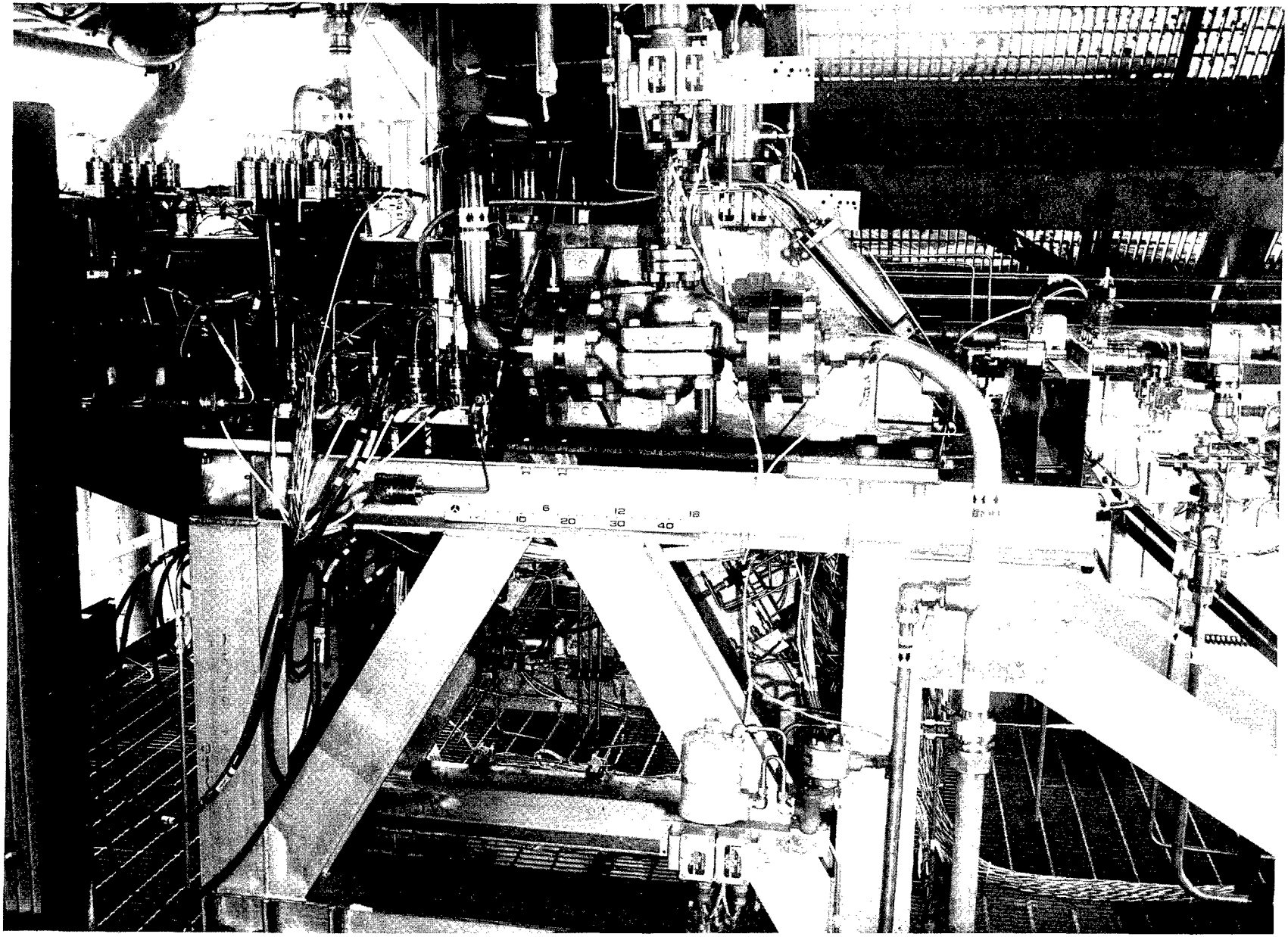

Figure 201. Combustor Hardware Installation 4LC31-6/21/77-S1 I

In general, the basic feasibility of the logic and sequencing used during this effort applied to all future tests. Some tailoring of the individual items to more readily fulfill test requirements was accomplished throughout the continued test effort. A brief description of the six tests conducted in this effort is as follows.

Test 032 was conducted on 24 June 1977, to demonstrate injector fuel and oxidizer manifold priming, a functional pressurized sequence, an instrumentation checkout, and to initiate main combustor ignition. The test resulted in LO_2/fuel communication internally which resulted in an overpressure and loss of the injector. An elaborate analysis of the incident was conducted and concluded the cause of the mishap was an unauthorized rework of the injector. The rework consisted of plugging an oversized hole and redrilling a new fuel manifold passage. This rework resulted in an interreactant wall that failed structurally when subjected to the high pressure cold LO_2. A discussion of this incident is covered in Appendix F.

Several significant items resulted from the injector incident that affected future testing. These items primarily pertained to the start sequence/logic used. Some of the more significant changes were:

(1) The continue signals used in the logic network were implemented with a fail-safe feature, causing the automatic sequence to go into cutoff if the continue signal was picked up prematurely.

(2) The ASI operation was extended for one second to ensure main combustor ignition. This was later changed back to termination at the main chamber pressure continue signal.

(3) The addition of a more effective LO_2 bleed system was implemented to permit adequate pretest chilldown of the system.

(4) The removal of the LO_2 flow meter and the addition of a LO_2 cavitating venturi to eliminate the significant pressure overshoot realized by a no-resistance start system.

On 5 October 1977, having fabricated a new injector and conducted all the leak tests and proof tests necessary to establish injector integrity, test 033 was conducted. This test was to actively define the LO_2 system characteristics, (feed system and injector priming) and LO_2 temperature vs time relationship. All timers and continue signals used during this test reflected the values determined for satisfactory hot fire test operation. The test results were analyzed and showed the test satisfactorily demonstrated dual ASI ignition, a full pressurized sequence check, instrumentation check and LO_2 manifold priming times. These test results were used to establish the requirements for the next hot fire test.

The next test attempt (034), was to demonstrate injector priming and main combustor ignition. The amount of reactant permitted in the combustor was restricted by limiting the opening of the fuel and oxidizer valves. The basic start sequence was followed until fuel valve operation. The main fuel valve signal was used to energize the mainstage timer and was set to initiate cutoff in 500 msecs from the signal. A faulty mainstage timer terminated this test. The fuel valve remained closed, and mainstage ignition did not occur. The timer was modified prior to the next test.

Test 035 (20 October 1977) was a successful test of 1400 msecs duration. Main combustor chamber pressure, (Pc), was established after a smooth ignition transition, fuel priming times were as predicted, and the injector LO_2 quality was better than anticipated. Posttest hardware inspection revealed a substantial carbon deposition over the internal surfaces of the combustor and over a large percentage of the injector face. The posttest data review showed the carbon deposition occurred after the cutoff signal and during the shutdown transition.

Test 036 was conducted on 25 October 1977, and satisfactorily demonstrated main combustor ignition realizing approximately 500 msecs of 30 atm chamber pressure. Analysis of the test data showed a smooth main combustor ignition transition but a fuel rich environment during a portion of the shutdown transition. The shutdown anomaly resulted in a complete carbon coating on the chamber inner surfaces and the injector face. Prior to the next hot fire test, shutdown purge and valve closure sequences were revised to attempt to eliminate this phenomena.

Hot fire test 037 was conducted satisfactorily on 4 November 1977, and realized approximately two seconds of nominal chamber pressure of 30 atm. Analysis of the test data showed a smooth main combustor ignition and mainstage, low characteristic velocity efficiency of 95.5%, and still a period of time during the shutdown transition where a fuel rich environment was evident. The shutdown anomaly resulted in traces of carbon in all four corners and random wall streaks. During a visual posttest inspection, the fuel bleed showed signs of sediment and SPAN-80 droplets. Analysis verified that the droplets were caused by the SPAN-80 surfactant. The contamination observed in the system was a heavy concentration of SPAN-80, which was thought to be in solution with the JP-4. The mixing procedures specified for mixing 7% SPAN-80 by wt in JP-4 permitted the SPAN-80 to migrate to the bottom of the tank without completely going into solution. Laborabory experiments showed a rigorous agitation was required to put the SPAN-80 in solution with the JP-4 and when a mixture was made, any precipitate that settled out had to be removed. This technique was applied to the run tank; that is, draining off the residual on the bottom of the tank, leaving a uniform solution. The remaining solution was analyzed and resulted in a 7% SPAN-80 concentration. The run tank remained dormant for a period of time and was rechecked. A sample showed the fuel was clear with no residue.

The five centimeter fuel feed system was removed and cleaned with a caustic solution. The mixer was flushed through the seed valve and subsequently through the injector assembly. This cleaning operation was then followed by a water rinse and subsequently dried with a GN_2 purge. The cleaned fuel system was reinstalled and was checked periodically to ensure good quality reactant.

Posttest, the solid wall combustor was modified to accommodate four hot gas photocons. Two of these measurements were used during normal testing, a third was incorporated during the stability test series.

Based on the analysis of test 037, the MOV closing time was delayed to increase the LO_2 lag at cutoff in an attempt to further reduce or eliminate the carbon buildup in the combustor.

c. Conclusions

During this development test series, several problems were encountered. The two most significant problems were the photocon attachment degradation and the fuel contamination. Both problems were solved and testing continued satisfactorily. The problem encountered with the sealing/torque retention of the high frequency pressure transducers appeared to be caused by the local relaxation of the copper threads in the solid wall combustor. The contamination was a result of SPAN-80/JP-4 mixture impurities and condensation forming on the internal plumbing surfaces. This was solved by cleaning of the entire fuel system and draining the impurity from the tank.

At the conclusion of this test series, the operational sequence typical parameter values were:

Timing		Continue Signals	
T_1	= 1000 msec	P_1	= 11.2 atm
T_2	= 650 msec	P_2	= 24.8 atm
T_4	= 500 msec	P_3	= 14.6 atm
T_6	= 2400 msec	P_4	= 24.8 atm
T_m	= 3300 msec	VSC	= 100 g P-P for 50 msec

At the conclusion of the operational sequence test series, the typical start-up time from ignition start was 1400 msecs to main Pc continue signal and 840 msecs from the cutoff signal to LO_2 main valve closed. Figures 202 and 203 detail the start and cutoff sequence established after hot fire test. The times illustrated resulted in a smooth start and cutoff transition.

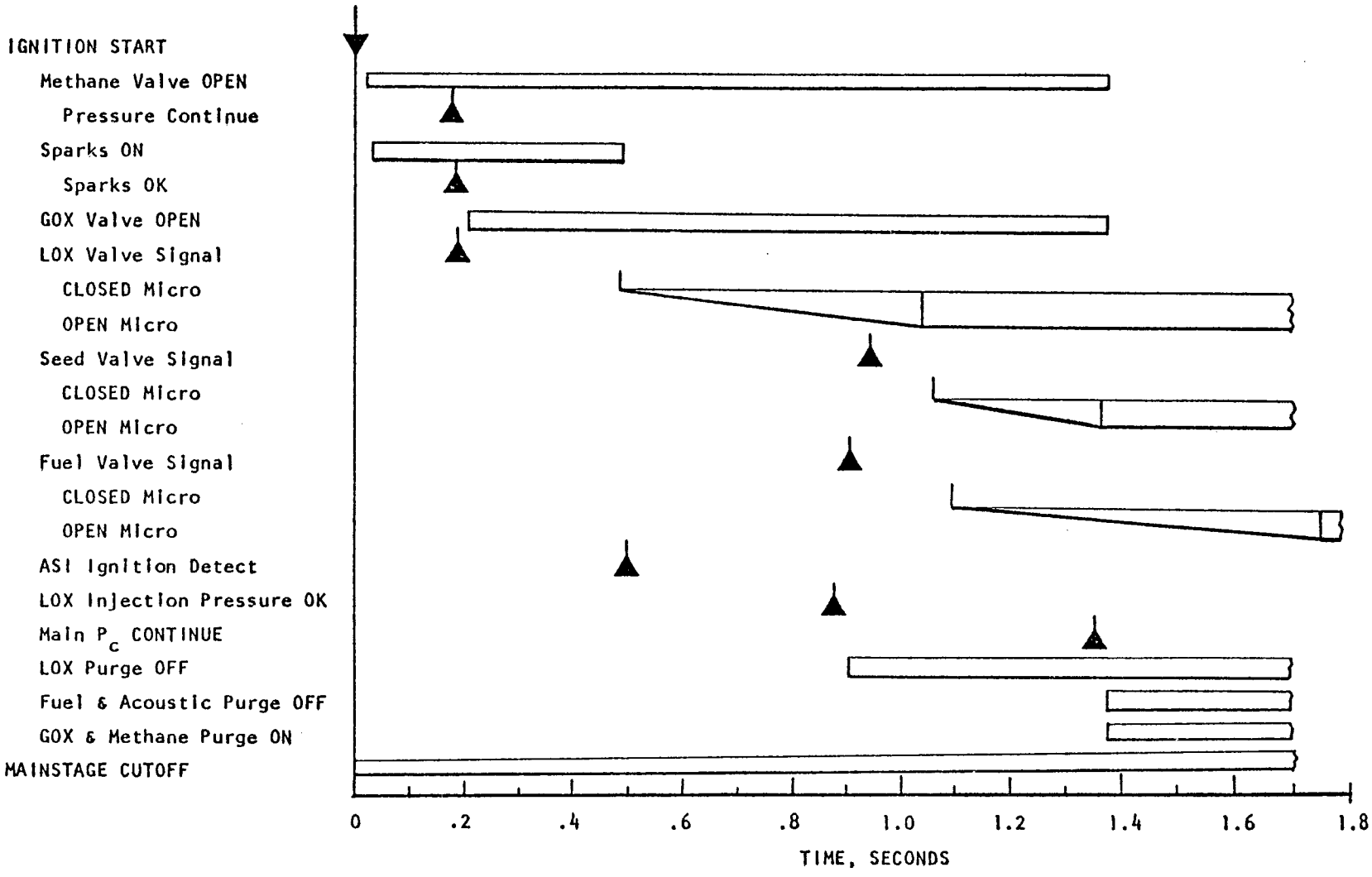

Figure 202. MHD Combustor Start Transition.

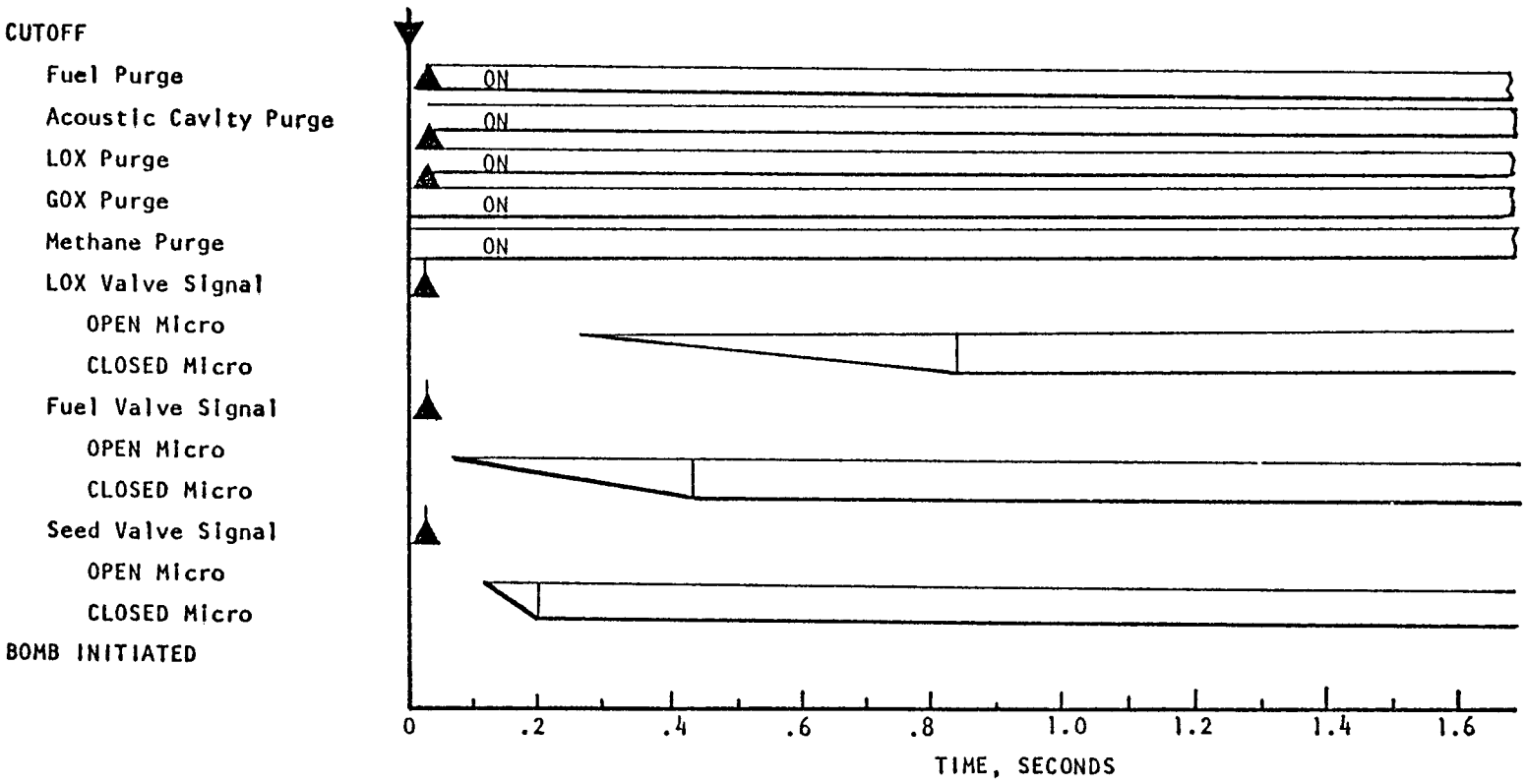

Figure 203. MHD Combustor Shutdown Transition.

The injector was satisfactorily characterized, and the injector pressure drops are illustrated in Figure 204. The oxidizer side of the injector was established at ~105 K, and the fuel side was determined using ambient fuel.

4. Injector Tests

A series of combustor tests were conducted using the basic logic established in the previous section to evaluate the combustor performance at various operational conditions. In an attempt to evaluate the combustor performance at several mixture ratios and chamber pressure levels, seven hot fire tests without seed and five tests with seed were conducted.

Entering into this test series several areas of concern were still prevalent: (1) performance; (2) carbon deposition/wetting on shutdown; (3) stability; and (4) combustor heat load. The combustor performance initially demonstrated resulted in a lower than expected 95.5% characteristic velocity efficiency. This low performance was attributed to the LO_2 flow measuring device. The shutdown procedure was not detrimental on the previous tests but required solving prior to the channel test series. The combustor stability was acceptable by JANNAF criteria, but steps would be taken during this series to attenuate the combustor pressure oscillations.[2] The heat load imposed on the combustor in the previous test series appeared low, and an attempt to resolve the variances in the value was made during this series.

Several problems were encountered during the hot fire series causing substantial delays in the schedule and resultant increased costs. These problems will be discussed in detail in a later section. At the conclusion of this test series, conditions were fixed and the diagnostics channel tests were initiated.

a. Test Setup

The hardware and test setup used for this test series was identical to that described in the previous section. Minor changes were made to the valve sequencing in an attempt to alleviate start/shutdown anomalies realized as testing progressed.

b. Injector Test Description

During the injector development test phase, twelve hot fire tests were conducted to define and characterize the combustor performance at varying mixture ratios, chamber pressure levels, and seed percentages. Throughout this series, updating of the operational logic and sequencing continued. A brief description of the twelve hot fire tests conducted in this effort are as follows.

[2] "Combustion Stability Specifications and Verification Procedures for Liquid Propellant Rocket Engines," CPIA Publication 247, October 1973.

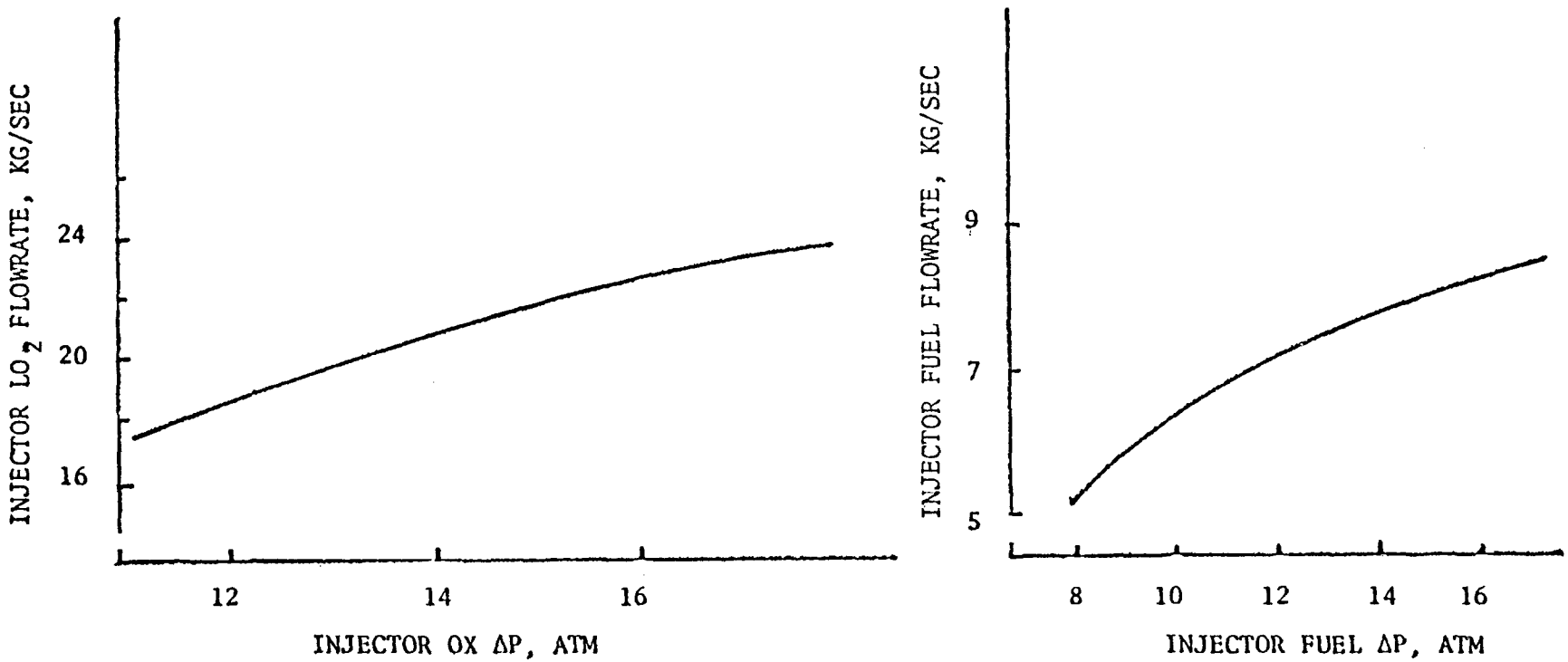

Figure 204. Injector Pressure Drop Summary.

Having cleaned the fuel system after test 037, hot fire test 038 was conducted. This satisfactory test, conducted on 22 November 1977, was run at nominal chamber pressure conditions of 30 atm with two seconds mainstage combustion.

Two hot fire test attempts were made on 29 November 1977, 039 and 040. Test 039 was conducted to demonstrate combustor characteristics at Pc and 3.0 mixture ratio. The test was satisfactory. Test 040 was conducted to demonstrate combustor characteristics at 2.7 mixture ratio. This test was aborted because of a facility procedural malfunction.

The performance of the high power MHD combustor was increased from approximately 95.5% to approximately 98% characteristic velocity efficiency after an in-house recalibration of the LO_2 measuring venturi. The discrepant vendor calibration values were revised and were used in the data reduction program on all subsequent tests.

Of the four hot fire test attempts made during the December period, three were successful. On 5 December 1977, test 041, the second attempt to test the low mixture ratio investigation requirements was completed successfully.

On 5 December 1978, test 042 was attempted and aborted because of a procedural malfunction. The main Pc continue signal was not received, and the test was subsequently terminated by a protective circuit. The circuit switched to a cutoff mode when the continue signal was not satisfied within the predetermined time increment.

Posttest, the LO_2 pressurizing system was analyzed, and a larger pressurizing regulator in the LO_2 tank was installed. On 8 December 1977, two hot fire tests were conducted, 043 and 044, a low Pc and high Pc, respectively. Test 043 was conducted to demonstrate combustor characteristics at 24 atm chamber pressure, and 3.34 mixture ratio. The test was successful but showed a delay in opening of the ASI methane solenoid valve by 260 msecs. Prior to the next hot fire test, the valve was replaced. Test 044 was conducted to demonstrate high Pc 36 atm combustor characteristics at 3.34 mixture ratio. This test was successful, but a decreasing chamber pressure with time caused by a decaying LO_2 tank pressure occurred. This anomaly was rectified by removing the check valve from the system. Posttest, a small copper movement in the throat was observed, this area was subsequently blended with no visible discontinuity evident. Several modifications were made to minimize recurrence: (1) the combustor pressure was reduced to a nominal value; (2) the nozzle throat coolant flow was increased; and (3) the injector was flushed and subsequently water flowed verifying unobstructed orifice flow.

Based on the past hot fire tests, the elimination of the posttest carbon deposition and residual fuel wetting appeared to be an anomaly that could not be simply corrected by modifications to the shutdown sequence or by adjusting the GN_2 purge pressures. From the test data the problem appeared to arise from the various liquid traps evident in the horizontal firing test hardware. A possible explanation for this phenomena was that during the expulsion of the residual fuel, carbon was being formed and rapidly deposited on the combustor walls. Once the combustion flame had been extinguished, the incoming fuel dribbled into the combustor and was either being cracked on the hot surface depositing carbon or wetting the walls. An analysis of the problem resulted in the requirement for an increased GN_2 purge flow rate capable of maintaining the injector design face pressures differentials during the shutdown sequence.

In order to implement this modification, the main fuel valve was reworked. A 2.5 cm purge system was installed to permit the attainment of this increased flow rate without exceeding the fuel manifold operating pressures. This modification eliminated the posttest fuel wetness and carbon deposition present in all of the earlier tests.

In preparation for the next series of tests, the cesium carbonate seed solution was mixed. Tanking was initiated on 12 December 1977, but before the tanking was completed, a 10 μ inlet filter clogged. The residue found in the filter was analyzed and found to contain cesium bicarbonate, calcium carbonate, aluminum, rhobidium, silicon, etc. All contaminants were listed in the certification impurities sheet. Further investigations involving electron microprobe X-ray spectrometry, X-ray diffraction, atomic absorption and infrared spectrophotometry revealed that two basic types of residue were encountered: (1) fallout of cesium carbonate caused by temperature cycling, and (2) the presence of an insoluble impurity in the technical grade cesium carbonate as received. Proper filtering of the solution removed the impurities, and the results showed that a stable solution remained.

On 9 January 1978, two hot fire test attempts were made, 001 and 002. The first test, conducted with $\approx 5\%$ by mass $Cs_2\ CO_3$ was successful and resulted in $\approx 0.5\%$ increase in the characteristic velocity efficiency.

The second test, which was with 10% by mass $Cs_2\ CO_3$ seed, was terminated during the startup transition by the fail safe circuitry when the main Pc buildup was not achieved in the predetermined time increment. The posttest analysis showed that the pressure transducer port used to satisfy this requirement was restricted by carbon buildup.

On 13 January 1978, the first stability test attempt was made. At 490 msec after the main Pc continue signal was received, the first bomb detonation signal was sent. Immediately on detonation of the 10 grain bomb, unstable combustion was realized at 2800 Hz, the first transverse mode in the long or vertical direction.

The test conditions realized to identify the potential dynamic instabilities were: (1) Pc = 30.2 atm; (2) M/R = 3.38; and (3) $Cs_2 CO_3$ = 9.96% by mass. The test was scheduled for 2.5 sec mainstage with two bombs scheduled to be detonated at 500 and 1500 msec after attaining main Pc. At 1770 msec after ignition start, the first of two pyrotechnic bombs was electrically initiated to generate a pressure pulse. The damping or lack of damping of this pulse was a measure of the dynamic stability of the combustor.

Immediately following the bomb initiation, large amplitude pressure oscillations began. The vibration safety cutoff (VSC), which was monitoring an accelerometer mounted on the injector, initiated cutoff when the accelerometer measured more than 100 g for 50 msec. The shutdown occurred at approximately 750 msec after the bomb initiation. During this period the combustor pressure oscillations were severe and accelerometer readings were greater than 200 g.

Posttest inspection revealed that the second bomb mounted in the combustor had detonated. The bomb was not initiated by the control system and was presumed to have been thermally ignited. The ignition time could not be identified from the test records.

The hardware was inspected after disassembly and photographs of the hardware damage were taken. The damage assessment was: (1) minor erosion of the combustor on inlet edge at the top and bottom adjacent to the acoustic cavity; (2) significant erosion damage to the acoustic cavity spacer in top and bottom cavities, minor erosion in side cavities; and (3) minor erosion on top and bottom edge of the injector adjacent to the acoustic cavity with considerable slag in the cavities.

In order to completely assess the injector damage, the injector was cleaned, and the top and bottom edges were beveled. After this operation, the injector assembly was subjected to a 110 atm dynamic proof test on the fuel side and visually inspected and then subjected to a 7.8 atm helium leak check. After the leak check, the injector assembly was flow checked, and both manifolds were flow checked to quantitatively establish free orifice flow and good impingement.

High frequency pressure measurements were made at five locations: three combustor positions, the fuel manifold, and the LO_2 manifold. In addition, three three accelerometer readings were recorded. A review of this data showed that the

instability was a classical combustion instability. No feed system coupling was observed. The instability occurred at a frequency of 2800 Hz, which corresponded to the first transverse mode of the combustor in the longer or vertical dimension. This was corroborated by the fact that the top and bottom regions of the injector incurred the most damage.

Subsequent to this test, a series of injector modifications and acoustic suppression methods were reviewed for use in suppressing the 2800 Hz instability.

An overall review of the gas generator stability problem was held on 25 January 1978. A major area of discussion was: (1) redesign of the stability aid for maximum damping at 2800 Hz or (2) redesign to provide increased damping at each of the major resonant frequencies. An approach which provided increased damping was selected.

In order to demonstrate combustor/injector integrity with the revised acoustic cavity prior to the diagnostics channel installation, two tests were conducted. On 24 February 1978, tests 004 and 005 were successfully conducted. The hot fire test demonstration of the modified acoustic cavity configuration resulted in the demonstration of stable engine operation and a performance evaluation with 10% by mass $Cs_2 CO_3$. The posttest evaluation after the first test showed some cavity erosion damage. This was primarily in the steel spacer lower cavity and the related dams. Minimal damage was realized in the top or side cavities. The second test, mainstage was reduced to 1.5 sec, and the test was successfully conducted. Posttest, the erosion damage was again observed. This time most of the increased erosion was concentrated in the upper cavity. An assessment of the hardware was made, and a decision to remove the injector resulted.

The injector was removed and the erosion damage was evaluated. All the damage was confined to the steel acoustic cavity spacer/enclosure with no erosion damage present on the copper combustor or injector. A review of the data and hardware initiated a new design concept. The acoustic cavity spacer redesign consisted of an OFHC cooled copper insert in a 321 steel mounting flange.

The posttest data evaluation showed no change in combustor characteristic velocity efficiency, but did show an operating combustor more stable than previously realized, over a range of mixture ratios from 2.97 to 3.4. The revised acoustic cavity absorber, although increasing cavity gas recirculation, had a significant attenuating effect on the combustor pressure oscillations.

c. Combustor Performances

The combustor performance was measured in terms of a characteristic velocity efficiency. The pressure was measured as a static wall pressure in the constant area section of the combustor and corrected to a nozzle stagnation value using a theoretical correction. The reactant flow rates were measured individually using calibrated venturi flow meters.

Values of characteristic velocity efficiency for several tests are presented in Figure 8. Three effects were noted. First, the efficiency decreased as mixture ratio was decreased. Since the momentum ratios of the injector elements were selected at a mixture ratio of 3.4, this decreased efficiency at off design mixture ratios was not unexpected. Second, combustion efficiency increased when the seed solution was added. This increase of 0.8% occurred in a test with the cesium carbonate solution amounting to 5% of the total flow or approximately 20% of the fuel flow. Third, the efficiency value of $\approx 98.5\%$ at the 3.1 mixture ratio was very high for LO_2/hydrocarbon combustors. Rocket engine combustors, which have undergone extensive development using LO_2/RP-1, have had characteristic velocity efficiencies several percent lower than this value. This high efficiency was attributed to the injector orifices which were a factor of two smaller than in previous LO_2/hydrocarbon injectors.

A plot of the static wall pressure measurements in the combustor is presented as Figure 9. Prior to the contraction section, the major mechanism for pressure drop was the heat addition resulting from combustion. The pressure profile, therefore, gave an indication of the completeness of the combustion. The pressure profile indicated that the major portion of the combustion occurred within 25-30 cm of the injector. This indicated that the pressure measurement at the 48 cm point, which was used in the c* calculations, should have been a reliable indicator of ηc^*, and that there was some potential for reducing combustor length.

d. Heat Transfer

In addition to the thermal data calculated and presented in the data printout, a more extensive and precise analyses was conducted. Data was taken on all tests and has been processed.

The experimental gas side heat transfer coefficients were determined from temperature measurements at the eleven "heat flux" meters located along the combustor wall. In these measurements, temperatures at a point approximately 2.5 to 3.0 cm from the hot gas wall were measured as a function of time.

These temperatures were compared to a transient thermal analysis based on a series of probable film coefficients and keyed to the actual combustor operating sequence. By matching the temperature data profile to a given predicted profile, a gas film coefficient was inferred.

A sample film coefficient profile is illustrated in Figure 205. Because of the limited space, this type of measurement was not possible at the throat. By scaling the measurements with theoretical profile the throat values are approximately 60% of the values initially predicted for LO_2/JP-4. The following text documents the results of all tests run to date with a 68.6 cm long combustor.

The results of the tests indicated that the mixture ratio definitely affected the heat load to the combustor and the gas side heat transfer coefficient. Results of tests with 4% to 5.2% by mass $Cs_2\ CO_3$ resulted in a heat transfer coefficient, in the convergent zone, of 0.303 w/cm^{2}K and 0.371 w/cm^{2}K for mixture ratios of 3.01 and 3.28, respectively. (See Figure 206). Also, the results of the 10% Cs_2CO_3 seed in fuel indicated the gas side heat transfer coefficients to be in the convergent zone, 0.268 w/cm^{2}K and 0.394 w/cm^{2}K for mixture ratios of 2.98 and 3.40, respectively. (See Figure 207).

The throat and nozzle exit heat loads, which were determined by the cooling water temperature change, were plotted against the mixture ratio, and the highest mixture ratio was observed to have caused the maximum heat loss. Added cesium carbonate solution in the fuel caused the heat transfer coefficient to increase. The test results showed that the experimental heat transfer coefficient with 10% of the mass flow $Cs_2\ CO_3$ and with the mixture ratio above 3.0 can be as high or higher than the values predicted by the boundary layer for the combustion zone. The effect of the seed solution percentage for the fuel was not as great in the nozzle as it was in the combustor although an effect of mixture ratio was still present. The exit nozzle coolant passage data was reduced for all tests and plotted. The results agreed with the data of heat flux meters #10 and #11.

The results of the tests with 5% of the mass flow being $Cs_2\ CO_3$ indicated that for a mixture ratio of 3.0, the heat transfer coefficient of 0.235 w/cm^{2}K were about 67.7% and 73.8% of the predicted value in the combustion zone and in the nozzle, respectively.

If the combustor had been designed for a mixture ratio of about 2.8 to 2.9 and a 5% by mass $Cs_2\ CO_3$, the possibility of a short regeneratively cooled combustor with a length of 33-36 cm upstream of the throat would have been feasible. In order for the exact combustor length allowable to be determined, a detailed thermal analysis must be completed to define the wall temperatures, fuel bulk temperature and pressure drop.

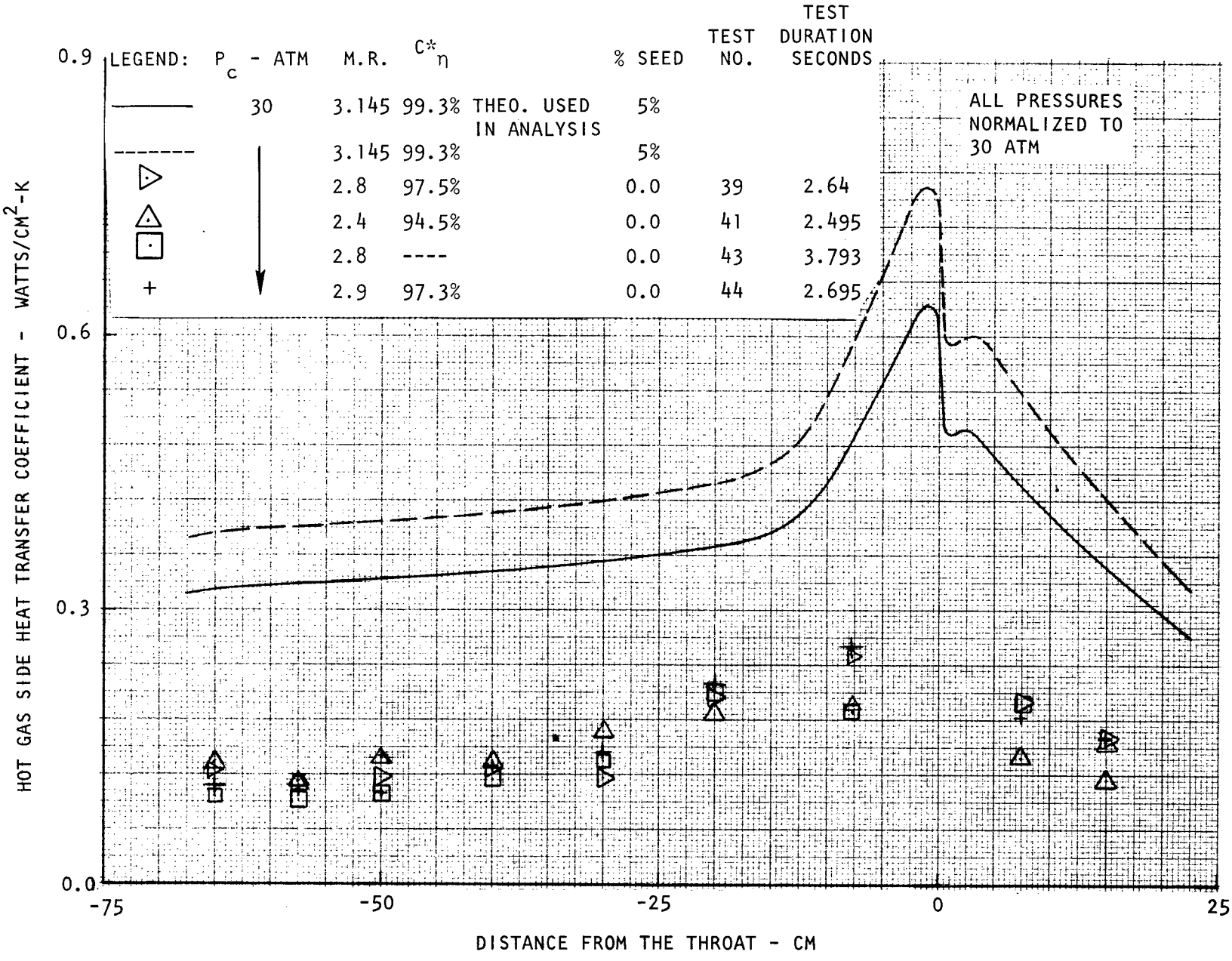

Figure 205. Hot Gas Side Heat Transfer Coefficient vs Distance From the Throat for the 30 MW MHD Hot Gas Generator

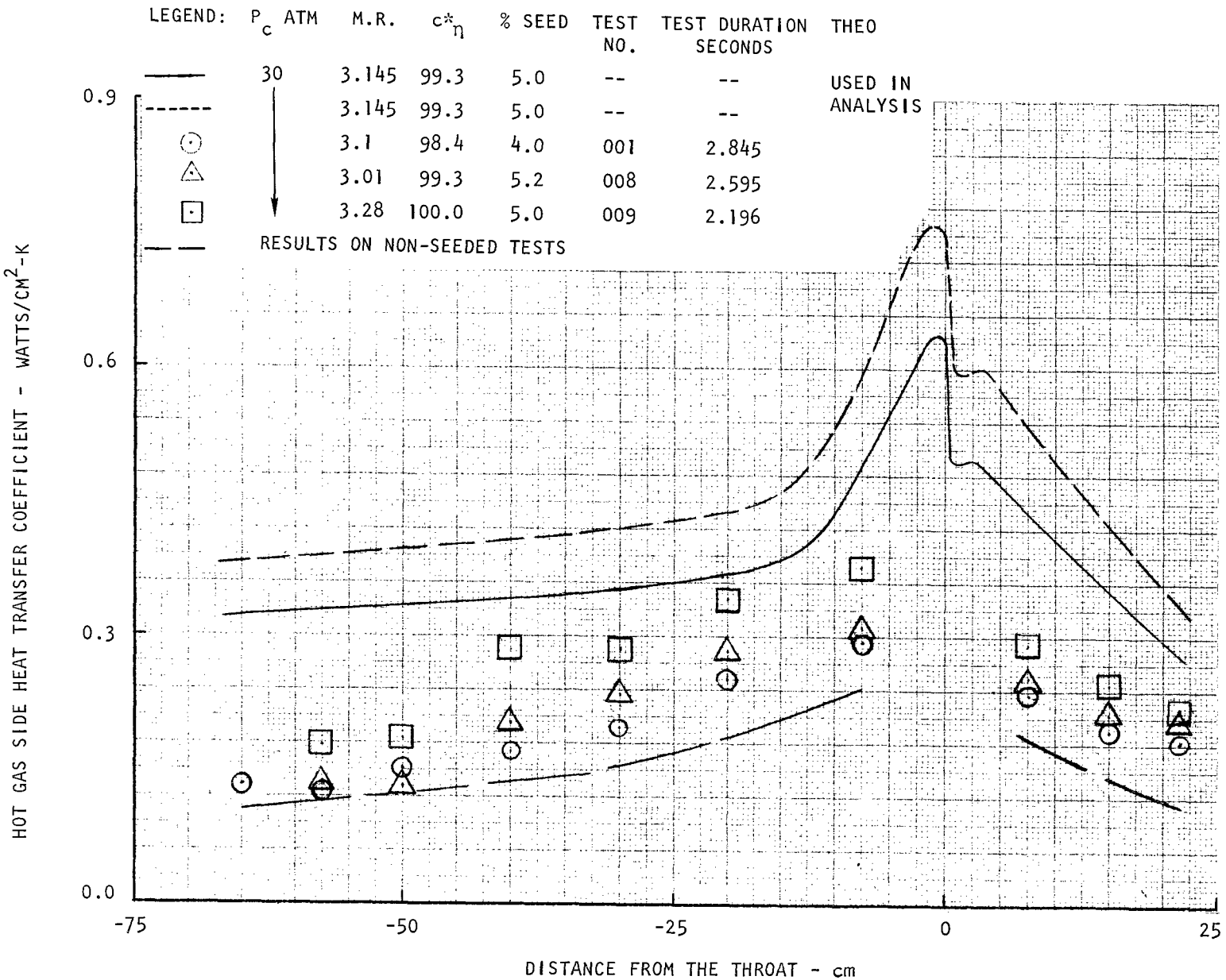

Figure 206. Hot Gas Side Heat Transfer Coefficient vs Distance From the Throat for the 300 MW MHD Hot Gas Generator

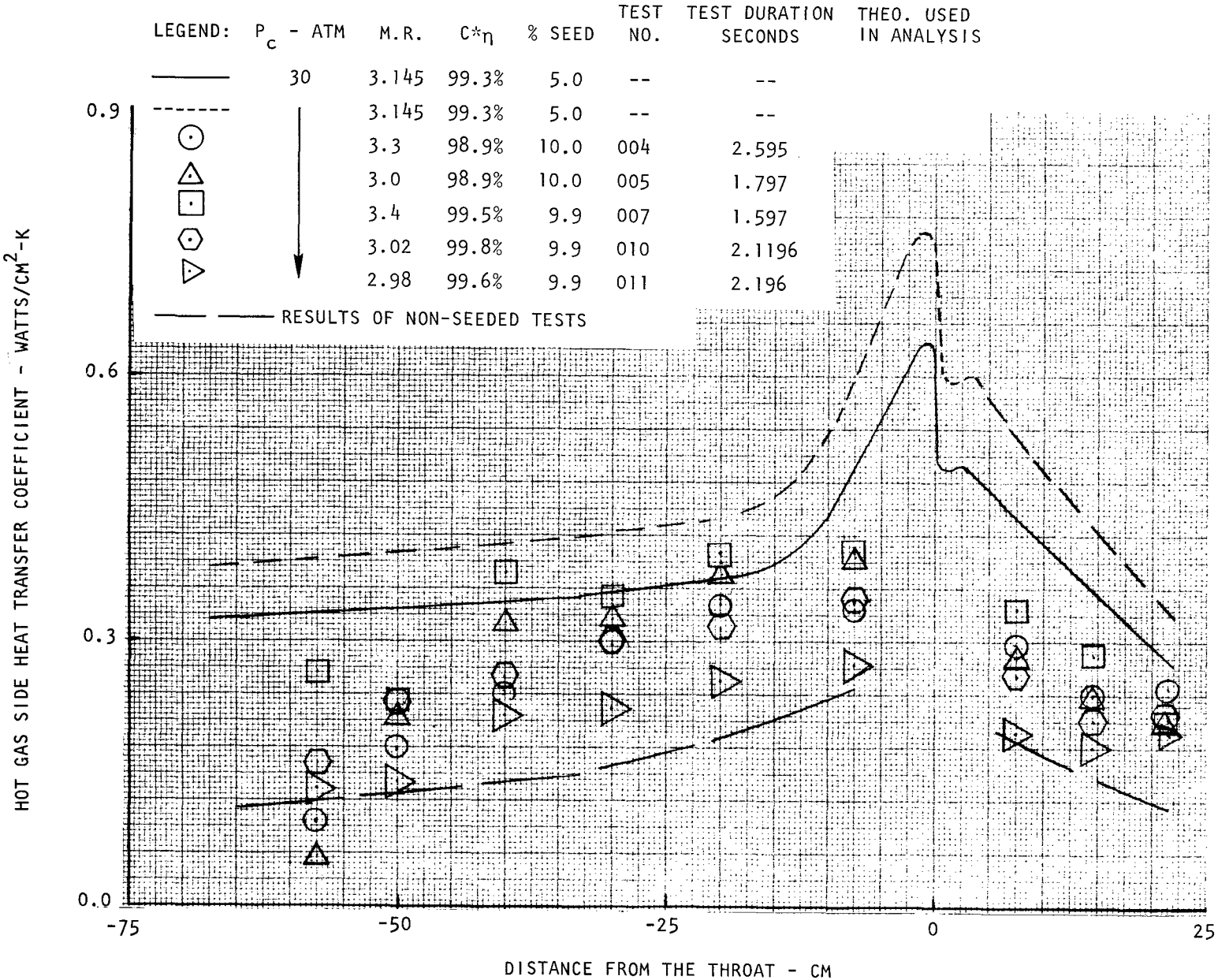

Figure 207. Hot Gas Side Heat Transfer Coefficient vs Distance From the Throat for the 30 MW MHD Hot Gas Generator

The data of the diagnostic channel tests were reduced and in the early part of the test, the experimental data was observed to fall above the curve indicating a heat transfer coefficient higher than 0.294 w/cm^{2}K. As time increased the test data crossed the analytical curve. The slope of the experimental curves tended to decrease with time almost from the start. The extent and time of the crossover depended on the mixture ratio. A typical heat flux meter profile is presented in Figure 208 and shows the crossover.

Test 007 was conducted at a mixture ratio of 3.4 and contained 10% by mass $Cs_2 CO_3$ in solution. The results of the tests were plotted, and the test data followed the curve of the analytical results very well and no line crossing took place. Although test 007 was only 1.497 sec in duration, the experimental data of other tests at lower mixture ratios indicated the analytical curve was crossed well below 1.597 sec. Therefore, at the low mixture ratios the carbon deposition on the wall did indeed occur, which led to the reduction of heat transfer coefficient with time. Again, the effect of mass flux on carbon deposition was evidenced by the fact that, even for low mixture ratio tests, the extent of crossover was less severe in the higher mass flux region (convergent zone).

The data for the nozzle exit coolant passage was reduced to determine the heat transfer coefficient at the nozzle exit. The raw data consisted of the water flow rate and the water bulk temperature rise as a function of time. The heat removed by the water was $Q = \dot{m}\, C_p(T_2-T_1)$[watts].

The length associated with this coolant passage was 2.5 cm in the axial direction which, when multiplied by the periphery, gave an area equal to 211.2 cm^2. The minimum coolant wall thickness was 0.64 cm and its diameter was 1.55 cm. The coolant side heat transfer coefficient was determined by means of

$$h_c = 1.47\,(N_{Re})^{0.95}(N_{Pc})^{0.4}\ \frac{K}{D}\ \left[\frac{\text{watts}}{\text{cm}^2\text{K}}\right]$$

The overall heat transfer coefficient, U, was:

$$U = \frac{1}{\frac{1}{hg} + \frac{X}{K} + \frac{1}{hc}}\ ;$$

and can also be determined by:

$$U = \frac{Q/A}{\Delta T}$$

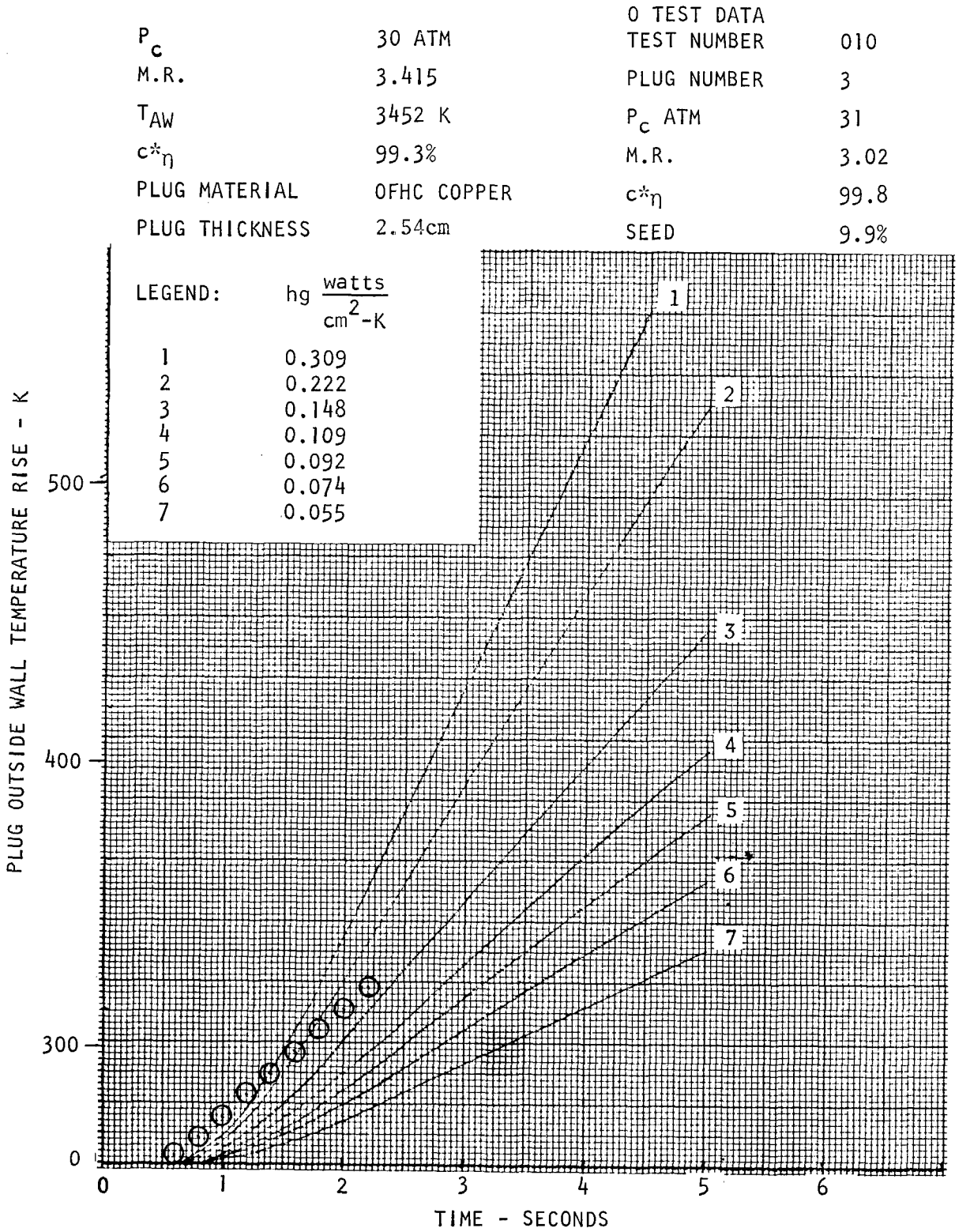

Figure 208. Plug Outside Wall Temperature Rise vs Time for the 30 MW MHD Gas Generator Heat Flux Meter in the Combustion Zone

Since the hot gas and the water temperatures were known, the calculation of ΔT could be made. The value of Q/A was simply determined from

$$Q/A = \frac{\dot{m} C_p (T_2 - T_1)}{211.2} \left[\frac{\text{watts}}{\text{cm}^2}\right]$$

An average wall thickness of 0.89 cm was assumed for the coolant passage. Therefore, having U, X/K, and $1/h_c$ the value of hg was calculated for each test. The heat transfer coefficient determined for the nozzle exit coolant passage was plotted for X = 21.9 cm. In the appropriate figures good agreement between the results of heat flux meters 10 and 11 and the coolant passage data was observed. Since the maximum resistance to heat transfer occurred on the hot gas side (in general about 90% of total), a slight error in coolant wall thickness assumption would not affect greatly the value of the heat transfer coefficient determined by this method.

Test Result. The results of tests 007, 008, 009, 010, and 011 are tabulated in Tables 62 through 66. Figure 209 shows the results of non-seeded tests 039, 041, 043, and 044. Also, the data collected by means of nozzle exit coolant passage are plotted in this figure at X = 21.9 cm. Very good agreement existed between the heat flux meter data and the coolant passage data.

The results of various tests are plotted in Figure 210 for the 4% to 5.2% by mass $Cs_2 CO_3$. Again a fairly good agreement was obtained in the nozzle between data collected by means of heat flux meters and the calorimeter. The effect of mixture ratio is again evident with test 009 having the highest mixture ratio, 3.28, resulting in the highest heat transfer coefficient. The heat transfer coefficients of 0.371 w/cm^2K were about 77.3% and 72.99% of the predicted values in the combustion zone and in the nozzle, respectively, for test 009.

The results of tests 004, 005, 007, 010, and 011, which were for 10% by mass $Cs_2 CO_3$ solution, are plotted in Figure 207. The calorimetric data for these tests are also plotted at X = 21.9 cm. Figure 207.shows that in the combustion zone the result of test 007 with a mixture ratio of 3.4 on the average was about the same as was predicted (solid line) for the 5% Cs_2CO_3 seed condition. Again, the effect of mixture ratio was quite evident when the results of test 007 (MR of 3.4) and test 011 (MR of 2.98) were compared. For example, in the convergent zone, the heat transfer coefficients showed an increase of 46%. The influence of mixture ratio was also noticed in the nozzle where from the throat to 14.7 cm, the heat transfer coefficients were 0.277 $w/cm^2 K$ and 0.175 $w/cm^2 K$ for mixture ratios of 3.4 and 2.98, respectively.

TABLE 62. PRELIMINARY RESULTS OF TEST 007

FOR THE HIGH POWER MHD GAS GENERATOR

Pc = 30.6 atm MR = 3.40 $\eta_c{}^*$ = 99.5% Seed % = 9.9

Plug No.	Distance From Injector Face (cm)	Uncorrected hg ($w/cm^2 K$)	T_O (K)	T_{AWC} (K)	T_{WGT} (K)	Corrected hg ($w/cm^2 K$)
1C	2.54	Not Recorded	3453			
2C	10.2	0.2586	3453	3395	542	0.2586
3C	17.8	0.2215	3453	3395	503	0.2259
4C	27.9	0.3698	3453	3395	658	0.3777
5C	38.1	0.3401	3453	3395	549	0.3468
6C	48.0	0.3921	3453	3395	682	0.4004
7C	60.7	0.3921	3453	3395	686	0.4004
8S	60.7	0.0865	3453	3395	357	0.0882
9S	60.7	0.3806	3453	3395	676	0.3886
10C	76.3	0.3253	3453	3353	611	0.3371
11C	83.4	0.2733	3453	3343	557	0.2839

$$hg_c = hg_M \frac{T_O - T_{WGM}}{T_{AWM} - T_{WGM}}$$

C - Contour Wall; S - Side Wall

hg_c - Corrected hg for $\eta_c{}^*$

hg_M - Measured hg

T_O - Theoretical T

T_{AWM} - Measured T_{AW}

T_{WGM} - Measured T_{WG}

T_{AWC} - $T_{AW(corrected)}$

T_{WGT} - $T_{WG(test)}$

TABLE 63. PRELIMINARY RESULTS OF TEST 008

FOR THE HIGH POWER MHD GAS GENERATOR

Pc = 30.5 atm MR = 3.01 η_c* = 99.3% Seed % = 5.2

Plug No.	Distance From Injector Face (cm)	Uncorrected hg ($w/cm^2 K$)	T_O (K)	T_{AWC} (K)	T_{WGT} (K)	Corrected hg ($w/cm^2 K$)
1C	2.54	Not Recorded	3453			
2C	10.2	0.1362	3453	3466	467	0.1356
3C	17.8	0.1285	3453	3466	456	0.1280
4C	27.9	0.2033	3453	3466	558	0.2024
5C	38.1	0.2362	3453	3466	606	0.2350
6C	48.0	0.2844	3453	3466	672	0.2890
7C	60.7	0.3112	3453	3466	719	0.3097
8S	60.7	0.2018	3453	3466	558	0.2009
9S	60.7	0.3056	3453	3466	710	0.3042
10C	76.3	0.2512	3453	3423	628	0.2539
11C	83.4	0.2106	3453	3413	569	0.2136

$$hg_c = hg_M \frac{T_O - T_{WGM}}{T_{AWM} - T_{WGM}}$$

C - Contour Wall; S - Side Wall

hg_c - Corrected hg for η_c*

hg_M - Measured hg

T_O - Theoretical T

T_{AWM} - Measured T_{AW}

T_{WGM} - Measured T_{WG}

T_{AWC} - $T_{AW(corrected)}$

T_{WGT} - $T_{WG(test)}$

TABLE 64. PRELIMINARY RESULTS OF TEST 009
FOR THE HIGH POWER MHD GAS GENERATOR

Pc = 31.3 atm MR = 3.28 η_c* = 100% Seed % = 5.0

Plug No.	Distance From Injector Face (cm)	Uncorrected hg ($w/cm^2 K$)	T_O (K)	T_{AWC} (K)	T_{WGT} (K)	Corrected hg ($w/cm^2 K$)
1C	2.54	Not Recorded	3453			
2C	10.2	0.1847	3453	3507	508	0.1815
3C	17.8	0.1921	3453	3507	517	0.1886
4C	27.9	0.2956	3453	3507	647	0.2900
5C	38.1	0.2956	3453	3507	647	0.2900
6C	48.0	0.3551	3453	3507	719	0.3483
7C	60.7	0.3921	3453	3507	781	0.3845
8S	60.7	0.1441	3453	3507	456	0.1415
9S	60.7	0.3689	3453	3507	753	0.3615
10C	76.3	0.2956	3453	3463	647	0.2945
11C	83.4	0.2512	3453	3453	594	0.2512

$$hg_c = hg_M \frac{T_O - T_{WGM}}{T_{AWM} - T_{WGM}}$$

C - Contour Wall; S - Side Wall

hg_c - Corrected hg for η_c*
hg_M - Measured hg
T_O - Theoretical T
T_{AWM} - Measured T_{AW}
T_{WGM} - Measured T_{WG}
T_{AWC} - $T_{AW(corrected)}$
T_{WGT} - $T_{WG(test)}$

TABLE 65. PRELIMINARY RESULTS OF TEST 010
FOR THE HIGH POWER MHD GAS GENERATOR

Pc = 31 atm MR = 3.02 η_c* = 99.8% Seed % = 9.9

Plug No.	Distance From Injector Face (cm)	Uncorrected hg (w/cm^2 K)	T_O (K)	T_{AWC} (K)	T_{WGT} (K)	Corrected hg (w/cm^2 K)
1C	2.54	Not Recorded	3453			
2C	10.2	0.1627	3453	3435	481	0.1636
3C	17.8	0.1774	3453	3435	499	0.1786
4C	27.9	0.2586	3453	3435	602	0.2603
5C	38.1	0.2733	3453	3435	619	0.2750
6C	48.0	0.3180	3453	3435	675	0.3200
7C	60.7	0.3459	3453	3435	719	0.3483
8S	60.7	0.1238	3453	3435	428	0.1244
9S	60.7	0.3459	3453	3435	719	0.3483
10C	76.3	0.2586	3453	3392	602	0.2642
11C	83.4	0.2068	3453	3383	536	0.2118

$$hg_c = hg_M \frac{T_O - T_{WGM}}{T_{AWM} - T_{WGM}}$$

C - Contour Wall; S - Side Wall

hg_c - Corrected hg for η_c*
hg_M - Measured h_g
T_O - Theoretical T
T_{AWM} - Measured T_{AW}
T_{WGM} - Measured T_{WG}
T_{AWC} - $T_{AW(corrected)}$
T_{WGT} - $T_{WG(test)}$

TABLE 66. PRELIMINARY RESULTS OF TEST 011
FOR THE HIGH POWER MHD GAS GENERATOR

Pc = 30.7 atm MR = 2.98 η_c* = 99.6% Seed % = 9.9

Plug No.	Distance From Injector Face (cm)	Uncorrect hg (w/cm^2 K)	T_O (K)	T_{AWC} (K)	T_{WGT} (K)	Corrected hg (w/cm^2 K)
1C	2.54	Not Recorded	3453			
2C	10.2	0.1324	3453	3420	441	0.1338
3C	17.8	0.1400	3453	3420	450	0.1415
4C	27.9	0.2142	3453	3420	544	0.2165
5C	38.1	0.2215	3453	3420	556	0.2239
6C	48.0	0.2512	3453	3420	593	0.2541
7C	60.7	0.2709	3453	3420	621	0.2742
8S	60.7	0.0691	3453	3420	353	0.0697
9S	60.7	0.2768	3453	3420	628	0.2800
10C	76.3	0.1921	3453	3378	517	0.1971
11C	83.4	0.1739	3453	3369	494	0.1789

$$hg_c = hg_M \frac{T_O - T_{WGM}}{T_{AWM} - T_{WGM}}$$

C - Contour Wall; S - Side Wall

hg_c - Corrected hg for η_c*
hg_M - Measured h_g
T_O - Theoretical T
T_{AWM} - Measured T_{AW}
T_{WGM} - Measured T_{WG}
T_{AWC} - $T_{AW(corrected)}$
T_{WGT} - $T_{WG(test)}$

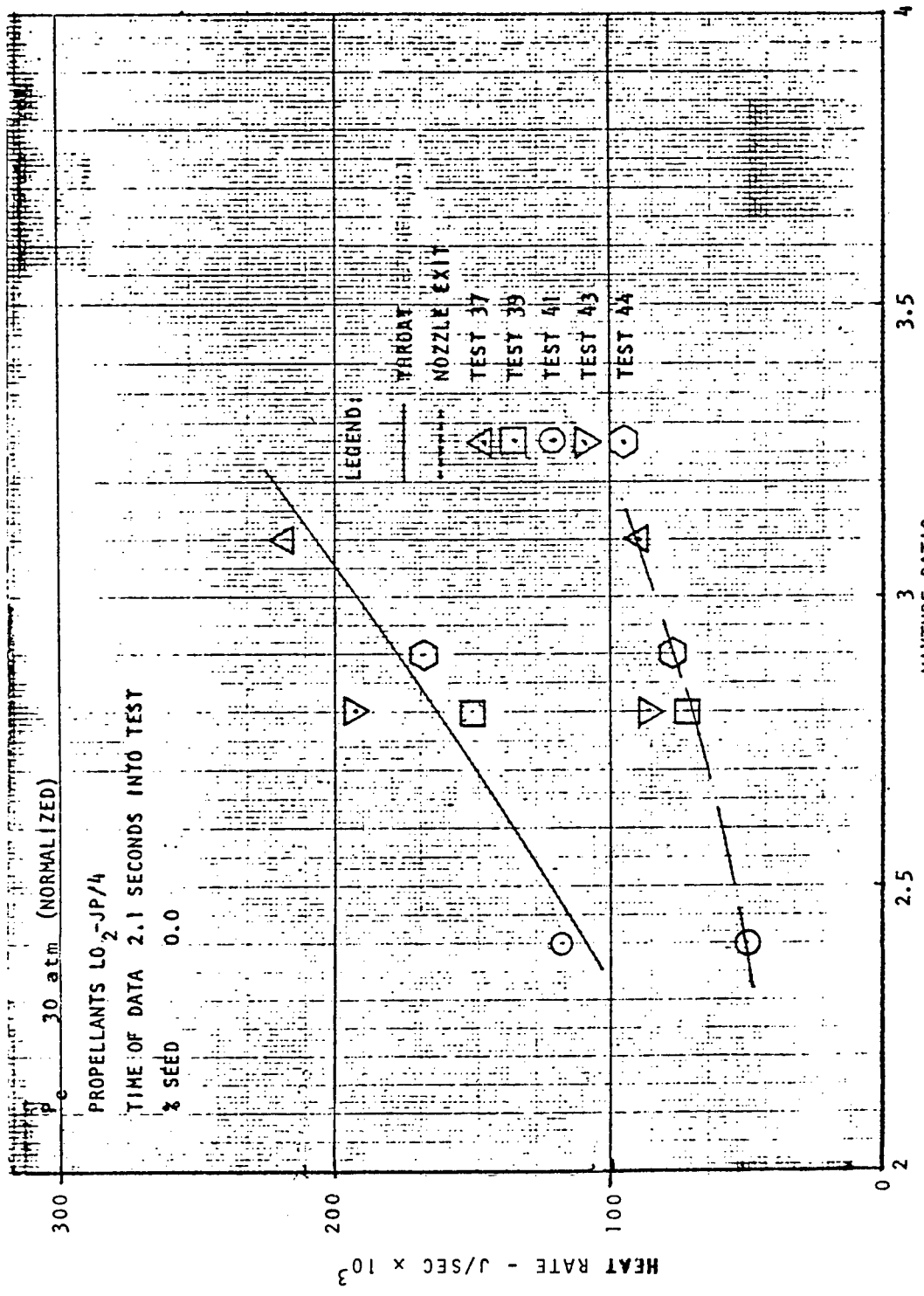

Figure 209. Heat Rate vs Mixture Ratio for the Gas Generator.

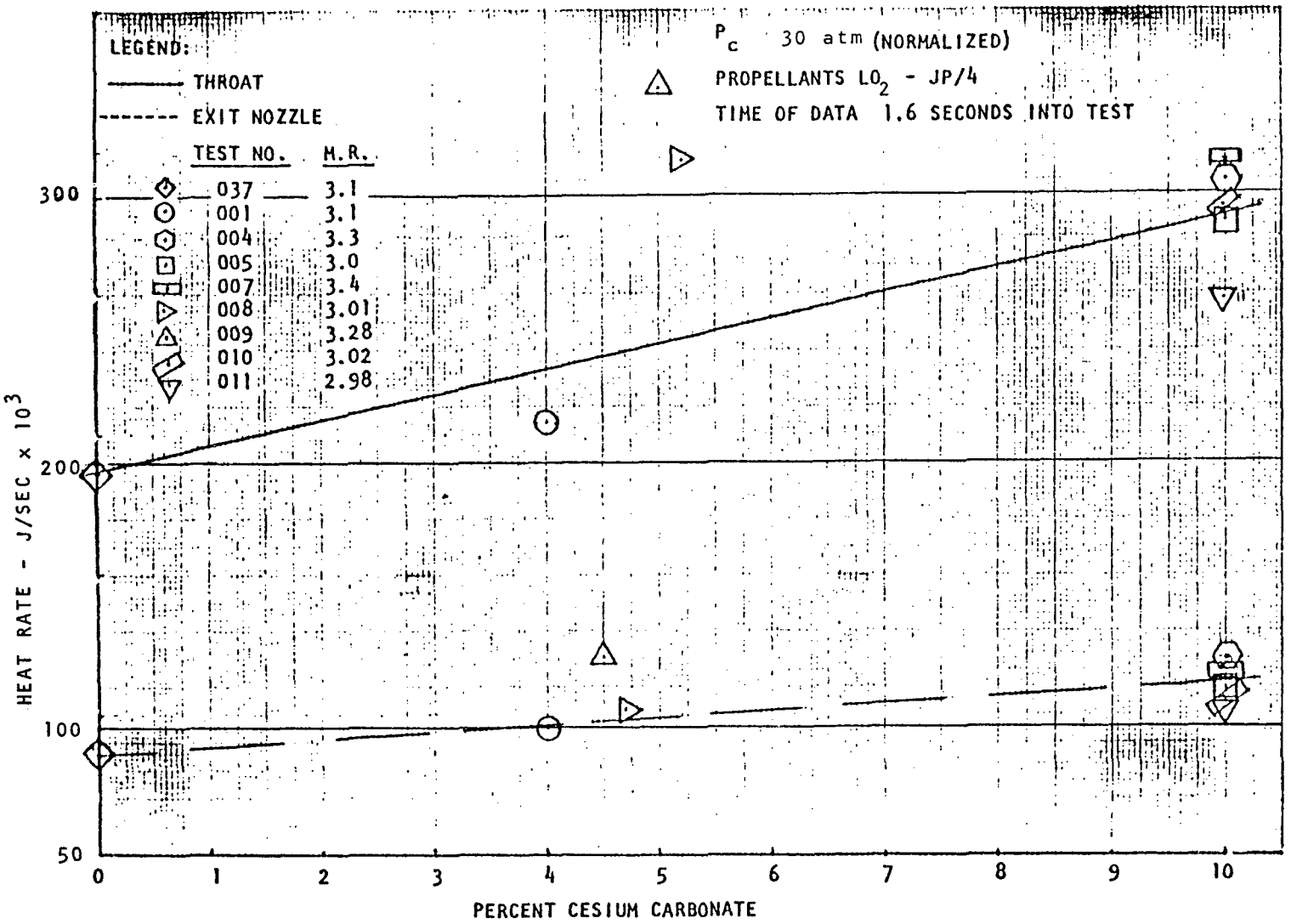

Figure 210. Heat Rate vs Cs_2CO_3 Percentage for the Gas Generator.

Mixture Ratio Effect. Figure 209 shows the effect of mixture ratio on the heat rate both for the throat and for the nozzle exit coolant passages for the non-seeded tests. The high mixture ratio resulted in higher heat loss. This was another confirmation of a resistance buildup to heat transfer at the lower mixture ratios. The reduction in heat flux might very well have been caused by carbon deposit on the wall during the run.

Seeding Effect on Throat and Nozzle Exit Heat Load. A plot of heat load at the throat and nozzle exit vs percent seed, shown in Figure 210, was prepared to evaluate the influence of Cs_2CO_3 seeding on the heat load. The result of test 037 was chosen for non-seeded fuel because the mixture ratio of this test was about the same as the seeded fuel tests. Again, the data for all tests were normalized to a Pc of 30 atm to eliminate the chamber pressure effect. Since test 007 was the shortest duration test, only 1.597 sec, all other heat loads were evaluated at 1.6 sec into the test. Although the data scatter for the throat, the data for the nozzle exit seemed to correlate fairly well. The reason for the heat load increase with seeding was not clear at this time. The seeding, however, was assumed to cause either an increased radiation heat flux, a reduced thickness of carbon buildup on the wall, or added heat because of particle impingement.

e. Combustor Stability

The high power MHD combustor was designed originally to contain acoustic slots around the entire injector periphery as shown in Figure 211. These slots were tuned to damp pressure oscillations corresponding to the 1T mode of instability, either 2819 Hz or 3570 Hz. The calculated frequencies for the various chamber acoustic modes are summarized below:

	Order of Mode		
Dimension	1st	2nd	3rd
19.69 cm	2819 Hz	5638 Hz	8457 Hz
15.54 cm	3570 Hz	7140 Hz	10710 Hz
Injector-to-Throat	910 Hz	1820 Hz	2730 Hz

Steady-state LO_2/JP-4 main stage combustion without any Cs_2CO_3 seed showed small but significant pressure oscillations whose predominant frequencies were 4800 Hz and 800 Hz. Tests with 5% and 10% by mass $Cs_2\ CO_3$ seed also showed evidence of the 4800 Hz and 800 Hz oscillations, although at somewhat lower levels. The detonation of an explosive bomb during main stage on a 10% seed test resulted in a sustained 1T mode of instability at 2800 Hz in the 19.69 cm combustor dimension. The high amplitude dynamic instability is shown in the pressure time trace presented in Figure 212.

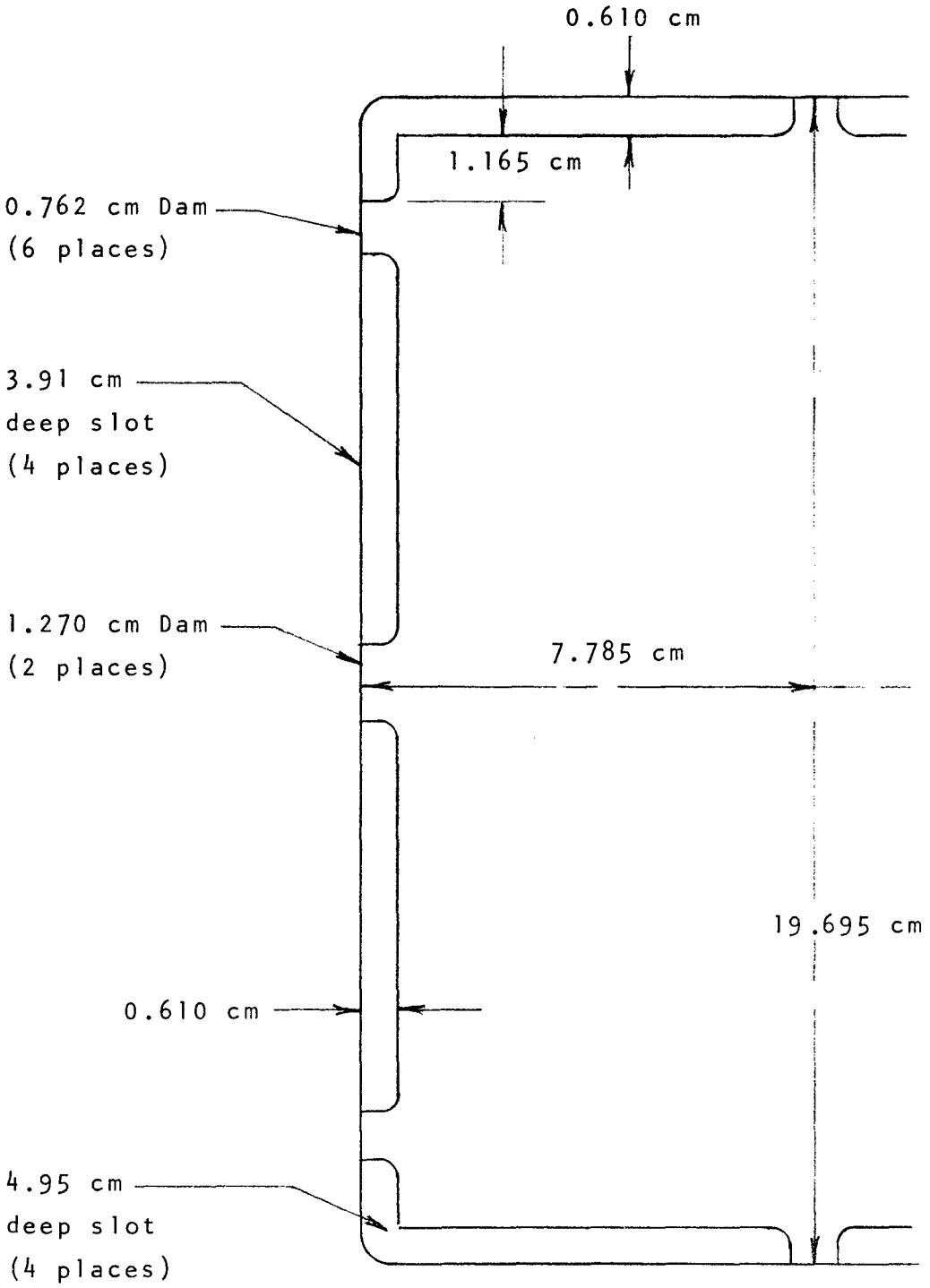

Figure 211. Top View of Original Acoustic Slot.

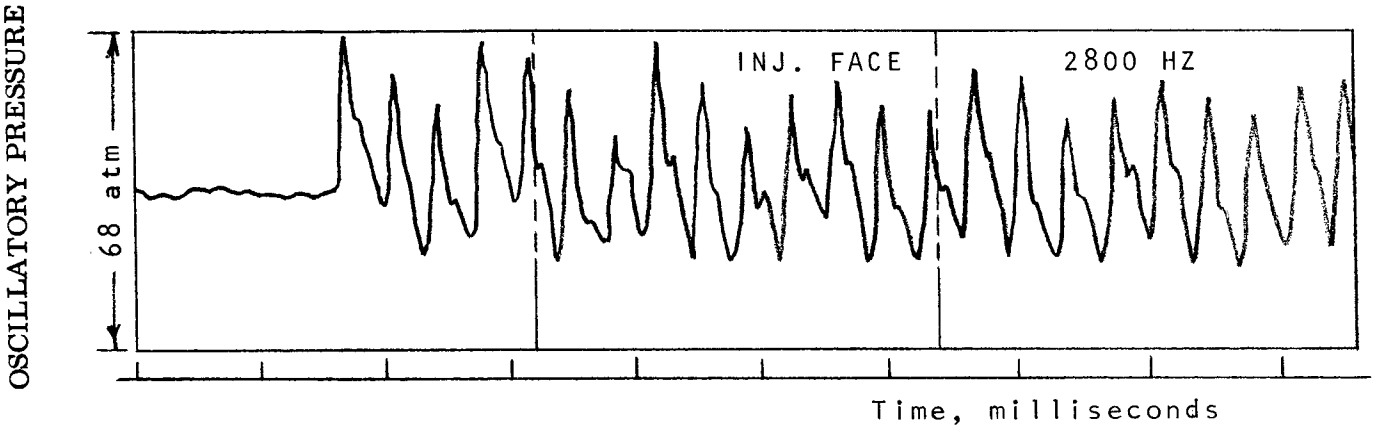

Figure 212. Combustion Pressure Time History; Combustion Instability AC Pressure Trace.

The acoustic slots positioned around the injector periphery were believed of insufficient open area to prevent the occurrence of the 1T mode of instability at 2800 Hz in the 19.69 cm dimension when the combustor was bombed. The injector pattern was also thought to strongly favor this mode. The acoustic slots were subsequently modified as shown in Figure 213 to: (1) significantly increase the amount of acoustic damping for the 2800 Hz mode; (2) slightly increase the amount of acoustic damping for the 3570 Hz mode; and (3) add significant acoustic damping for the 4800 Hz mode.

The damping coefficient for each frequency or mode of interest was predicted using Figure 214 in the manner outlined as follows: (1) calculate the tuned frequency and percent open area of each slot; (2) calculate effective slot open area assuming 100% effectiveness if slot was positioned at an antinode, or between an antinode and the midpoint between node and antinode, for mode of interes; (3) to determine the damping coefficient for the tuned frequency, use Figure 214 with the peak aligned with the tuned frequency and the effective open area; and (4) to determine the damping coefficient for other than the tuned frequency, use Figure 214 with the peak aligned with the tuned frequency and with the effective open area for the frequency of interest.

Using the method outlined damping coefficients for 2800 Hz, 3570 Hz, and 4800 Hz modes were calculated and are summarized in Table 67. Protection against the 2800 Hz mode was greatly improved in the modified acoustic absorber with the damping coefficient for the mode increasing from 1190 sec^{-1} to 3672 sec^{-1}. Protection against the 3570 Hz mode was increased slightly from 1070 sec^{-1} to 1128 sec^{-1}. A significant amount of protection against the 4800 Hz mode (i.e., $\alpha 4800 = 360\ sec^{-1}$) was also provided.

The threefold increase in slot width resulted in increased recirculation at the injector face. This, of course, resulted in increased temperatures in the slot, thus retuning the slots to slightly higher frequencies. Based on past experience, however, the beneficial effect of the increased slot width dominated any possible harmful effect because of slot mistuning. Several tests with 5 and 10% by mass Cs_2CO_3 seed have been conducted subsequent to the acoustic slot modification. A comparison of the combustor pressure oscillations recorded on these latter tests with those recorded on the earlier tests was made.

Results. Pressure oscillation characterization from the high frequency pressure transducer denoted as Pc_{21} and located at the injector face was obtained for tests 038, 001, 003, 004, and 005. All tests were conducted at a nominal chamber pressure of 30 atm. Tests were further categorized by the percentage of seed and acoustic configuration as shown below:

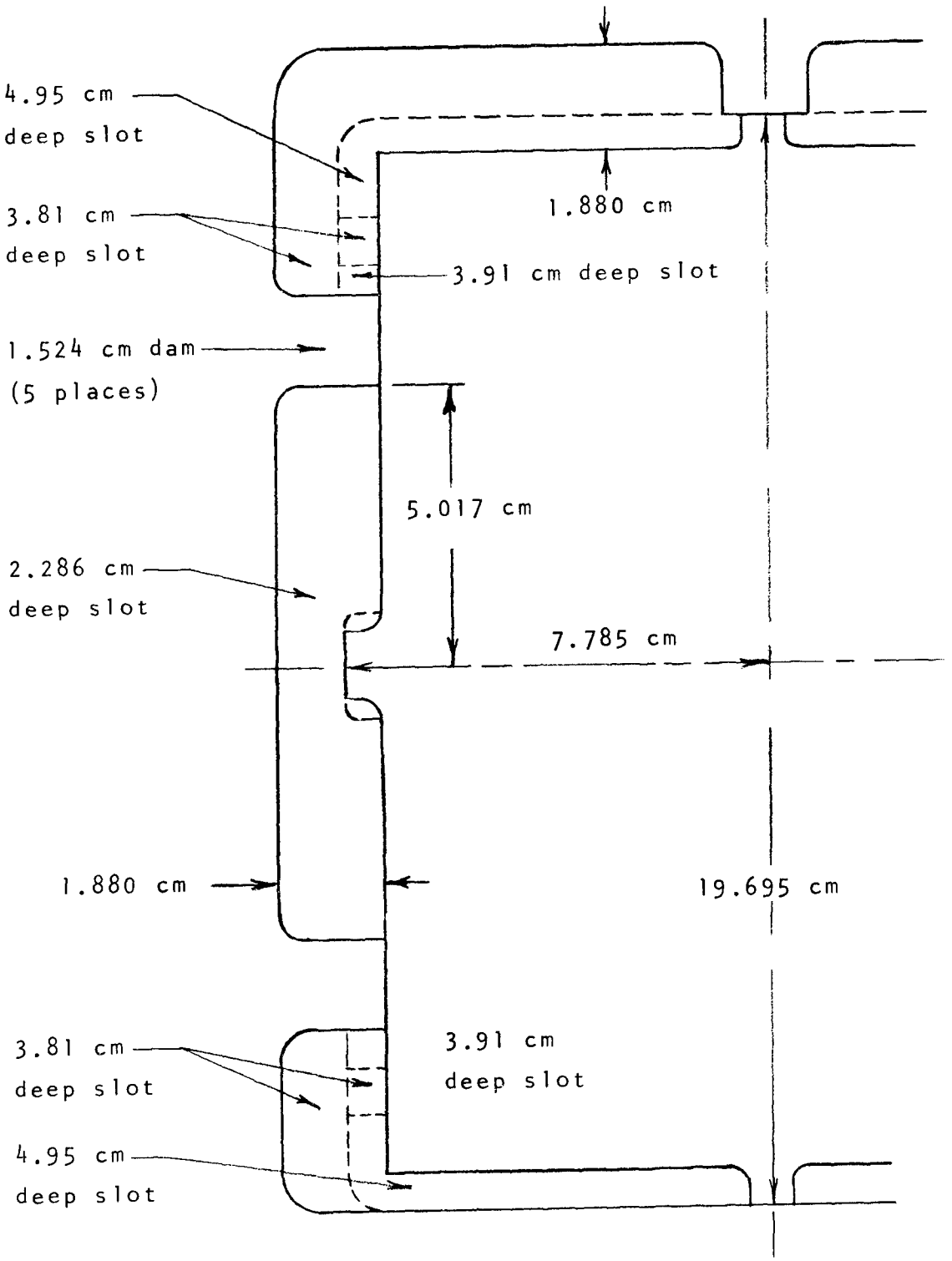

Figure 213. Top View of Modified Acoustic Slot.

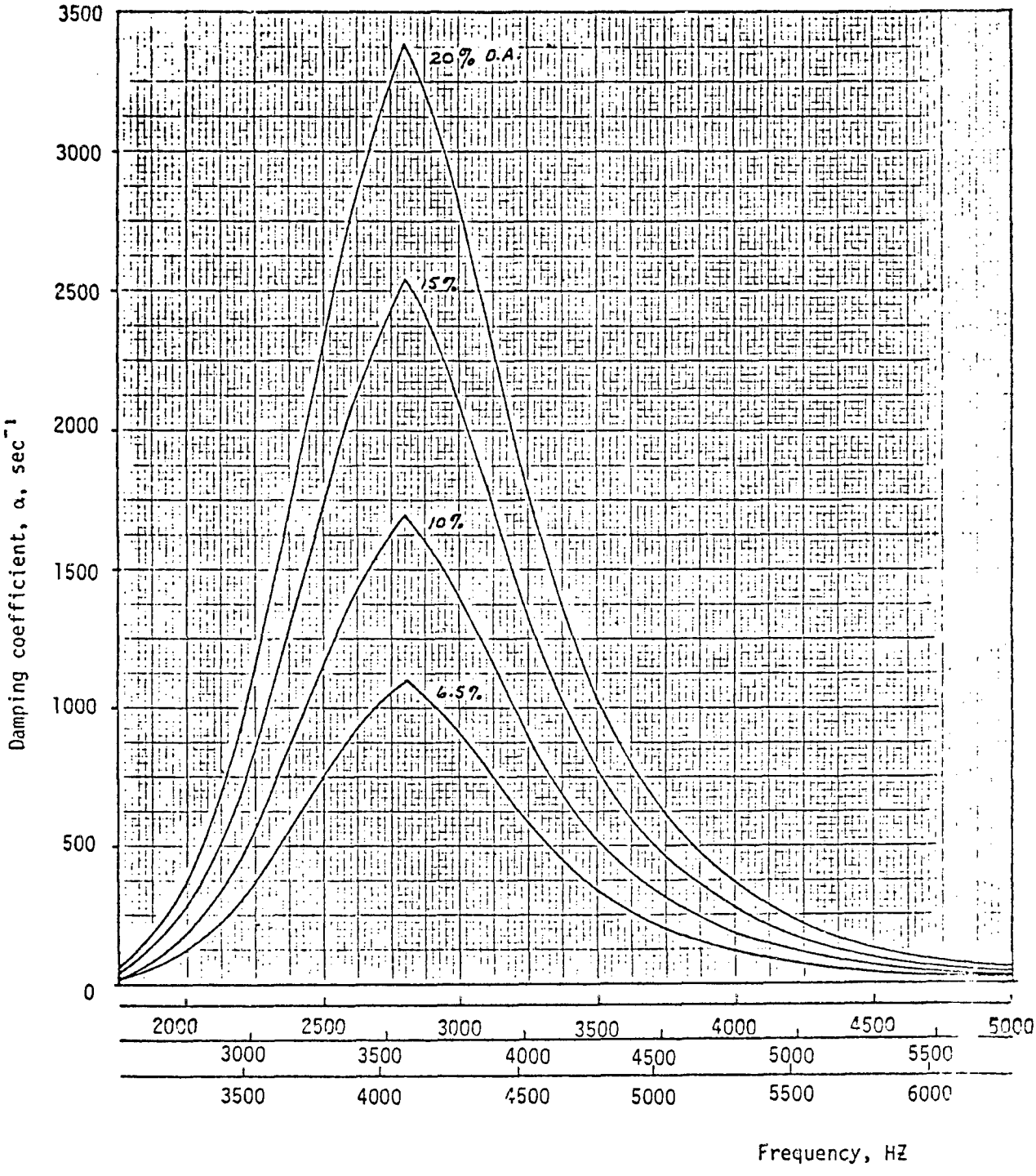

Figure 214. Acoustic Slot Bandwidth.

TABLE 67. PREDICTED DAMPING COEFFICIENTS

	Original Slot Design	Modified Slot Design
Open Area of Top/Bottom Slots	6.8%	21.7%
Tuned Frequency of Top/Bottom Slots	2800 Hz	2800 Hz
Open Area of Side Slots	5.3%	11.5%
Tuned Frequency of Side Slots	3570 Hz	4100 Hz
TOP/BOTTOM SLOTS		
Effective Open-Area for 2800 Hz	6.8%	21.7%
Effective Open-Area for 3570 Hz	4.0%	8.7%
Effective Open-Area for 4800 Hz	6.8%	19.8%
α Contribution for 2800 Hz	1150 sec^{-1}	3672 sec^{-1}
α Contribution for 3570 Hz	170 sec^{-1}	392 sec^{-1}
α Contribution for 4800 Hz	20 sec^{-1}	75 sec^{-1}
SIDE SLOTS		
Effective Open-Area for 2800 Hz	1.9%	0%
Effective Open-Area for 3570 Hz	5.3%	11.5%
Effective Open-Area for 4800 Hz	1.5%	7.0%
α Contribution for 2800 Hz	40 sec^{-1}	0 sec^{-1}
α Contribution for 3570 Hz	900 sec^{-1}	736 sec^{-1}
α Contribution for 4800 Hz	20 sec^{-1}	285 sec^{-1}
SUMMATION		
α for 2800 Hz	1190 sec^{-1}	3672 sec^{-1}
α for 3570 Hz	1070 sec^{-1}	1128 sec^{-1}
α for 4800 Hz	40 sec^{-1}	360 sec^{-1}

Test No.	% Cs_2CO_3	Acoustic Slot
038	0	Original
001	5	Original
003	10	Original
004	10	Modified
005	10	Modified

The steady-state main stage portion of test 003 was marginally, if at all, attained before the bomb detonation which resulted in a sustained high amplitude instability of 37 atm peak-to-peak at 2800 Hz.

Steady-state main stage PSD results for the various tests are summarized in Table 68. Table 68 indicates the predominant oscillation frequencies, frequencies at which "spikes" are seen in the PSD plots, and their respective power level "amplitudes."

A summary of the steady-state main stage AMS (1-t) results is presented in Table 69 which compares both root-mean-square atm^2 and atm peak-to-peak between the various tests. Actual AMS traces are shown in Figure 215 and the actual time history traces are shown in Figures 216 through 218.

Discussion of Results. Expanded pressure time traces from the steady-state portion of test 038 showed typical oscillations as depicted in Figure 216. Oscillations at both 4800 Hz and 800 Hz are seen to co-exist. The 800 Hz oscillations were believed to be the 1L mode while the 4800 Hz oscillations were believed to be the 2T mode in the 19.69 cm direction. This latter mode was predicted by the Dykema model to be the "most likely" mode. The PSD of test 038 showed spikes at both 750 Hz and 4800 Hz and was in agreement with Figure 216.

Steady-state PSD's for test 001 with 5% Cs_2CO_3 seed and for pre-bomb conditions on test 003 with 10% Cs_2CO_3 seed also showed spikes at 800 Hz and 4800 Hz and, therefore, were in agreement with the PSD from test 038. A minor spike at 1600 Hz, which was possibly the 2L mode, was observed on all three tests. The amplitude of the 800 Hz and 4800 Hz spikes was lower on tests 001 and 003 than on test 038. Thus, the use of seed appeared to decrease the inherent pressure oscillation amplitude at these two frequencies.

Steady-state PSD's for tests 004 and 005 with 10% Cs_2CO_3 seed also showed spikes at $\approx$ 700 Hz and $\approx$4800 Hz. A minor spike at $\approx$2000 Hz was also observed. The amplitude of these spikes was greatly decreased when compared to tests 038, 001, and 003 which were conducted with the original slot. Thus, the modified slot

TABLE 68. STEADY-STATE PSD SUMMARY

(AMPLITUDE OF "SPIKES")

Frequency	Test 038 ($matm^2/Hz$)	Test 001 ($matm^2/Hz$)	Test 003 ($matm^2/Hz$)	Test 004 ($matm^2/Hz$)	Test 005 ($matm^2/Hz$)
730-850 Hz	787	185	509	60	69
4800 Hz	972	416	648	26	46

TABLE 69. STEADY-STATE AMS AND TIME HISTORY SUMMARIES

	1/4 Wave Cavities			Modified Absorber Cavities					
	Test 038	Test 001	Test 003	Test 004	Test 005	Test 007	Test 008	Test 009	Test 010
AMS									
atm^2_{rms}	0.230	0.148	0.222	0.089	0.078	0.041	0.044	0.070	0.043
$atm^*_{peak\text{-}to\text{-}peak}$	1.34	1.07	1.32	0.84	0.78	0.56	0.59	0.74	0.58
TIME HISTORIES									
$atm_{p\text{-}p,}$ main stage	3.81	--	--	1.96	2.18				
$atm_{p\text{-}p,}$ pre-run noise	1.09	--	--	1.20	1.31				
$atm_{peak\text{-}to\text{-}peak,}$ net	2.72	--	--	0.76	0.87				

* Calculated from rms value assuming perfect sine wave waveform,

i.e., $atm_{p\text{-}p} = 2.8\ atm_{rms}$

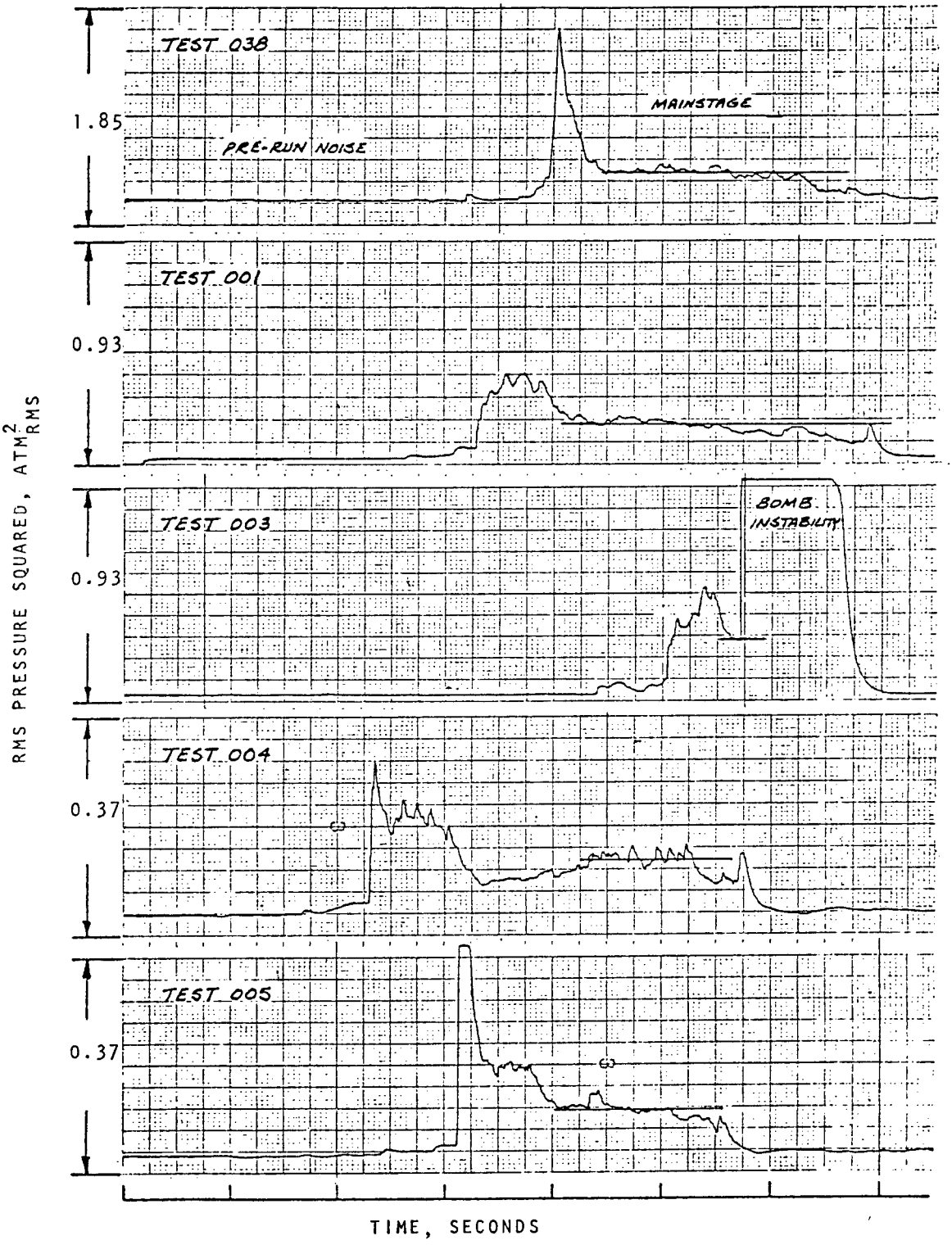

Figure 215. AMS Traces.

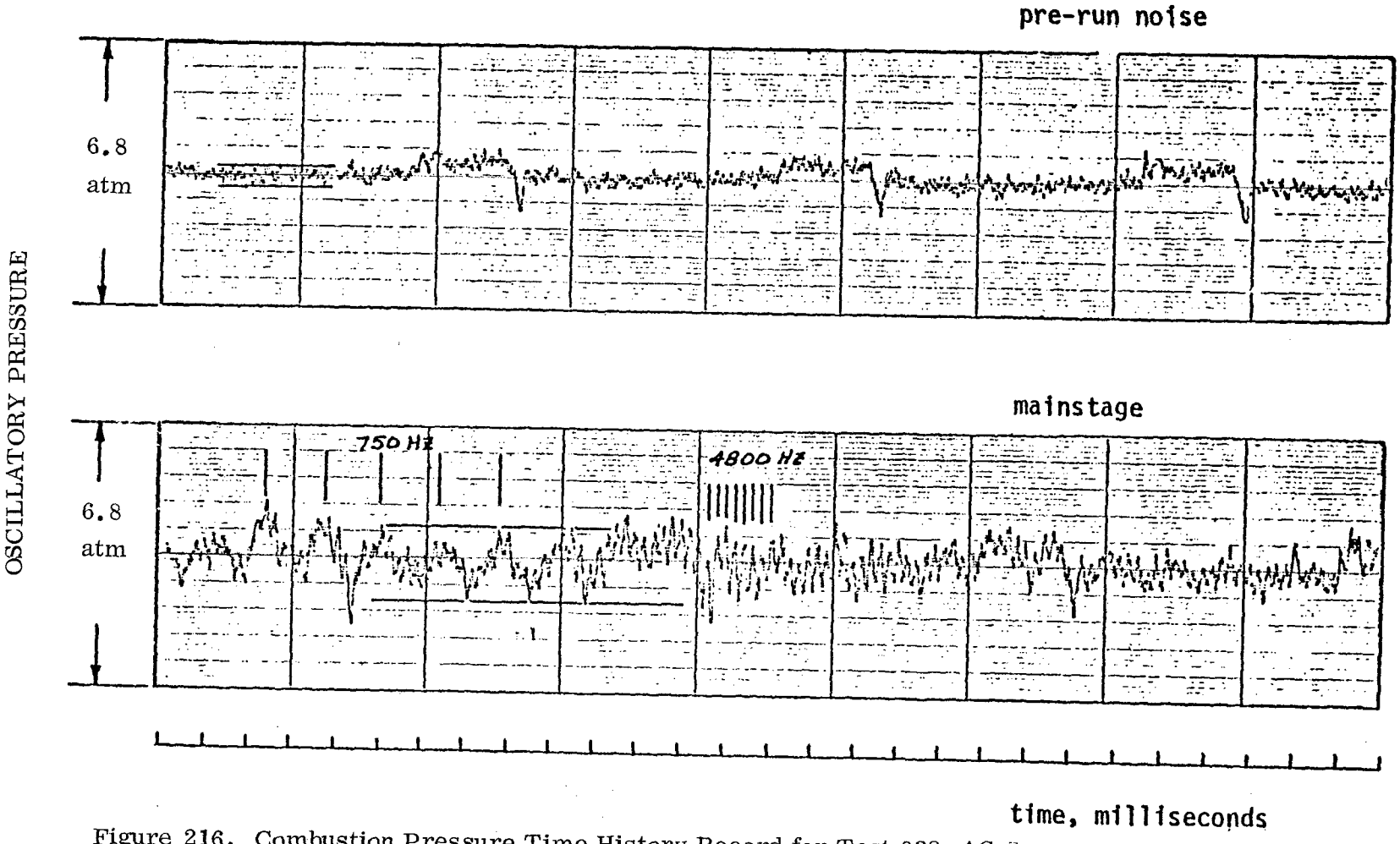

Figure 216. Combustion Pressure Time History Record for Test 038; AC Pressure Trace.

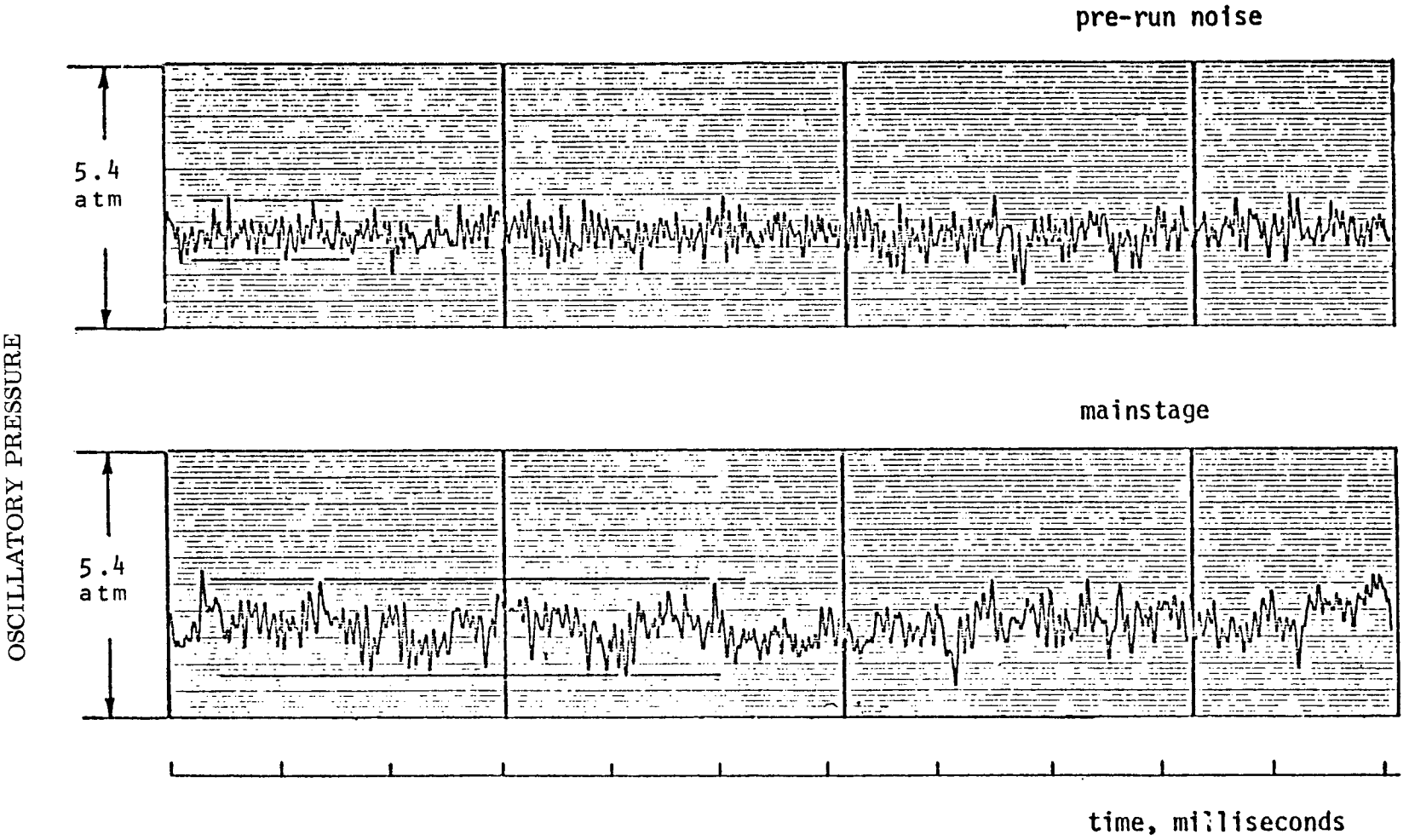

Figure217. Combustion Pressure Time History Record for Test 004; AC Pressure Trace.

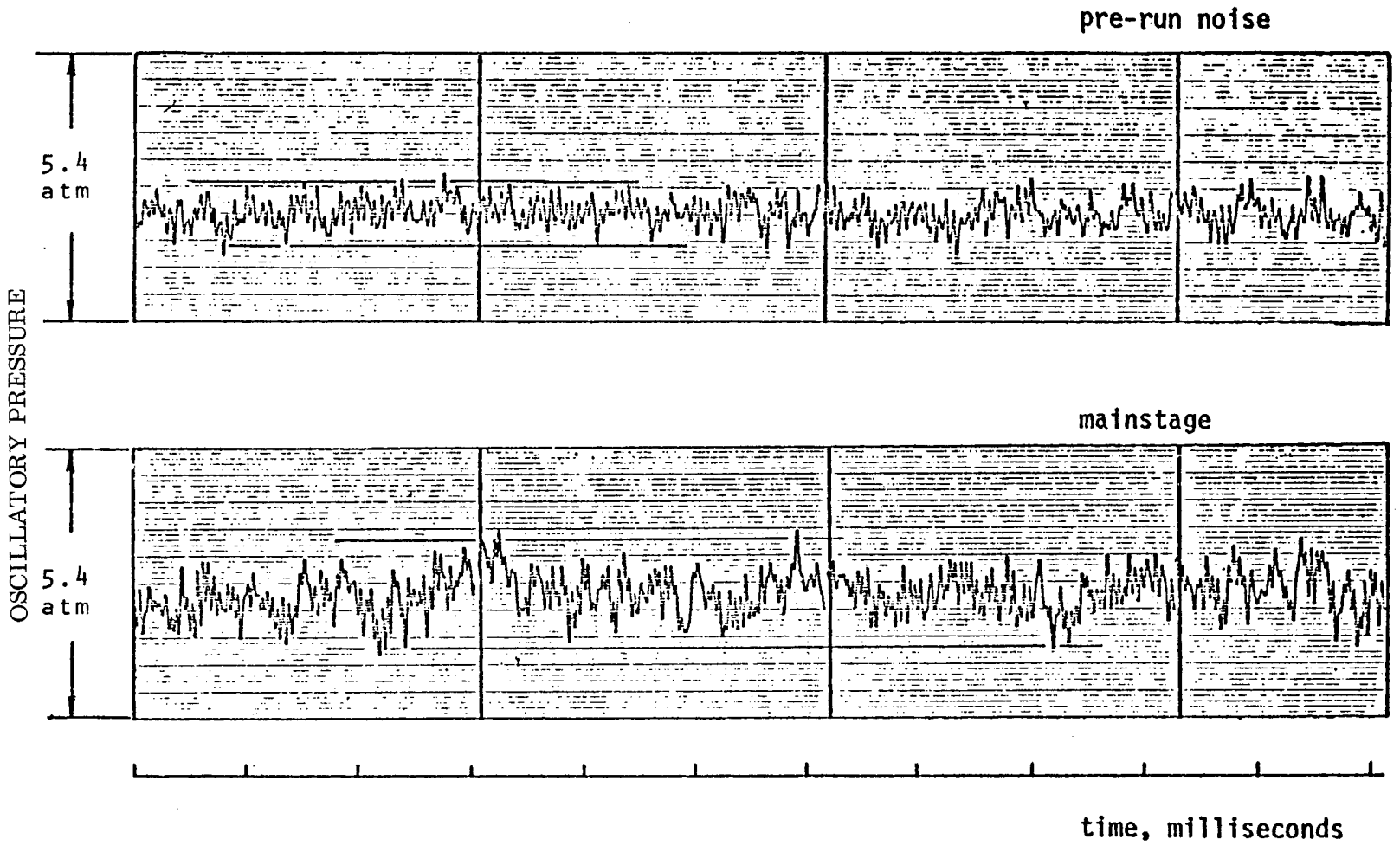

Figure 218. Combustion Pressure Time History Record for Test 005; AC Pressure Trace.

design appeared to be quite effective in providing greater damping for the ≈800 Hz mode as well as the 4800 Hz mode. Indeed, the 800 Hz and 4800 Hz frequencies were not visually observed on the time-history records of tests 004 and 005. These are shown in Figures 217 and 218.

The decrease in the pressure oscillation amplitude achieved with the modified acoustic slot design was quantitatively expressed by comparison of the atm^2_{rms} values for the various tests as shown in Table 69. These atm^2_{rms} values were obtained from AMS processing using a 20 Hz to 10 kHz band pass filter.

The net peak-to-peak atm values for pressure oscillation amplitude obtained from the time-histories or the expanded P-t traces also exhibited a significant decrease with the modified slot design. This is also shown in Table 69. These peak-to-peak atm values were in some cases, higher than peak-to-peak atm values determined from the AMS data, as indicated in Table 69. This was caused by the fact that the peak-to-peak atm values determined from the AMS data assumed a perfect sinusoidal waveform; whereas, in actuality, the waveform was quite complex.

f. Conclusions

The reduction and interpretation of the experimental data obtained during this test series showed the MHD combustor operating at nominal Pc of 30 atm and varying seed ratios to exhibit stable combustion, when disturbed artificially, with inherent pressure oscillations whose peak-peak amplitude was ≈2.7% of the mean combustion chamber pressure. This value was approximately half of that realized prior to the acoustic cavity redesign. The attenuation of all predominant frequencies appeared with the cavity redesign.

Combustion ignition occurred reliably in each combustor start. Since the seed solution was introduced after combustor ignition occurred, the seed had no impact on the gas generator start. In the early tests the shutdown of the gas generator produced very fuel-rich operation which resulted in carbon formation on the combustor/nozzle walls. Since attempts to eliminate the carbon formation through sequence modification were unsuccessful, the purge flow rate and pressure were increased. This modification resulted in a clean, carbon-free shutdown.

The thermal data reduction and interpretation led to the following conclusions: (1) the heat load for non-seeded fuel was lower than predicted by the boundary layer program; (2) a clean combustor chamber wall increased the heat load level; (3) heat flux levels were affected by mixture ratio and seed ratio, i.e., higher mixture ratio/seed ratio, higher heat flux; (4) the maximum heat transfer coefficient realized was 82% of that predicted in the throat and occurred at 3.4 M/R and 10%by mass Cs_2CO_3 seed; (5) individual heat flux meters indicated some deposition of carbon

on the combustor walls during low mixture ratio tests; (6) in the convergent section, the heat transfer coefficient for the contoured wall was higher than for the flat wall at the same axial station; (7) the calometric result of the nozzle exit coolant passages agreed with the nozzle heat flux meters; and (8) the results of the tests at 5% by mass $Cs_2 CO_3$ and mixture ratio of 3 or lower showed the average heat transfer coefficient to be approximately 60% of the predicted value, which would allow regenerative cooling of a 33 to 36 cm combustor.

5. Diagnostics Channel Tests

a. Introduction

A series of diagnostics channel tests were conducted using the procedure established during the previous combustor only tests. The diagnostics channel was designed to be used to measure the electrical conductivity of the gas, and hence, provided an evaluation of the performance of the combustor as a source of ionized gas. The test objectives of the diagnostics channel tests were: (1) measurement of the gas electrical conductivity during the SSFL development test program; (2) verification of the nozzle/channel interface design for the high power MHD system; and (3) provide structural, thermal, and hydraulic design data for the verification of the lightweight, high power MHD channel/diffuser design.

Six hot fire tests were conducted with varying seed percentages and mixture ratios. To establish the electrode frame temperatures, one test was conducted without electrical current flow to the diagnostics channel. All tests that were conducted at the nominal chamber pressure level were successful. The first diagnostics channel test, which was conducted at a reduced chamber pressure, experienced an early termination. This test series accomplished the objectives of gas conductivity measurement, mechanical design information, and nozzle/channel interface verification.

b. Test Setup

The basic hardware and test setup used for this test series was identical to that used for the previous tests with the exception of the water cooled acoustic cavity spacer and the diagnostics channel. The 7.6 cm water system previously used for the combustor coolant only was modified to accommodate the additional requirements. A 1.9 cm system was tapped off the combustor inlet manifold and orificed to provide approximately 2.3 kg/sec of coolant for the acoustic cavity spacer. The diagnostics channel coolant supply required an independently controlled water system, which was tapped off the 7.6 cm system. A new 5.1 cm system was installed to feed the diagnostics channel using a flow meter, flow screen, annin valve and orifices to control the flow distribution. The entire system was fed from a single run tank. Consequently, several tests were made to characterize the system. By adjusting the orifices a satisfactory flow distribution was established.

In addition to the coolant requirements, the diagnostics channel had an electrical power requirement. A dc power supply supplied by Maxwell Laboratories was installed and checked out prior to the first test. This unit supplied 15 to 30 A dc to the diagnostics channel for the gas conductivity measurements. A substantial quantity of additional instrumentation was also utilized for the diagnostics channel system to characterize the channel operation. This instrumentation was installed and checked out prior to the first test. Figure [219] shows the location of the diagnostics instrumentation used for the diagnostics channel tests. All of the instrumentation was utilized for all of the development tests, except that the electrode frame thermocouples were not used to record the frame temperatures unless the power supply was disconnected. One test of this type was conducted during the development test program. Additionally, unused voltage tap connections were provided for electrode frames #5, #11, #23, #29, and #35. These were included to provide additional flexibility in measuring the electrical conductivity of the gas. In addition to the static pressure tap locations indicated, three other pressure taps were provided.

c. Test Description - Combustor

During the diagnostics channel test series six hot fire tests were conducted to characterize the combustor performance at various mixture ratios and seed percentages. Throughout the series continuous updating of the instrumentation was realized. A brief description of the six hot fire tests conducted during this effort is presented in the following paragraphs.

Prior to test initiation, the diagnostics channel was installed, a water blowdown conducted to size the control orifices, and an electrical power check conducted to determine instrumentation reactions. The Beckman recording system was protected against voltage surges by installing a diode/fuse circuit.

Hot fire test 006 was conducted on 28 March 1978. This was the first diagnostics channel test. The test was conducted at a reduced chamber pressure and with current supplied to the diagnostics channel. The test was terminated prematurely because of a vibration safety cutoff (VSC). A review of the test data showed the test to have a normal start transition, but the accelerometer channels were noisier than normal during the pretest period. A 50 msec accumulation of spikes in excess of 100 g triggered the VSC circuit. The test data from this test showed some anomalies; i.e., noisy high frequency data channels, cross talk into the exciter output voltage monitor and diagnostics channel differential voltage, etc. A subsequent facility review showed some anomalies in the ground circuits. These items were corrected and checked out prior to the next test. A review of the high frequency channel noise showed a grounding problem was encountered

ACCELEROMETERS: 5 REQUIRED

BBN MODEL 506

10 mV/g ± 10%
3 Hz to 15 KHz
.25" X .31" X .40"
.07 oz (3gms)
TITANIUM CASE ISOLATED
2' COAXIAL CABLE WITH MICRODOT TYPE 858 CONNECTOR

BBN MODEL P16 POWER SUPPLY: 5 REQUIRED

PROVIDES 0.5mA DC BIAS CURRENT TO ACCELEROMETER
15V BATTERY, NEDA TYPE 220, 100HR LIFE
INPUT CONNECTOR: MICRODOT TYPE 560
OUTPUT CONNECTOR: BNC

ADAPTOR MALCO MICRODOT

03301030001 5 REQUIRED
03301010001 5 REQUIRED
UG914 10 REQUIRED

PRESSURE TRANSDUCER: 3 REQUIRED

TYCO MODEL AB (OPTIONS D, E)
SEMI CONDUCTOR STRAIN GAGE TYPE
100 PSI ≈ 100mV OUT
WHEATSTONE BRIDGE 150Ω INPUT
5V MAX INPUT
FLUSH .749" DIAMETER
1KHz FREQ. RESP.
COMPENSATED RANGE 80 - 180° F
CONNECTORS - MS3101A-14S-6-S 3
MS3106A-14S-6-P 3
MS3057-10007 6

THERMO COUPLES: 15 REQUIRED

IRON - CONSTANTAN 0.005" DIA (.013 cm)
OMEGA INCO-005 12" LEADS UNSHEATHED
CONNECTOR
OMEGA NMP-INCO-MF (BLACK)

POWER SUPPLY: ONE REQUIRED

MLI SUPPLIED
460V, 15A, 60Hz, 1φ, INPUT
200V, 30A, DC OUTPUT (NOMINAL)

AC INPUT CONNECTOR
HUBBELL 21419/21415

DC OUTPUT CONNECTOR
LUGS, T & B #P4-10

CURRENT SHUNT: ONE REQUIRED

GE 50-146034 NTAA
50A, 100mV

VOLTAGE DIVIDER: 6 REQUIRED

2000/1 (1MΩ - 500Ω)

CONNECTIONS TO E1 THROUGH E12
VIA LUGS T&B #RA10-6

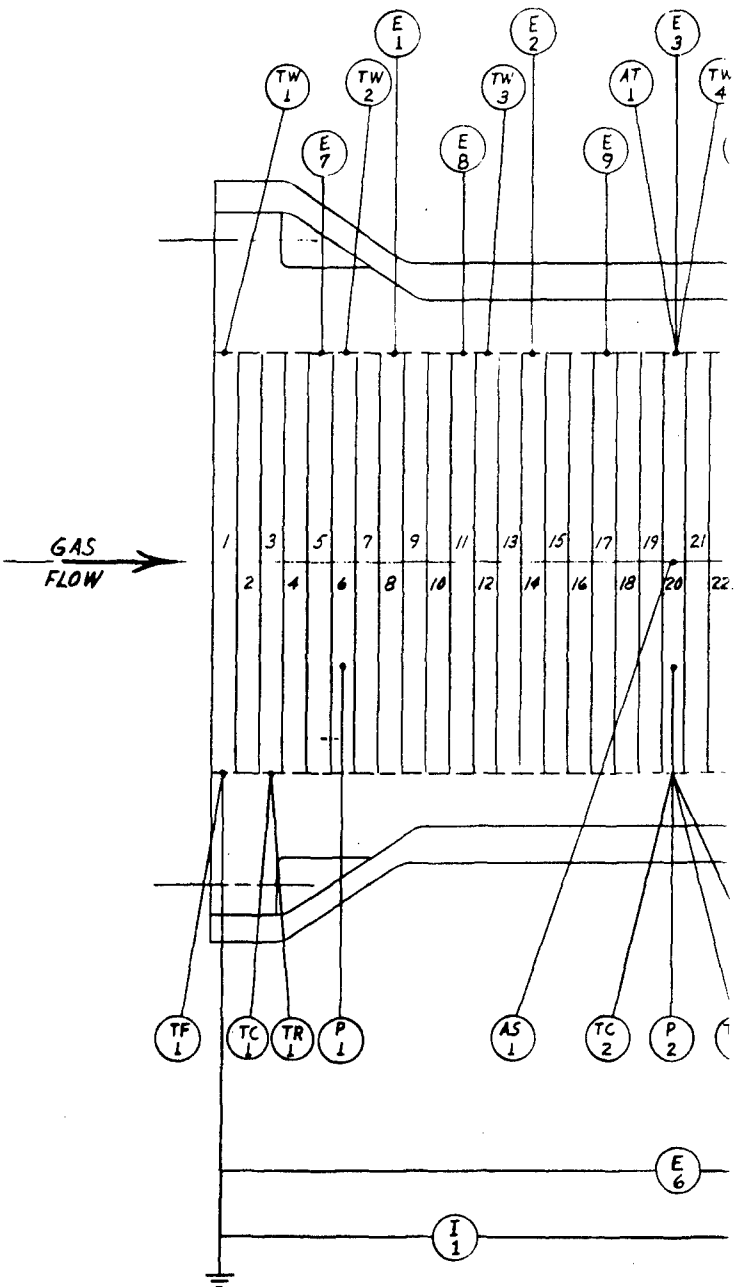

1

LEGEND	
SYMBOL	NOMENCLATURE
E	VOLTAGE
I	CURRENT
P	PRESSURE
T W	WATER TEMPERATURE
T F	FRAME TEMPERATURE
T C	CASE TEMPERATURE
A T	ACCELEROMETER ON TOP (RADIAL ORIENTATION)
A S	ACCELEROMETER ON SIDE (RADIAL ORIENTATION)
A	ACCELEROMETER ON SIDE (LONGITUDINAL ORIENTATION)
T R	RTV TEMPERATURE

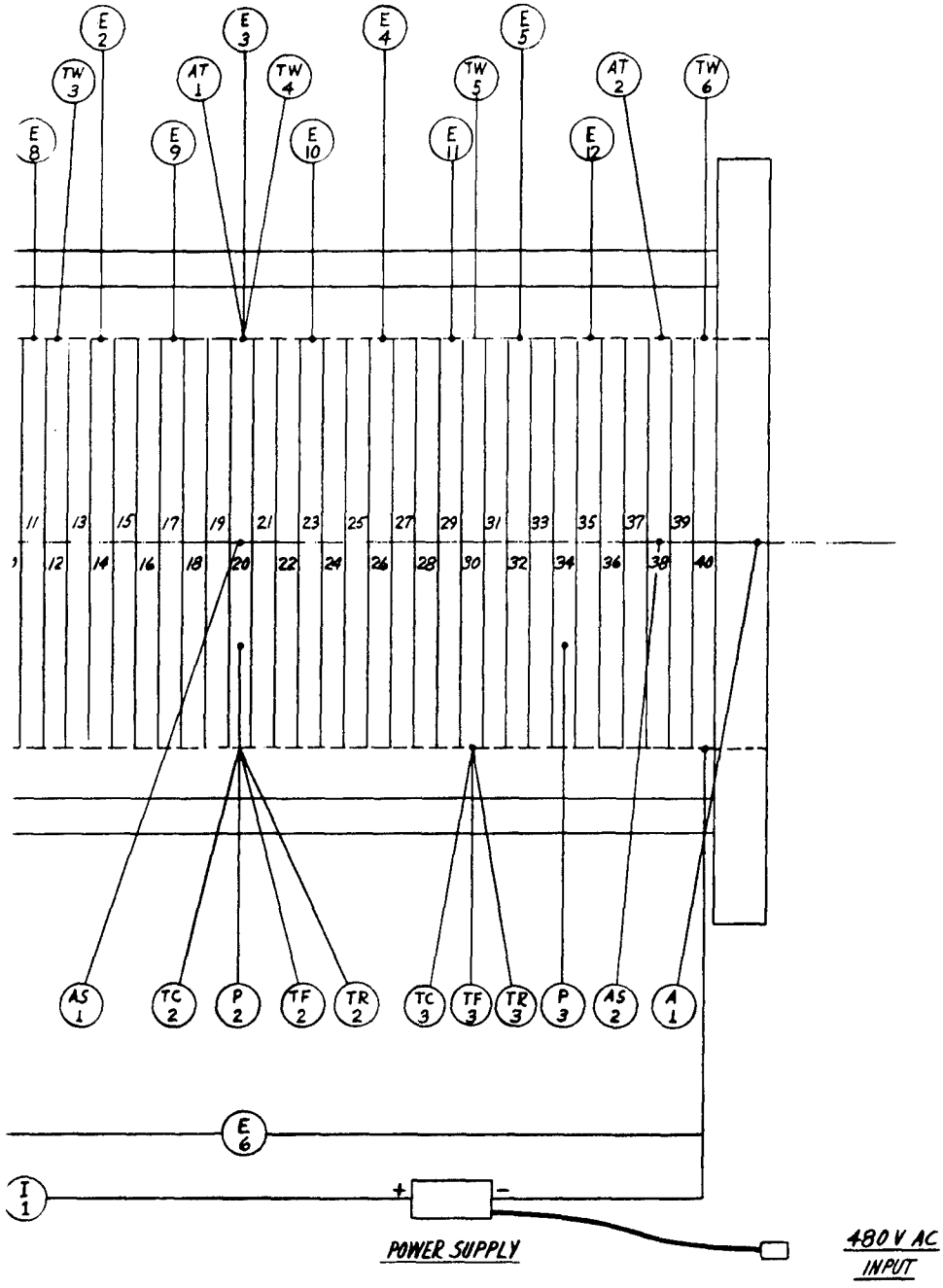

Figure 219. Diagnostics Channel Instrumentation.

(2)

because of the addition of the diagnostics channel instrumentation. In addition, instrumentation channel noise was realized because of the added water coolant flow and the added cantilevered diagnostics channel mass. The grounding modifications which were made to the instrumentation system, improved the electrical output signals and substantially eliminated the cross talk between the exciter output voltage monitor and the diagnostics channel differential voltage measurements.

On 5 April 1978, hot fire tests 007 and 008 were conducted with 20 A of electrical current supplied to the diagnostics channel. The 5% and 10% by mass $Cs_2 CO_3$ seed flow rates at 30 atm chamber pressure were evaluated during these successful tests.

On 7 April 1978, hot fire tests 009, 010, and 011 were successfully conducted evaluating the mixture ratio and seed percentage effects at 30 atm chamber pressure. Test 011 was a repeat test of 010, except that electrical current was not supplied to the diagnostics channel. This test was conducted to determine the heat load on the diagnostics channel during a hot fire test condition.

d. Test Description - Diagnostics Channel

For the diagnostics channel development test program the channel was cantilevered from the nozzle exit. This arrangement minimized the difficulties of the channel installation and eliminated the cost and complexity of providing a downstream support structure for the channel. Figure 220 shows the diagnostics channel installed on the Bravo test stand ready for testing.

As mentioned previously, six hot fire tests were conducted during this phase of the test program. Except for the first test which experienced a VSC termination, the tests were all successful. The test descriptions are given for each of the six tests in the preceding subsection and will not be repeated in this subsection. Figure 221 shows the diagnostics channel internal surface prior to test 007. The view shown is looking upstream from the exit end of the diagnostics channel. Figure 222, from the same location and orientation, shows the channel after test 011. Some ablation of the exit ring was evident after each test. This was caused by the turbulent gases at the exit plane.

e. Results - Diagnostics Channel

For each of the diagnostics channel tests, data was recorded to measure the electrical conductivity of the gas, heat transfer to the channel walls and channel vibrations. Each of these items are discussed in the following paragraphs. This data was used to evaluate the combustor performance as a source of ionized gas and to provide design verification information for the high power MHD channel/diffuser.

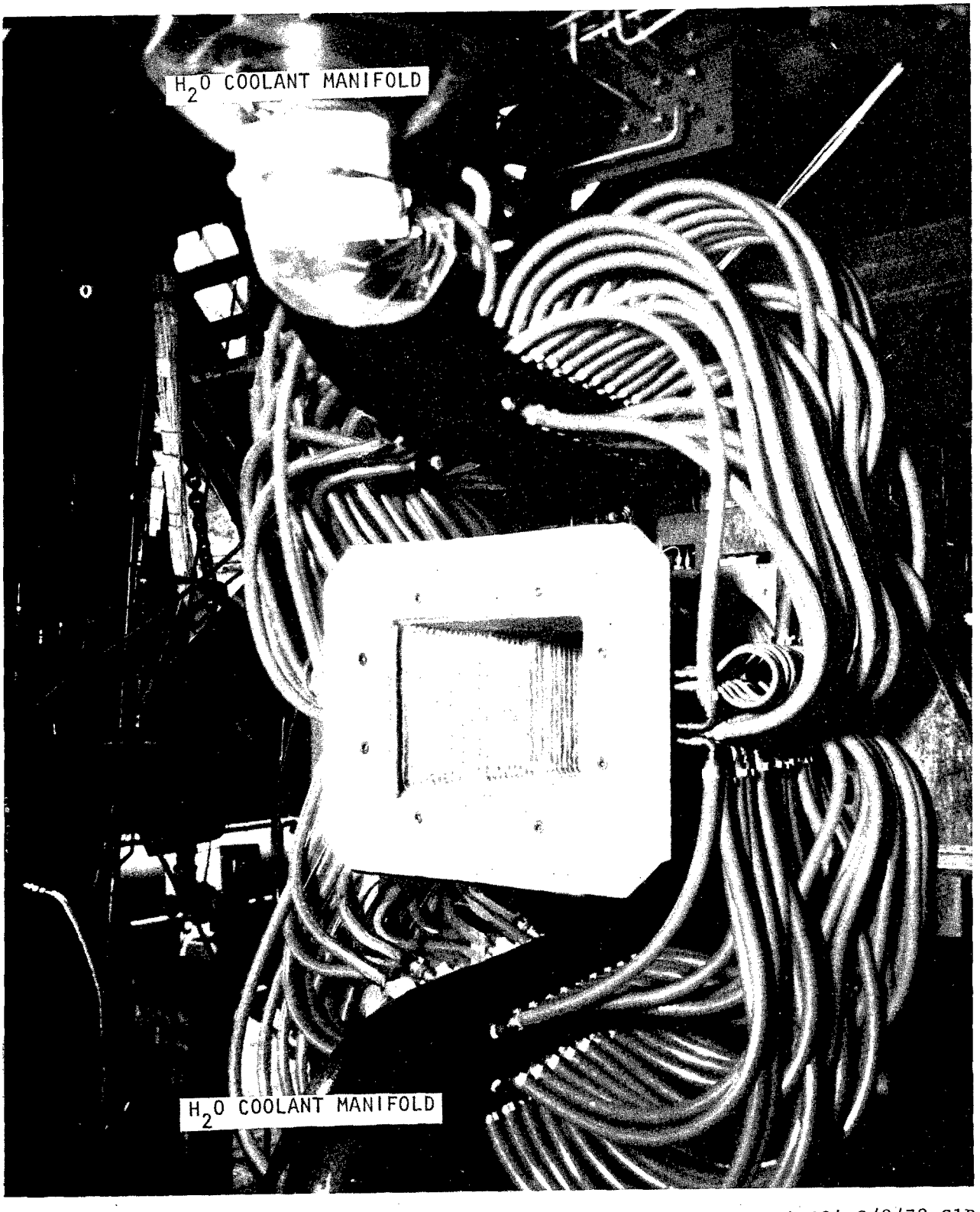

4LC34-3/8/78-S1B

Figure 220 . Diagnostics Channel Installed for Testing

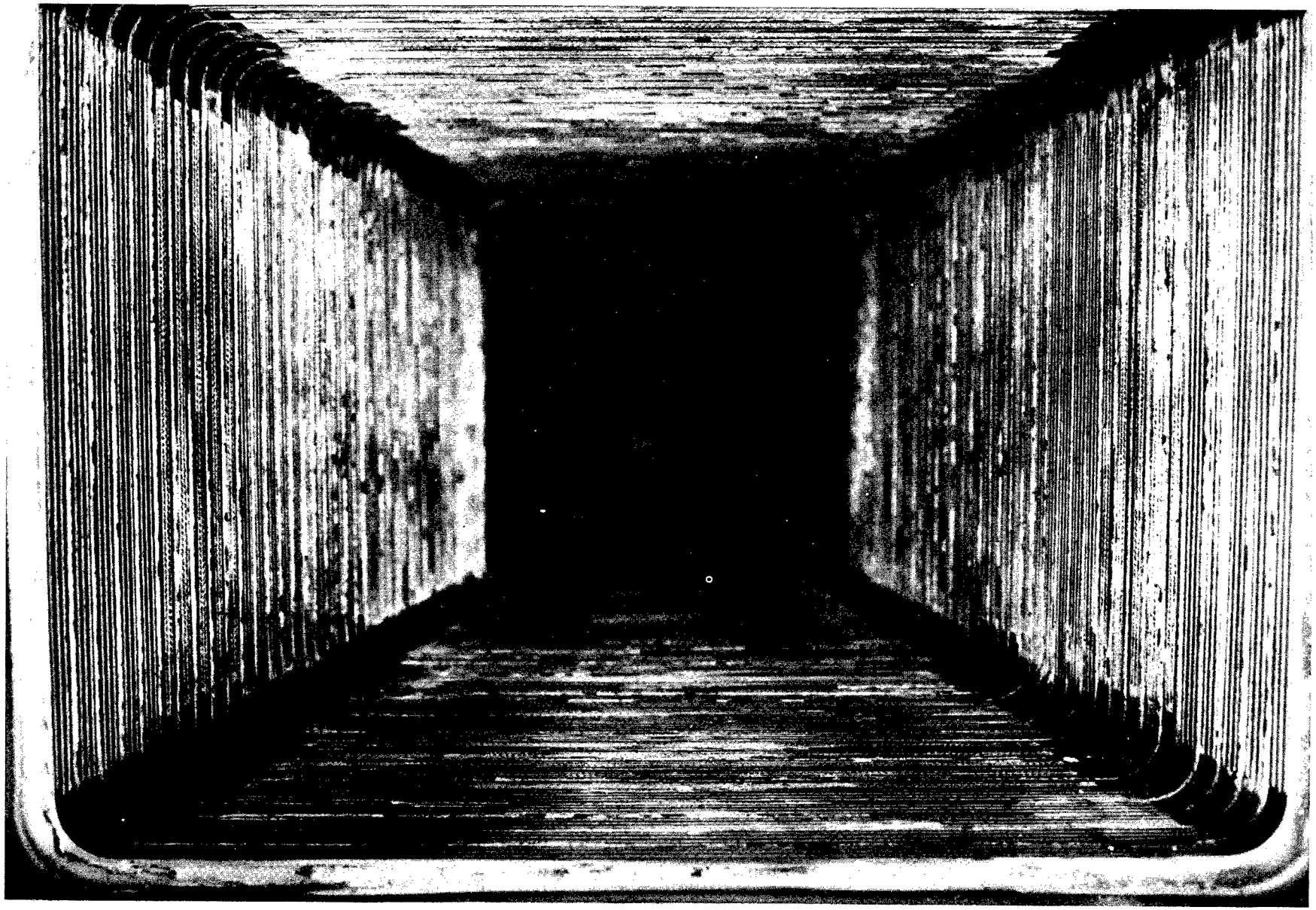

Figure 221. Diagnostics Channel Prior to Test.

Figure 222. Diagnostics Channel After Tests.

Conductivity. One of the most important results of the development test program was the determination of the electrical conductivity of the ionized gas. This was accomplished by supplying electrical current to the channel as shown in Figure 217 and then measuring the differential voltages between various electrode frames. The electrical conductivity, σ, was then determined from the equation: $\sigma = (\Delta L/A)(I/\Delta V)$; where ΔL = distance of electrode separation, A = cross sectional area, I = total current flow, and ΔV = voltage difference between the electrodes separated a distance, ΔL.

The results of the four tests conducted to determine the electrical conductivity at the diagnostics channel inlet are shown in Table 70. All of these tests were conducted at the nominal chamber pressure of 30 atm. The Cs_2CO_3 water solution was approximately 71% Cs_2CO_3 for all tests. The power supply current settings were also unchanged during the test program. For each test only the percentage of Cs_2CO_3 and/or the mixture ratio (MR) were changed. The values of 5% and 10% refer to the mass flow of the Cs_2CO_3 as a percentage of the total reactant mass flow. As the table shows, the highest conductivity of 15.0 mhos/m was obtained for a MR of 3.01 and a Cs_2CO_3 flow of 5.15% of the total reactant flow.

The measured axial conductivity is shown in Figure 223 for each of the four conductivity tests. Except for the conductivity measured in the region of electrode frame #23, the data were consistent. Only test 007 showed an increase of gas conductivity with axial location in the channel. Based on the theoretical calculations, this decrease in conductivity with axial location in the channel was expected. Figure 224 shows the theoretical conductivity calculations for various combustor conditions. By comparing the two figures, a total enthalpy loss of approximately 120 cal/g appears to provide reasonable agreement with the inlet conductivity for test 009. For test 008 the inlet conductivity appeared to indicate a slightly greater enthalpy loss. The 120 cal/g enthalpy loss can be compared to a theoretical stagnation enthalpy in the combustor for the conditions of test 008 of 2220.7 cal/g. By accounting for the C* efficiency and the accumulated heat transfer losses, the theoretical enthalpy loss was approximately 100 cal/g.

The anomaly associated with the conductivity measurement in the region of frame #23 was not resolved during the short development test program. The increase in conductivity with axial location, which occurred during test 007, was also not resolved in view of the decreasing trend apparent in the other conductivity tests. Since the test program was limited to five conductivity tests, repeating any of the tests at identical test conditions or varying the test parameters to test for sensitivity was not possible.

TABLE 70. CONDUCTIVITY TEST RESULTS

Test No.	MR	% Cs_2CO_3	Inlet Conductivity (mhos/m)
007	3.40	9.90	13.9
008	3.01	5.15	15.0
009	3.28	5.01	14.3
010	3.02	9.86	14.7

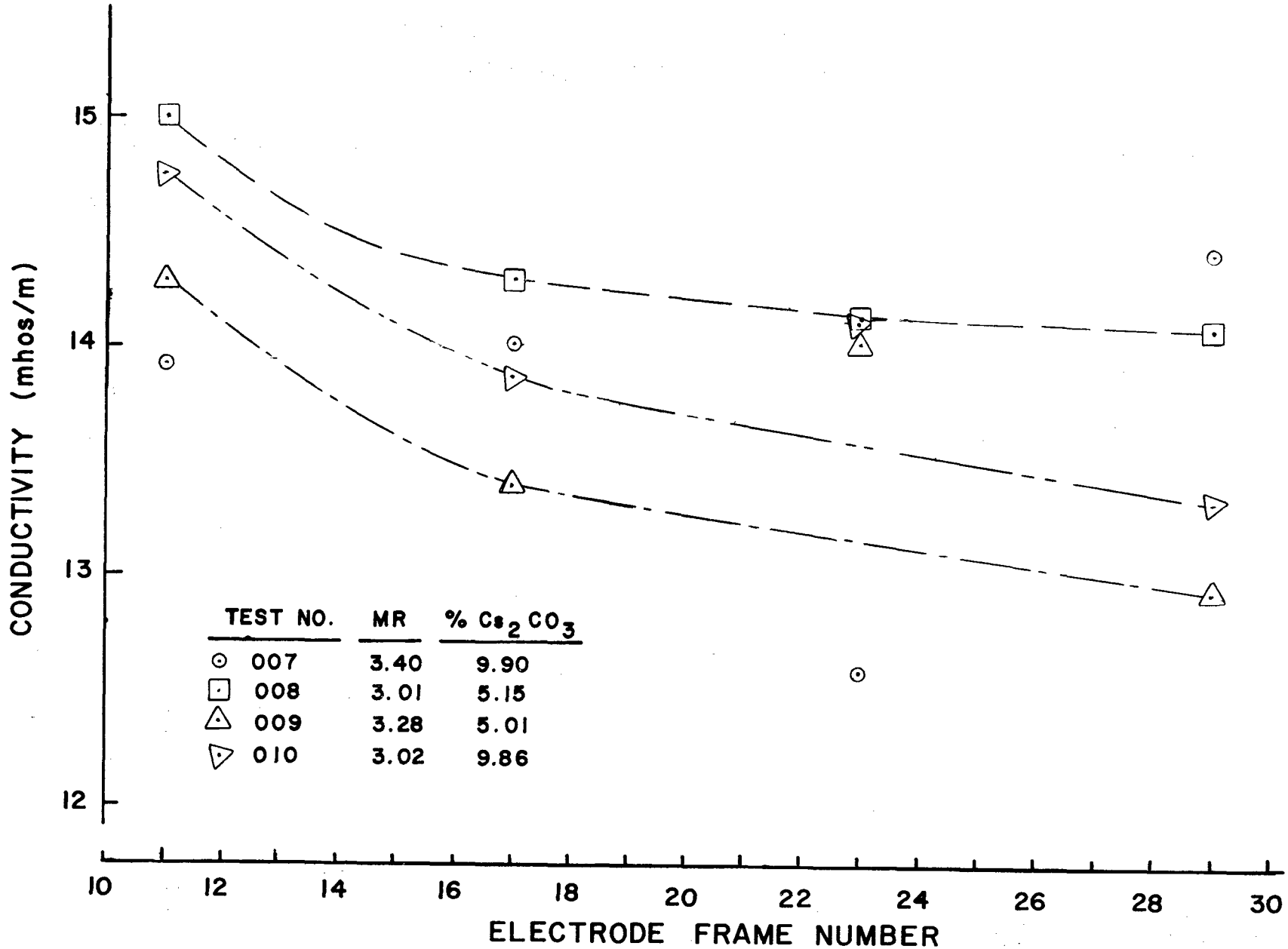

Figure 223. Gas Electrical Conductivity.

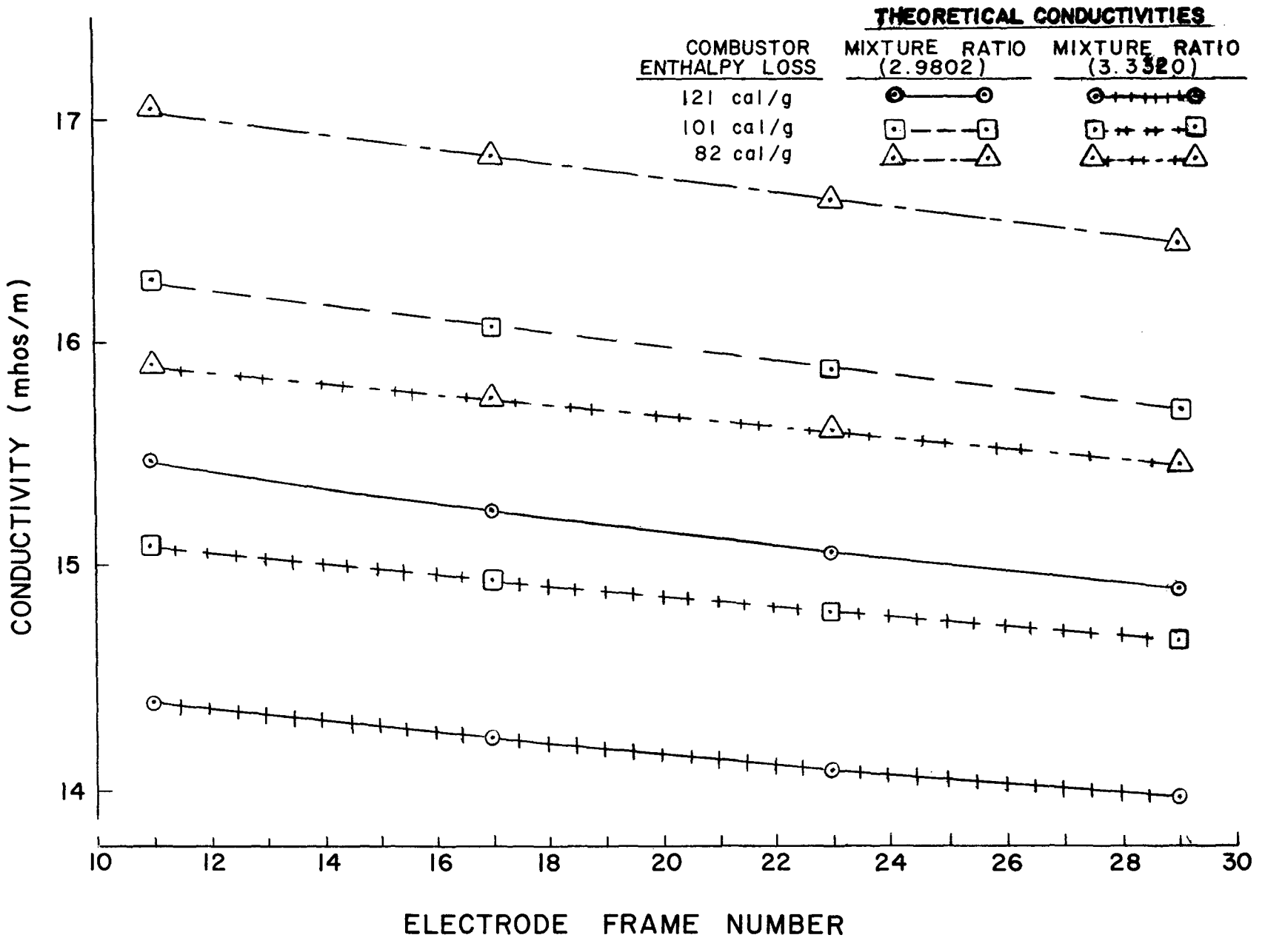

Figure 224. Theoretical Electrical Conductivity.

Heat Transfer. Measurements of the wall heat flux were made at selected axial locations during each of the development tests that utilized the diagnostics channel. The heat flux was determined by measuring the water temperature rise of individual electrode frame cooling loops. This temperature rise was then reduced to a wall heat flux. Water side film coefficients were also calculated to determine the maximum water-side wall temperature. In addition, the thermal gradient across the electrode was calculated to obtain the approximate gas-side wall temperatures. Since steady-state conditions were not achieved in these tests, unsteady-state methods of analysis were applied as necessary. Consideration was given to the fact that in many cases involving unsteady flow or complex geometry, steady-state relationships could be used as a simplifying approximation.

The experimental heat transfer curves for five of the six diagnostics channel tests are shown in Figures 225 and 226. These figures show the heat flux to the walls from the combustor/nozzle throat downstream to the exit of the diagnostics channel. Six cooling water temperature measurements were made in the diagnostics channel at the locations shown in Figure 219. The three heat flux values for the expansion section of the nozzle were obtained from the heat flux meters, which is discussed in the previous subsection, "Injector Tests."

The resultant heat flux for the electrode frame located approximately 240 mm from the channel/nozzle interface was lower because the electrode contained more ceramic and less copper than the other electrodes. The result was consistent for all of the diagnostics channel tests. The electrode frame heat flux for the electrode located approximately 130 mm from the channel/nozzle interface was inconsistent with the general heat flux curve for all tests. During the limited test program no explanation for this anomaly was found.

The heat flux at the diagnostics channel inlet for the 5% Cs_2CO_3 tests increased as the mixture ratio increased; however, the trend was reversed for the 10% Cs_2CO_3 tests. The highest heat flux of 644 w/cm^2 occurred at a mixture ratio of 2.98 and a Cs_2CO_3 percentage of 9.9%. For the low mixture ratio tests the heat flux increased as the Cs_2CO_3 percentage increased. The lowest heat flux of 467 w/cm^2 occurred during the first test, which was conducted at a mixture ratio of 3.4 and a Cs_2CO_3 percentage of 9.9%. While the downstream heat fluxes varied less than 10% from the average value at each axial location, the inlet heat flux steadily increased during the test program. This could be interpreted as an indication of a hardware change during the test program. However, an inspection of the hardware did not reveal any anomalies.

As stated in the previous paragraph, the heat flux at the downstream end of the channel varied less than 10% from the average value. The maximum heat flux of 363 w/cm^2 occurred at a mixture ratio of 3.02 and a Cs_2CO_3 percentage

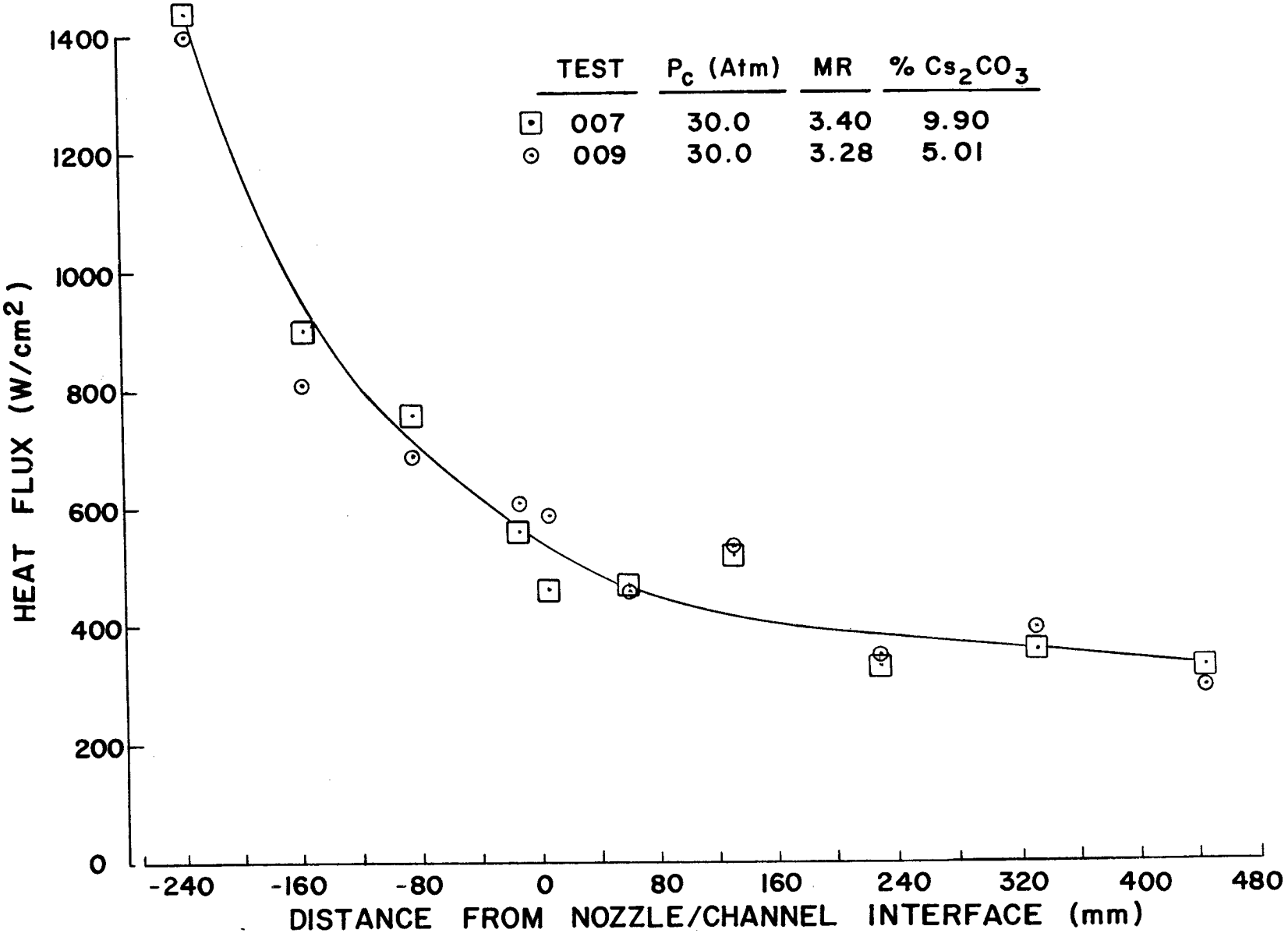

Figure 225. Axial Heat Flux Distribution.

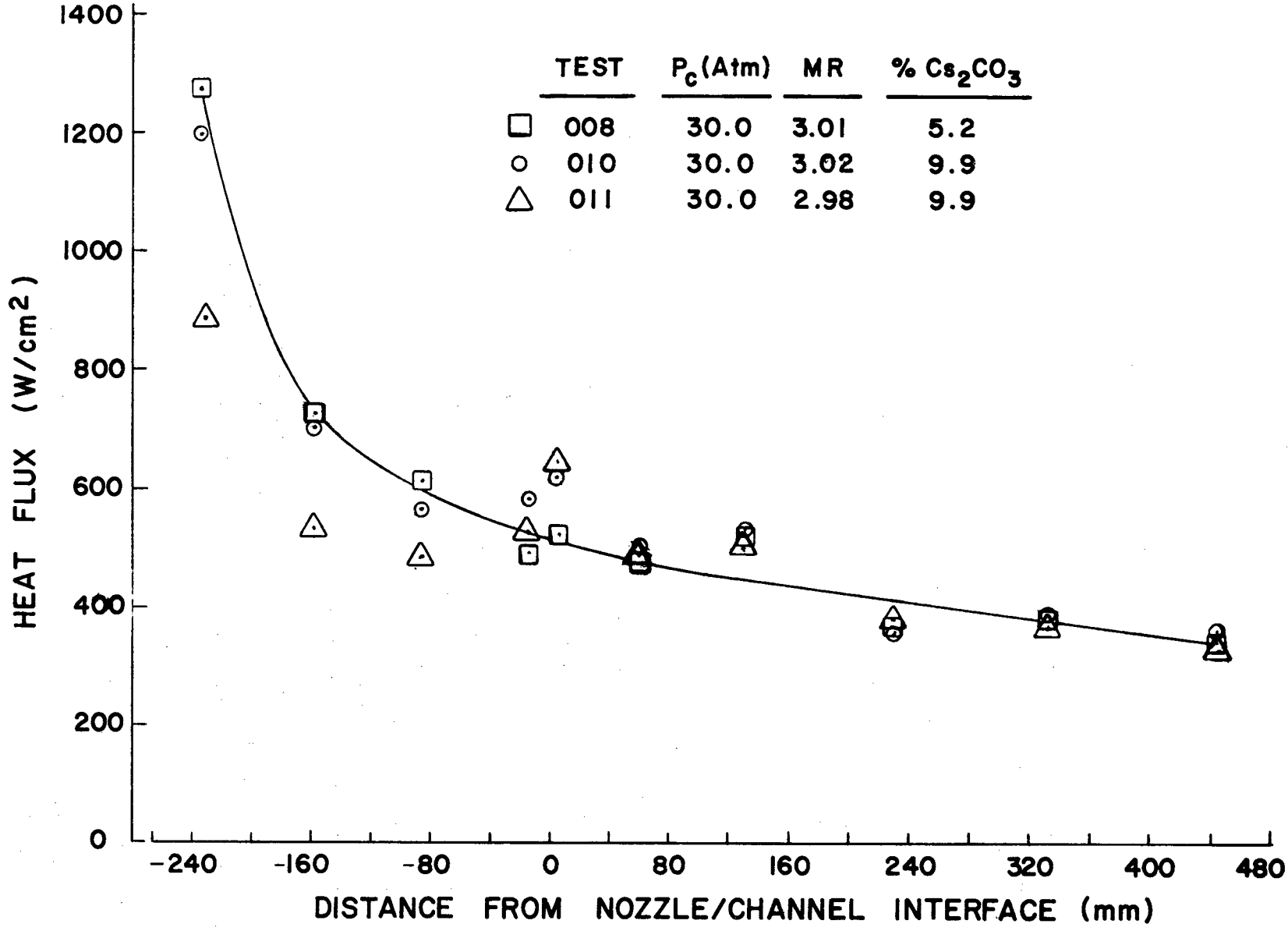

Figure 226. Axial Heat Flux Distribution.

of 9.86% while the minimum heat flux of 298 w/cm^2 occurred at a mixture ratio of 3.28 and a Cs_2CO_3 percentage of 5.01%. At the axial locations upstream from the exit end also exhibited relatively small variances as the test conditions were varied.

A comparison between the measured heat flux for test 008 and the calculated heat flux for the conditions of test 008 is shown in Figure 227. Since the diagnostics channel heat flux calculations were based on matching the boundary layer conditions at the channel/nozzle interface, the resultant calculated heat transfer curve for the diagnostics channel exceeded the measured heat transfer curve by an amount proportional to the combustor/nozzle comparisons.

Water side film coefficients were calculated using the equation for forced convection of water in turbulent flow in tubes.[43] Values were calculated for test 008 ranged from 7.3 w/cm^{2}K at the channel inlet to 5.9 w/cm^{2}K at the channel exit. These values nearly constant along the length of the cooling channel since the water temperature changed very little during the run. Table 71 shows a summary of the water side film coefficients for test 008.

Once the water side film coefficient was determined, the average and maximum water side wall temperatures were calculated. Since the bulk water temperature varied only slightly between the water passage inlet and outlet, the average and maximum wall temperatures were nearly identical. The values calculated for test 008 are also shown in Table 71. The temperature difference between the wall and the water bulk temperature was in the range of 60-70K. The copper surface temperatures for test 008 are also illustrated in Table 71.

Channel Vibrations. During the diagnostics channel development tests, vibration data was recorded to characterize the channel environment. The diagnostics channel accelerometers were mounted to the channel at the locations shown in Figure 219. Three types of reduced vibration data were available: (1) time history records of the amplitude vs elapsed time; (2) AMS traces which provide the adjusted rms amplitude vs time*; and (3) PSD plots of the frequency spectrum of the vibrations.

Figures 228 and 229 show segments of the time history records taken at discrete time elements from test 008. These figures showed the noise level which was present on the instrumentation during the pretest checkout, the increase

* Essentially an integration of the PSD plot between two frequency bounds.

43 J. M. Coulson and J. F. Richardson, Chemical Engineering, Vol. 1, 2nd Ed. Pergamon Press, 1970.

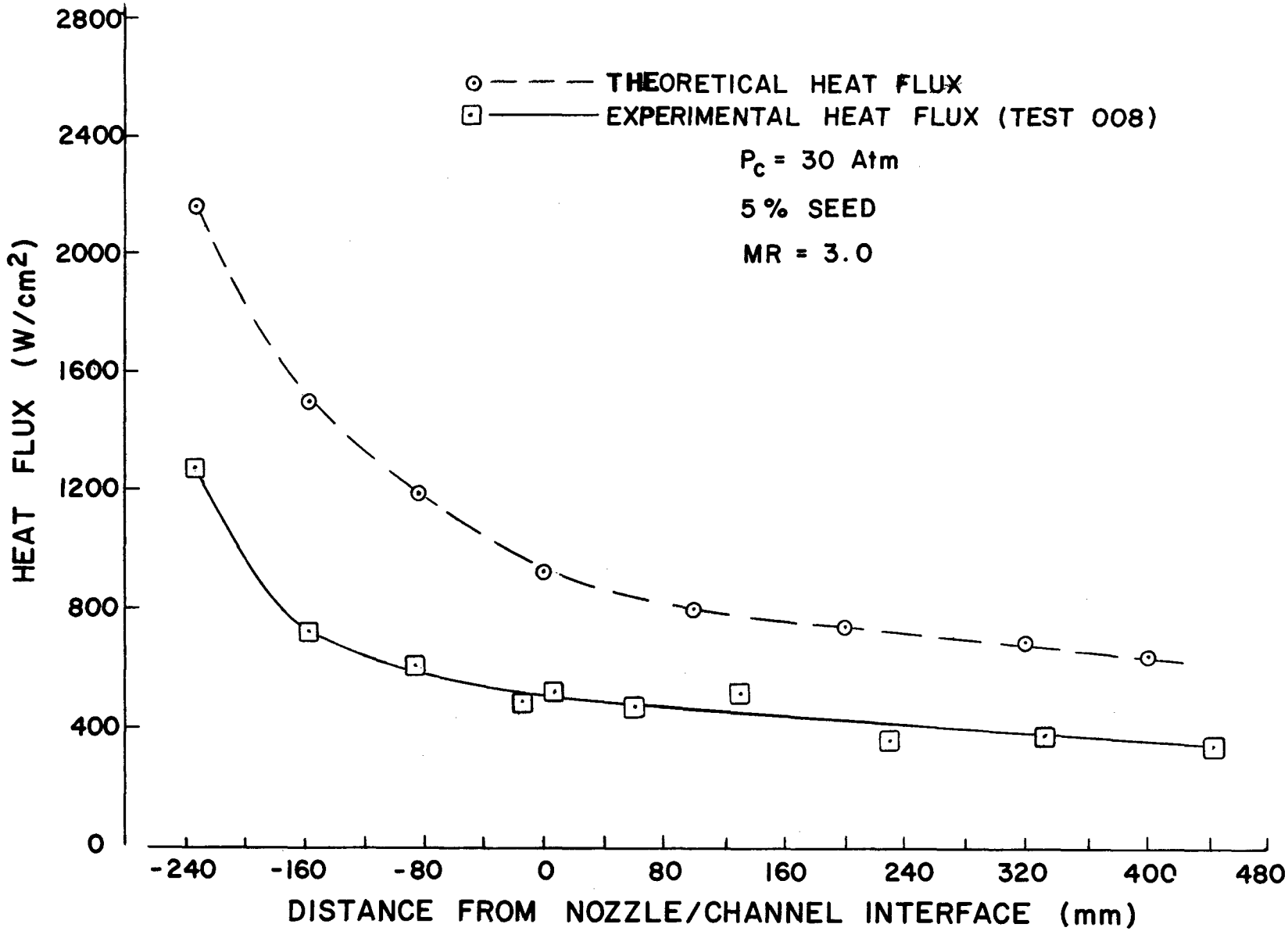

Figure 227. Comparison of Measured and Theoretical Heat Flux.

TABLE 71. RESULTS OF TEST 008

Frame No.	Water Side Film Coefficient ($w/cm^2 K$)	Maximum Water Side Copper Wall Temperature (K)	Maximum Gas Side Copper Temperature (K)
1	7.3	360 K	438
6	7.3	354 K	423
12	7.2	359 K	433
20	5.8	359 K	393
30	5.8	362 K	403
40	5.9	374 K	423

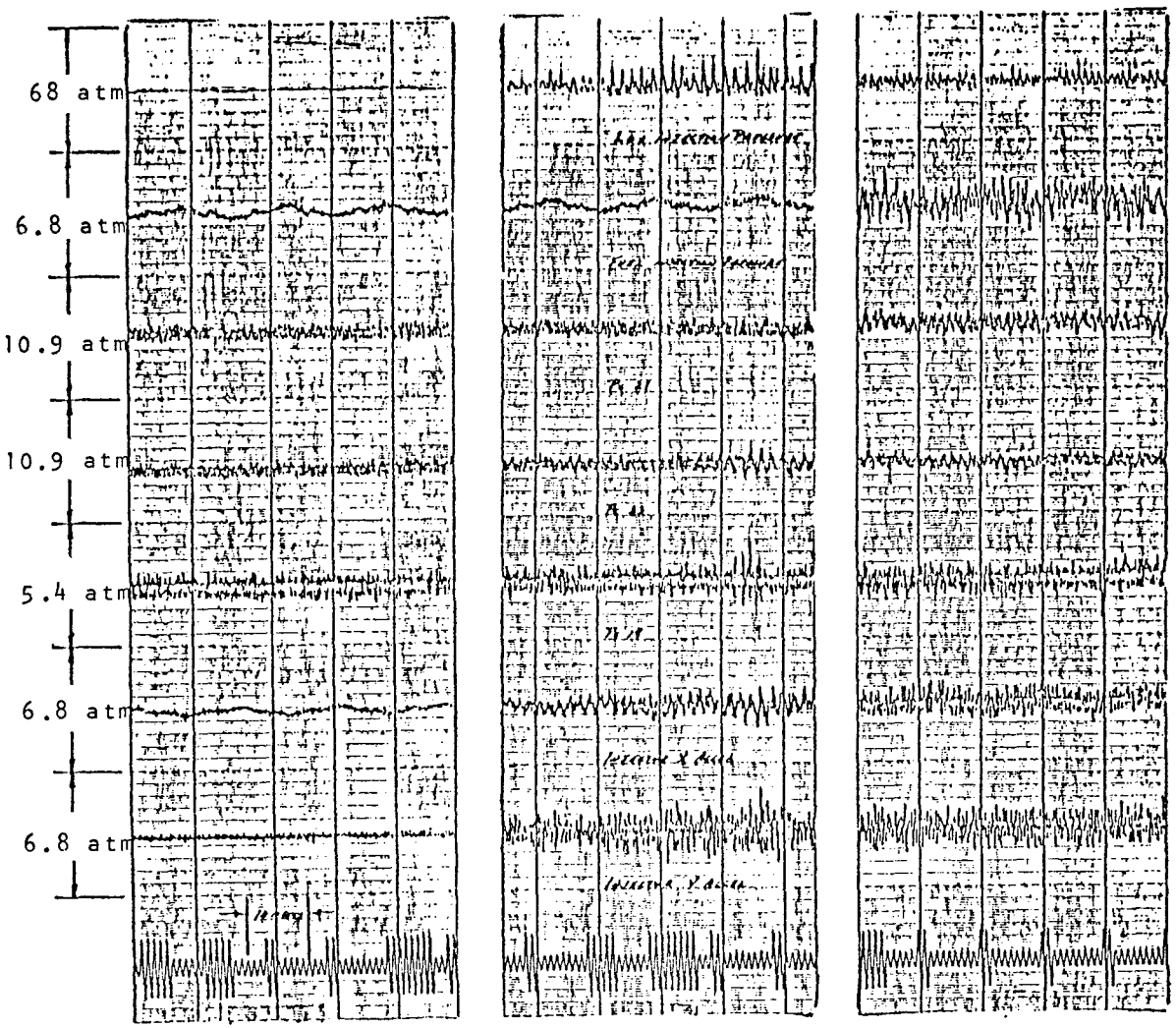

Figure 228. Pressure Time History Records.

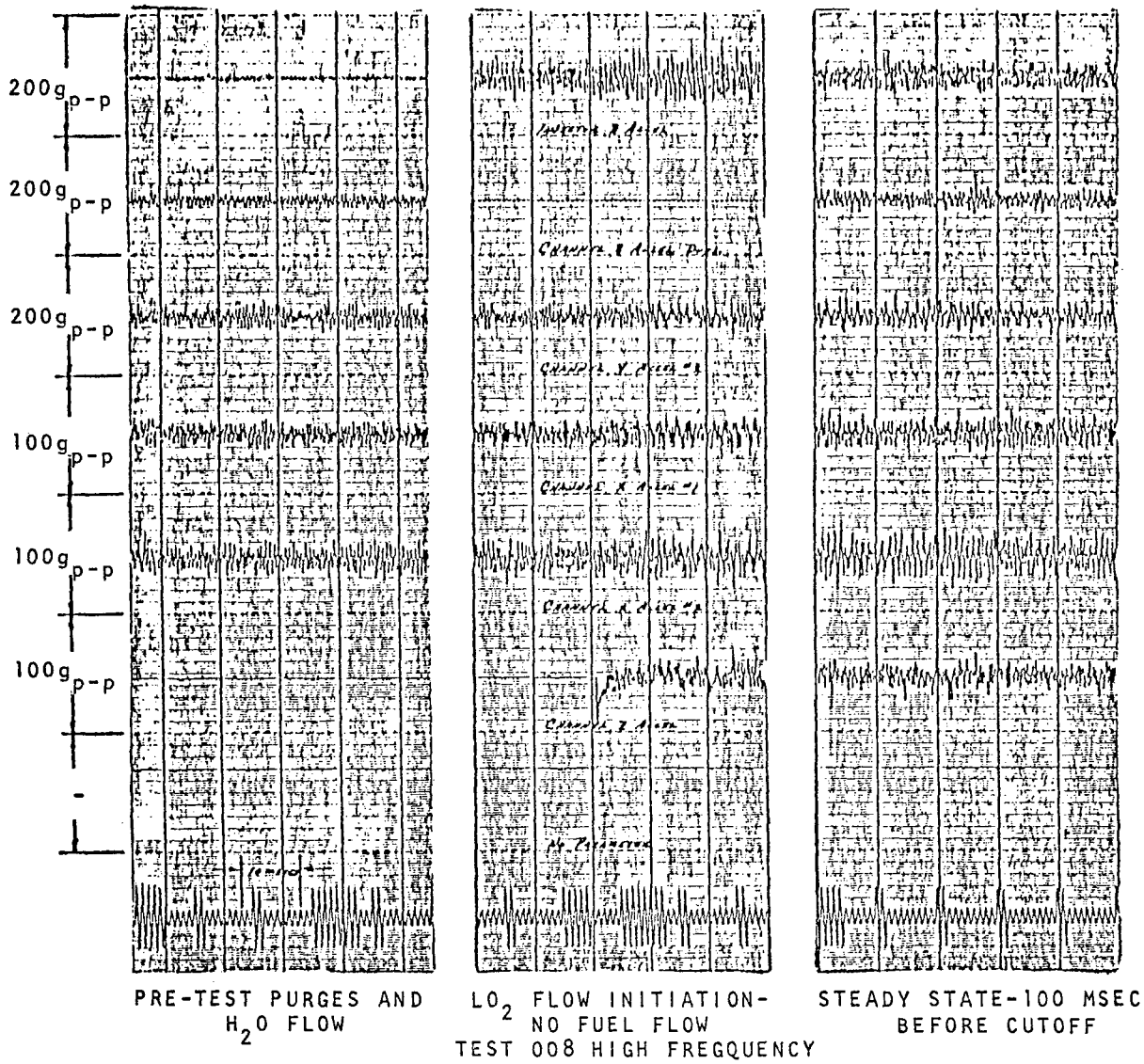

Figure 229. Vibration Time History Records.

in the noise level during the introduction of LO_2, and then a steady-state condition 100 msec prior to cutoff. A substantial portion of the steady-state level was superimposed noise created by such items as the high pressure water flow, etc. The maximum single amplitude of the prerun vibration signal appeared to be of the order of 20 g. The traces shown in Figure 229 indicated that the lowest frequency was 80 Hz, with intermediate values at 100 and 400 Hz and a high of 1100 Hz.

The AMS plots of the combustor photocon traces for Pc_{21} for the four tests are shown in Figure 230. This high frequency recording pressure transducer was located at an axial location 5.1 cm from the injector face in the bottom flat surface. Figure 231 shows the AMS traces of the channel accelerometers for test 010. The plots shown in these figures are net values of vibration after the flow noise has been subtracted. Table 72 shows a summary of the AMS results from tests 007, 008, 009, and 010. As shown in Figure 219 the top accelerometers were mounted in the middle of the top side of the channel, and the side accelerometers were mounted in the middle of the side wall of the channel. The #1 accelerometers were located approximately 220 mm from the channel/nozzle interface, and the #2 accelerometers were located near the exit plane of the diagnostics channel, approximately 450 mm from the channel/nozzle interface. As the table shows, the highest levels of vibration of 27 g occurred at the point farthest from the diagnostics channel support.

During the diagnostics channel design a vibration analysis was conducted to determine the natural frequencies expected for the various modes of response. These frequencies were: axial, 107 Hz; pitch or yaw, 55 Hz; case wall deflection, 533 Hz; and electrode frames, 400 Hz.

The experimental frequencies were above the theoretical pitch and yaw values. Consequently, the channel appears to have been isolated from these modes. The wall bending deflection frequency and the frame bending frequency were of the same order of magnitude as the 400 Hz frequency recorded during the experiments. The observed frequencies involved lateral motion only; hence, no assessment was made of the axial response prediction.

During the design of the diagnostics channel, a definite value for the expected vibration input to the channel from the combustor/nozzle was not available. Consequently, the channel was designed for a 25 g load in each direction, single amplitude. Considering the mass per unit area of the channel wall, this effect corresponded to an equivalent pressure of 0.20 atm, and was included as a component of the total stress in the diagnostics channel. For axial, pitch, and yaw movements of the channel as a rigid body, the input frequencies were assumed to be most severe above 1000 Hz. In this range, the diagnostics channel was isolated. The experimental results have verified that assumption.

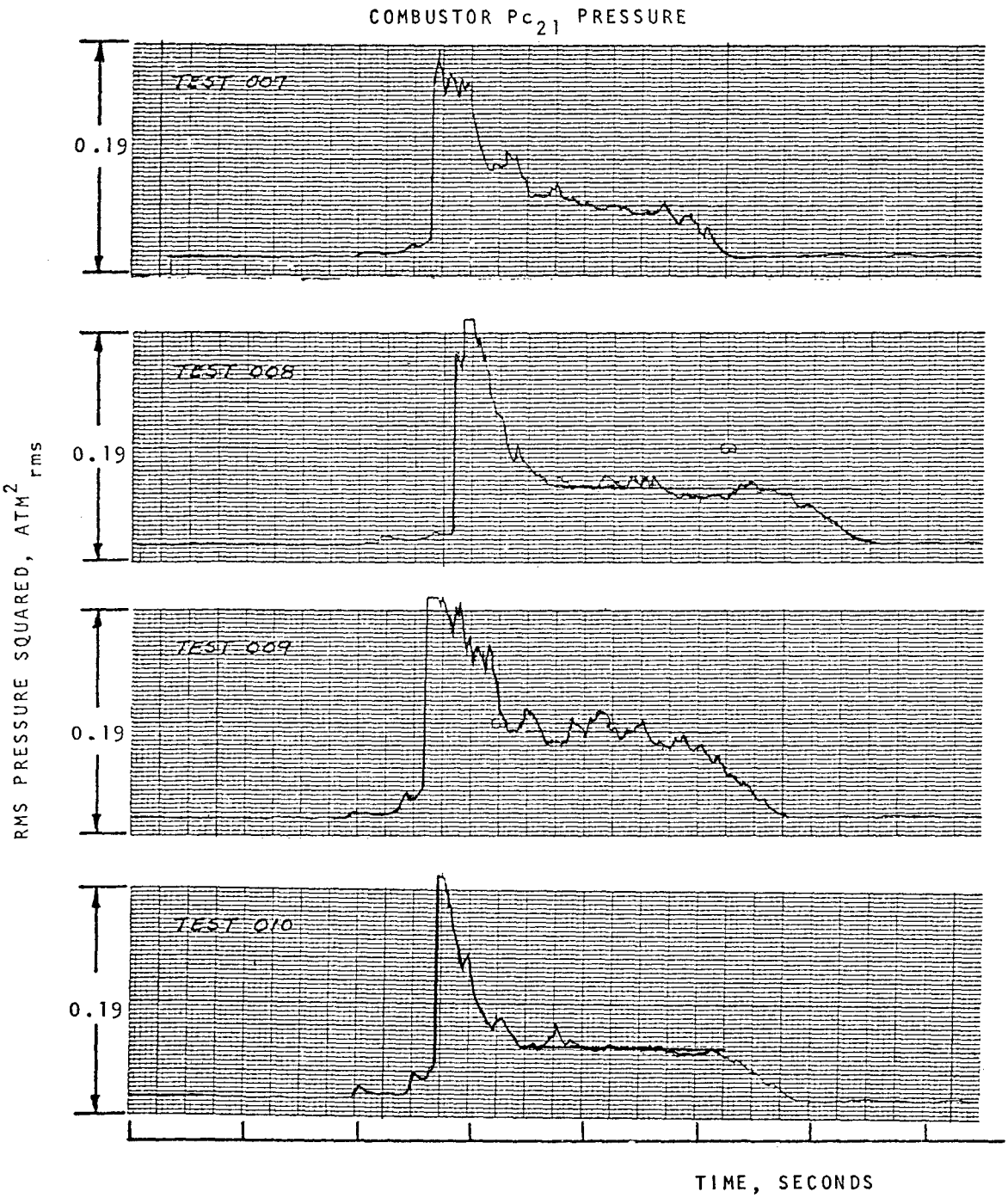

Figure 230. AMS Pressure Traces.

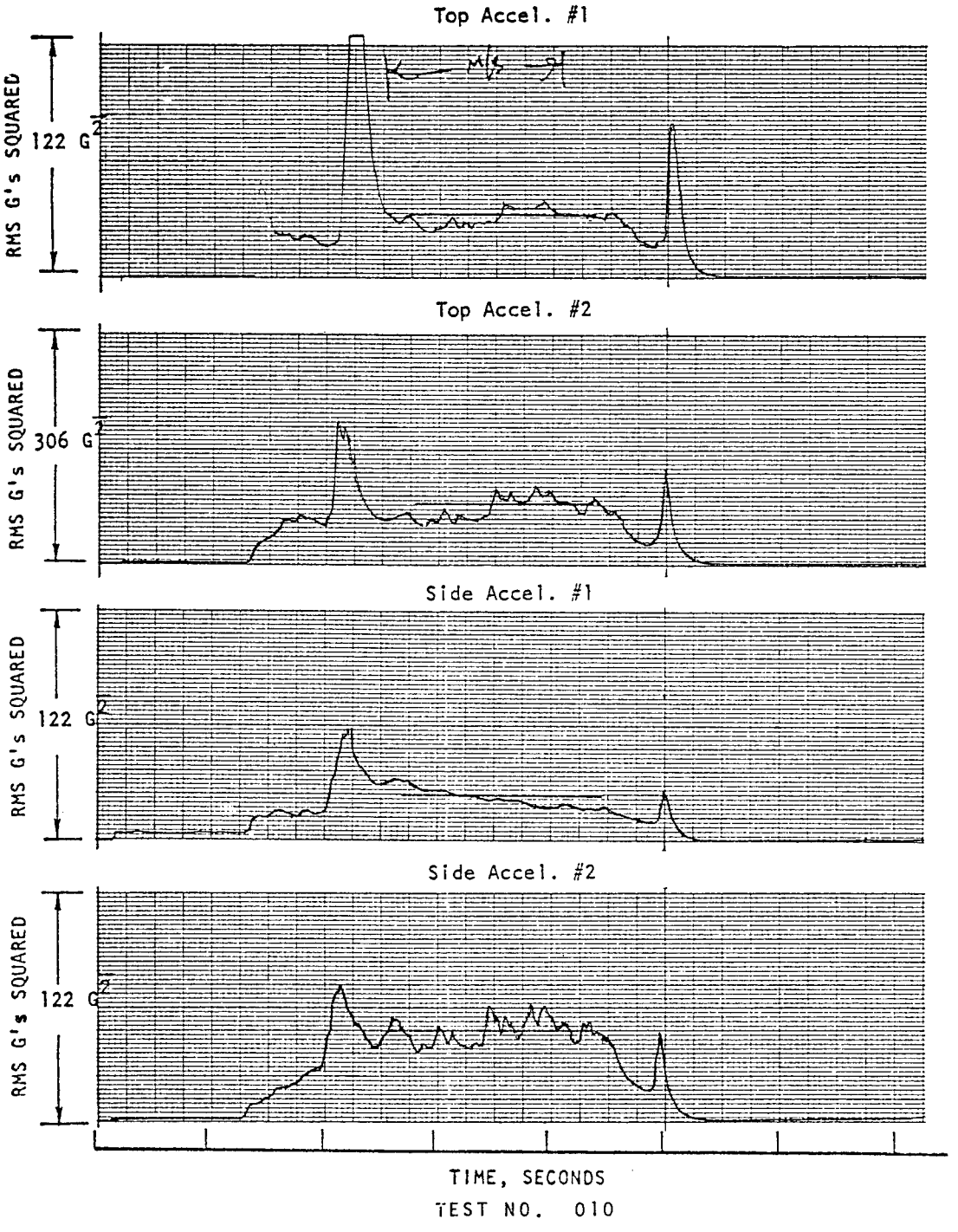

Figure 231. AMS Vibration Traces.

TABLE 72. AMS TRACE SUMMARY

	Units*	Test 007	Test 008	Test 009	Test 010
Top Accelerometer #1	$\overline{G}^2$	--	36.7	51.2	34.2
	G_{p-p}	--	17.0	20.0	16.4
Top Accelerometer #2	$\overline{G}^2$	64.7	91.8	91.8	76.5
	$\overline{G}_{p-p}$	22.5	26.8	26.8	24.5
Side Accelerometer #1	$\overline{G}^2$	22.0	18.0	25.6	20.7
	$\overline{G}_{p-p}$	13.1	11.9	14.2	12.8
Side Accelerometer #2	$\overline{G}^2$	41.5	63.4	53.7	46.4
	G_{p-p}	18.0	22.3	20.5	19.1
Pc_{21}	$\overline{atm}^2$	0.041	0.044	0.070	0.043
	atm_{p-p}	0.56	0.59	0.74	0.58

* The accelerometers are measuring vibration at various channel locations. The pressure transducer is measuring combustor pressure fluctuations.

f. Conclusions

The experimental data obtained during the diagnostics channel tests showed the channel to operate reliably for the range of mixture ratios and Cs_2CO_3 percentages tested. Measurements of the electrical conductivity of gas, the channel wall heat flux rates, and the channel vibrations were obtained, the data reduced, and interpretation of the data was completed. Only the first test of this test series, which was conducted at a reduced mass flow rate, showed any anomalies.

The electrical conductivity of the gas was greatest for a mixture ratio of 3.0, and 10% by mass $Cs_2\ CO_3$ did not increase the gas conductivity. The test results from the stoichiometric mixture ratio tests also resulted in a lower gas conductivity than the fuel rich tests at a mixture ratio of three. The increase in electrical conductivity for the lower mixture ratios was consistent with the theoretical predictions. The maximum inlet conductivity of 15 mhos/m occurred at a mixture ratio of 3.01 and a Cs_2CO_3 percentage of 5.15%. This conductivity was within 10% of the original estimate, and indicated sufficient electrical conductivity to verify the channel design assumptions.

The reduced heat transfer data indicated wall heat fluxes which were substantially lower than the theoretical predictions. The maximum inlet heat flux was approximately 75% of the calculated value. This resulted from the fact that the theoretical calculations were based on matching the boundary layer conditions at the channel/nozzle interface. Consequently, any variation in the calculated heat flux in the nozzle region also was present in the calculated heat flux for the diagnostics channel. Except for the inlet region of the diagnostics channel, the wall heat fluxes for the diagnostics channel were relatively insensitive to variations in the mixture ratio or Cs_2CO_3 percentage. As expected, the heat flux was lower for the electrode which contained more ceramic. The results were within the upper limits of the high power MHD channel/diffuser system cooling design. While some modifications to the electrode design may be required, these are expected to be relatively easily accomplished.

The high frequency vibration data analysis showed that the diagnostics channel behavior was within the design limits. While the diagnostics channel system was markedly different from the high power MHD channel/diffuser system in length and support method, some conclusions concerning the dynamic structural integrity of the high power MHD channel/diffuser can be formulated.

The vibration frequencies in the entrance region of the high power MHD channel/diffuser should be slightly lower in the wall bending mode because the frames will undergo a transition from perpendicular to slanted in the channel/diffuser. Therefore, these electrode frames in the MHD channel will be longer than any of the electrode frames in the diagnostics channel. Since the frequency

is inversely proportional to the square of the span of a plate or beam, the frequencies downstream will decrease rapidly as the high power MHD channel/diffuser walls increase in width. Since most of the frames in the channel/diffuser were oval in cross section as opposed to relatively square for the diagnostics channel, this may affect the character of the flow noise. Therefore, the relation among the relevant parameters could be changed considerably. As a result, the flow noise that was observed at SSFL may not be experienced in the channel/diffuser.

The fiberglass case thickness increased with downstream distance on the high power MHD channel/diffuser. This might be expected to increase the capacity of the case to damp vibrations. However, the natural frequency of the wall also decreased downstream, which could tend to offset that effect. The lowest frequency observed for the diagnostics channel tests was 80 Hz. This frequency would be expected to occur approximately two-thirds of the distance downstream of the entrance if simple beam bending behavior was assumed for the frame case subsystem. This might not be a problem since the case upstream of that location could damp a significant portion of the input energy at 80 Hz, leaving a small proportion to travel downstream.

The same bolting arrangement through belleville springs and three-pin alignment used for the diagnostics channel/nozzle interface will be used on the high power MHD channel/diffuser. The greater mass of the high power MHD channel/diffuser should provide a greater measure of isolation from the high frequency vibrations parallel to the channel/diffuser axis.

SECTION IX

AEDC TEST PROGRAM

A. INTRODUCTION

The gas generator system and the high power MHD channel/diffuser were designed for use in a performance test program in the HPMS test facility at the Arnold Engineering and Development Center (AEDC). In these tests the gas generator system with the cooled wall combustor and a modified support provided by Rocketdyne would supply hot ionized gas to the high power MHD channel/diffuser supplied by Maxwell Laboratories. This equipment would be installed in the HPMS magnet supplied by the AFAPL. In support of this performance test program, the facility requirements were identified, a detailed test plan prepared, subsystem interfaces defined, an interface control system established, and an interface control document issued. The AEDC test plan and the interface control document were prepared for use during Phase C of the overall HPMS program. These two documents were also prepared using as a baseline the cooled combustor and high power MHD channel/diffuser designs. All of the activities described in this chapter represent the plans developed during Phase B of the HPMS program, and do not reflect exactly what may be implemented during Phase C.

B. TEST FACILITY DESCRIPTION

The tests will be conducted at the HPMS test facility of the Propulsion Wind Tunnel (PWT) complex of the Arnold Engineering and Development Center located at Tullahoma, Tennessee. A simplified illustration of this installation is shown in Figure 232.

The high power MHD channel/diffuser will be located within the modified HPMS magnet at AEDC, which can be separated to facilitate installation. The channel/diffuser assembly was designed to be supported at one end by the gas generator and at the other by a mechanical support to the facility. The exact axial location of the high power MHD channel/diffuser is to be selected on the basis of the measurements of the actual magnetic field.

The gas generator provided the hot gas directly to the MHD channel/diffuser. The combustor and flow control valves were all designed to be mounted on a support structure which was fixed to the facility floor. This structure supported the components and resisted the thermal load of the hot gas flow train.

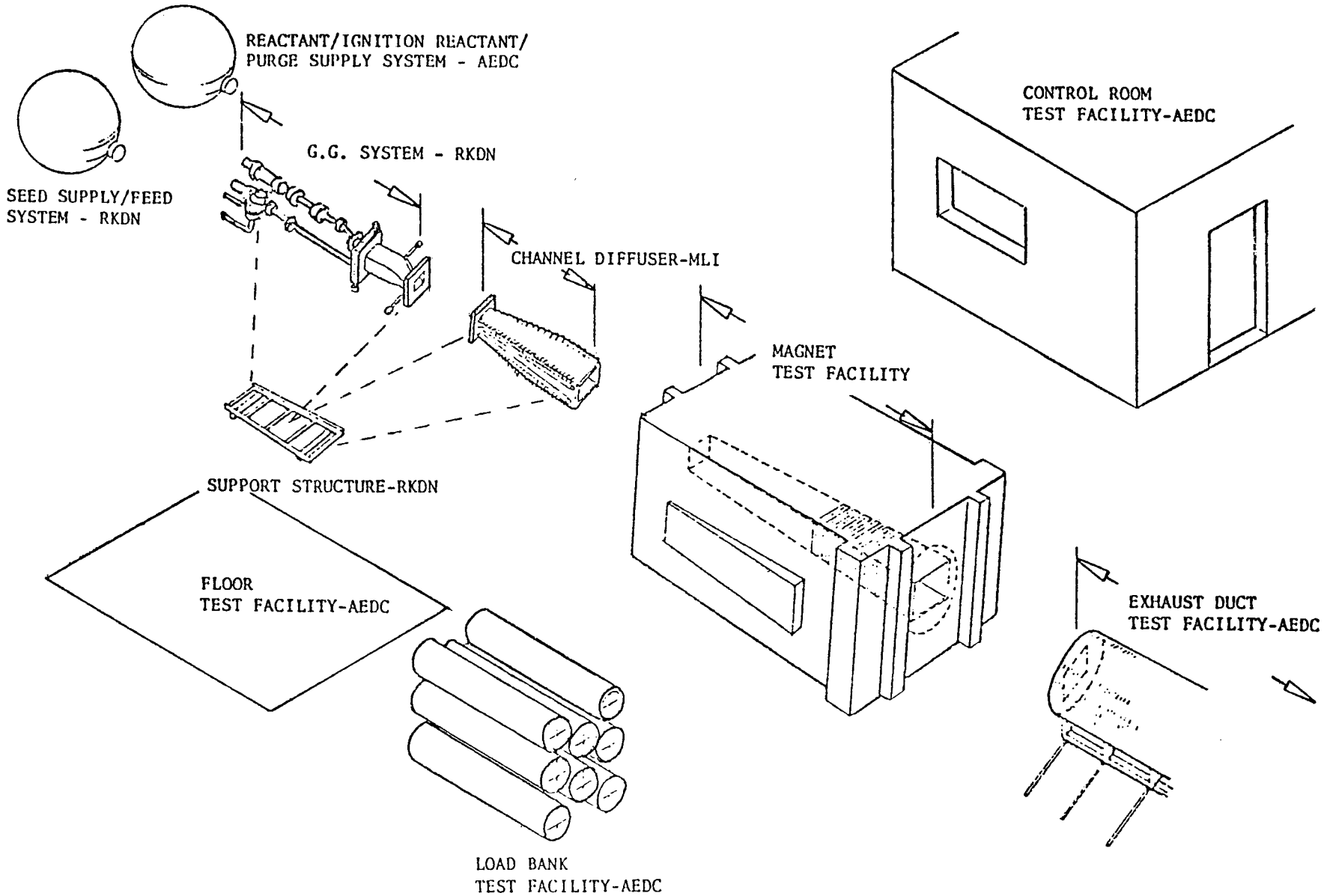

Figure 232. AEDC Test Facility.

Reactants are fed to the gas generator from the facility tanks located external to the test building. The reactants are fed by pressurized gas. The seed solution system was used in the development test program at SSFL and will be located in the test area. The fluids for valve actuation, purges, etc., are supplied by the facility. The cooling of the combustor is accomplished with a closed circuit deionized water system. The high power MHD channel/diffuser cooling system uses a separate facility water system.

The entire system is operated from an existing control and data acquisition facility. The generated electrical power is dissipated in a test facility load bank. Exhaust gases from the channel enter a facility exhaust duct which conveys them outside the test building.

C. TEST PROGRAM SUMMARY

The objective of the planned AEDC performance test program was to test an advanced liquid fueled high power MHD generator system into a single passive load.[44] The critical performance objectives were a power density of 200 MW_e/m^3, an enthalpy extraction of 1 MJ/kg, and an electrical output power level of 30 MW. This MHD power generator system will consist of the following components:

(1) High Power MHD Channel/Diffuser System
   (a) Channel
   (b) Diffuser
   (c) Cooling Manifold

(2) Gas Generator System
   (a) Combustor Assembly
   (b) Feed System
   (c) Igniter System
   (d) Support Structure
   (e) Purge System

(3) Seed Solution Fluid Supply System
   (a) Storage Tank
   (b) Fluid Feed System

(4) HPMS Magnet
(5) Reactant/Coolant Supply System
(6) Facility Control/Data Acquisition Systems

---

[44] "AEDC Test Plan," MLI No. MHD 218-10-1, January 1978.

Following a gas generator system checkout a total of 37 tests have been defined to verify the performance goals of the MHD generator system. The test program logic is illustrated in Figure 233. Table 73 provides a summary of the planned test program. The test duration, type of test, and purpose of each test are shown. These tests have an accumulated duration of 572 sec and could be conducted during a test program of four months duration. Each of the eight test series are described in the following paragraphs.

Gas Generator Checkout Test Series. The test program will be initiated with a series of gas generator system checkout tests using a combustor checkout duct in place of the high power MHD channel diffuser. Following a series of ignition checkout tests, three combustor hot fire tests will be conducted to verify the operating sequence of the gas generator system in the single shot and multipulse operating modes. These tests will confirm the mass flow rates, combustor performance, and dynamic behavior of the gas generator before the installation of the channel/diffuser.

MHD Generator Checkout Test Series. This initial series of five tests with the high power MHD channel/diffuser will be conducted to establish the thermal and structural behavior of the channel as well as verify satisfactory functioning of the interfaces. These generator checkout tests will be completed and the results analyzed before proceeding to the power and performance tests. The test durations will be approximately three sec. The mixture ratio and Cs_2CO_3 seed rates will be selected based on the results of the development test program at SSFL.

Performance Characteristics Test Series. Eleven performance tests will be conducted to establish the electrical performance characteristics of the MHD generator system. Each of these will be approximately three sec duration. These tests will vary the seed mass flow rate, the load resistance, the magnetic field, and the combustor mixture ratio. A baseline performance for comparison with future performance tests will be established by these tests.

Extended Power and Multiple Test Series. During this series of three tests, one ten-second power run and two multipulse tests will be completed. These tests will be completed at the experimentally determined optimum operating conditions.

Power Test Series. Five power tests will be conducted for various operating conditions. These tests will be completed to maximize the electrical output power. The seed rate, mass flow rate, and magnetic field will be varied during this test series. Variations from the nominal operating conditions will be limited to $\pm$ 20%.

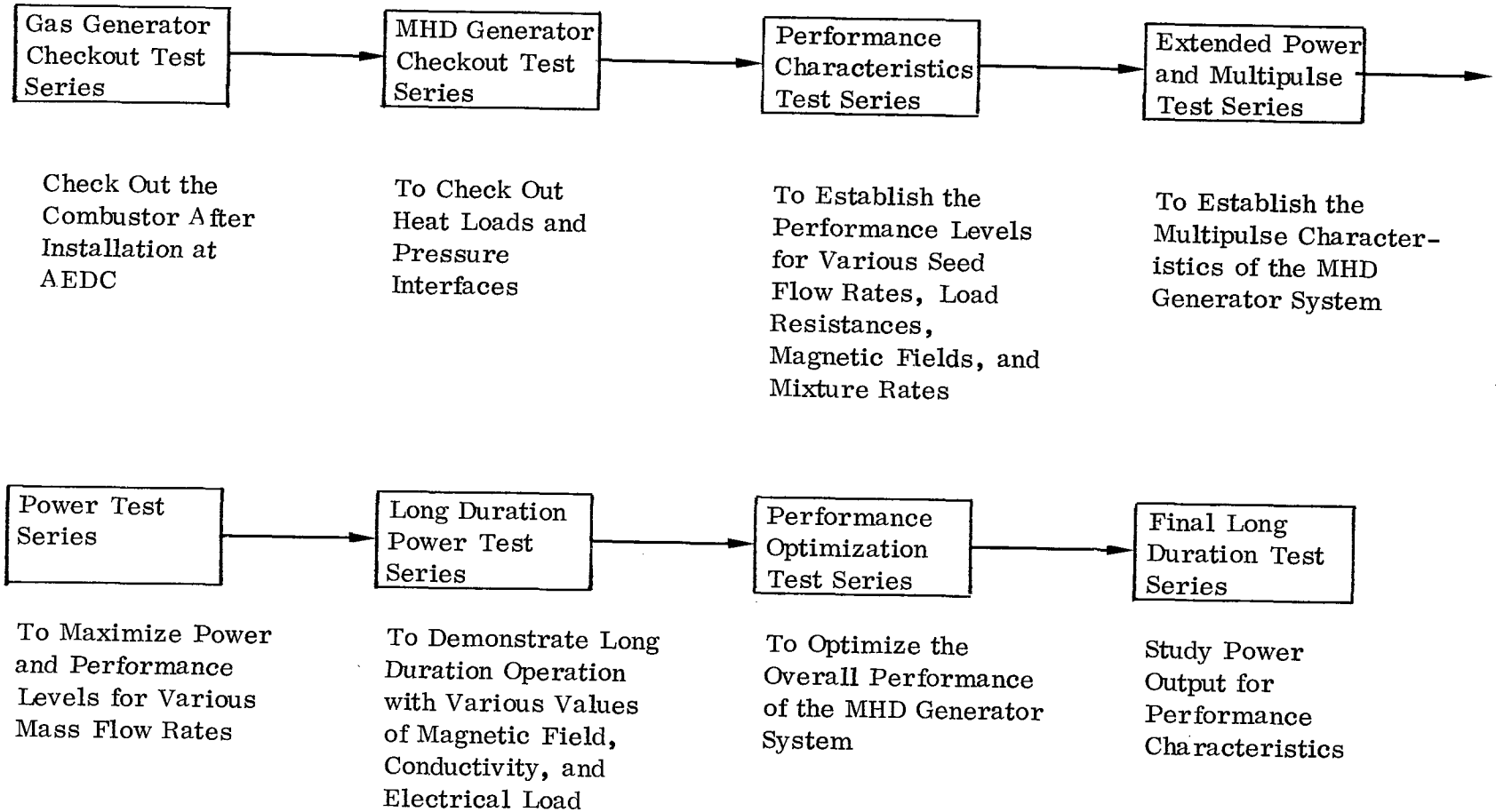

Figure 233. AEDC Test Program Logic.

TABLE 73.

30 MW CHANNEL/DIFFUSER TEST PLAN AT AEDC

TEST NUMBER AND SEQUENCE	TEST DURATION (SECS)	TYPE OF TEST	PURPOSE AND/OR VARIABLES
1	3	GAS GENERATOR CHECKOUT	COMBUSTOR CHECKOUT, MASS FLOW
2	3	" " "	" " " "
3	6	PULSE CHECKOUT	3 SEC ON, 3 SEC OFF, 3 SEC ON
4	3	MHD GENERATOR CHECKOUT	HEAT LOADS, PRESSURE INTERFACE
5	3	" " "	" " " "
6	3	" " "	" " " "
7	3	" " "	" " " "
8	3	" " "	" " " "
9	3	PERFORMANCE CHARACTERISTICS	30 MW, SEED MASS, LOAD, MIX, CONDUCTIVITY, VI
10	3	" "	" " " " "
11	3	" "	" " " " "
12	3	" "	" " " " "
13	3	" "	" " " " "
14	3	" "	" " " " "
15	3	" "	" " " " "
16	3	" "	" " " " "
17	3	" "	" " " " "
18	3	" "	" " " " "
19	3	" "	" " " " "
20	10	POWER, EXTENDED TIME	CONSTANT POWER
21	6 (PULSED)	MULTIPULSE	3 SEC ON, 3 SEC OFF, 2 PULSES
22	21 (PULSED)	"	7 SEC ON, 4 SEC OFF, 3 PULSES
23	5	POWER	± 20% MASS, MIX, CONDUCTIVITY
24	5	"	" " " "
25	5	"	" " " "
26	5	"	" " " "
27	5	"	" " " "
28	60	POWER, EXTENDED TIME	FIELD, CONDUCTIVITY, LOAD
29	150	" " "	" " "
30	5	PERFORMANCE OPTIMIZATION	VARIABLES AS REQUIRED
31	5	" "	" " "
32	5	" "	" " "
33	5	" "	" " "
34	5	" "	" " "
35	5	" "	" " "
36	60	POWER, EXTENDED TIME	STUDY OUTPUT
37	150	" " "	" "
[APPROX 37 TESTS TOTAL]	[TOTAL TIME "ON" SECS - 572]		

Long Duration Power Test Series. Two long duration power tests, one of 60 sec duration and the other of 150 sec duration, will be completed. These tests will be used to establish the steady-state performance of the high power MHD generator system. During the tests the magnetic field and conductivity may be varied.

Performance Optimization Test Series. A series of six performance optimization tests, each of five sec duration, will be completed to maximize the electrical power output of the generator. The test variables will be altered as required to maximize the output of the MHD generator.

Final Long Duration Test Series. The final series of two tests will be completed to establish the optimum operating conditions and to study the output and the characteristics of the generator operating under these conditions. One test will be of 60 sec duration and the other will be of 150 sec duration.

D. INTERFACE CONTROL SUMMARY

The identification, description and control of interfaces between the six general subsystem areas was accomplished through an Interface Control Working Group (ICWG) and an Interface Control Document (ICD). The ICWG identified interfaces, coordinated the development of interface descriptions, documented the descriptions and controlled modifications to these descriptions. The ICD was initially established to document interfaces and describe methods for coordinating and controlling the physical and functional interface descriptions. As the subsystem designs developed, interface descriptions were generated and included in the ICD. These descriptions now form a basis for control of the individual subsystem designs to assure compatibility.

This method was used to control the interface between the heat sink combustor and diagnostic channel used in the development test program at SSFL. From an interface standpoint these components were identical to the AEDC test hardware. These two components matched perfectly, and the installation of them at SSFL was readily accomplished.

The Interface Control Document addressed the interface requirements of the AEDC test article which was comprised of the fluid supply system, combustor/nozzle, channel/diffuser, and magnet.[45] The system for generation, control, and change of documents that identified the physical, environmental, and functional interface requirements between the components and/or subsystem of the high power MHD system was defined. Instructions were provided for the formation of Interface Control Working Group (ICWG). The information contained in this document was compatible with the MHD system drawings, but was not used to fabricate, procure or inspect fabricated hardware.

[45] "Interface Control Document," MLI No. MHD 218-9-1, April 1978.

Over 300 interfaces have been identified and described. These interfaces were coded with a five digit number for identification. The interface descriptions were provided through a series of drawings and tables. Because the ICD was used to control mechanical interfaces, dimensions were in the English system of units. Interface information is briefly described in the following paragraphs.

MHD System Envelope Drawing. These drawings defined allowable overall MHD system external dimensions for each of the major components. An allowable volume envelope was established for the fluid feed system, combustor/nozzle, channel/diffuser, and magnet.

MHD Interface Drawing. These drawings were pictorial views, dimensional data, and mating characteristics of each MHD system interface connect points.

MHD Mechanical Interface Description. These data provided information about the physical characteristics of each MHD interface connect point in terms of responsibility, material, location and maximum allowable loading.

MHD Electrical Interface Description. These data provided information about pin function, voltage limits, current limits, resistance values, and connector type for each MHD system electrical interface connect point.

MHD Operational Interface Description. These data provided information about fluid cleanliness limits, operational limits, operational characteristics, fluid connection operating criteria and limits, and operational sequence limits.

MHD Instrumentation Interface Description. These data provided information on pin or wire function, voltage limits and current limits for each instrumentation interface connect point.

SECTION X

RELIABILITY AND MAINTAINABILITY ANALYSIS

A. INTRODUCTION

The purpose of the Reliability and Maintainability Analysis (RMA) was to eliminate or minimize the probability of occurrence of the failure modes that could have affected the system performance or operation. The hot gas flow train and ancillary equipment were given careful consideration and study at all of the critical phases of the design and fabrication efforts that occurred during this program. Although no testing was performed specifically for the purpose of the RMA, the heat sink combustor, and diagnostics channel system tests have provided actual test information from the development test program relating to this analysis.

The reliability and maintenance characteristics of the gas generator components and the feed and control system were evaluated. The evaluation included the subsystems to be used in the AEDC performance testing: combustor assembly, the feed system, and the structural support. Facility systems such as the oxidizer and fuel tanks, magnet, gaseous nitrogen supply, test control sequencer, and data recording system were excluded. Emphasis was placed on the items that affected the successful operation of the hot gas flow train as opposed to items that would lead to a hardware damage-type of failure.

Each component of the channel/diffuser and manifold system is identified and analyzed with respect to its function, failure mode, failure effects, probability of failure, maintainability provisions and maintenance frequency. The results of this analysis, arranged in a criteria matrix, are presented in both qualitative and numerical form. The probability of failure, based on the design system operation within the performance requirements of the contract, was given an estimated numerical rating of percent probability of failure. A rating less than 5% implied that the failure was not likely to occur within the design life of the component while a rating greater than 95% implied that the failure was most likely to occur.

B. GAS GENERATOR COMPONENT RELIABILITY

The gas generator components include the cooled wall combustor/nozzle, injector, seed mixer, and two igniter combustors. Each of these components was to be demonstrated prior to use in the performance test program at AEDC.

Following this successful demonstration, these components would be expected to have a very high reliability relative to the feed system components as long as system operation remained within the design limits. There were no moving parts to deteriorate, and the only operational factor to impact reliability was the accumulated cyclic life. The cooled wall combustor was designed for a life of approximately 375 full thermal cycles. Up to this point, the probability of successful operation should effectively be 100%. After this point there is the potential for the development of small cracks in the combustor walls that could lead to the leakage of the coolant into the interior of the combustor. While the appearance of a crack would not jeopardize the test, further testing would involve the risk of additional cracking and the eventual deterioration of the combustor liner.

The cyclic life of the injector, igniters, and seed mixer were in excess of 375 cycles. The probability of successful operation should effectively be 100% up to 700 to 800 cycles as long as the gas generator is operated within proper limits.

C. FEED AND CONTROL SYSTEM RELIABILITY

The reliability of feed and control components of the gas generator system was evaluated. This evaluation was based on the cooled wall combustor system described in Figures 179 and 201 The reliability evaluation was based on the probability of the system successfully operating for a given test. Since the system had a comprehensive safety circuit, the possibility of hardware damage was very low; therefore, the emphasis was placed on the probability of a successful startup steady-state operation, and shutdown for any given operation. The vast majority of the unsuccessful test operations would result in a shutdown of the system which could then be inspected and restarted.

As a result, transducers necessary to the system start and shutdown were included. Instrumentation for the purpose of a data gathering was excluded, as well as items such as timers which were part of the facility sequencer. Joints and tubing also were excluded from the direct evaluation. The tubing had a very high reliability and would have negligible impact. Joints were periodically leak checked and, therefore, had a high reliability.

To determine reliability, individual components were identified and failure rates determined. The failure rates were determined from data in References 46 and 47 The results are summarized in Table 74. The overall probability of a

---

[46] Earles, D.R. and M.F. Eddins, Reliability Engineering Data Series Failure Rates, Avco Corporation, April 1962.

[47] Nonelectric Reliability Notebook, Hughes Aircraft Company, January 1975.

TABLE 74. GAS GENERATOR SYSTEM - PROBABILITY OF SUCCESSFUL OPERATION

Subsystem	Probability of Successful System Operation
Purge	0.999692
CH_4	0.999732
GO_2	0.999882
Fuel and Seed	0.999322
LO_2	0.999686
Cooling	0.999618
Miscellaneous	0.999722
Total	0.997776

successful test was approximately 99.8%. One component, the pressure transducer, had a relatively high failure rate and was used extensively in the system to provide continue signals in the start sequence and in "blueline" and "redline" safety circuits. These components played a major part in reducing the probability of a successful system operation.

D. GAS GENERATOR SYSTEM MAINTENANCE

Maintenance and checkout requirements that were recommended for implementation at the system operating site are described below. Listed are general requirements, inspections that should be performed prior to system installation, verification tests that should be done after system installation, requirements to be fulfilled prior to system operation, activities for securing the system after operation, and postoperation inspection and tests. Periodic maintenance requirements are identified, and corrective maintenance is discussed.

Within the cyclic life limit, there were no components that require periodic replacement. Emphasis was, therefore, placed on inspection and identification of nonperiodic maintenance items.

1. System Installation Inspection

The inspections outlined below should be completed to ensure that no damage has occurred during shipment. These following tasks should be performed before connecting the system to the facility:

Interfaces	Remove covers; inspect all exposed portions of the system.
Electrical Connectors	Inspection connectors for cleanliness, corrosion damage, and correct identification.
Fluid/Pneumatic Line	Inspect sealing surfaces for foreign particles, nicks, scratches, and imperfections that could impair sealing capability.

2. Post-Installation System Verification

The tasks below should be conducted to verify that no damage had occurred during installation, that interface connections were properly made, and that all systems operated satisfactorily when integrated with the facility.

a. Leak/Functional Checkout

The following systems should be leak and function tested: (1) pneumatic control; (2) hydraulic control; (3) purge; (4) ASI CH_3 and O_2 supply; (5) seed solution feed; (6) JP-4 feed; (7) LO_2 feed; and (8) combustor coolant water supply. During this check, the valve actuation times should be recorded to verify the operational sequence.

b. Combustor Seal Checkout

The combustor exit test plug should be installed, and the combustor pressurized to approximately 5 atm with an inert gas. The combustor/injector seals should be leak tested as well as line connections downstream of the main valves.

c. Injector Purge

A trickle GN_2 purge must be maintained through the gas generator injector oxidizer manifold whenever system is in a standby mode. If the system is to be inactive for one month or longer, the purge may be discontinued. However, if the purge is discontinued, the LO_2 side of the gas generator injector must be flushed with a suitable solvent and dryed to remove any hydrocarbons prior to system operation.

3. Pre- and Post-Operation Requirements

These tasks verify that the systems were ready to receive fluids and pneumatics for system operation and that the systems were properly secured after the test was completed.

a. Pre-Operation Requirements

Closure Removal - Remove covers and closures from bleeds and other system openings.

Inspection - Inspect exposed and accessible portions of the systems for general physical condition.

Valve Check - Verify position of all system control valves.

Pressure Check - Pressure check combustor seals at pressure of about 2 atm purge flow.

Pressure check line connections using inert gas.

b. Post-Operation Maintenance

Check purge system gauges for proper pressure setting.

Verify injector oxidizer manifold trickle purge.

Cover Installation - Install covers as necessary.

Seed Mixer Cleaning - Circulate fuel through mixer and bleed system to remove residual seed solution.

External Inspection - Visual inspect system exterior for evidence of leaks or fire damage.

Post-Operation Data Review - Fault isolation is primarily done through analysis of test operating data. This is an important part of identification of maintenance.

Verify valve times for proper operation; record times for future trend analysis.

Verify pressure and temperature readings at all points for proper range.

Internal Inspection - Inspect internal areas of combustor and injector face for erosion or cracks. If the channel is not removed, perform inspection through igniter port using borescope and light source.

Torque Check - Torque check the following:

Injector-to-combustor bolts
Combustor-to-channel bolts
ASI-to-combustor bolts
Main fuel valve flange bolts
Main LO_2 valve flange bolts

Record results of torque check. Discontinue postoperation torque check on connection when all bolts on the connection do not move during torque check.

4. Periodic Maintenance

Within the limits of the gas generator cyclic life, there were no components that were designed to require periodic replacement. The following activities, therefore, are primarily inspection and checkout.

Combustor Interior Inspection - At the completion of six operations of the system with the channel installed, remove channel and perform the following:

Inspect combustor interior/injector face.
Leak Check - install test plate on combustor exit; maintain closing pressure on main valves and pressurize injector/combustor; leak test all connections on injector/combustor.

Test Abort Inspection - During system operation, if a test is terminated by an over temperature condition (redline cutoff), or if an abnormal coolant bulk temperature change is observed, perform gas generator injector/combustor leak test as specified above.

Relief Valve Check - Functionally check relief valves annually.

Instrumentation Calibration - To maintain data accuracy, instrumentation should be recalibrated on a six to twelve month period.

Pressure Transducer Inspection - Because of their importance to system operation, pressure transducers should be checked both by reviewing test records and period recalibration.

Combustor, Injector, Igniter Replacement - These components are designed for 375 full thermal cycles. A record of the number of system operations should be maintained. At approximately 375 cycles, these components should be replaced. However, not all operations constitute a complete thermal cycle, and even an aborted test may be a full thermal cycle.

5. Corrective Maintenance and System Reverification

The system was designed so that a component malfunction can be readily determined and isolated to the item requiring replacement or repair.

Component Replacement - In the majority of the cases, system problems will be remedied through component replacement or repair of the component when removed from the system.

Component Accessibility - Component removal and installation is affected by accessibility, the need to use special handling equipment for heavy items, and the number of connections. Location of the gas generator injector is such that it is necessary to remove the channel and combustor to gain access for removal. The remaining components are directly accessible.

Reverification - System reverification after maintenance consists of performing a leak test on the disturbed or opened joints and a function test of the replaced component.

E. CHANNEL/DIFFUSER AND MANIFOLDS

The high power MHD channel/diffuser and manifold system components were grouped according to their functions: electrode system, cooling system, gas seals, channel and diffuser cases, and instrumentation and electrical. Each subsection presents the results of the RMA for each of the five system components.

1. Electrode System

The electrode system components were the electrode frame assemblies, the electrode screen, the electrode ceramic, and the insulator ceramic. Of these the electrode ceramic and the insulator ceramic have the highest probability of failure of the electrode system components. The insulator ceramic was particularly vulnerable because of the ceramic susceptibility to cesium carbonate penetration, and hence, the ceramic becomes more of an electrical conductor than was desired. The electrode ceramic also was susceptible to the same type of damage from impurities, thus decreasing the performance of the electrode ceramic. Table 75 provides a summary of the results of the RMA for the electrode system.

TABLE 75. ELECTRODE SYSTEM RMA

Component Identification	Component Function	Failure Mode	Failure Effects	Probability of Failure	Maintainability Provisions	Maintenance Frequency
Electrode Frame Assemblies	Extract energy from plasma	Burnout because of excessive temperatures	Decrease power output	< 5%	Cut through case and replace frame	Seldom
Electrode Screen	Conduct electric current and heat	Thermal erosion	Decrease current flow	< 5%	Require replacement of electrode frame	Seldom
Electrode Ceramic	Electric current collector and emitter	Spalling and erosion	Increase Electrode voltage drop	20%	Cast replacement ceramic from inside of channel	Periodic with operation, as required
Insulator Ceramic	Prevent electric current flow between frames	Spalling, erosion and contamination by conductive seed and moisture	Decrease output voltage	20%	Cast replacement ceramic from inside of channel	Periodic with operation, as required

2. Cooling System

The cooling system components were the water manifolds for the channel and diffuser, the cooling tubes for the channel electrodes, the cooling tubes for the diffuser wall, and the water hoses for the channel and diffuser. Of these the water hoses and connections for the channel and diffuser had the highest probability of failure of the cooling system components. The problem was most severe at the connections where minor leaks could occur after prolonged usage. Table 76 provides a summary of the results of the RMA for the cooling system.

3. Gas Seals

The gas sealing system components were the nozzle/channel interface seal, the channel/diffuser to exhaust duct interface seal, and the channel cooling tube gas seals. The probability of failure for each of these three components was approximately equal, and if properly installed, failure was not likely to occur during the design life. After prolonged periods of operation, leaks may develop from the effects of repeated thermal and mechanical cycling. Table 77 provides a summary of the results of the RMA for the electrode system.

4. Channel/Diffuser Case

The case system component was the composite channel/diffuser case. Within the design cycle life this component was not likely to fail. A summary of the results of the RMA for the channel/diffuser case system is given in Table 78.

5. Instrumentation and Electrical Components

The instrumentation and electrical system components were the accelerometers, the channel/diffuser pressure transducers, the channel/diffuser pressure taps, the channel/diffuser case and cooling water thermocouples, and the electrical wiring. Of these the channel/diffuser pressure taps and the channel/diffuser case and cooling water thermocouples had the highest probability of failure of the instrumentation and electrical system components. The pressure taps were particularly vulnerable to blockage from the products of combustion. The blockage was easily removed, and the only loss is the information from that pressure transducer for only the tests conducted while the blockage was present. The thermocouples may also fail because of overheating or the breakage of the wire leadouts. These thermocouples are easily disconnected and replaced by a new one whenever a failure occurs. Table 79 provides a summary of the results of the RMA for the instrumentation and electrical system.

TABLE 76. COOLING SYSTEM RMA

Component Identification	Component Function	Failure Mode	Failure Effects	Probability of Failure	Maintainability Provisions	Maintenance Frequency
Water Manifolds, Channel/ Diffuser	Distribute and collect channel/ diffuser coolant	None	N/A	0%	N/A	N/A
Cooling Tubes, Channel Electrodes	Control electrode temperature	Leaks	Degrade performance Possible electrical short to ground.	< 5%	Repair or replace	Seldom
		Blockage	Overheating	< 5%	Remove blockage	Seldom
Cooling Tubes, Diffuser Wall	Control diffuser wall temperature	Leaks	Possible electrical short to ground.	< 5%	Repair or replace	Seldom
		Blockage	Overheating	< 5%	Remove blockage	Seldom
Water Hoses, Channel/ Diffuser	Transfer coolant water between manifolds and channel/diffuser	Leaks at connections after prolonged operation, blockage	Component destruction through burnout, if coolant lost or blocked.	< 5% with proper operation	Tighten or replace hoses and/or fittings	Seldom

TABLE 77. GAS SEALS RMA

Component Identification	Component Function	Failure Mode	Failure Effects	Probability of Failure	Maintainability Provisions	Maintenance Frequency
Interface Seal, Nozzle/ Channel	Prevent leakage of pressurized hot gas	Leaks may occur after prolonged operation from the effects of temperature, pressure, and thermal expansion	Hot gas might degrade composite channel case and damage adjacent non-metallic components.	< 5% (if properly applied at assembly)	Reassemble channel to nozzle with replacement gasket and new application of silicon rubber sealant	Very low
Interface Seal, Channel/ Diffuser to Exhaust Duct	Prevent entrance of atmospheric air	Leaks may occur after prolonged operation from the effects of temperature, pressure, and thermal expansion	Substantial air leakage into gas flow stream would degrade generator performance and decrease output	< 5% (if properly applied at assembly)	Reassemble exhaust duct to channel/diffuser with replacement gasket and new application of silicone rubber sealant.	Very low
Gas Seals, Channel Cooling Tubes	Prevent gas leakage	Leaks may occur after prolonged operation from the effects of temperature, pressure, and thermal expansion	Degrade performance, damage adjacent non-metallic components	<5%	Reapply silicone rubber to repair seals	Seldom

TABLE 78. CHANNEL AND DIFFUSER CASES RMA

Component Identification	Component Function	Failure Mode	Failure Effects	Probability of Failure	Maintainability Provisions	Maintenance Frequency
Composite Case, Channel/ Diffuser	Main structural member of channel/diffuser primary pressure vessel	Progressive cracking with extended number of run cycles	Loss of structural integrity	< 1% (within the design number of cycles)	Fiberglass epoxy composite is readily repaired	Seldom

TABLE 79. INSTRUMENTATION AND ELECTRICAL RMA

Component Identification	Component Function	Failure Mode	Failure Effects	Probability of Failure	Maintainability Provisions	Maintenance Frequency
Accelerometer	Measure vibrations imparted to the case	Overheating because of localized thermal problem	Loss of measurement	< 1% (if properly installed and operated)	Replace transducer	Seldom
Pressure Transducers, Channel/Diffuser	Measure gas pressure	Most likely mode: mechanical abuse resulting in external damage	Loss of measurement	< 1% (if properly installed and operated)	Replace transducer	Seldom
Pressure Taps, Channel/Diffuser	Conduct pressure pulse to transducer	Blockage from products of operation	Loss of pressure measurement	40%	Remove blockage with flexible probe	As Required
Thermocouples, Channel Case and Cooling Water	Measure temperature of case and cooling water	Burnout because of excessive temperatures or lead breakage because of abuse	Loss of measurement	10%	Remove and replace thermocouple, or disconnect leads and install a replacement nearby	Low
Electrical Taps	Conducts electrical current from frames to load bank	Overheating because of electrical current overload	Loss of output power	< 1% (if properly sized and installed)	Verify proper connections and installation	Low

6. Requirements at Operating Site

a. Installation Inspection

The inspections outlined below are accomplished to ensure that no damage has occurred during shipment. These tasks should be performed before connecting the system to the gas generator and the facility equipment.

Interface	- Remove covers; inspect all exposed portions of the system.
Electrode Surfaces	- Inspect channel interior surfaces to verify condition of electrode and insulating ceramic material.
Channel/Diffuser Case	- Inspect glass-epoxy case for damage.
Electrical Connections	- Inspect connectors for cleanliness, damage, and correct identification.
Coolant Lines	- Inspect sealing surfaces and connections for foreign particles, nicks, scratches, and imperfections or damage that could impair sealing capability. Particular attention should be given to the copper tubes projecting through the glass-epoxy case.

b. Post-Installation System Verification

The tasks below should be conducted to verify that no damage has occurred during installation, that interface connections were properly made, and that all systems operate satisfactorily.

Gas Seals Leak/ Functional Checkout	- The nozzle/channel and channel/exhaust gas seals should be leak checked to verify proper installation.
Channel Coolant Leak/Functional Checkout	- The coolant manifolds and lines should be leak and flow checked.

c. Pre-Operation Requirements

These tasks verify that the system is ready for operation.

Frames resistance check to ground.

Output power circuit continuity check.

Coolant water flow/leak check.

Instrumentation checkout.

d. Post-Operation Maintenance

Internal Inspection - Inspect internal surfaces of channel for damage to electrode and insulator ceramic.

Cover Installation - Install diffuser/exhaust blankoff cover and fill channel interior with dry nitrogen gas at a positive pressure of approximately 0.1 atm.

External Inspection - Visual-inspect the channel/diffuser exterior for evidence of hot gas leaks or fire damage; check manifolds for evidence of water leaks.

e. Periodic and Corrective Maintenance

These items are covered by the detailed listings in the charts previously presented.

APPENDIX A

SAFETY AND HAZARD ANALYSIS

1. INTRODUCTION

This operating Safety and Hazard Analysis (SHA) for the hot gas flow train and ancillary equipment tests at AEDC was conducted in accordance with Section 5.8.2 of MIL-STD-882 of 15 July 1969. The analysis was performed to determine safety requirements for personnel, procedures, and equipment used in installation, maintenance, support, testing, transportation, storage, operations, emergency escape, agress, rescue, and training during all phases of intended use as specified in the system requirements. Engineering data, procedures, and instructions developed from the engineering design and initial test programs were used in support of this effort. Results of these analyses provided basis for:

i Design changes where feasible to eliminate hazards or provide safety devices, and safeguards.

ii The warning, caution, special inspections, and emergency procedures for operating and maintenance instructions including emergency action to minimize personnel injury.

iii Identification of a hazardous period time span and actions required to preclude such hazards from occurring.

iv Special procedures for servicing, handling, storage, and transportation.

Section 2 of this Appendix presents the SHA which was completed for the combustor/nozzle and ancillary. Section 3 presents the SHA for the channel/diffuser and manifold.

2. COMBUSTOR/NOZZLE AND ANCILLARY PRELIMINARY HAZARD ANALYSIS

a. Summary

A preliminary hazard analysis of the MHD gas generator system was conducted to identify and classify the major hazards and to define the design and operational features for elimination or control of the hazards. Table A.1 summarizes the specifically identified hazards by subsystem and indicates the classification and applicable operational phase associated with each.

TABLE A.1

HAZARD SUMMARY

SUBSYSTEM	HAZARD	CLASSIFICATION	PHASE			
			Standby	Start	Operate	Shutdown
CH_4	1. Leakage - Toxic Fume	III	X	X	X	X
	2. Rupture - Fragmentation/Fire	III		X	X	X
	3. Failure to supply - fire/explosion	IV		X		
	4. Failure to terminate	I		X		
GO_2	1. Leakage - Possible fire	II	X	X	X	X
	2. Rupture - Fragmentation/Fire	III		X	X	X
	3. Failure to supply - Fire/Explosion	IV		X		
	4. Failure to terminate	I		X		
JP4	1. Leakage - Possible Fire	II	X	X	X	X
	2. Rupture - Fragmentation	III		X	X	X
	3. Failure to supply - LOX Flow	II		X	X	X
	4. Failure to terminate - High Temp	II				X
LO_2	1. Leakage - Possible Fire	II	X	X	X	X
	2. Rupture - Fragmentation/Fire	III		X	X	X
	3. Failure to supply - Possible explosion	II/IV		X	X	X
	4. Failure to terminate - High Temp	II				X
CS_2CO_3	1. Leakage	II	X	X	X	X
	2. Rupture	III		X	X	X
	3. Failure to Supply	II		X	X	X
	4. Failure to terminate	II				X
HYDRAULIC	1. Leakage - Fire hazard	II	X	X	X	X
	2. Rupture - Control Loss/Fire hazard	III		X	X	X
	3. Fail to Supply - Control loss	III		X	X	X
GN_2	1. Leak	I	X	X	X	X
	2. Rupture - Purge and valve failure	III	X	X	X	X
	3. Fail to supply - Purge and valve failure	III		X	X	X
COMBUSTOR COOLANT WATER	1. Leak	I	X	X	X	X
	2. Rupture - Overheat/burnthru	III	X	X	X	X
	3. Fail to supply - Overheat/burnthru	III		X	X	X
ASI	1. Fail to start - Possible explosion	IV		X		
	2. Fail to cutoff - negligible	I		X		
COMBUSTOR	1. Poor mixing - overtemp	III		X	X	X
	2. Propellant communication - explosion	IV		X	X	X
	3. Vibration - instability	III		X	X	X

b. Potential Hazards

The following potentially hazardous characteristics of the fluids and the system are significant. Special attention should be given to these areas:

(1) Fuel. The fuel was JP-4. This had a higher vapor pressure than RP-1 and should be treated similar to gasoline.

(2) Seed. Cs_2CO_3 was the seed material. In most cases, this will be mixed with the water in the seed tank. However, during the mixing operation, the Cs_2CO_3 will be a fine, dry powder. Although not a dangerous chemical, personnel protection should be used when handling the material.

(3) Exhaust. Cesium compounds will be in the combustor exhaust during the seed tests. Most of the seed tests are 5 sec duration. Longer test runs in the cooled wall combustor tests of 50-150 sec are planned.

(4) Hot Gas at Channel Exit. The hot gas exhausting the channel exit will be at elevated temperature ($\sim$ 2500 K), and be flowing at supersonic velocity.

(5) Oxidizer. Liquid oxygen (LO_2) is used. This is a cryogenic liquid ($T \sim 110$ K); personnel protection from contact with the liquid should be provided. LO_2 is also a vigorous oxidizer. This demands exceptional attention to maintaining the oxygen systems clean and free from reactive contaminants.

(6) Liquid Oxygen/Hydrocarbon Mixture - (JP-4, asphalt, for example). Unignited mixtures of LO_2 with hydrocarbons form shock-sensitive explosives. Situations which could lead to unignited LO_2/hydrocarbon mixtures should be avoided. All fueld should be removed from areas where LO_2 leaks or spills could occur.

(7) Pressurized Tanks. The reactant tanks operated at pressures approaching 137 atm.

(8) Hydraulic Fluid. The oxygen and fuel valves were actuated with hydraulic fluid, which was another fuel.

c. Hazard Avoidance

The following items were recommended as a minimum to avoid unsafe operating conditions:

(1) The test installation should be reviewed and checked for consistency prior to test initiation.

(2) A control sequence employing safety interlock should be used. These interlocks prevent the operating sequence from proceeding until all previous critical operations have safely occurred. The gas generator system sequence logic provided by Rocketdyne should be modified to include the high power MHD channel interlocks identified by Maxwell Laboratories. This logic should be reviewed prior to the initial test by a team selected by Maxwell Laboratories and AEDC. An electrical sequence check shall be made following any sequence change and before each test series or test day.

(3) The test facility should provide an on line secondary control electrical power supply in the case of primary power supply failure.

(4) Blue Lines/Red Lines

Blue line parameters should be used to maintain a critical parameter within safe operating limits. A visually observed parameter value which, if exceeded either before or during a test, should inhibit progression into the test and brought to the Test Engineers' attention for appropriate action.

Red line parameters should be used to provide an automatic cutoff when a critical parameter is exceeded. These parameters are present to provide an automatic shutdown.

(5) Other recommendations, including system leak tests, personnel exclusion, visual observation during tests, etc., are presented in the body of the hazard analysis.

d. Format And Content

The preliminary hazard analysis format was designed to comply with the requirements of MIL-STD-882 and Data Item Description DI-H-3278 "Hazard Analysis Report," paragraph 3, "Preliminary Hazard Analysis" (PHA). Table A.3, following the data entries discussion, provides the PHA for the gas generator system. Data entries are:

(1) Subsystem. The MHD fluid flow system was divided into subsystems for this analysis. Each fluid circuit was designated as a subsystem.

(2) Operational Phase. The following operational phases were defined:

Standby - System primed with fluids but not operating.

Start - Ignition sequence and transient operation to steady-state (Figure 202, "Start Sequence").

Operate - Steady-state operation for the specified test durations.

Shutdown - Cutoff sequence including purges and coolant flow until the system is secured (Figure 203, "Shutdown Sequence").

(3) Hazard. Brief description of the source of the hazard. For the MHD fluid flow systems, the following malfunctions were considered to be hazard sources:

Gross leakage of a fluid.

Burst or rupture of a fluid supply component.

Failure to provide a required fluid to the combustor - start or pulsing.

Failure to terminate flow of a fluid to the combustor if safety-critical.

Burnthrough or erosion of the combustor.

The following were outside the scope of the hazard analysis:

Control valve sequencing and operational failures or errors that were facility controlled, but critical to safety of the system.

Fluid cleanliness and chemical composition that were facility controlled, but could be critical to proper operation.

Facility safety systems such as barriers and firex.

High power MHD channel/diffuser which is discussed in the following section.

(4) Hazard Classification. The general hazard classification of MIL-STD-882, para. 3.14 applies (Table A.2).

TABLE A.2 HAZARD LEVELS

3.14 Hazard Level. A qualitative measure of hazards stated in relative terms. For the purposes of this standard the following hazard levels are defined and established: Conditions such that personnel error, environment, design characteristics, procedural deficiencies, or subsystem or component failure or malfunction:

(a) Category I - Negligible

.... will not result in personnel injury or system damage.

(b) Category II - Marginal

.... can be counteracted or controlled without injury to personnel or major system damage.

(c) Category III - Critical

(d) Category IV - Catastrophic

.... will cause death or severe injury to personnel, or system loss.

(5) Hazard Control. Actions implemented or recommended (see "Remarks") to eliminate or control the hazard. The preferred order of precedence for hazard control actions, singularly or in combination, was suggested by MIL-STD-882 and further amplified as follows:

Design for Minimum Hazards. To the maximum extent practical, hazards were eliminated by design and by selection of qualified components. The hazard analysis reviewed the selections to ensure compatibility with the stated operational requirements.

Safety Devices. Hazards which could not be controlled by design or were reduced through use of safety devices, such as mechanical internal barriers or inhibiting mechanisms, relief valves, failsafe concepts, etc. Red lines initiate cutoff of a test if a safety critical parameter is violated.

Warning Devices. When a risk cannot be eliminated by the foregoing means, a detection and warning system was used, in conjunction with procedures for appropriate response and remedial action. Blue lines inhibit start of a test unless safety critical parameters are acceptable.

Special Procedures. When none of the above measures will eliminate the risk, procedures are developed to avoid initiation of a hazardous event.

Remarks. Applicable information not covered in other entries such as recommended actions, applicable documents, test history, etc.

3. CHANNEL/DIFFUSER AND MANIFOLDS

a. Areas to be Considered for the Channel/Diffuser and Manifolds

The following areas, which are required to be reviewed by Section 5.8.2.1 of MIL-STD-882, were reviewed to determine their applicability.

(1) Isolation of Energy Sources - Applicable.

(2) Fuels and Propellants - Not Applicable.

(3) System Environmental Constraints - Not Applicable.

(4) Explosive Devices - Not Applicable.

(5) Compatibility of Materials - Applicable.

(6) Transient I, Electrostatic, EMR, Ionizing Radiation - Applicable.

TABLE A.3 PRELIMINARY HAZARD ANALYSIS

SUBSYSTEM: CH_4 SYSTEM

LRU:

DATE:

REPORT:

HAZARD SOURCE	OPERATIONAL PHASE	HAZARD	HAZARD CLASSIFICATION	HAZARD CONTROL	REMARKS
1. EXTERNAL LEAKAGE OF CH_4 FROM SEALS, JOINTS OR PORTS.	STANDBY START OPERATE SHUTDOWN	TOXIC FUME HAZARD TO PERSONNEL. FIRE HAZARD.	III - CRITICAL	1.1 PERSONNEL EXCLUDED WHEN SYSTEM OPERATING. 1.2 SYSTEM LEAK TEST PRIOR TO CHARGING WITH CH_4. 1.3 PERIODIC LEAK TESTS	
2. RUPTURE OF CH_4 SYSTEM LINES OR COMPONENTS CAUSED BY EXCESS PRESSURE OR COMPONENT FAILURE.	START OPERATE SHUTDOWN	TOXIC FUME HAZARD TO PERSONNEL. FRAGMENTATION. BACKFLOW OF COMBUSTION GAS. FIRE HAZARD.	III - CRITICAL	2.1 PERSONNEL EXCLUDED FROM AREA DURING START, OPERATE, SHUTDOWN. 2.2 RELIEF VALVE (VF6-4). 2.3 COMPONENT PROOF TEST. 2.4 DESIGN FACTOR OF SAFETY. 2.5 MATERIAL SELECTION APPROVED BY M&P.	
3. FAILURE TO SUPPLY CH_4 TO ASI (VF6-3 FAILS TO OPEN, REG. RF6-2 FAILS CLOSED).	START	FIRE/EXPLOSION: FLOW OF GASEOUS OXYGEN, LIQUID OXYGEN AND JP-4 INTO COMBUSTOR, IGNITER FIRING.	IV - CATASTROPHIC	3.1 METHANE SUPPLY PRESSURE IS A BLUELINE. 3.2 ASI IGNITION IS A REDLINE.	
4. FAILURE TO TERMINATE CH_4 FLOW (VF6-3 FAILS TO CLOSE).	START	MINOR ADVERSE EFFECT ON COMBUSTOR MIXTURE RATIO.	I - NEGLIGIBLE	-	

TEST FORM 55-1136

TABLE A.3 PRELIMINARY HAZARD ANALYSIS (Cont'd)

SUBSYSTEM: GASEOUS OXYGEN

DATE:

LRU:

REPORT:

HAZARD SOURCE	OPERATIONAL PHASE	HAZARD	HAZARD CLASSIFICATION	HAZARD CONTROL	REMARKS
1. EXTERNAL LEAKAGE OF GOX	STANDBY START OPERATE SHUTDOWN	NONE, UNLESS A FUEL SOURCE IS PRESENT - THEN, INTENSIFIED FIRE HAZARD.	II - MARGINAL	1.1 SYSTEM LEAK TEST	
2. RUPTURE OF O_2 SYSTEM LINES, OR COMPONENTS CAUSED BY OVERPRESSURE OR COMPONENT FAILURE.	START OPERATE SHUTDOWN	FRAGMENTATION, OXYGEN-FED FIRE. POSSIBLE DAMAGE TO ADJACENT COMPONENTS. COMBUSTION GAS BACKFLOW.	III - CRITICAL	2.1 RELIEF VALVE (VG04) 2.2 COMPONENT PROOF TEST 2.3 DESIGN FACTOR OF SAFETY 2.4 MATERIAL SELECTION INCLUDING LOX COMPATIBILITY APPROVED BY M&P.	
3. FAILURE TO SUPPLY GOX TO ASI (VG03 FAILS TO OPEN, REG. RG02 FAILS CLOSED).	START	FIRE/EXPLOSION. LOX, JP-4 AND CH_4 APPLIED TO COMBUSTOR; IGNITER FIRING.	IV - CATASTROPHIC	3.1 GOX SUPPLY PRESSURE IS A BLUELINE. 3.2 ASI IGNITION IS A REDLINE	
4. FAILURE TO TERMINATE GOX FLOW TO ASI (VG03 FAILS TO CLOSE).	START	POSSIBLE ADVERSE EFFECT ON MIXTURE RATIO DURING OPERATION.	I - NEGLIGIBLE		

TEST FORM 89-1136

TABLE A.3 PRELIMINARY HAZARD ANALYSIS (Cont'd)

SUBSYSTEM: JP-4 FUEL SUPPLY

DATE:

LRU:

REPORT:

HAZARD SOURCE	OPERATIONAL PHASE	HAZARD	HAZARD CLASSIFICATION	HAZARD CONTROL	REMARKS
1. EXTERNAL LEAKAGE OF JP-4 FROM SEALS OR JOINTS	STANDBY START OPERATE SHUTDOWN	FUEL FOR POSSIBLE FIRE HAZARD.	II - MARGINAL	1.1 SYSTEM LEAK TESTS 1.2 LEAKAGE VISIBLE - ALLOWS TIME FOR CORRECTIVE ACTION.	
2. RUPTURE OF JP-4 SYSTEM LINES OR COMPONENTS CAUSED BY EXCESS PRESSURE OR COMPONENT FAILURE.	START OPERATE SHUTDOWN	FRAGMENTATION - FIRE HAZARD.	III - CRITICAL	2.1 NONCOMPRESSIBLE FLUID IN OPEN-LOOP (NO LOCKUPS) SYSTEM. 2.2 JP-4 MAIN VALVE UPSTREAM PRESSURE IS A REDLINE.	
3. FAILURE TO SUPPLY JP-4 TO GAS GENERATOR OR PREMATURE TERMINATION (VALVE VJ4 FAILS CLOSED).	START OPERATE	EXPLOSION IN GAS GENERATOR OR BURNTHROUGH FROM LOX-RICH OPERATION.	II - MARGINAL	3.1 LOX LEAD 3.2 CHAMBER PRESSURE REDLINE 3.3 JP-4 TANK PRESSURE IS A BLUELINE.	
4. FAILURE TO TERMINATE JP-4 FLOW.	SHUTDOWN	POSSIBLE TEMP SPIKE AT CUTOFF - CONTAMINATION OF MHD CHANNEL.	II - MARGINAL	4.1 VALVE DESIGNED TO FAIL SAFE (NORMALLY CLOSED).	

TEST FORM 55-1156

TABLE A.3 PRELIMINARY HAZARD ANALYSIS (Cont'd)

SUBSYSTEM: LIQUID OXYGEN SUPPLY

DATE:

LRU:

REPORT:

HAZARD SOURCE	OPERATIONAL PHASE	HAZARD	HAZARD CLASSIFICATION	HAZARD CONTROL	REMARKS
1. EXTERNAL LEAKAGE FROM JOINTS OR SEALS.	STANDBY START OPERATE SHUTDOWN	NONE, UNLESS A FUEL SOURCE IS PRESENT--THEN, FIRE HAZARD.	II - MARGINAL	1.1 SYSTEM LEAK TESTS	
2. RUPTURE OF LOX SYSTEM OR COMPONENTS DUE TO OVERPRESSURE OR COMPONENT FAILURE, OR IGNITION OF A NONCOMPATIBLE SUBSTANCE.	START OPERATE SHUTDOWN	FRAGMENTATION - OXYGEN-FED FIRE. POSSIBLE CASCADING DAMAGE. COMBUSTION GAS BACKFLOW.	III - CRITICAL	2.1 OPEN LOOP LOX SYSTEM - NO LOCKUPS IN SYSTEM. 2.2 COMPONENTS PROOF TESTED. 2.3 DESIGN FACTOR OF SAFETY. 2.4 MATERIAL SELECTION INCLUDING LOX COMPATIBILITY, APPROVED BY M&P. 2.5 CHAMBER PRESSURE REDLINE. 2.6 MAIN LOX VALVE UPSTREAM PRESSURE REDLINE. 2.7 ELIMINATE FUEL SOURCES IN VICINITY.	
3. FAILURE TO SUPPLY LO_2 TO GAS GENERATOR (VALVE VL03 FAILS TO OPEN OR TO REMAIN OPEN).	START OPERATION SHUTDOWN	INTRODUCTION OF FUEL INTO GG WITHOUT LOX LOAD. NO COMBUSTION. POSSIBLE PRESSURE SPIKE. CONTAMINATION OF MHD.	II - MARGINAL IV - CATASTROPHIC IF LOX FLOW DELAYED.	3.1 P_C REDLINE. 3.2 LOX TANK PRESSURE - BLUELINE	
4. FAILURE TO TERMINATE LO_2 FLOW AT CUTOFF.	SHUTDOWN	CONTINUED LO_2 FLOW - POSSIBLE ADVERSE THERMAL EFFECTS - POSSIBLE FIRE HAZARD AT EXIT.	II - MARGINAL	4.1 VALVE IS DESIGNED FOR FAIL SAFE TO THE CLOSED POSITION.	

TEST FORM 59-1198

TABLE A.3 PRELIMINARY HAZARD ANALYSIS (Cont'd)

SUBSYSTEM: AQUEOUS CESIUM CARBONATE (CS_2CO_3) DATE:

LRU: REPORT:

HAZARD SOURCE	OPERATIONAL PHASE	HAZARD	HAZARD CLASSIFICATION	HAZARD CONTROL	REMARKS
1. LEAKAGE OF CS_2CO_3 POST SEALS/JOINTS.	STANDBY START OPERATION SHUTDOWN	RELEASE OF CAUSTIC SUBSTANCE IN TEST AREA; POSSIBLE ADVERSE EFFECT ON STRUCTURAL AND OTHER MATERIALS.	II - MARGINAL	1.1 SYSTEM LEAK TEST 1.2 MATERIALS MUST BE COMPATIBLE WITH CHEMICAL CHARACTERISTICS OF FLUID. 1.3 STANDBY WATER SOURCE FOR FLUSHING AREA. 1.4 LEAK CAN BE VISUALLY DETECTED.	
2. RUPTURE	START OPERATE SHUTDOWN	FRAGMENTATION. GROSS RELEASE OF CAUSTIC SOLUTION; POSSIBLE BACKFLOW AND RELEASE OF FUEL (JP-4) INTO AREA; FIRE HAZARD.	III - CRITICAL	2.1 DESIGN MARGIN 2.2 PROOF TEST 2.3 WATER FLUSH AVAILABLE.	
3. FAILURE TO SUPPLY CS_2CO_3	START OPERATE SHUTDOWN	POSSIBLE FUEL-RICH OPERATION OF COMBUSTOR.	II - MARGINAL	3.1 SEED TANK PRESSURE IS A BLUELINE.	
4. FAILURE TO TERMINATE FLOW	SHUTDOWN	POSSIBLE CONTAMINATION OF SYSTEM WITH CAUSTIC FLUID.	II - MARGINAL	4.1 CONTROL VALVE FAIL-SAFE (NORMALLY CLOSED).	

TEST FORM 88-1196

TABLE A.3 PRELIMINARY HAZARD ANALYSIS (Cont'd)

SUBSYSTEM: HYDRAULIC SUPPLY
LRU:
DATE:
REPORT:

HAZARD SOURCE	OPERATIONAL PHASE	HAZARD	HAZARD CLASSIFICATION	HAZARD CONTROL	REMARKS
1. LEAKAGE	STANDBY START OPERATE SHUTDOWN	POSSIBLE FIRE HAZARD.	II - MARGINAL	1.1 LEAK TEST SYSTEM 1.2 LEAKAGE IS VISIBLE; PERMITS READY DETECTION AND CORRECTION.	
2. RUPTURE	STANDBY START OPERATE SHUTDOWN	FRAGMENTATION; FIRE HAZARD; LOSS OF CONTROL TO MAIN OXIDIZER VALVE AND MAIN FUEL VALVE	III - CRITICAL	2.1 DESIGN FACTOR OF SAFETY. 2.2 SUPPORT LINES AGAINST FLEXING AND VIBRATIONS. 2.3 MAIN VALVES SPRING-LOADED FAIL-SAFE - CLOSE ON LOSS OF HYDRAULICS OR 2.4 CLOSE COUPLED, PNEUMATIC CHANGED HYDRAULIC ACCUMULATOR, CHECK VALVE ISOLATED FROM MAIN SUPPLY, CAPABLE OF POWERING VALVES CLOSED.	
3. LOSS OF SUPPLY PRESSURE	START OPERATE SHUTDOWN	LOSS OF CONTROL TO MAIN VALVES.	III - CRITICAL	3.1 SAME AS 2.3 AND/OR 2.4 ABOVE.	

TEST FORM 55-1196

TABLE A.3 PRELIMINARY HAZARD ANALYSIS (Cont'd)

SUBSYSTEM: GASEOUS NITROGEN

DATE:

LRU:

REPORT:

HAZARD SOURCE	OPERATIONAL PHASE	HAZARD	HAZARD CLASSIFICATION	HAZARD CONTROL	REMARKS
1. EXTERNAL LEAKAGE OF GN_2	STANDBY START OPERATE SHUTDOWN	NEGLIGIBLE	I - NEGLIGIBLE		
2. RUPTURE OF GN_2 LINES OR COMPONENTS DUE TO OVERPRESSURE OR COMPONENT FAILURE.	STANDBY START OPERATE SHUTDOWN	FRAGMENTATION. FAILURE TO ACTUATE SAFETY-CRITICAL VALVES (SEE RELATED FLUID SYSTEM) OR PURGE OPERATIONS: (A) ASI GO_2 (B) COMBUSTOR LO_2 (C) ASI CH_4 (D) JP-4 (E) INJECTOR	III - CRITICAL	2.1 DESIGN SAFETY FACTOR 2.2 COMPONENT PROOF TEST 2.3 REDLINES ON PURGE VALVE POSITIONS. 2.4 CHECK VALVES PREVENT BACKFLOW INTO PURGE SYSTEM.	
3. FAILURE TO SUPPLY GN_2 FOR PURGE OR ACTUATION OF SAFETY-CRITICAL VALVES (FAILURE OF VALVE CONTROLS OR PURGES.	START OPERATION SHUTDOWN	FAILURE TO ACTUATE SAFETY-CRITICAL CONTROL VALVES AND SHUTDOWN PURGES (SEE HAZARD #2, RUPTURE, ABOVE).	III - CRITICAL	3.1 BLUELINES AND REDLINES FOR CRITICAL FUNCTIONS ARE DESCRIBED UNDER THE RESPECTIVE SUBSYSTEM. 3.2 BACKUP POWER FOR PURGE VALVE CONTROLS. 3.3 USE OF NORMALLY OPEN PURGE VALVES (POWERED CLOSE) FOR CRITICAL FUNCTIONS SHOULD BE CONSIDERED.	

TABLE A.3 PRELIMINARY HAZARD ANALYSIS (Cont'd)

SUBSYSTEM: COMBUSTOR COOLANT WATER

DATE:

LRU:

REPORT:

HAZARD SOURCE	OPERATIONAL PHASE	HAZARD	HAZARD CLASSIFICATION	HAZARD CONTROL	REMARKS
1. LEAKAGE	ALL	NEGLIGIBLE	I - NEGLIGIBLE		
2. RUPTURE	START OPERATE SHUTDOWN	LOSS OF COMBUSTOR COOLANT. POSSIBLE OVERHEATING AND BURNTHROUGH OR EROSION OF COMBUSTOR.	III - CRITICAL	2.1 COOLANT WATER PRESSURE IS A REDLINE.	
3. FAILURE TO SUPPLY WATER TO COMBUSTOR (VALVE VWI FAILS TO OPEN)	START OPERATE SHUTDOWN	SAME AS ABOVE.	III - CRITICAL	3.1 COOLANT WATER PRESSURE IS A BLUELINE. 3.2 COOLANT WATER PRESSURE IS A REDLINE.	

TEST FORM 55-1136

TABLE A.3 PRELIMINARY HAZARD ANALYSIS (Cont'd)

SUBSYSTEM: COMBUSTOR ASI

LRU:

DATE:

REPORT:

HAZARD SOURCE	OPERATIONAL PHASE	HAZARD	HAZARD CLASSIFICATION	HAZARD CONTROL	REMARKS
1. ASI FAILURE TO ENERGIZE IGNITER	START	NO IGNITION - CONTINUED FLOW OF UNBURNED MIXED PROPELLANTS. POSSIBLE EXPLOSION.	IV - CATASTROPHIC	1.1 DUAL REDUNDANT ASI SPARK IGNITERS. 1.2 ASI PRESSURE REDLINE.	
2. ASI FAILURE TO DEENERGIZE	START	NEGLIGIBLE - CONTINUED IGNITION SOURCE - POSSIBLE DETERIORATION OF IGNITER.	I - NEGLIGIBLE	-	

TABLE A.3 PRELIMINARY HAZARD ANALYSIS (Cont'd)

SUBSYSTEM: COMBUSTOR

LRU:

DATE:

REPORT:

HAZARD SOURCE	OPERATIONAL PHASE	HAZARD	HAZARD CLASSIFICATION	HAZARD CONTROL	REMARKS
1. POOR PROPELLANT INJECTION OR MIXING	START OPERATE CUTOFF	OVERTEMPERATURE, LOCAL HOT SPOTS OR COMBUSTOR WALL EROSION. POSSIBLE BURNTHROUGH.	III - CRITICAL	1.1 PROVEN INJECTION PATTERN 1.2 COMBUSTION CHAMBER PRESSURE REDLINE 1.3 COOLANT WATER TEMP EXIT REDLINE	
2. MIXING OF FUEL AND OXIDIZER IN MANIFOLDS OR LINES	START OPERATE CUTOFF	EXPLOSION; FRAGMENTATION HAZARD; RELEASE OF PROPELLANTS, CASCADING DAMAGE.	IV - CATASTROPHIC	2.1 POSITIVE SEPARATION OF PREPELLANTS. 2.2 PURGE SEQUENCES TO ASSURE INITIAL INERTING OF MANIFOLDS. 2.3 PURGE VALVE POSITION REDLINES. 2.4 PURGE SEQUENCES AT CUTOFF FOR POST-SHUTDOWN INERTING AND ISOLATION. 2.5 CHECK VALVES IN PURGE SYSTEM PREVENT PROPELLANT BACKFLOW AND COMMUNICATION IN PURGE MANIFOLDING.	TEST HISTORY: EARLY INJECTOR EXPLOSION DUE TO FUEL/LO_2 COMMUNICATION VIA A DEFECTIVE PART.
3. ACOUSTIC OR VIBRATION INSTABILITIES IN THE COMBUSTION ZONE.	START OPERATE SHUTDOWN	COMBUSTION INSTABILITY; POSSIBLE DETRIMENTAL STRUCTURAL DAMAGE; POSSIBLE THERMAL DAMAGE BY OSCILLATORY PRESSURES NEGATING BOUNDARY COOLANT.	III - CRITICAL	3.1 CHAMBER ACCELERATION REDLINE 3.2 DESIGN OF COMBUSTOR GEOMETRY FOR STABILITY.	TEST HISTORY: SUSTAINED INSTABILITY EXPERIENCED IN BOMB TEST.

(7) Pressure Vessels and Plumbing - Applicable.

(8) Crash Safety - Not Applicable.

(9) Safe Operation and Maintenance - Applicable.

(10) Training and Certification In Operations and Maintenance - Applicable.

(11) Egress, Rescue, Survival - Not Applicable.

(12) Life Support Requirements - Not Applicable.

(13) Fire Ignition and Propagation Sources and Protection - Applicable.

(14) Resistance to Shock Damage - Not Applicable.

(15) Fail Safe Design Considerations - Applicable.

(16) Environmental Factors, Layout, Lighting, Safety Implications in Manual Systems - Not Applicable.

(17) Safety From Vulnerability Standpoint, Armor, Fire Suppression, Redundancy - Not Applicable.

(18) Protective Clothing, Equipment or Devices - Applicable.

(19) Lightning and Electrostatic Protection - Not Applicable.

(20) Human Error Analysis of Operation Function and Tasks - Applicable.

b. Component Identification by Hazard Areas

The subsystem hazard analysis per Section 5.8.2.2 identifies all components and equipment comprising each subsystem whose failure could result in hazardous conditions. Those components are identified below by the hazard area noted above.

(1) Isolation of Energy Sources

(a) Electrical signals and signal power

(b) MHD Power

i. Channel Electrodes
ii. Insulation/Isolation for Diffuser

(2) Fuels and Propellants - Not Applicable

(3) System Environmental Constraints - Not Applicable

(4) Explosive Devices - Not Applicable

(5) Compatibility of Material

(a) Liquids

i. Hard Water - corrodes carbon steel fittings, restricts coolant flow; contains suspended material, plugs coolant channels.

ii. Treated Water - corrodes carbon steel fittings, restricts coolant flow.

iii. Electrolytic Action - deteriorates brasses, steels.

(b) Solids

i. Cs_2CO_3 - penetrates channel insulator and electrode ceramic material.

(6) Transient Current, Electrostatic Discharge, EMR, Ion Radiation

(a) Current Surges

i. Unsteady MHD operation
ii. Load Switching
iii. Arcing to Ground

(b) Static Discharge - Not Applicable

(c) Electromagnetic Radiation

i. Unsteady MHD operation
ii. Load Switching

(d) Ionizing Radiation - Not Applicable

(7) Pressure Vessels and Plumbing

(a) Pressure Gauge

(b) Pressure Transducers

(c) High Pressure H_2O System

i. Pipes, hoses, fittings

(8) Crash Safety - Not Applicable

(9) Safe Operation and Maintenance

(a) Use of Check List

(b) Safety Planning for Tests

(c) Regularly scheduled, progressive maintenance

(10) Training and Certification in Operation and Maintenance

(a) Certification - Not Applicable

(b) Operators and technician trainees should operate under direction of past operators.

(11) Egress, Rescue and Survival - Not Applicable

(12) Life Support Requirements - Not Applicable

(13) Fire Ignition and Propagation Sources and Protection

(a) Ignition Sources

i. Damaged channel/diffuser
ii. Short circuits, sparks

(b) Fire Propagation Sources

i. All combustible materials in presence of gaseous oxygen

(c) Fire Protection - Not Applicable

(14) Resistance to Shock Damage - Not Applicable

(15) Fail Safe Design Considerations

(a) Electrode frame cooling system

(b) Ceramic insulators

(16) Environmental Factors, Layout, Lighting, Safety Implications in Manual Systems - Not Applicable

(17) Safety from Vulnerability Standpoint - Not Applicable

(18) Protective Clothing, Equipment, Devices

(a) Protective gloves, goggles, and dust masks when handling electrode and insulating ceramics and seed contaminated components and materials.

(19) Lightning and Electrostatic Protection - Not Applicable

(20) Human Error Analysis of Operator Functions and Tasks

(a) Impossible to evaluate as all functions are error prone.

c. Hazard Analysis by Components

(1) Isolation of Energy Sources

(a) Electrical Signals and Signal Power (5, 10, 15, 28 V dc)

Hazard Potential: Numerous exposed cables

Hazard: Loss of power, damaged power supplies, fire

Hazard Level: II - Marginal

Cause: Short circuits due to abrasion and/or cutting of insulated cables by normal activity

Correction/Prevention: All signal cables and signal power should be encased within flexible protective sheaths and routed through cable ways. All electrical power requirements should be reviewed to insure a safe shutdown under electrical power failure conditions.

(b) MHD Power - Characteristically a noisy dc signal of 5000 V dc maximum and 10,000 Adc maximum, but not simultaneously.

i. Channel Electrodes

Hazard Potential: Voltage instrumentation leads from various electrode frames to the voltage divider located in test cell.

Hazard: Short circuit to ground through various paths. Fire, explosion of various devices, electrocution.

Hazard Level: IV - Catastrophic

Cause: Insulation breakdown, voltage divider breakdown arc over in voltage divider, arc over to manifolds or instrumentation.

Correction/Prevention: Extreme care to assure sufficient voltage potential gap between high voltage sources and conductors or wet and/or dirty surface. Need high voltage, high current shunt to earth ground or signal side of the voltage divider.

ii. Insulation/Isolation for Diffuser

Hazard Potential: High voltage end of the channel/diffuser.

Hazard: Short circuit to ground through various paths, fire, explosion of various components, electrocution.

Hazard Level: IV - Catastrophic

Cause: Insulation breakdown, arc over to coolant manifold or instrumentation leads, dirty or wet insulation surfaces.

Correction/Prevention: Extreme care taken to assure unbroken or cracked insulations, maintain insulating surfaces in a clean and dry condition - need fuse shunts for all high voltage end instrumentation leads to shunt arc over current to earth ground.

(2) Fuels and Propellants - Not Applicable

(3) Systems Environmental Constraints - Not Applicable

(4) Explosive Devices - Not Applicable

(5) Compatibility of Liquids and Solids

(a) Hard Water

Hazard Potential: Hard water is used wherever possible for coolant.

Hazard: Corrosion, burnout of components.

Hazard Level: II - Marginal

Cause: Carbon steel parts and pipe are corroded by hard water, causing decreased heat flow rates. Suspended material clogs flow passages.

Correction/Prevention: All hard water lines should have large filter screens for removal of suspended material. All fittings and tubing should be stainless steel or copper.

(b) Treated Water

Hazard Potential: Treated water is used wherever higher quality water is needed, but de-ionized water is not required.

Hazard: Corrosion, burnout of components.

Hazard Level: II - Marginal

Cause: Carbon steel parts and pipe are corroded by the treated water, causing reduced heat flow rates where coolant lines have been restricted. Corrosion particles can obstruct coolant passages.

Correction/Prevention: All treated water lines should have large filter screens for removal of corrosion particles. Screens should be inspected regularly. All fittings and tubing should be stainless steel or copper.

(c) Electrolytic Action

Hazard Potential: Dissimilar metal materials in contact with water.

Hazard: General deterioration of components - leaks and weakening of joints.

Hazard Level: I - Negligible

Cause: Highly dissimilar materials can be expected to sustain electrolytic activity.

Correction/Prevention: Care should be taken in specifying materials to reduce electrolytic potential. Materials, where possible, should be treated with inorganic protective coatings to reduce electrolytic activity.

(d) Cs_2CO_3

Hazard Potential: Cs_2CO_3 is required to achieve the proper plasma conductivity, but material is corrosive to electrode/insulator system ceramic materials.

Hazard: General deterioration of the insulator ceramic eventually leading to electrical shorts between electrode frames.

Hazard Level: II - Marginal

Cause: Cs_2CO_3 penetration into the castable ceramics.

Correction/Prevention: Controlled shutdown procedure at conclusion of test where seed flow termination leads hot gas flow termination by more than one second. Operation with the minimum Cs_2CO_3 flow rate to achieve required plasma conductivity.

(6) Transient Current, Electrostatic Discharge, EMR, Ion Radiation

(a) Current Surges

i. Unsteady MHD Operation

Hazard Potential: Operation of the MHD generator primarily involves unsteady operation.

Hazard: No direct hazard without a failure of another type additionally.

Hazard Level: I - Negligible

Cause: Natural operation of MHD generator.

Correction/Prevention: None known at this time.

ii. Load Switching

Hazard Potential: Operations involving load switching.

Hazard: Large arcs (open to atmosphere) drawn by opening circuits. Source of ignition. No direct hazard without additional failure.

Hazard Level: I - Negligible

Cause: Normal Operation.

Correction/Prevention: Load switches might be housed in an inert atmosphere.

(b) Static Discharges - Not Applicable

(c) Electromagnetic Radiation

i. Unsteady MHD Operation

Hazard Potential: Unsteady generation of power is normal, but unusual or strong surging occurs.

Hazard: Electrical shocks, data biasing, computer errors, adverse test sequence influence.

Hazard Level: II - Marginal

Cause: Rapid variation of power can cause transient and randomly induced voltages during periods of strong MHD generator surging. The result is loss of data, erroneous data, erroneous computer operation. Extreme cases should conceivably cause minor electrically shocking from ungrounded metal objects and erroneous test sequence signal.

Correction/Prevention: All metallic objects should be grounded to earth ground - all cabling should be shielded and grounded to earth ground. All cabinetry for computers, controls, etc., should completely enclose the components and be grounded to earth ground.

ii. Load Switching

Hazard Potential: Operations involving load switching.

Hazard: Same as Unsteady MHD Operation.

Hazard Level: II - Marginal

Cause: Rapid variation of loading by load switching can cause randomly induced voltages.

Correction/Prevention: Same as for Unsteady MHD Operation.

(d) Ionizing Radiation - Not Applicable.

(7) Pressure Vessels and Plumbing

(a) Pressure Gauges

Hazard Potential: Bourdon tube gauges are used for calibration, setting points, and monitoring critical pressures.

Hazard: Explosive rupture of the gauges, incorrect indication response to applied pressure.

Hazard Level: II - Marginal

Cause: Overpressurization, incorrect calibration, malfunctioning, deterioration.

Correction/Prevention: Periodic inspection and calibration, shatterproof plexiglass shields over gauges.

(b) Pressure Transducers

Hazard Potential: Strain gauge pressure transducers are used to monitor various pressures.

Hazard: Incorrect readings (indications).

Hazard Level: I - Negligible

Causes: Incorrectly positioned calibration valves, transducer shorting (water leaks can do this), improper or obsolete amplifier calibration settings.

Correction/Prevention: Transducer connections should be protected from short circuiting influences. Check lists must be strictly adhered to in valve positioning. Transducer amplifiers must be calibrated prior to each test run to reduce drift errors.

(c) High Pressure Water System

i. Pipes, hoses, fittings, valves

Hazard Potential: Water is routed through stainless steel pipes, reinforced nylon tubing, copper tubing and brass barbed fittings.

Hazard: Ruptures, leaks, clogging.

Hazard Level: II - Marginal

Cause: Overpressure, deterioration of materials or joints, corrosion.

Correction/Prevention: System should be provided with pressure-relieve valves and/or vents; lines should be leak tested and flow tested periodically.

(8) Crash Safety - Not Applicable

(9) Safe Operation and Maintenance

(a) Use of Check List - Check lists for system operation must be strictly adhered to.

(b) Safety Planning for Tests - Each test must be analyzed concerning expected operation of the test cell and where deviations from normal operation are to be expected. These deviations must be thoroughly analyzed to provide safety precautions in areas where abnormal operation may create unsafe conditions.

(c) Regularly Scheduled Progressive Maintenance - All items of hardware involved in operation should be placed on a table of periodic maintenance operations which should include regular inspection.

(10) Training and Certification in Operation and Maintenance

(a) Certification - Not Required.

(b) Operators and trainee technicians should receive on-the-job training and operate the system under the direction of persons experienced in its operation.

(11) Egress, Rescue and Survival - Not Applicable.

(12) Life Support Requirements - Not Applicable.

(13) Fire Ignition and Propagation Sources and Protection

(a) Ignition Sources

i. Channel/Diffuser

Hazard Potential: High temperature combustion gases.

Hazard: Burnout of components.

Hazard Level: II - Marginal

Cause: Burn-through or deteriorating gasketing plus burn-through of electrode frame insulation and channel composite case have the potential to burn the magnet coil insulation causing short circuiting.

Correction/Prevention: No simple means of interlocking against burnouts is possible; it is necessary that the operator know what to expect and what to look for and shut down the system through the dead man switch in these events.

ii. Short Circuits or Sparks

Hazard Potential: Ignition of combustible products present as vapors in the test cell.

Hazard: Overloaded electrical circuits or open arc current concentrations.

Hazard Level: II - Marginal

Cause: Overheating caused by electrical conditions forcing electric current through a reduced number of circuits. Sparks caused by shorting of high voltage components to ground.

Correction/Prevention: Verify that all electrical connections are properly installed and that all lug/terminal connections are securely attached. Review operation to insure that all water sprays, test leads, etc., do not provide short circuit or grounding conditions.

(b) Fire Propagation Sources

i. All Combustible Materials in Presence of Gaseous Oxygen

Hazard Potential: Oxygen rich atmosphere.

Hazard: Metal oxidation.

Hazard Level: III - Critical

Cause: Hot metal components exposed to oxygen rich conditions.

Correction/Prevention: Operate components with the surface temperatures below the combustion temperature of the component.

(14) Resistance to Shock Damage - Not Applicable.

(15) Fail Safe Design Considerations

(a) Electrode Frame Cooling System

Hazard Potential: Overheating of electrode frames and adjacent case area.

Hazard: Loss of cooling system integrity without interlock signal.

Hazard Level: III - Critical

Cause: Reduced water flow rate because of leaks and/or partially blocked tubes.

Correction/Prevention: Cooling water flow rates should be interlocked with the operating system to cause a system shutdown if proper water flow rates are not maintained.

(b) Ceramic Insulators

Hazard Potential: Degradation of the insulator material.

Hazard: Electrode frame short circuit.

Hazard Level: II - Marginal

Cause: Seed penetration of the insulator ceramic.

Correction/Prevention: Controlled shutdown procedure at conclusion of test where seed flow termination leads hot gas flow termination by more than one second. Operation with minimum Cs_2CO_3 flow rate to achieve required plasma conductivity.

(16) Environmental Factors, Layout, Lighting, Safety Implications in Manual Systems - Not Applicable.

(17) Safety from Vulnerability Standpoint - Not Applicable.

(18) Protective Clothing, Equipment, Devices

(a) Protective gloves, goggles, and dust masks when handling electrode and insulating ceramics and seed contaminated materials.

Hazard Potential: Cesium carbonate or cesium nitrate compounds are used as seeding agents. Ceramic materials used in channel electrodes.

Hazard: Cesium compounds are extremely caustic and can cause severe skin burns as well as lung irritation. Cesium and its oxides form caustic hydroxides on contact with moisture. Ceramic materials are irritants to skin, eyes, and lungs.

Hazard Level: II - Marginal

Cause: During operation of the channel/diffuser, deposits form on the walls due to condensation of seed and slight corrosion of the walls.

Correction/Prevention: Protective clothing, when handling all ceramic and seed materials such as cesium and potassium compounds, should include gloves, goggles, and a dust mask as a minimum. The same precautions should be observed when handling the internal surfaces of the channel and diffuser after system operation with seed materials.

(19) Lightning and Electrostatic Protection - Not Applicable.

(20) Human Error Analysis of Operator Functions and Tasks

(a) Hazards involved in operator functions are impossible to evaluate; therefore, it is imperative that check lists be carefully prepared and strictly adhered to. The use of interlock bypasses to facilitate test operations is extremely hazardous and should not be used except for "dummy" test, calibration checks, and other non-combustion type tests.

APPENDIX B

SUPPLEMENTARY SSFL TEST DATA

The SSFL development test program was completed successfully after 55 hot fire tests were conducted. Table B1. illustrates the test data summary realized during the igniter test series and Table B.2 illustrates the data summary from the main combustor and diagnostics channel tests.

TABLE B.1 IGNITION SYSTEM DEVELOPMENT TEST DATA SUMMARY

Test Stand No. 632-	Date	ASI No.	Comments
001	15 Apr 77	1	Sequence problems
002	15 Apr 77	1	Facility problems
003	15 Apr 77	1	Red Line restraints
004	15 Apr 77	1	Nitrogen dilution
005	15 Apr 77	1	Transition
006	15 Apr 77	1	Fuel regulator failed - high system ΔP
007	19 Apr 77	2	Resized shutoff valves - reduced fuel flow
008	19 Apr 77	Both	Resized shutoff valves - reduced fuel flow
009	20 Apr 77	Both	New fuel venturi - dump coolant starves main fuel
010	20 Apr 77	Both	New fuel venturi - dump coolant starves main fuel
011	22 Apr 77	1	Eliminated dump coolant - changed fuel venturi
012	22 Apr 77	2	Eliminated dump coolant - changed fuel venturi
013	22 Apr 77	Both	Premature cutoff
014	3 May 77	2	Changed oxygen orifice diameter - recess spark plug
015	3 May 77	1	Changed oxygen orifice diameter - recess spark plug
016	3 May 77	Both	Eliminated dump coolant
017	3 May 77	Both	Ignition on #1 only
018	3 May 77	Both	Ignition on #2 only
019	3 May 77	Both	Satisfactory
020	3 May 77	Both	Ignition on #1 only

TABLE B.1 IGNITION SYSTEM DEVELOPMENT TEST DATA SUMMARY (Cont'd)

Test Stand No. 632-	Date	ASI No.	Comments
021	4 May 77	Both	Test series M/R excursions with final configuration. Installed independent reactant control orifice.
022	4 May 77	Both	
023	4 May 77	Both	
024	4 May 77	Both	
025	4 May 77	Both	
026	4 May 77	Both	
027	4 May 77	Both	
028	21 Jun 77	Both	Spark continue circuit cutoff error in setting. Test series with main injector and functional purges and sequence logic.
029	21 Jun 77	Both	
030	21 Jun 77	Both	
031	21 Jun 77	Both	

TABLE B.2 GAS GENERATOR AND DIAGNOSTICS CHANNEL DEVELOPMENT TEST DATA SUMMARY

Test Stand #632-	Date	Time (msec)	LO_2	JP-4	Seed	Pc_4* (atm)	MR	% Seed	*** η_c*	Temp (K)	Comments
032	6/24/77	--	NA	NA	--	NA	--	--	--	--	Inter-reactant communication
033	10/5/77	--	NA	NA	--	NA	--	--	--	--	Function check, no fuel
034	10/17/77	--	NA	NA	--	NA	--	--	--	--	Define Start/Cutoff
035	10/20/77	95	NA	NA	--	NA	--	--	--	--	Start seq. check
036	10/25/77	340	NA	NA	--	NA	--	--	--	--	Injector prime
037	11/4/77	1830	21.68	6.97	--	29.13	3.11	--	98.2	3566.6	Contaminated fuel at end
038	11/22/77	1950	22.38	7.04	--	29.14	3.18	--	--	3563.6	LO_2 flow error
039	11/29/77	2350	21.06	7.51	--	29.64	2.80	--	98.3	3569.8	
040	11/29/77	200	17.67	8.16	--	25.36	2.16	--	--	3486.1	Transition
041	12/5/77	2335	19.22	8.11	--	28.06	2.37	--	95.0	3526.4	Low mixture ratio
042	12/5/77	460	17.59	5.48	--	23.05	3.21	--	--	3528.1	Setup error
043	12/8/77	3520	15.87	5.49	--	23.30	2.89	--	--	3537.6	LO_2 flow error
044	12/8/77	2440	23.83	8.24	--	32.94	2.89	--	97.1	3587.5	Transient
001	1/9/78	2440	20.80	6.71	1.66	29.25	3.10	4.12	98.5	3516.8	First seed test
002	1/9/78	170	21.40	7.40	4.57	28.51	2.89	9.89	--	--	Restricted Pc port

TABLE B.2 GAS GENERATOR AND DIAGNOSTICS CHANNEL DEVELOPMENT TEST DATA SUMMARY (Cont'd)

Test Stand #632-	Date	Time (msec)	LO_2	JP-4	Seed	Pc_4* (atm)	MR	%*** Seed	η_{c*}	Temp (K)	Comments
003	1/13/78	560	21.38	6.32	4.43	30.22	3.38	9.96	97.3	3425.6	Stability Test
004	2/24/78	2515	20.63	6.28	4.31	29.92	3.28	9.98	98.7	3429.9	
005	2/24/78	1535	20.11	6.77	4.24	30.25	2.97	9.84	98.3	3444.7	
006	3/28/78	255	17.85	5.33	1.73	22.34	3.35	5.03	--	3455.3	VSC Cutoff
007	4/5/78	1380	21.35	6.29	4.39	30.62	3.40	9.90	87.8	3427.0	Chan.test - 20 A
008	4/5/78	2380	21.08	7.01	2.16	30.50	3.01	5.15	98.5	3511.6	Chan.test - 20 A
009	4/7/78	1960	21.91	6.67	2.13	31.29	3.28	5.01	**	3506.8	Chan.test - 20 A
010	4/7/78	1990	20.55	6.80	4.32	31.03	3.02	9.86	98.9	3448.0	Chan.test - 20 A
011	4/7/78	1790	20.28	6.81	4.29	30.72	2.98	9.90	98.4	3446.1	Chan.test - 20 A

* Nozzle Stagnation Pressure

** Unexplained η_{c*} anomaly.

***Seed percentage is based on the mass flow of $Cs_2 CO_3$ as a percentage of the total mass flow.

APPENDIX C

CHANNEL TOOLING AND MODELING

1. INTRODUCTION

The design of the high power MHD channel/diffuser incorporated many significant features that had not previously been fabricated. The only previous lightweight channel fabricating experience was that obtained from the 200 kW channel that was furnished to the Air Force Aero Propulsion Laboratory, Wright-Patterson Air Force Base, Ohio.[4] The results of that channel fabrication indicated areas that needed improvement. In addition, the greater size of the high power MHD channel raised the possibilities of encountering new problems. Consequently, various channel tooling and modeling tasks were performed in order to reduce the risks of encountering costly and time-consuming delays during actual fabrication. These tasks, as discussed in detail in the following sections, involved the channel/diffuser internal contour, the electrode frames, and the composite case.

2. CHANNEL/DIFFUSER INTERNAL CONTOUR

The design of the high power MHD channel/diffuser required close correlation with the planned process to be used for fabricating the contoured assembly mandrel and the channel/diffuser assembly. This correlation was simplified and expedited by constructing a full size plywood mockup of the channel/diffuser internal surface contours.

The contour mockup facilitated the design and process planning of the contoured assembly mandrel. The mandrel was designed in four sections that could be collapsed and removed from the inside of the completed channel. The mockup was used to evaluate the access to the inside of the channel to disassemble the mandrel. The mockup was also used to define and plan the process of machining the mandrel external corner radius along the intersections between the contoured top and bottom walls and the diverging side walls.

---

[4] D. W. Swallom, O. K. Sonju, D. E. Meader, G. T. Heskey, "MHD Lightweight Channel Development," AFAPL-TR-78-41, June 1978.

The mockup provided a full size model for evaluating the relation between the internal radius of the corner blocks and the external radius of the corners of the mandrel. It also served to evaluate the slenderness ratio of the long diagonal frame side rails for establishing the handling fixture requirements.

The planning for the fiberglass-epoxy shell fabrication process was also facilitated by using the full size contour mockup. This was particularly true for the evaluation of the floor space and equipment size requirements for winding and curing the fiberglass-epoxy shell and for removing the mandrel from the completed channel shell.

3. ELECTRODE FRAMES MODELING

The electrode frame modeling tasks involved five key features of the electrode frames: (a) attaching the Inconel current collector screens to the copper electrode frame rails; (b) fabricating the perpendicular electrode frames; (c) fabricating the diagonal frame corner blocks; (d) fabricating the diagonal electrode frames; and (e) forming the cooling tubes to conform to the complex three-dimensional external geometry of the electrode frames. These five tasks are discussed in detail in the next sections of this appendix.

a. Current Collector Screen Attachment

One of the most critical details affecting the performance of the electrodes was the method of attaching the Inconel current collector screen to the copper electrode frames. A successful joint provided an uninterrupted heat transfer path from the screen to the rail while maintaining clear openings between the screen wire strands shown in Figure C. 1, items A and B. This was a difficult task to accomplish because of the "miniature" details of the screen and groove features, but after investigating four different approaches, a successful process was developed.

The first approach was an attempt to bond the screen to the rail by electron beam welding. Very precise alignment of the screen and rail was needed because of the fine diameter of the electron beam. If the electron beam contacted the screen, the beam would instantly melt the screen at that point. In addition, the lack of sufficient flow of melted copper to fill the spaces around the bottoms of the screen strands was a problem. Consequently this approach was discontinued.

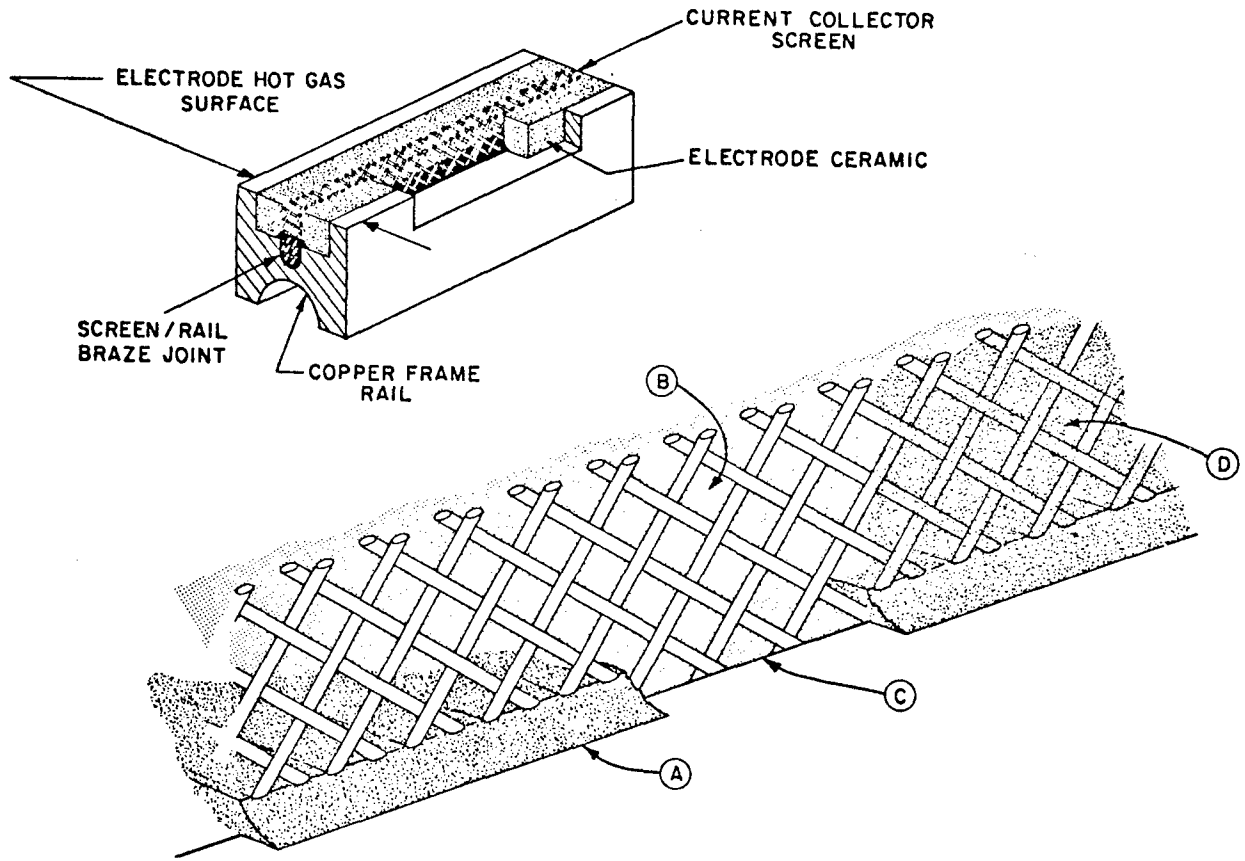

Ⓐ SUCCESSFUL BRAZE JOINT, NO VOIDS, MINIMUM FILLET
Ⓑ SCREEN OPENINGS FILLED WITH ELECTRODE CERAMIC
Ⓒ DEFECTIVE JOINT, VOIDS IN BRAZE JOINT
Ⓓ DEFECTIVE SCREEN, OPENINGS FILLED WITH BRAZE MATERIAL

Figure C.1 Electrode Screen Attachment.

The second approach used vacuum furnace brazing. The braze was applied in the form of a paste that contained both the braze material and a flux compound. The results were unacceptable because of either insufficient braze material in the joint between the screen and the rail as shown by C of Figure C.1 or excess braze material filling the openings in the screen as shown by D of Figure C.1.

The third approach was an attempt to electro-plate pure copper on to the base of the screen so the copper would completely surround the wire strands of the screen. This copper base would then have been brazed to the copper electrode rail. The plating process filled the spaces around the strands at the base of the screen, but the outer surfaces of the plated copper were quite irregular. Consequently, they would have required precision machining in order to fit the screen into the grooves of the electrode rails for brazing. Hence, this approach was discontinued.

The fourth approach, which finally proved successful, was the manual torch brazing process. The screen was first "tinned" in the base region using the following procedure. A steel block with machined grooves was placed in a tray of water. The water served as a heat sink, and the water level was kept well below the bottom of the grooves. Next, the screen was placed into one of the tight fitting grooves with the base uppermost and was held in place with Nichrome wire. After fluxing the exposed portion of the screen, the screen temperature was increased indirectly by torch heating of the steel block. Then a bead of braze alloy was deposited on the exposed portion of the screen. The amount of screen which was tinned was controlled by the depth and width of the grooves in the steel block.

The excess braze was then removed from the screens by sanding down the width to fit the frame rail grooves. The unbrazed area of the screen was coated with a "stop-off" material using a straight edge as a mask to keep the tinned area free from the stop-off. The screen was inserted into the frame rail and secured with Nichrome wire. The final braze joint was then made by heating the back side of the rail with a torch.

This technique was successfully used on the diagnostics channel where the maximum length of screen was approximately 250 mm. In the high power MHD channel the maximum length of screen was approximately 750 mm. The same technique was expected to be adapted to accommodate the longer screens but further modeling will be required before the full scale fabrication phase.

b. Prototype Perpendicular Frame Fabrication

Conventional MHD generator channels have been previously constructed with structurally rigid electrode bars or frames that were attached to or enclosed by thick walls of non-conductive materials. The electrode/frames were sufficiently massive to maintain the required internal hot gas surface contour of the generator channel. However, the electrode frames for the lightweight high power MHD channel were designed to minimize the channel mass, consequently they were considerably less rigid than conventional frames. The degree of dimensional accuracy that could be reasonably achieved was, however, an unknown. For this reason a few prototype perpendicular frames were fabricated.

Each perpendicular frame consisted of four corner blocks, four straight side rails which contained the current collector screens and grooves for the electrode ceramic, and continuous cooling tubes that were attached to the outside of the frame as shown in Figure C.2. The internal dimensions of these frames were approximately 400 mm by 460 mm, which represented the cross section at the large end of the high power channel.

The corner blocks and side rails were machined first with extra length allowed for the rails. At the same time a short section of an aluminum mandrel, shown in Figure C.3, was fabricated. The external surface of the mandrel was machined to the exact size and contour of the channel internal hot gas surface. The corner blocks were then positioned on the mandrel, and the rail lengths were cut to fit exactly between the corner blocks. The corners and sides were clamped in position on the mandrel and then were temporarily joined together with small tack welds. The frame was then removed from the mandrel, and the joints were permanently formed by manual torch brazing. Next, the frame was repositioned on the mandrel, and the cooling tubes were formed to fit closely to the external contour of the frame. The fitted tube and the frame were then removed from the mandrel, and the tubes were soldered to the frame. The completed frame was then repositioned on the mandrel, and using spacer shims between frames to produce the required insulation space, the next frame was fabricated.

This process proved very successful for the prototype frames. Four frames were fabricated and the dimensional results were very encouraging. In addition, the diagnostics channel was constructed with forty perpendicular frames using the same process. The dimensional contour of the internal surface contour and the intra-frame spacing was well within the design specifications.

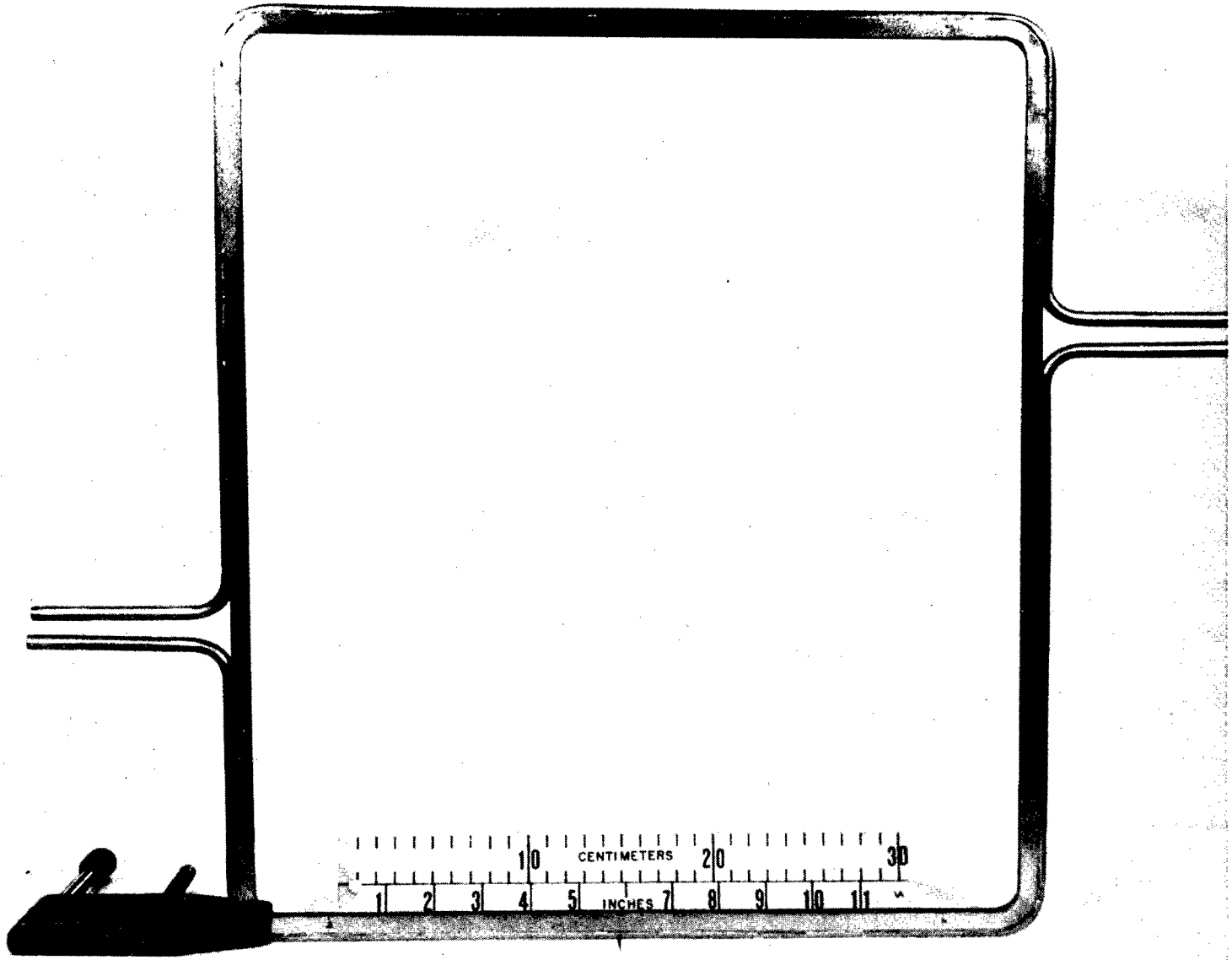

Figure C.2 Electrode Frame.

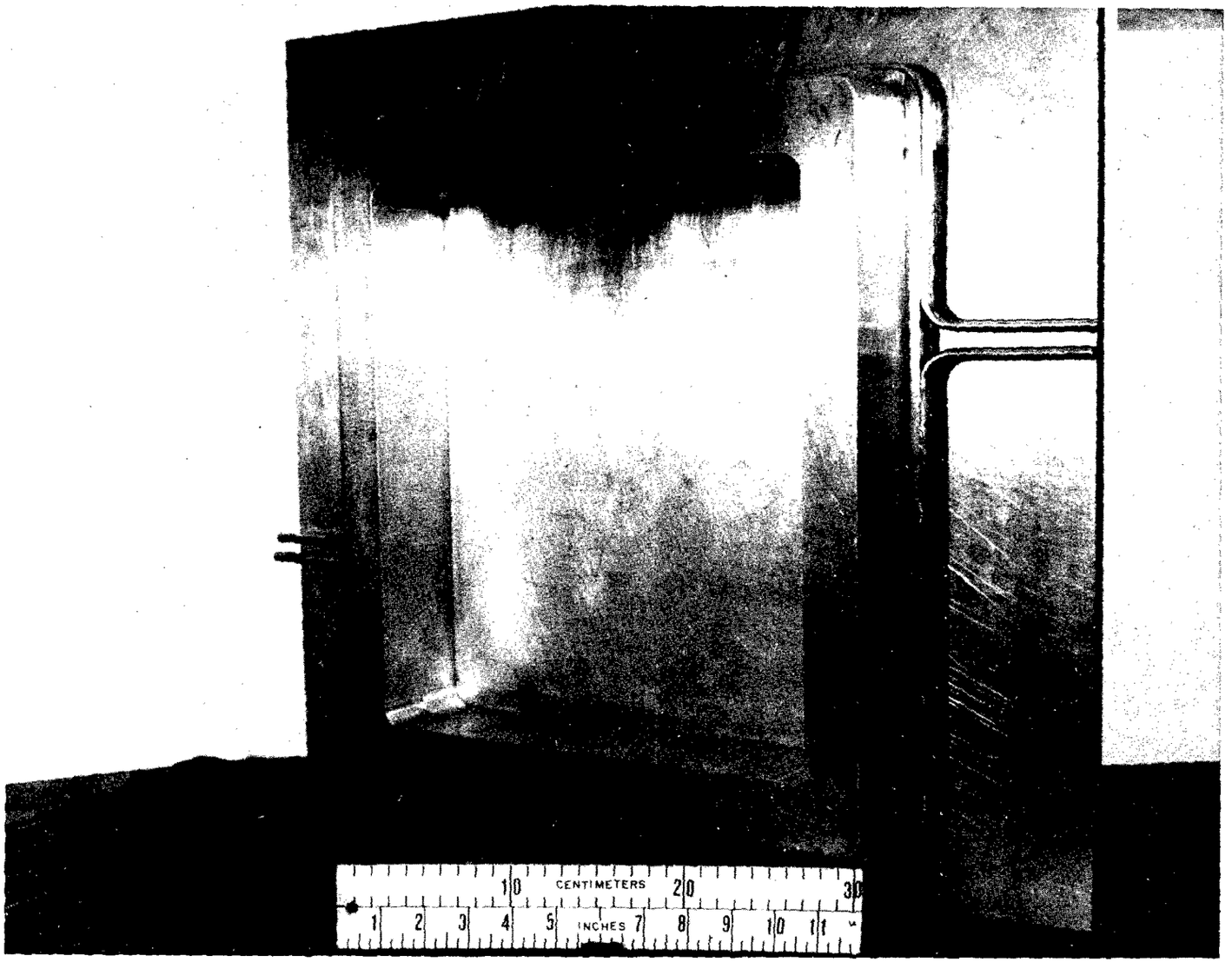

Figure C.3 Short Mandrel Section.

c. Prototype Diagonal Corner Fabrication

The construction of the internal corners of a high performance MHD channel was critical to maintain the axial voltage gradient present in the diagonal conducting wall channel. The corner regions of the diagonal electrode frames were the most complicated three-dimensional (3-D) geometry involved in the total channel hardware. These corners were very difficult to visualize on paper. Consequently, several models were fabricated to verify the design.

The required corner geometry is illustrated by Figure C.4. A constant width insulation space that was perpendicular to the internal hot gas surface was required between adjacent electrode frames. This requirement could only be met by making the diagonal side rails narrow and the top and bottom cross rails wide. The complexity arose as the frame made the transition from the narrow section to the wide section while forming an internal radius at the corner of the channel. This problem was resolved by fabricating the corner blocks as shown in Figure C.5. The required shape was formed by the intersection of two sets of parallel planes and two concentric cylindrical surfaces which lended itself to the use of conventional machining operations. Three model corners were constructed and mounted on a model mandrel section as shown in Figure C.6 which illustrated the uniform width insulation space between the adjacent blocks.

d. Prototype Diagonal Frame Fabrication

The diagonal frames, shown in Figure C.7, were constructed similar to the perpendicular frames, using four corner blocks, two straight side rails and straight top and bottom cross rails with continuous cooling tubes attached to the outside of the frame. The procedure for assembling the pieces into a frame was the same as described above for the perpendicular frames. However the diagonal side rails were more slender than the perpendicular side rails raising the question of what effects the increased slenderness could have on the fabrication of the frames. Another question concerned the problems that might be encountered in assembling the frames on the mandrel because of the diagonal location of the frames.

In order to evaluate these questions, a full scale section of a mandrel was fabricated as shown in Figure C.8, which resulted in frames that were approximately 690 mm long by 560 mm wide at the top and 460 mm wide at the bottom. Corner blocks were fabricated as discussed previously, and the straight side and cross rails were manufactured as discussed here. The parts were then assembled on the mandrel to form one electrode frame without cooling tubes and one frame with cooling tubes.

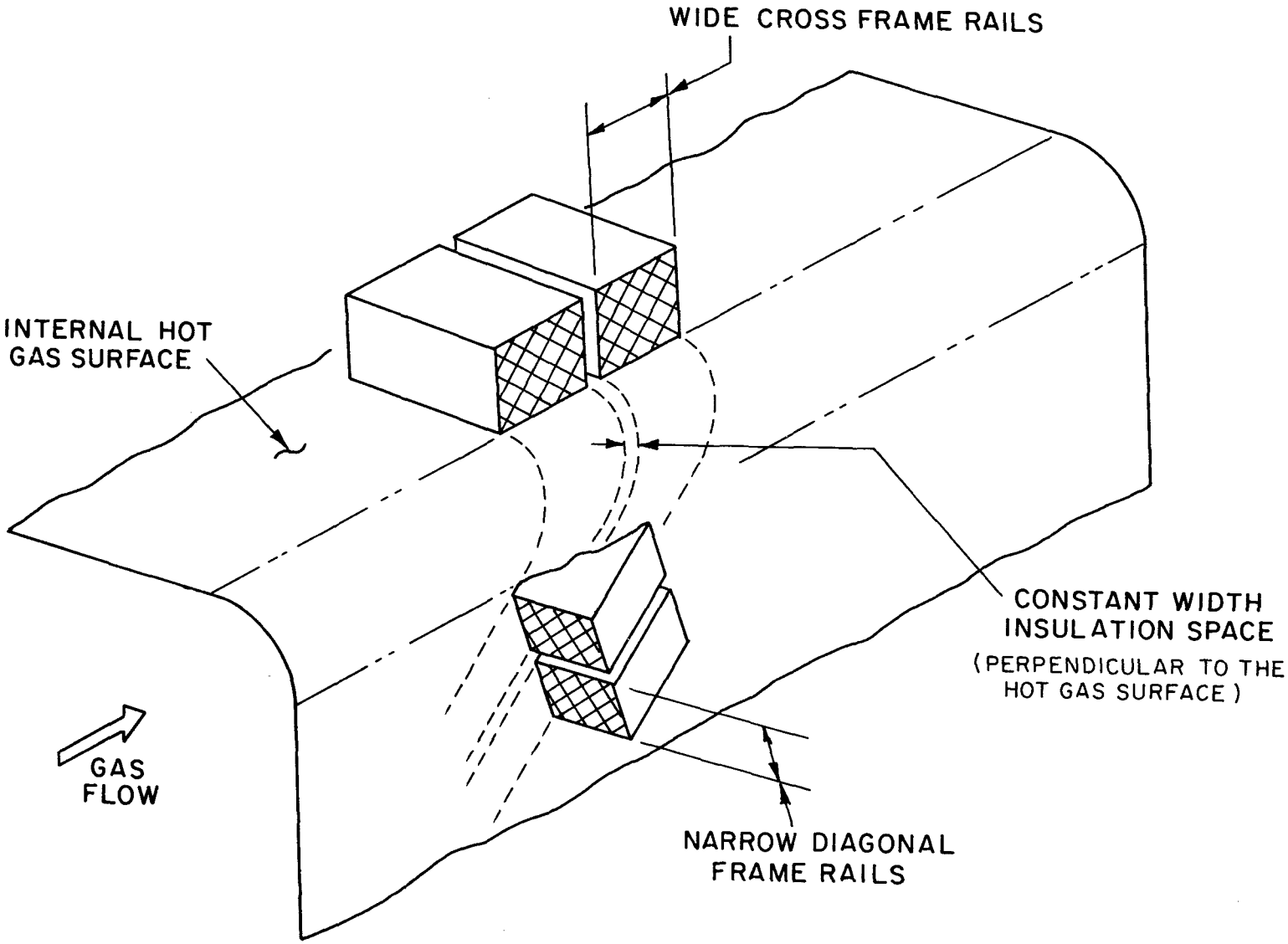

Figure C.4 Electrode Frame Corner Geometry.

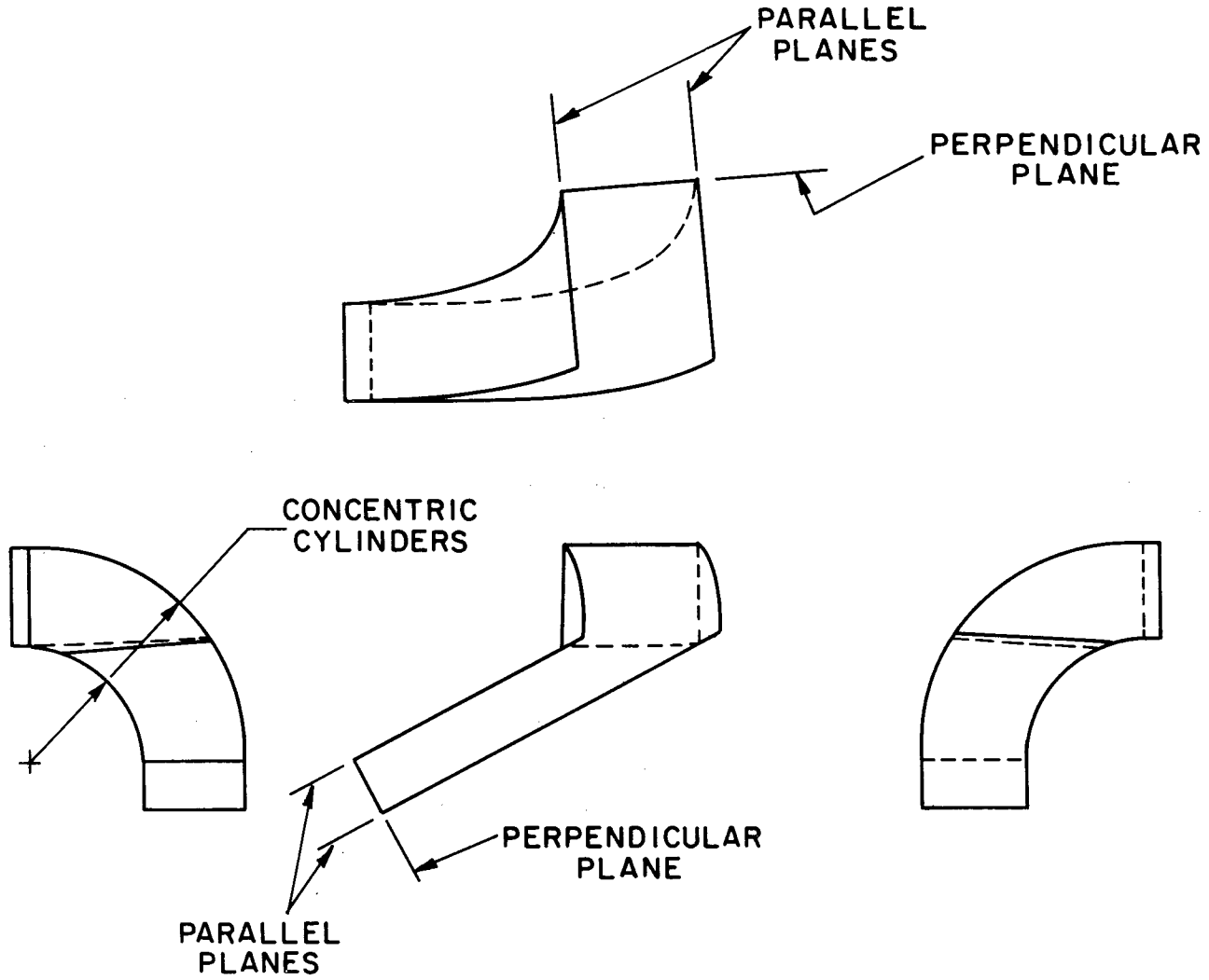

Figure C.5 Typical Diagonal Corner Detail.

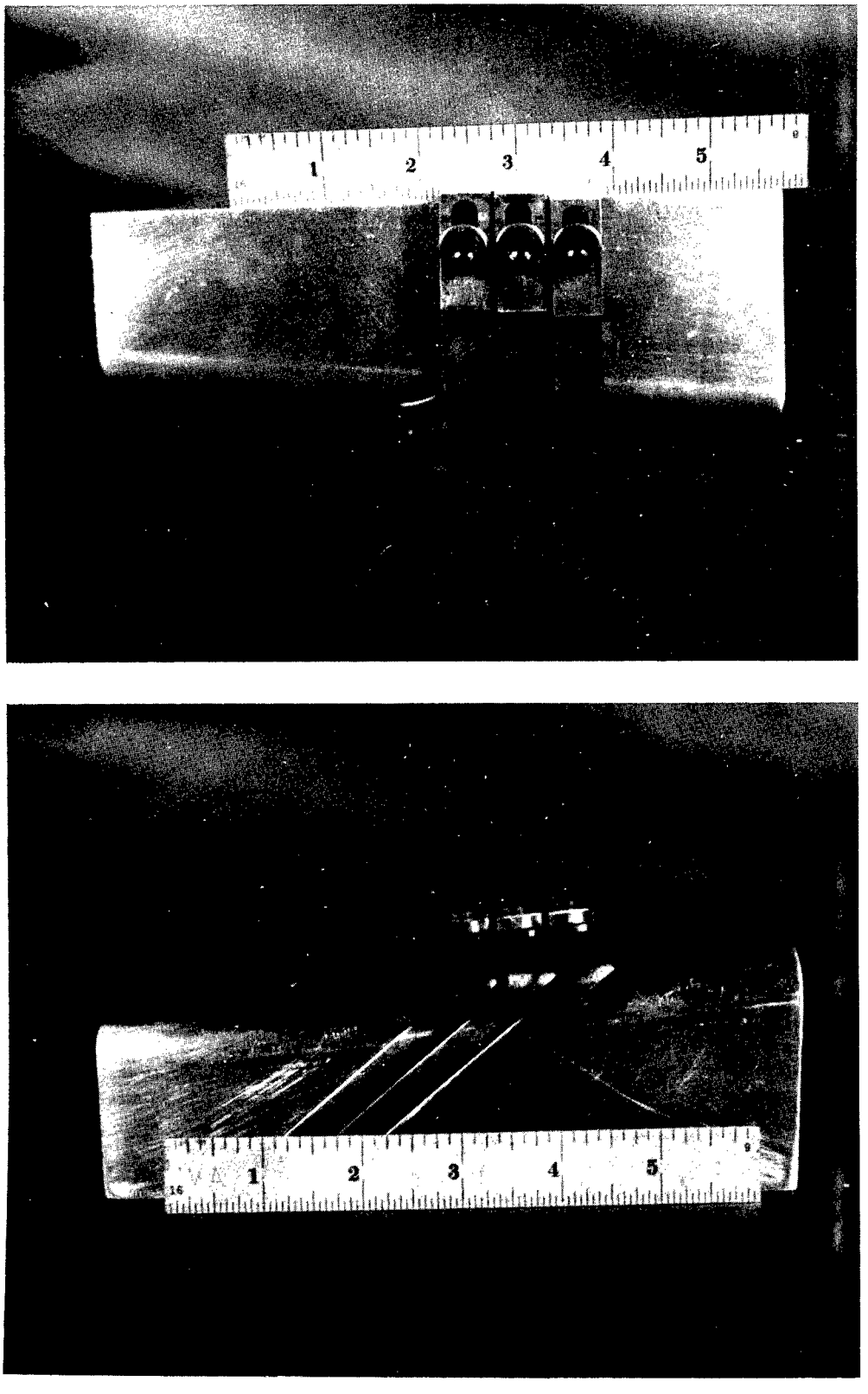

Figure C.6 Model Diagonal Corners.

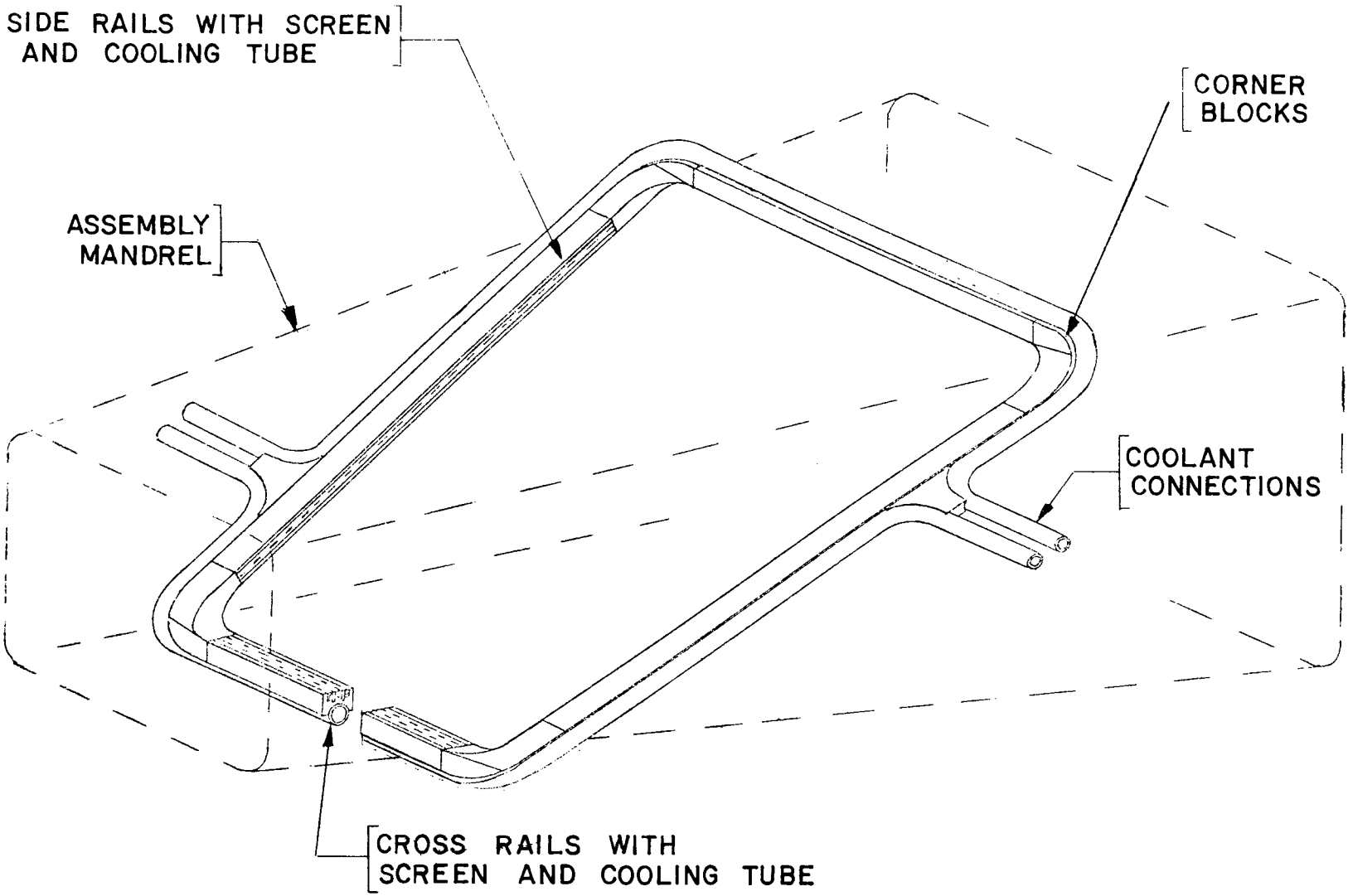

Figure C.7 Diagonal Electrode Frame Model.

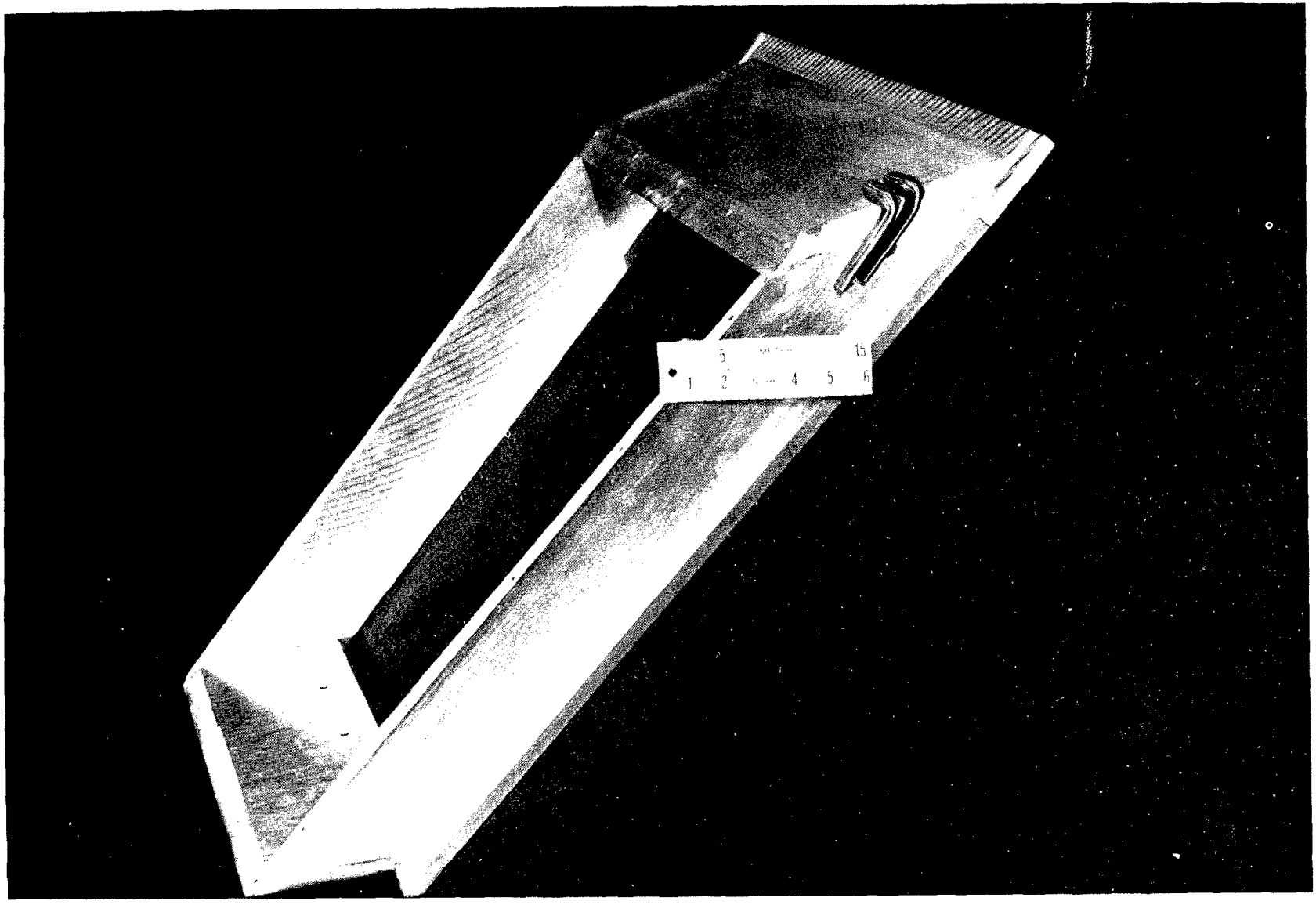

Figure C.8 Prototype Diagonal Frame Mandrel.

Assembling the loose frame parts on the mandrel was more difficult than with the perpendicular frames because no matter how the mandrel was oriented there were some parts that tended to slide off the mandrel. Consequently, more fixtures were required. Based on the limited experience with the fabrication of only two frames, the slenderness of the side rails did not appear to introduce any problems. The assembled frame without the cooling tubes was more rigid than expected, and the addition of the cooling tubes significantly increased the stiffness of the frames. Nevertheless, the frames will require careful handling during fabrication in order to prevent distortion until the composite fiberglass-epoxy shell is fabricated over the frames.

e. Cooling Tube Forming

The problems of designing and fabricating the diagonal corners of the electrode frames were previously described. The next most complex design and fabrication task was that of forming the cooling tubes around the complex external geometry of the diagonal electrode frames. A smooth internal tube contour, which minimized any restrictions to the high velocity cooling water flow that could arise from any sharp discontinuities, was also required. The tube forming requirements involve three types of geometry as shown in Figure C.9: (1) the frame corner regions; (2) the tube connections regions; and (3) the flattened straight sections along the diagonal side rails. The constant diameter copper tubing was formed into all of the complex geometry required without making any joints along the length of the tube. This was a key feature that greatly increased the reliability of the channel cooling provisions.

The tube geometry that was required at the corners is shown by Figure C.10. The tube shape must change from a round to a flattened cross section while making the transition around the corner radius of the channel. At the same time the tube must fit closely to the outer surface of the frame in order to form a reliable heat transfer joint, which was enhanced by cutting grooves in the corner blocks as shown in Figure C.11.

Conventional tube forming techniques were heavily dependent on the use of filler materials that were temporarily placed inside of the tubes to prevent the walls from buckling and collapsing. A variety of fillers were tried unsuccessfully, but after considerable effort, a technique was developed that successfully formed the tubes without using any internal fillers.

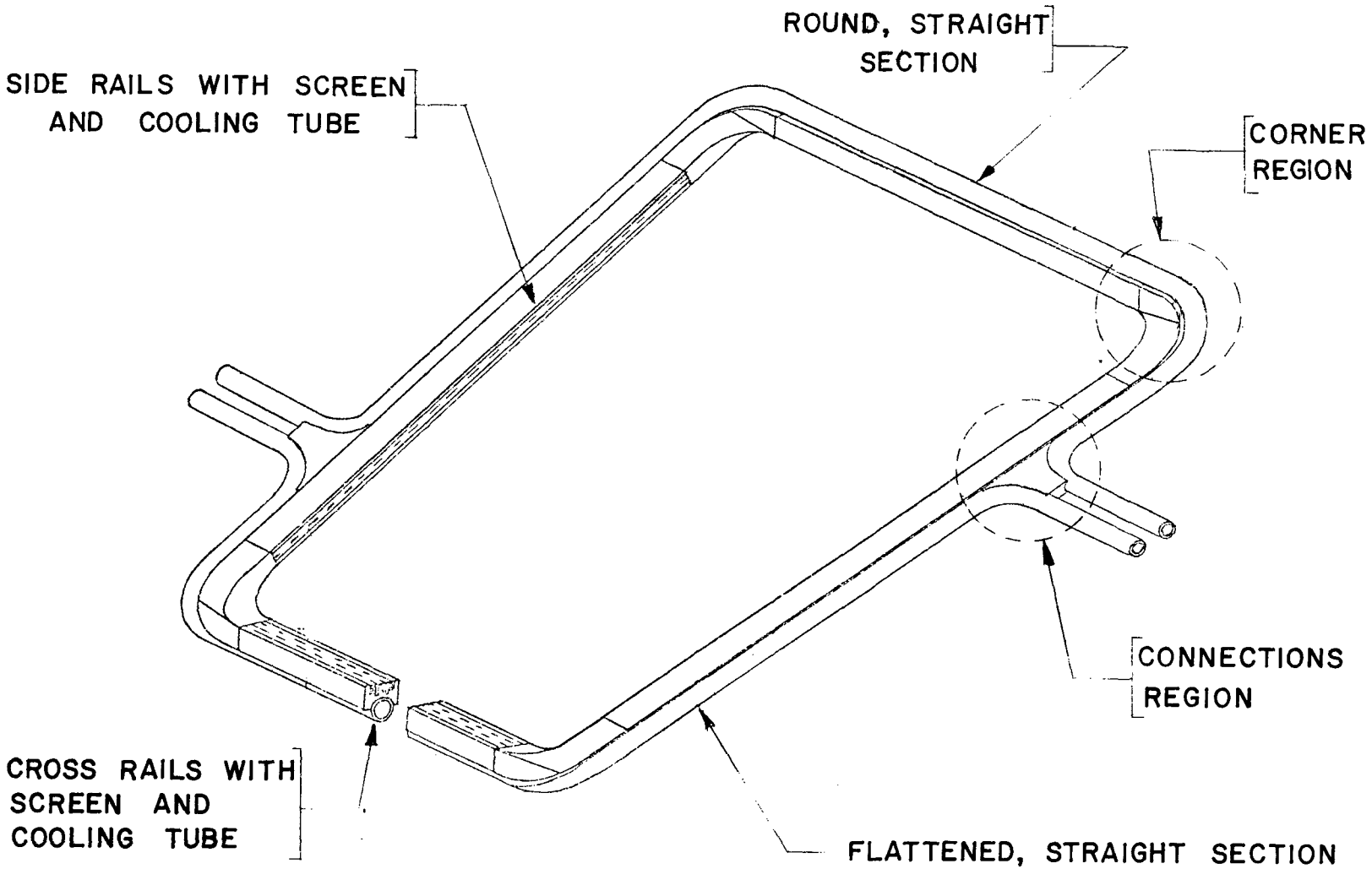

Figure C.9 Diagonal Frame Cooling Tubes.

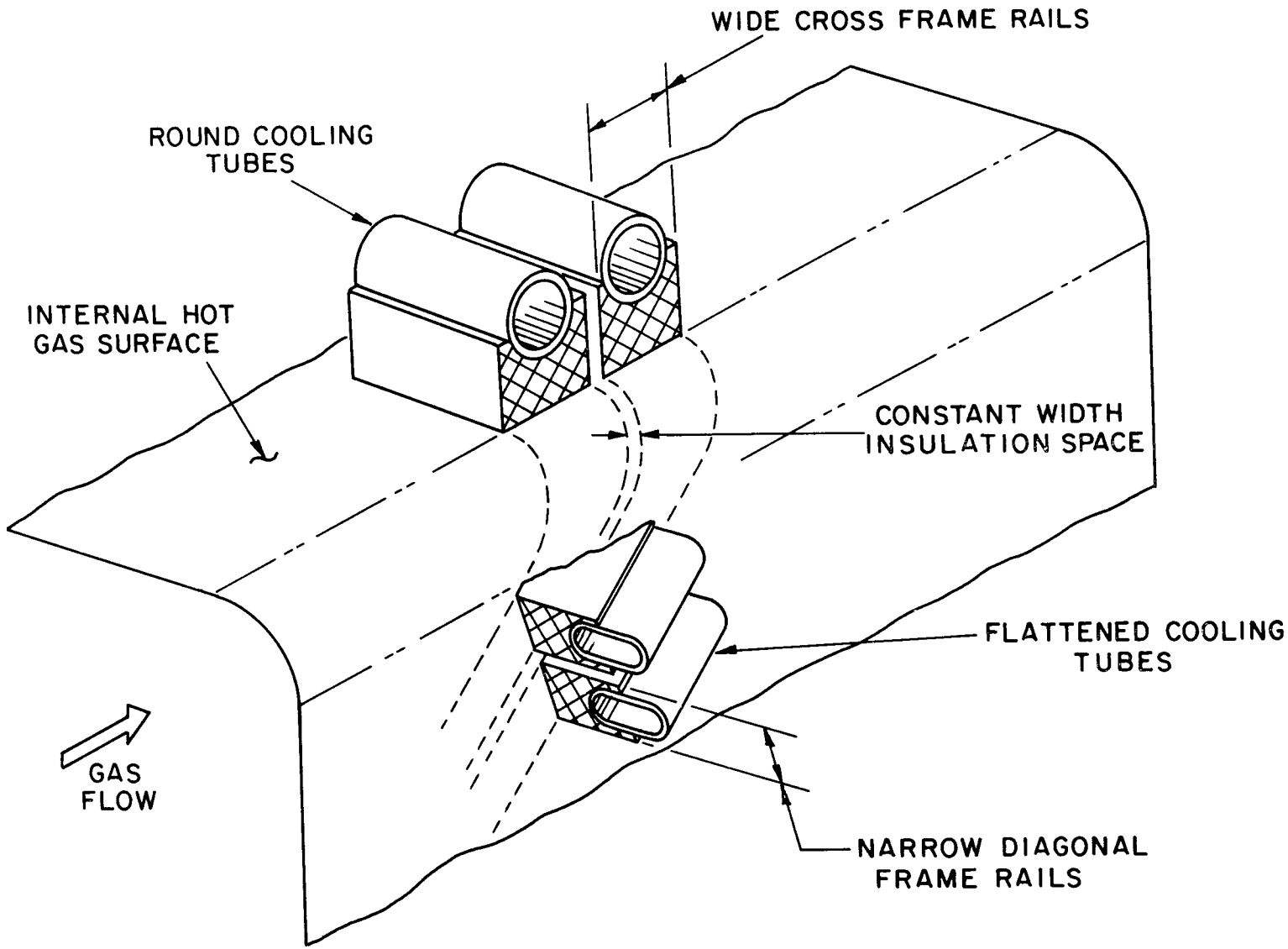

Figure C.10 Electrode Frame Corner Geometry.

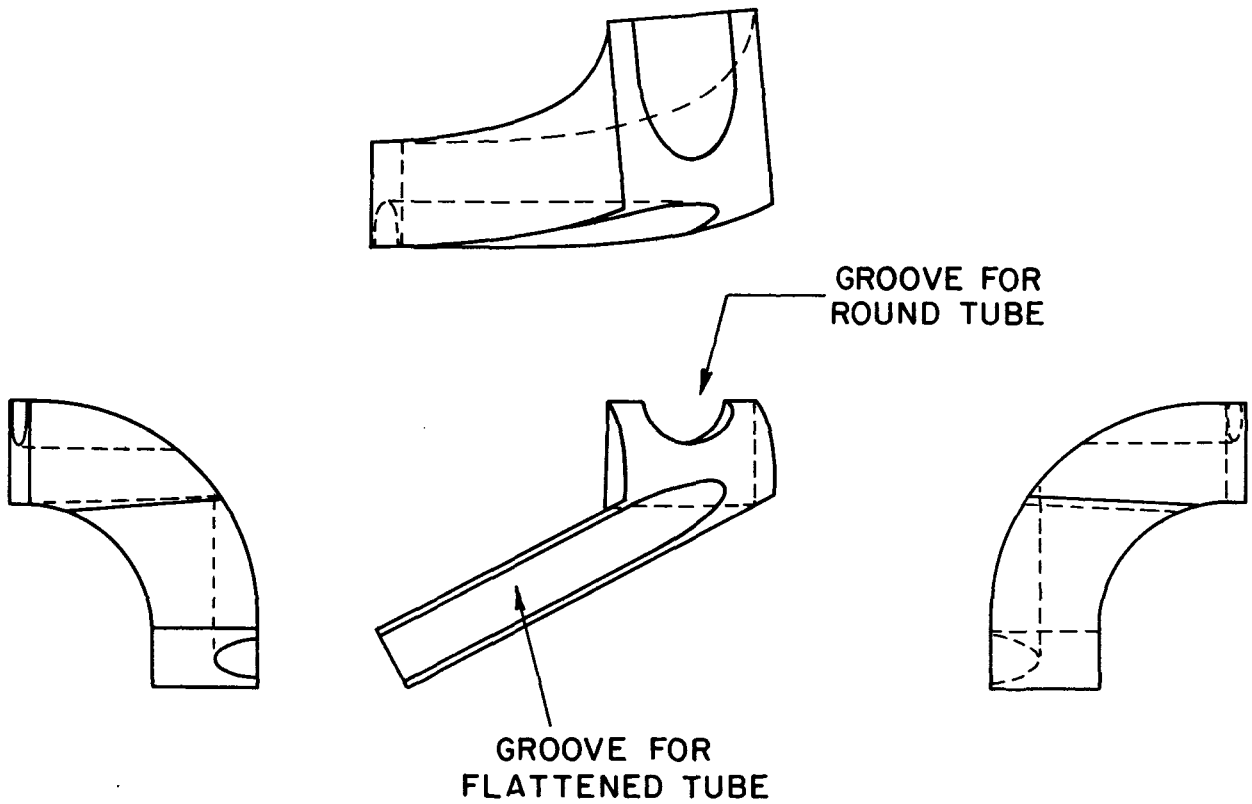

Figure C.11 Grooves in Corner Blocks.

A prototype corner forming tool was developed and is shown in Figure C.12A. The tool consisted of a main forming die block, a three-dimensional forming cam, and a roller/lever type cam follower. Figure C.12B shows a piece of tubing in place with the cam and follower in the starting position. Figure C.12C shows the cam and follower in the finished position. Figure C.12D shows the completed formed tube corner.

In the tube connection region the tube shape must change from a round to a flattened cross section while forming a 90 deg bend in the plane of the flattened section. This was accomplished by developing the special two piece forming die shown in Figure C.13A. The tube was placed in the die shown in Figure C.13B. Figure C.13C shows the flattened tube before removal from the die.

Figure C.14A shows two adjacent formed tubes with a heat transfer wedge block in place. The same tooling was used to produce offset connections where higher heat transfer rates may require closer spacing of the tubes. The cooling tubes formed to meet this requirement are shown in Figure C.14B. The flattened straight sections of the tubes were formed with the special two-piece forming die shown in Figure C.15A with a piece of tube before flattening. The resulting tube cross section after flattening is shown in Figure C.15B.

Because of the complexity of the corner forming tooling, the tubes were formed using a series of operations. At first this caused unacceptable deformations in the tube walls at the overlapping of the operations. This deformation was successfully eliminated by providing a gradual taper on the forming punch as shown in Figure C.16A. A sample tube was flattened in three steps, and the deformations were eliminated as shown in Figure C.16B.

In conjunction with the development of the foregoing tube forming tooling, a few full size completely formed tubes were subjected to water flow tests to evaluate the results of the forming operations. These tests showed that the major increase in the pressure drop over that of a round tube was the result of the flattened straight sections which were unavoidable with this electrode frame design. The complex tube corner forming added only a 5% increase to the pressure drop. The successful results of the foregoing tube forming modeling verified the design of the electrode frame cooling tubes.

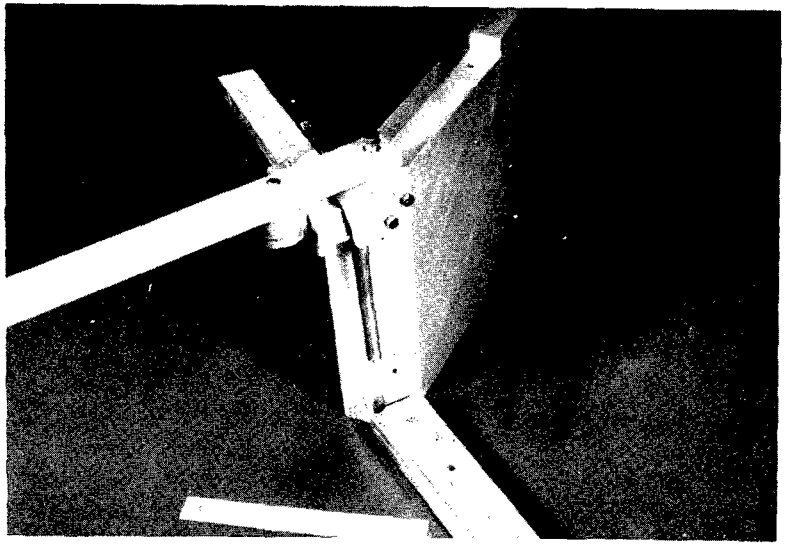

(A)

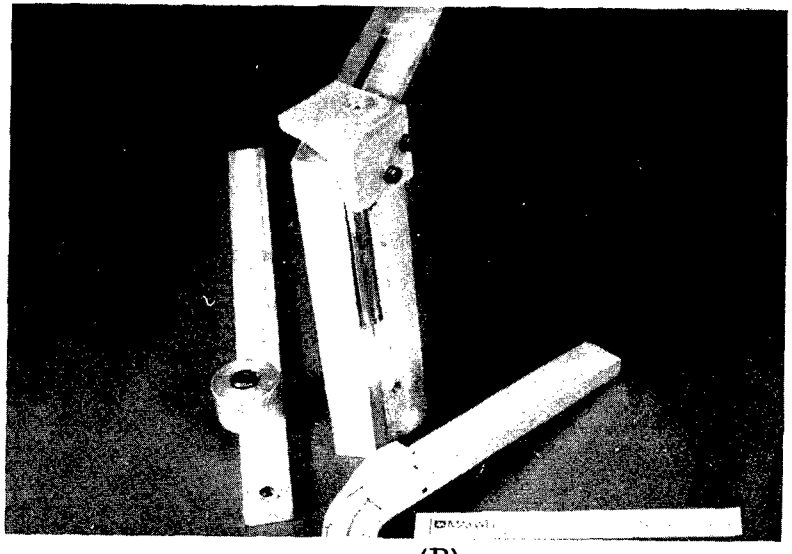

(B)

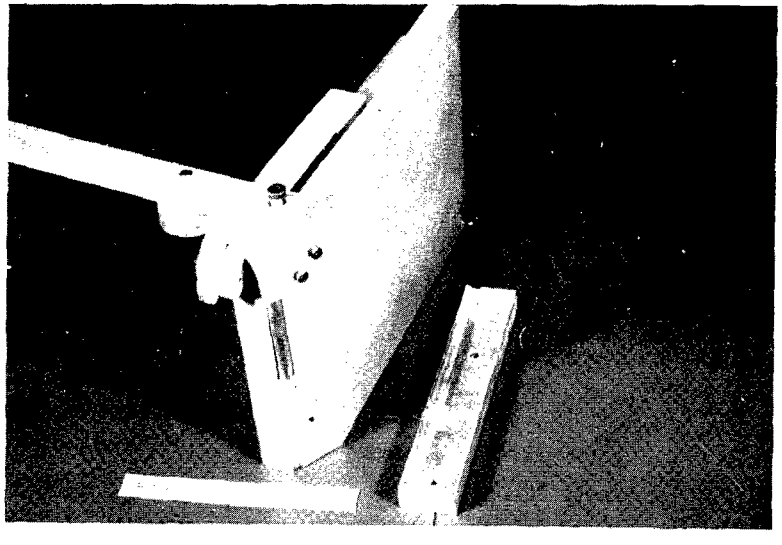

(C)

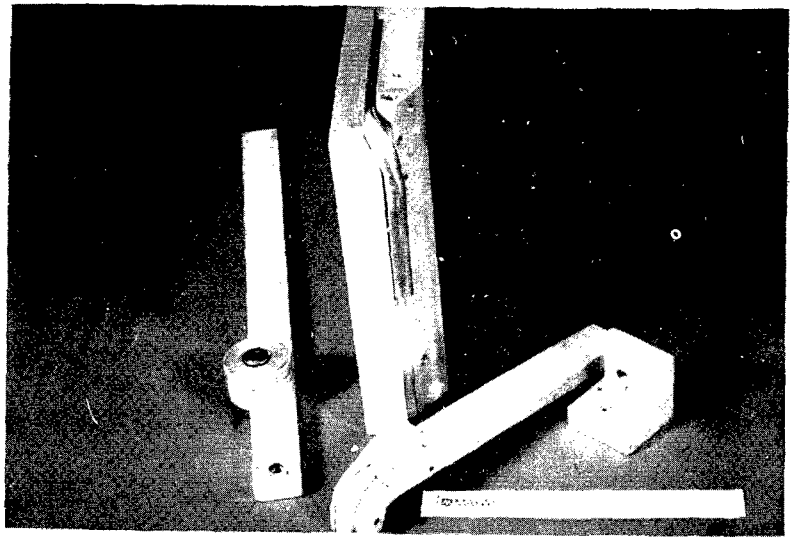

(D)

Figure C.12 Tube Corner Forming Tool.

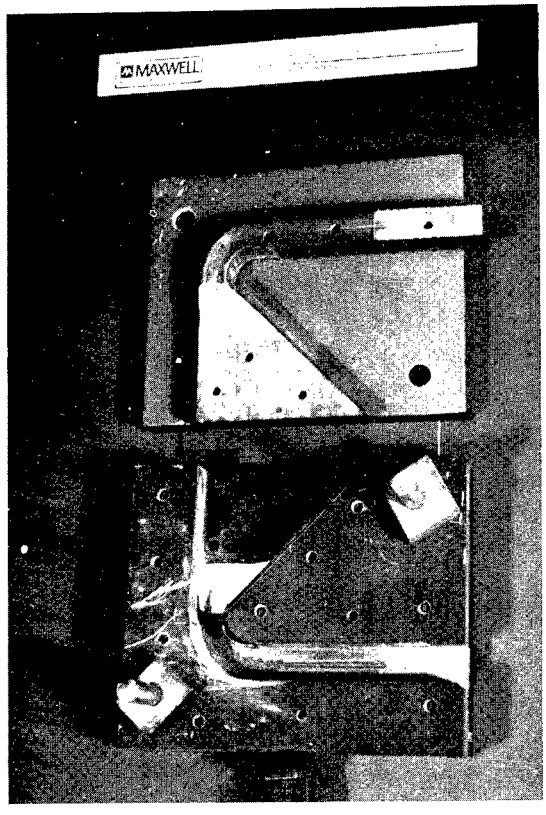

(A)

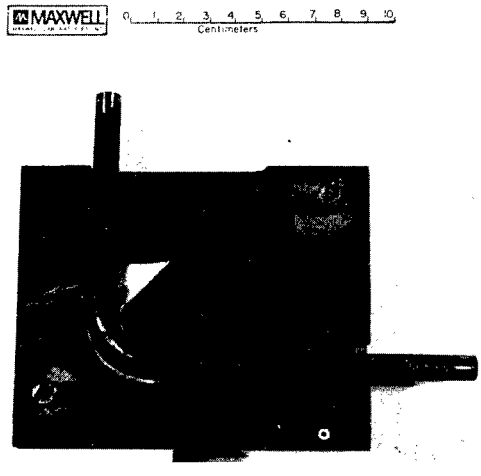

(B)

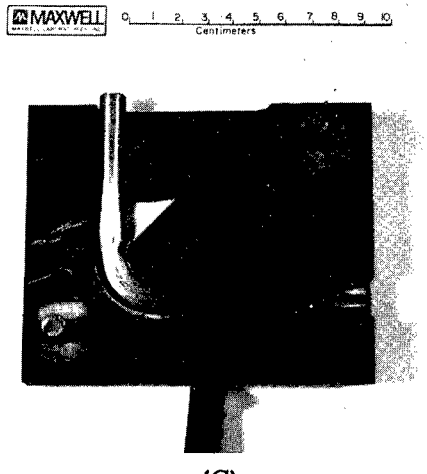

(C)

Figure C.13 Tube Connections Forming Tool.

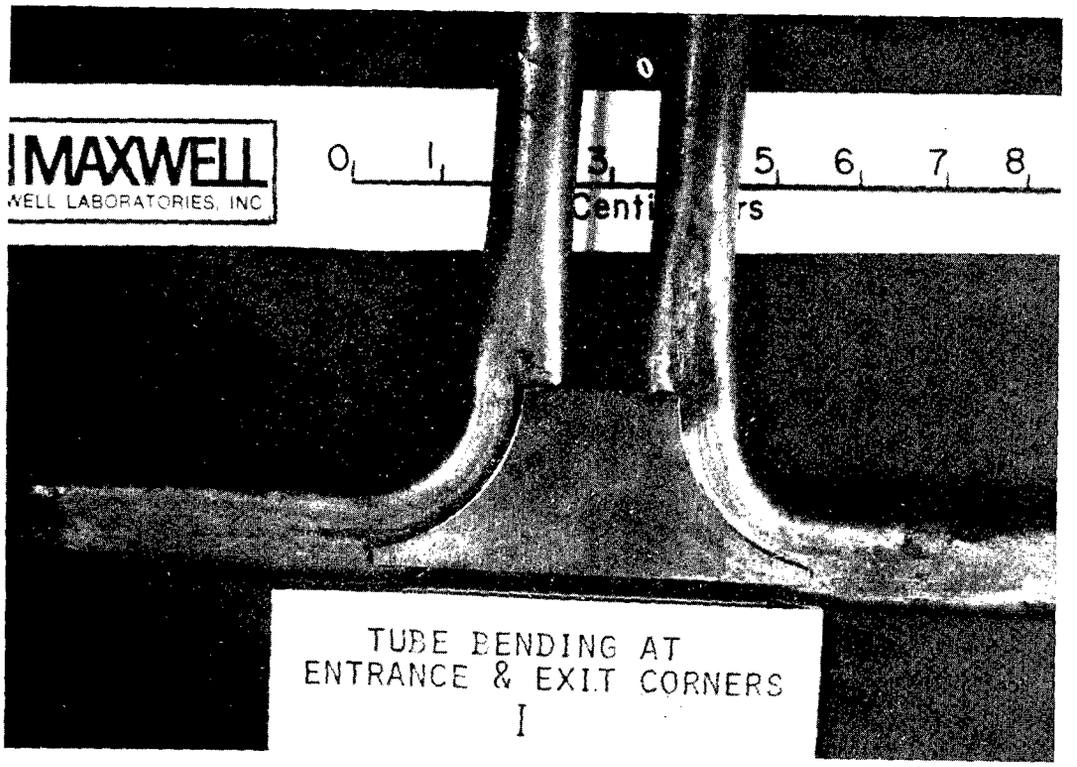

(A)

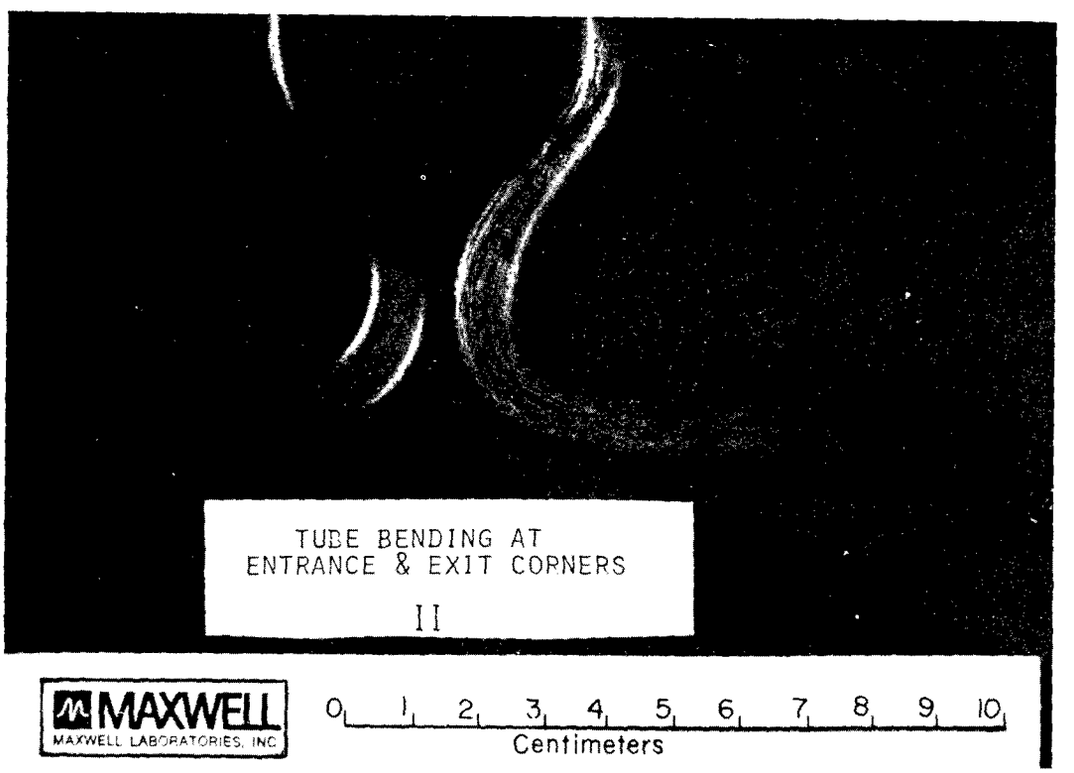

(B)

Figure C.14 Formed Connection Tubes.

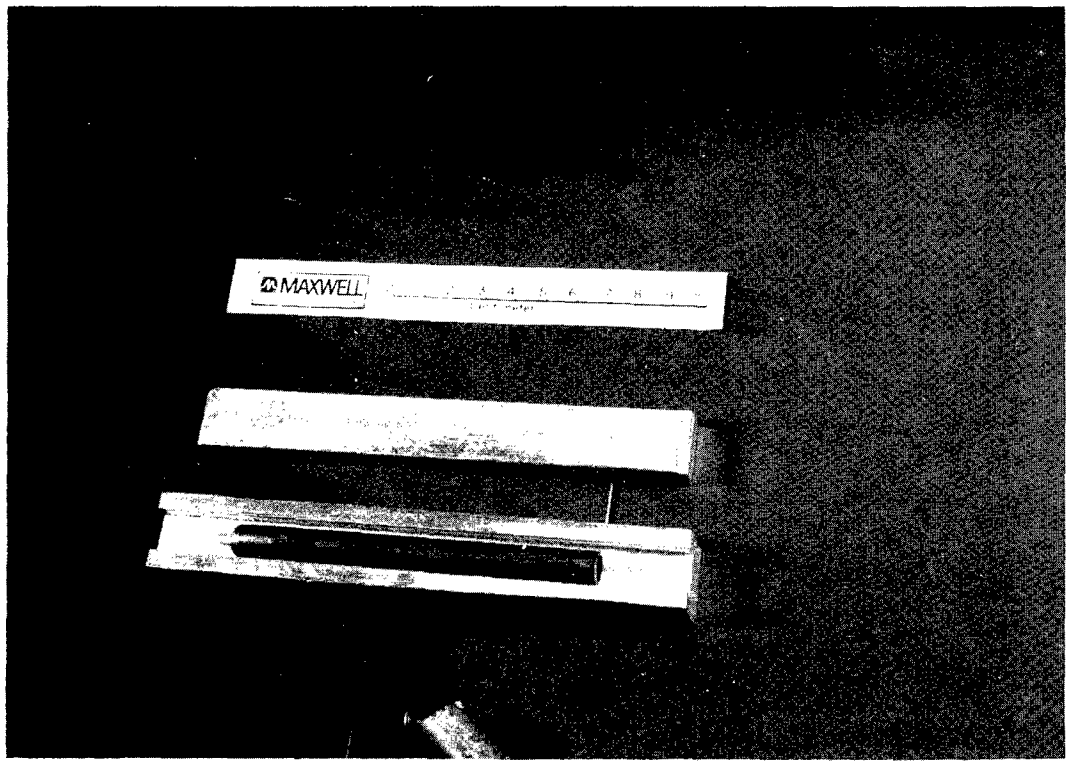

(A)

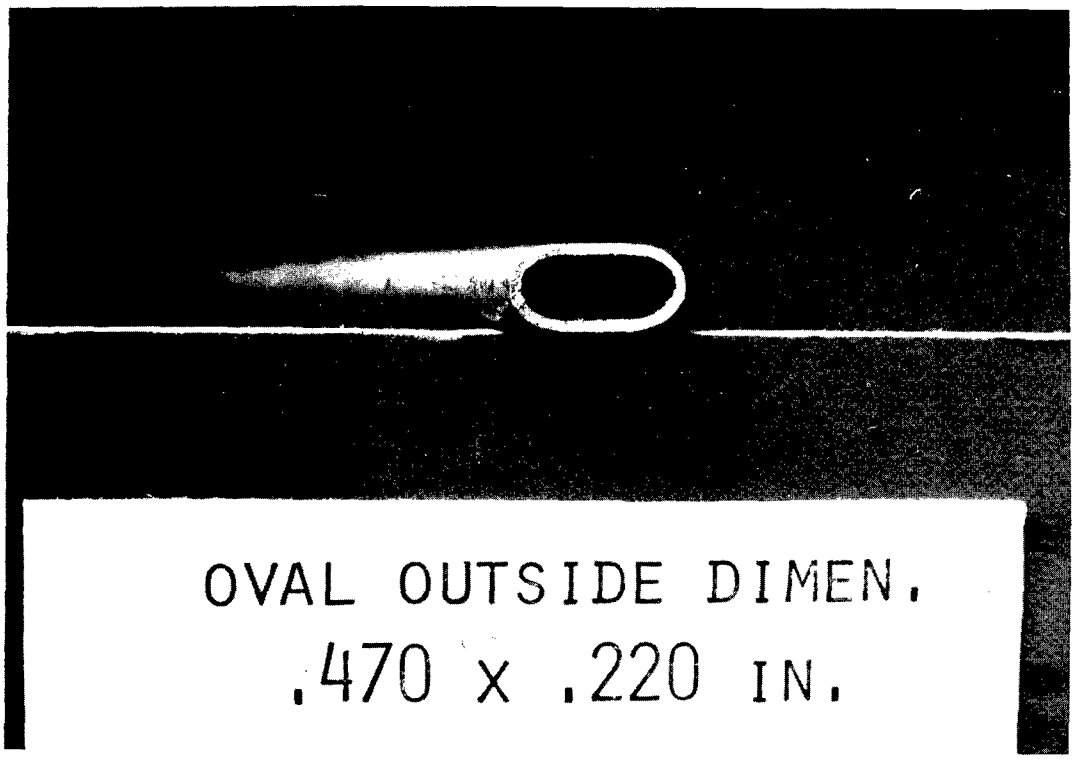

(B)

Figure C.15 Straight Tube Flattening Die.

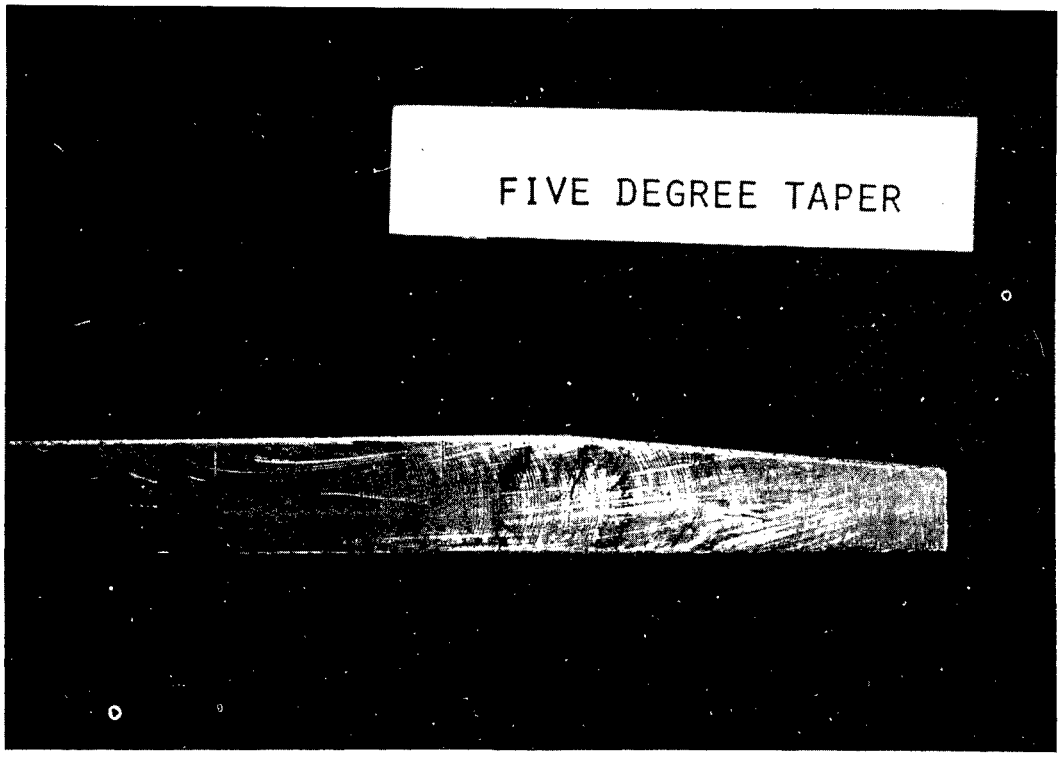

(A)

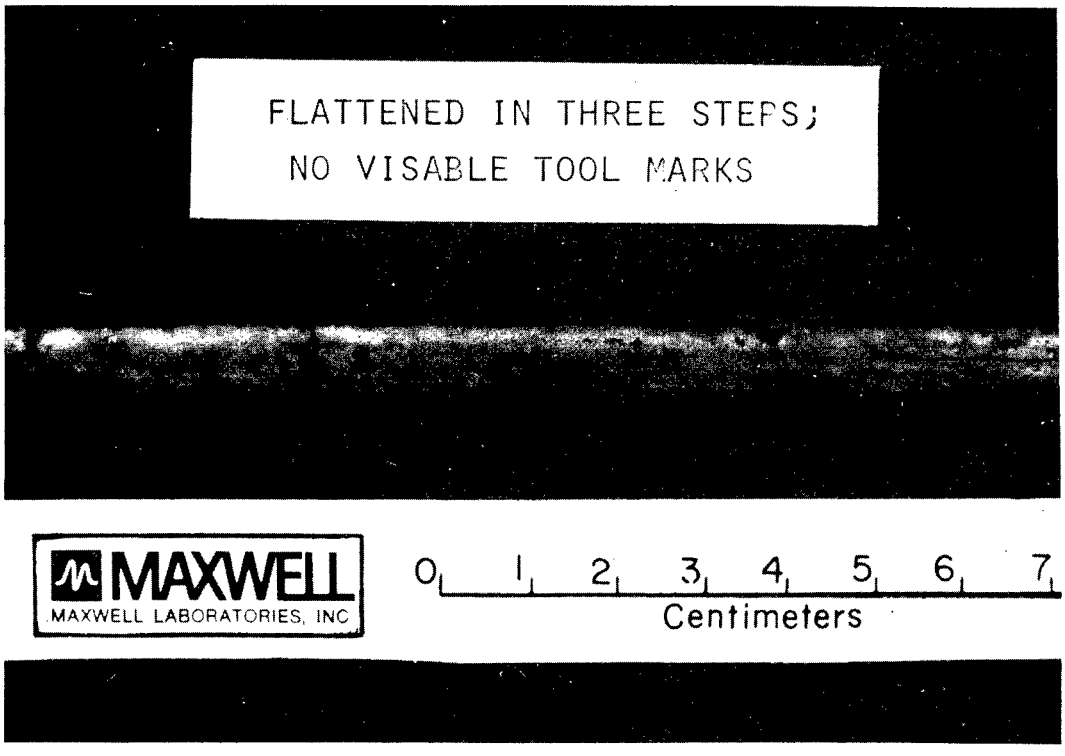

(B)

Figure C.16 Straight Tube Flattening Punch.

4. COMPOSITE CASE

The high power channel/diffuser composite case was designed as an integral fiberglass reinforced epoxy resin structure that was to be fabricated in place around the outside of the electrode frames and functioned as the primary structural member of the channel. Since the high power MHD channel was approximately three times as long and four times as wide at the exit end as the previous AFAPL lightweight channel,[4] a model section of the case was fabricated to evaluate the process of fabricating the case. In addition, a section of the model case was used for measuring the various design properties of the actual material composition that will be used in the channel case fabrication. The model case section which was approximately 360 mm square by 360 mm long is shown in Figure C.17A. This section was representative of the midsection of the high power MHD channel case.

The model was fabricated on a wooden mandrel section, using the fiberglass winding machine and the elevated temperature curing oven that was later used for the diagnostics channel fabrication process. The increased size of the channel case did not introduce any problems that affected the design of the case. The case walls were twice as thick at the midpoints as they were at the corners because of the nature of the fiberglass epoxy wet-winding process. However, the winding process was very slow because of the amount of materials involved and the application of only a few fiberglass filament strands at one time. Obviously further work is required to develop tooling, fixtures, equipment, and methods for speeding up the winding process before attempting to fabricate the high power channel/diffuser composite case.

The model was also used to study the process of separating and splicing together the case, which would be required if it were necessary to replace any defective channel electrode frames. The model was separated into two sections by making a diagonal cut as shown by Figure C.17B. The sections were then spliced together using fiberglass and epoxy resin. Preliminary tests indicated that the spliced walls were essentially as strong as the original walls for bending loads that would be applied by the static gas pressure inside the channel. However, the axial tensile strength of the joints was not tested. The joints would also require further reinforcement material (fiberglass-epoxy) to withstand the axial forces that would be involved when the operating channel is subjected to the bending loads related to the magnetic forces acting on the channel.

---

[4] D.W.Swallom, O.K.Sonju, D.E.Meader, G.T.Heskey, "MHD Lightweight Channel Development," AFAPL-TR-78-41, June 1978.

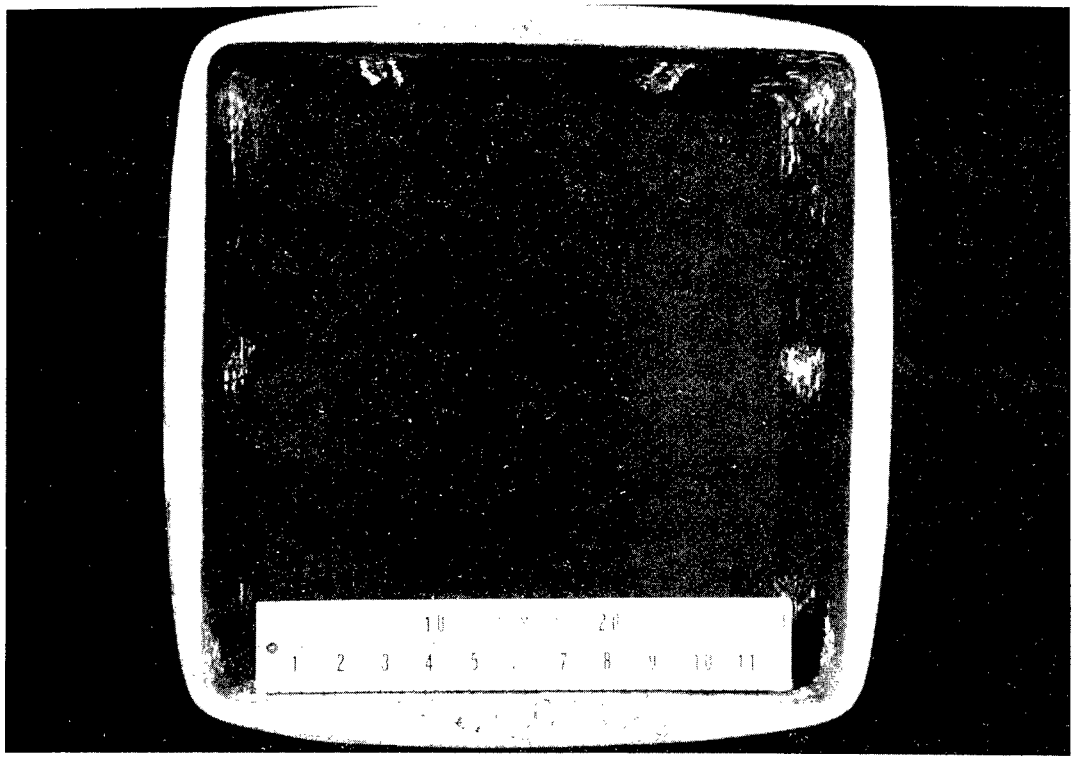

(A)

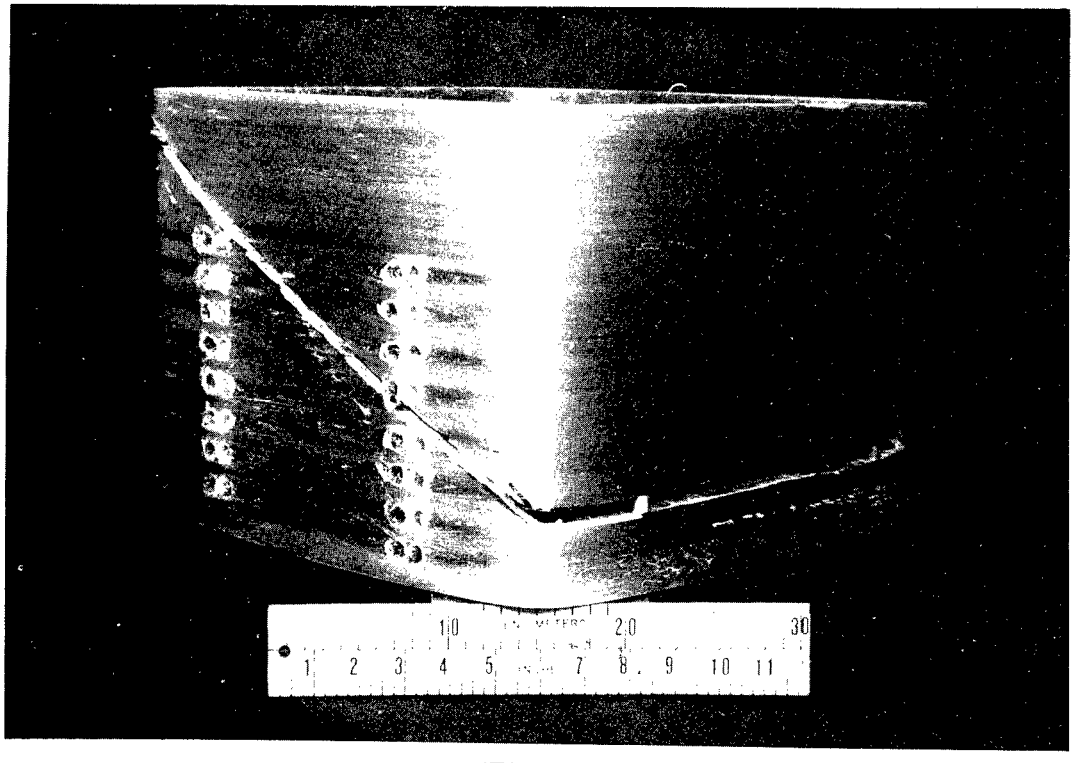

(B)

Figure C.17 Composite Case Model.

APPENDIX D

DYNAMIC ANALYSIS

To evaluate the dynamic performance of the system, a model was formulated and programmed for solution on an analog computer. The system simulated is shown schematically in Figure D. 1 and included: (1) the GO_2 and Methane igniter reactants supply; (2) the LO_2 feed system from the supply tank to the combustor; (3) the JP-4 feed system from the tank to the mixer; (4) the seed feed system from the tank to the mixer; (5) the fuel feed system from the mixer to the combustor; (6) the igniter, seed, fuel and LO_2 control valves; and (7) the combustor. The model was used to evaluate the system start and cutoff performance. The start studies included a determination of the effect of the valve sequencing and the system geometry on pressure surges, volume priming and overall start time. The cutoff studies consisted of determining the effect of valve area contour and closing time on surge pressures.

The nominal system values used were:

1) LO_2 and JP-4 feed lines of 5.25 cm i.d., 38.1 m long
2) Seed system feed line of 2.66 cm i.d., 11.6 m long
3) LO_2 priming volume of 3300 cm^3
4) Fuel priming volume of 1300 cm^3
5) 5 cm Annin Series 4500 fuel and LO_2 valves with a maximum $C_V = 1950$
6) 2.5 cm Annin Series 1600 seed valve with a maximum $C_V = 667$

1. VALVE CONTOURS

For Annin valves there were three standard throttle plug contours designated as: (1) semi-throttle, (2) linear, and (3) percentage. The contours referred to the shape of the C_V, defined as the liters/min flow of water/atm pressure drop, curve vs valve position as shown in Figure D. 2. The LO_2, fuel and seed valves originally had semi-throttle plugs.

To select the best plug for the fuel and oxidizer valves, a start and cutoff transient was predicted for each contour using 0.6 sec linear position vs time opening and 0.5 sec linear position vs time closure. The operating conditions used were those resulting in the maximum LO_2 system pressures, + 20% total flow with no seed flow, and the maximum fuel system pressures, + 20% total flow with 10% seed flow. The results from the starts and cutoffs are tabulated in Tables D. 1 and D. 2, respectively.

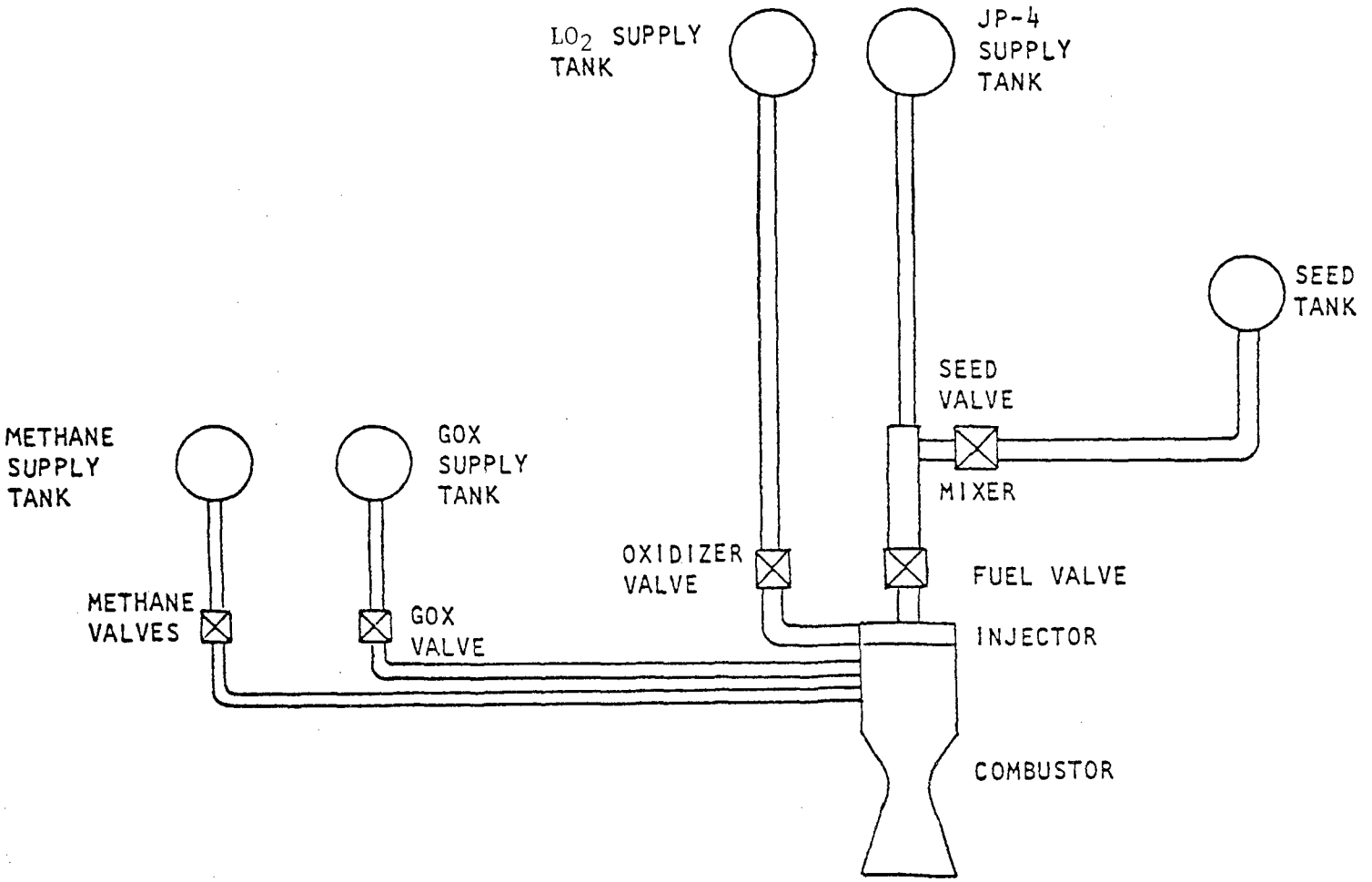

Figure D.1 Feed System Schematic.

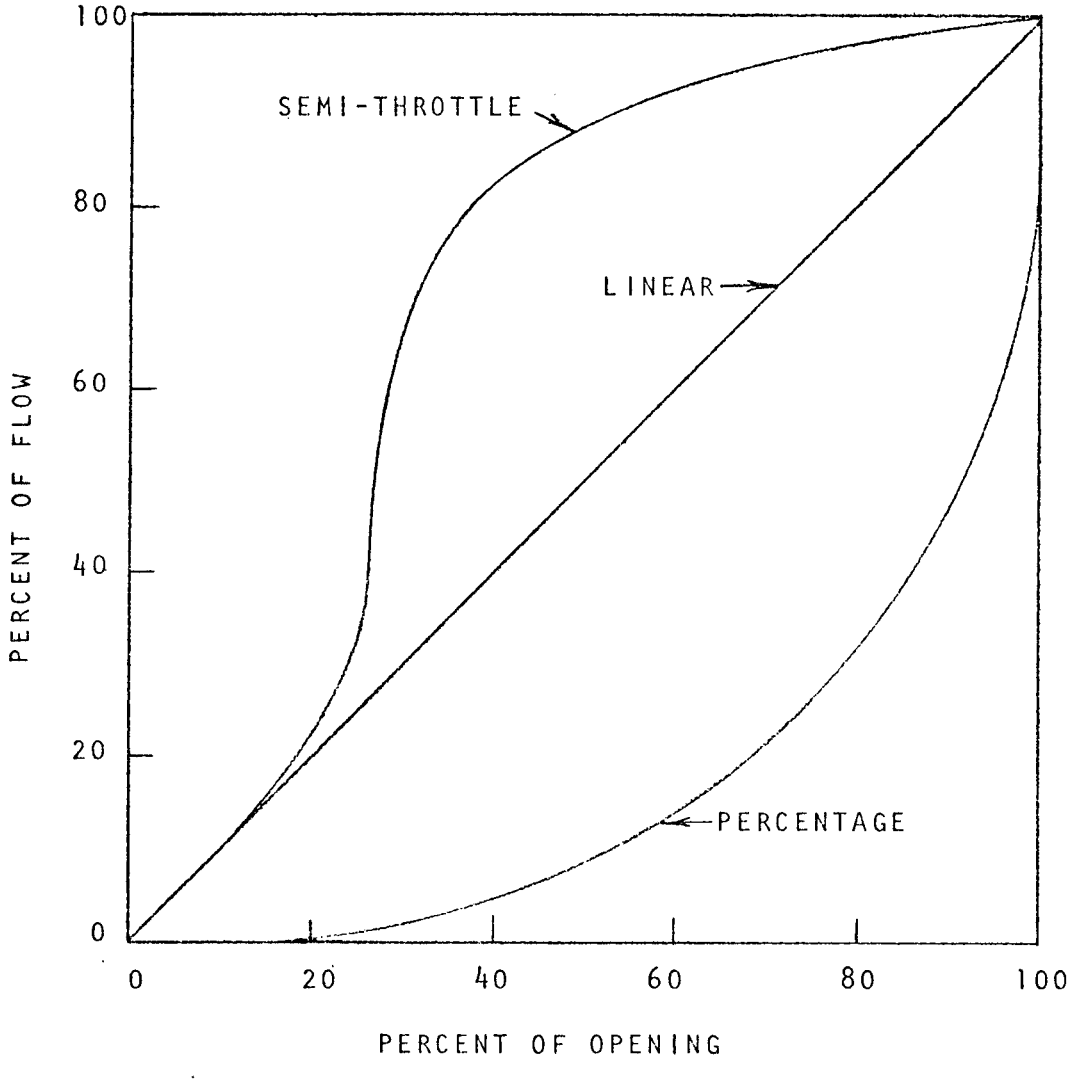

Figure D.2 Curve of Flow vs Valve Position.

TABLE D.1 MAXIMUM PREDICTED START TRANSIENT PRESSURES VS VALVE PLUG CONTOUR

	Normalized Pressure*		
Plug Location	Semi-Throttle	Linear	Percentage
LO_2 Injector	1.10	0.92	1.0
Fuel Injector	1.42	1.04	1.0
Chamber	1.14	0.98	1.0

* Normalized to Percentage Contour

TABLE D.2 MAXIMUM PREDICTED CUTOFF VALVE INLET PRESSURES VS VALVE PLUG CONTOUR (NORMALIZED TO PERCENTAGE CONTOUR)

	Normalized Pressure		
Plug Location	Semi-Throttle	Linear	Percentage
LO_2	1.27	1.08	1.0
Fuel Valve	1.14	1.13	1.0

To minimize the transient pressure surges to which the system can be subjected, percentage plugs were installed in the LO_2 and fuel valves.

The seed system was relatively short and the semi-throttle plug with a valve closing time of 0.250 sec resulted in a valve inlet pressure surge of only 6.8 atm above its tank pressure. This was no problem and did not warrant changing the plug. Subsequent start and cutoff studies were made using percentage plugs for the LO_2 and fuel valves.

The start and cutoff required accurate control of the three reactant valves to provide the short transient and to avoid introducing JP-4 into the combustor prior to the LO_2. The type of actuation system had a direct bearing on this accurate control. A pneumatic actuation system was a compressible force balance type and as such was susceptible to non-repeatable travel times, characteristics and delays because of such things as flow forces, mechanical friction and pneumatic fluid temperature changes. A hydraulic system was essentially a positive displacement system and resulted in predictable, repeatable sequencing. For these reasons a hydraulic actuation system was used.

2. START ANALYSIS

The goals for the start sequence analysis were: (1) the time from the ASI methane valve open signal to reaching 90% of operating chamber pressure less than or equal to 1.0 sec; and (2) chamber fuel flow must not be initiated prior to oxidizer flow. Both of these criteria were dependent on the volumes downstream of the valves, which had to be primed, and the priming characteristics. From previous rocket engine experience, the priming characteristics of a fuel like JP-4 were such that little if any fuel flow entered the chamber until enough flow had entered the priming volume to completely fill the volume. For an oxidizer like liquid oxygen, manifold heat transfer resulted in oxygen vaporization and some chamber flow during priming. Those characteristics have been accounted for in performing the start analysis.

The maximum priming times resulted for the operating condition which had the lowest LO_2 and fuel tank pressures. This occurred at -20% total flow with no seed flow for the fuel system and at -20% total flow with +10% seed flow for the oxidizer system. To preclude any fuel entering the chamber prior to oxidizer, the opening of the fuel valve was delayed approximately 150 msec with respect to the oxidizer valve. An alternate method which provided greater assurance of an LO_2 lead was to use a fuel valve opening signal keyed to an LO_2 manifold pressure. This however, led to slower start times.

Table D.3 summarizes the predicted time from the initial methane valve opening to achieving 90% of operating chamber pressure as a function of LO_2 and fuel valve opening times.

For initial testing the LO_2 and fuel valve opening times of 600 msec were used. This time minimized any transient pressures and stayed within the 1 second start criteria time. The effect of a 50% increase in volumes was to increase the buildup time from 700 to 770 msec. The effect of 20% longer feed lines was also considered and the results indicated no detectable change in priming time.

The complete recommended sequence for a rapid system start was: (1) the methane ASI solenoid actuated valve was energized open; (2) after 250 msec the GO_2 ASI solenoid valve was energized open; (3) when the ASI ignition was detected, the main LOX valve was started open at 167%/sec (4) after 150 msec the main fuel valve is started open at 167%/sec; and (5) the seed valve started open at 750 msec from methane valve opening at 400%/sec.

Figure D.3 shows predicted pressures and flow rates for this sequence with nominal flow rate and 5% seed flow. An array of operating conditions were surveyed to determine maximum pressures. During the start sequence, the maximum surge pressures occurred downstream of the main valve. The maximum pressure values were: (1) LO_2 injector pressure of 77 atm; (2) fuel injector pressure of 67 atm; and (3) combustor pressure of 38 atm. These amounted to approximately 12% overshoot of the steady-state values.

At nominal operating conditions the pressure overshoot was well within the channel limits. However, this pressure overshoot resulted in a nozzle exit pressure of approximately 2% higher than the maximum allowable pressure defined for the channel. Since the overshoot predictions were based on an analytical model, the transient operation was observed during the heat sink combustor prior to addressing any of the above alternatives. A pressure rise rate of 204 atm/sec was observed during the analysis.

3. CUTOFF ANALYSIS

The goal for cutoff was that the combustor be capable of initiating a restart between 2 and 10 sec after a cutoff signal, and that the chamber fuel flow rate be terminated prior to termination of the LO_2 flow rate. The first goal was met by selection of the valve closure times. The latter goal was assured by delaying the start of closing of the LO_2 valve and using injector purges.

TABLE D.3 TIME TO 90% CHAMBER PRESSURE
AS A FUNCTION OF VALVE OPENING TIME

Valve Opening Time, sec	.250	.500	.600	1.0
Start Time,* sec	0.45	0.60	0.70	0.98

Oxidizer Volume - 3300 cm^3

Fuel Volume - 1300 cm^3

* 90% of nominal combustor pressure; predefined fuel valve delay

TABLE D.4 MAXIMUM LO_2 AND FUEL VALVE INLET PRESSURES
VS VALVE CLOSING TIME *

	Maximum Valve Inlet Pressure - ATM			
Valve Closing Time, Sec	.25	.50	.75	1.0
LO_2	187	122	112	107
JP-4	125	100	98	95

* Based on Annin percentage plug characteristics with valve closure linear with time

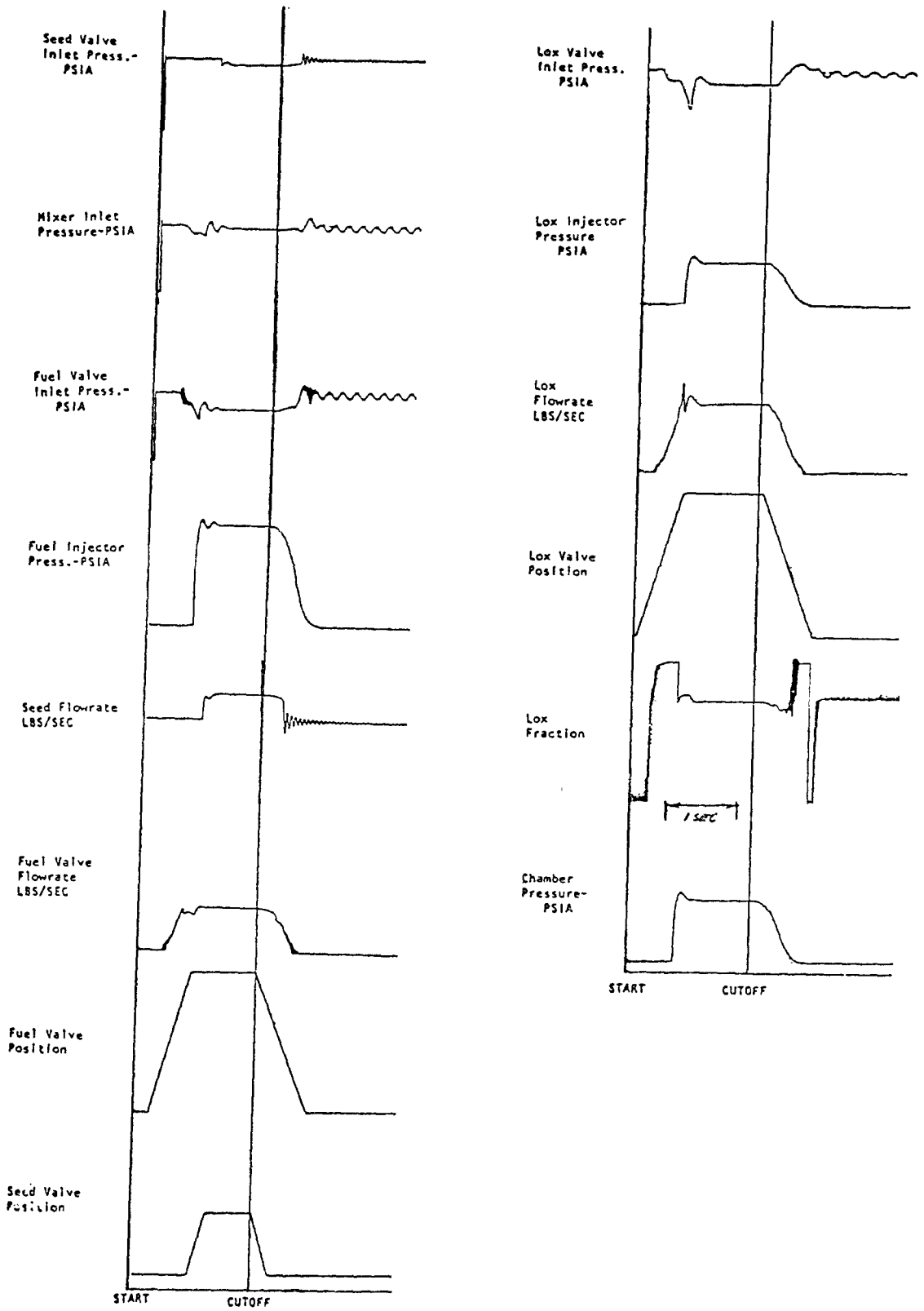

Figure D.3 Start and Cutoff for Nominal Test Flow Rate With 5% Seed Flow Rate.

In addition, predicted valve inlet pressure surge values were considered in arriving at valve closure times. Table D.4 lists the maximum predicted LO_2 and fuel valve inlet pressures as a function of valve closing time.

For initial testing, a closing time of 750 msec was used for the LO_2 and fuel valves. A seed valve closing time of 250 msec was used for these studies. Alternate times could be selected to avoid seed deposition at cutoff, if necessary. The predicted cutoff pressures and flow rates are shown in Figure D.3.

In addition to nominal LO_2 and fuel feed line lengths, the effect on cutoff surge pressures was predicted for 10% and 20% increase in line length. The pressures increased by 4-8%.

The complete cutoff sequence was: (1) the cutoff signal initiated closure of the fuel and seed valves at rates of 133%/sec and 400%/sec, respectively; and (2) after 50 msec, closure of the LO_2 valve was initiated at a rate of 133%/sec.

During the shutdown sequence the maximum surge pressures occurred upstream of the main valve. These pressures listed below were felt by the shutoff valves and adjacent line but were not detected downstream of the valve or in the supply tank.

		ΔP_{surge}
LO_2 Valve	-	22 atm
JP-4 Valve	-	13 atm
Seed Solution Valve	-	10.2 atm (upstream) 13 atm (downstream)

These values should be added to the tank pressure to obtain the actual surge pressure.

APPENDIX E

NOZZLE DESIGN FOR IMPROVED FLOW FIELD UNIFORMITY

1. INTRODUCTION

A source flow nozzle computer code was developed and used to design contours which yielded a non-parallel, uniform flow field for specified exit angle. These contours were analyzed by use of a second, existing, computer code to obtain profiles of exit flow properties.

2. DISCUSSION

For typical rocket nozzles, the properties of a uniform flow field were calculated by a computer program for a specified exit area ratio. The nozzles generated using this method were then truncated at the required exit angle. The result was a nozzle with uniform flow (no gradients) in the center region at the exit as shown in Figure E.1. However, depending on the degree of truncation, gradients existed in the outer regions. Also, as shown in Figure E.1, the region influenced by the truncated wall increased with the distance downstream. Since for MHD applications these nozzle contours produced an unacceptably large variation in exit gas uniformity, an improved nozzle contour design was developed. The approach used is described in the following sections.

The Rocketdyne nozzle design computer program was modified to determine a wall shape which generated source flow at the nozzle exit. This was accomplished by inputting a line which represented the desired source flow in place of the parallel, uniform flow-line calculated by the program. The remainder of the computer program was unchanged and was used to generate the wall which yielded the specified exit source flow as shown in Figure E.2.

For this nozzle, no gradients existed along the cylindrical surface (E-C) of the flow. When the nozzle divergency angle, θ, was small (3-6 deg), the radius, R, was large, and the maximum gradients between the cylindrical surface (E-C) and plane surface (E-D) were very low.

Nozzles were designed to obtain a uniform Mach number along a circular arc EC with the flow gradually varying from a specified fixed value at the wall point E to 0 deg at the centerline point C. In this two-dimensional source flow, EB described a left Mach line. The flow conditions along this left-line were completely defined by requiring the Mach number at E to be 1.9,

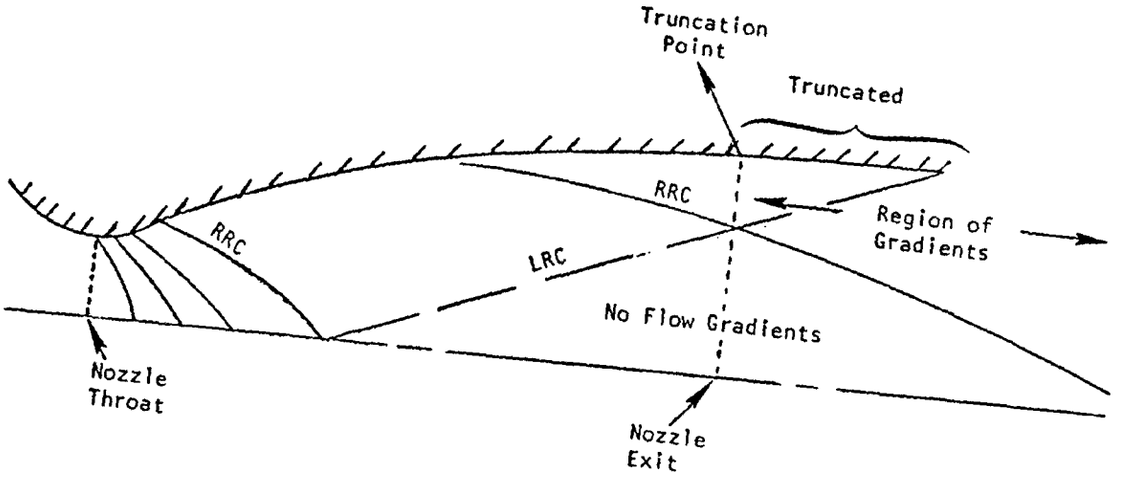

Figure E.1 Truncated Ideal Bell Flow Field.

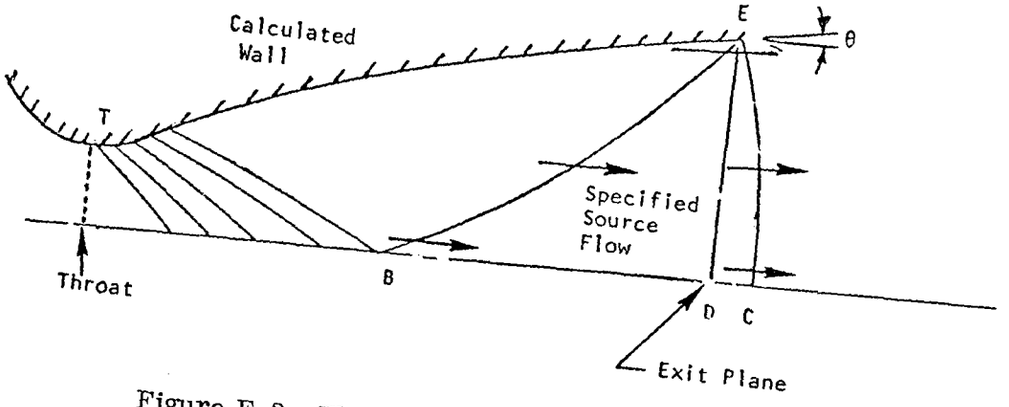

Figure E.2 Flow Field: Source Flow Nozzle.

and the choice of source type flow along BE. From the flow analysis in the throat region, a suitable right Mach line (TB) was found which matched the Mach number at B obtained from the source flow line EB. By constructing the right and left Mach lines in the region TBE and satisfying mass flow continuity, the wall contour between T and E was easily constructed. Thus, the nozzle wall contour gave source type (radial) flow along EC.

As a check to the new calculation procedures, the nozzles were analyzed using the Rocketdyne Nozzle Analysis Program. This computer program was used to determine the nozzle flow field for a specified wall geometry and has been shown to accurately predict experimental results. The results showed very uniform flow properties at the nozzle exit.

APPENDIX F

INJECTOR TEST FAILURE DESCRIPTION

1. INTRODUCTION

A detonation occurred while testing the MHD combustor assembly at the Rocketdyne Bravo 1B test facility on 24 June 1977. The resulting overpressure ruptured the oxidizer dome and severely distorted the injector face.

The injector failed because of an oxidizer dome detonation that occurred about 230 msec after the cutoff signal was given. The pressure, temperature and accelerometer data showed that the oxidizer dome detonation was because of an inter reactant leak. Post test analysis of the injector showed an unreported vendor machining error in one of the JP-4 cross passages near the face of the injector. Specifically, the following problems were determined to exist at the time of detonation:

a) An end cross-feed passage was drilled oversize causing thin walls and/or breakthroughs to exits at the oxidizer passages.

b) Repair was attempted by inserting copper rods (three separate pieces were used) into the oversize hole and redrilling to the specified diameter.

c) The new hole was eccentric and broke through the rods.

d) Fuel communicated with the oversize hole at three locations: (1) at the center where two rods did not seal against each other; (2) at the intersections of the two inlet holes with the cross-feed passage; and (3) along the axis of the cross-feed passage where the hole broke through the rods.

This error resulted in a leak capable of permitting more than enough JP-4 to flow into the oxidizer dome during the 230 msec prior to detonation that JP-4 injection pressure was higher than LO_2 and produce the type of detonation that occurred. Although the ignition source has not been defined, a spontaneous ignition of the LO_2/JP-4 mixture was the probable cause.

2. RECOMMENDATIONS

The results of the incident investigation review panel recommended that the following actions be accomplished.

a. Hardware Design/Fabrication

1) Review the injector design for design changes that enhanced quality of the part and/or ability to accomplish required proof and leak tests.

2) Review the fabrication sequence of the injector and impose quality source inspection requirements following critical operations.

3) Develop a new proof pressure and leak test plan to ensure the structural integrity of the injector internal passages and completed assembly.

b. Test

1) Implement a failsafe feature on the ASI ignition detect and the oxidizer injection pressure continue signals which would cause the automatic sequence to go into cutoff if the signals were picked up before they should be present.

2) Review, again, the complete automatic sequence to assure that failsafe provisions were sufficient and functionally adequate.

3) Develop a new plan for hardware blowdowns which would provide a check of the full-up automatic sequencing system and provide system priming pressure and temperature transient data.

The hardware design/fabrication items were completed and the replacement injector fabricated. The test items were completed, and the test program was completed.

APPENDIX G

DATA ANALYSIS DESCRIPTION

The data reduction procedure for performance evaluation of the high power MHD LO_2/JP-4 combustor was very similar to the approach which would be utilized with an equivalent rocket engine. The basic measure of combustion efficiency of any rocket engine system was the characteristic velocity (C*). This computation was based on chamber pressure, reactant mass flow, and nozzle throat area. The number was expressed as a velocity, primarily because of the dimensional residue of the calculation, since C* does not reflect any physical relationship. If gas species were assumed to be representative of the combustion chemistry, C* was most directly a reflection of the gas temperature. With constant gas properties C* was proportional to the square root of the combustion product stagnation temperature.

All of the parameters which went into the experimental and theoretical C* expressions were subject to various corrections to compensate for the physical processes involved with real combustion and data acquisition. The value was computed as defined below:

$$C^* = \frac{P_c A_t}{\dot{m}_t}$$

where

P_c = Nozzle stagnation pressure

A_t = Nozzle throat area

$\dot{m}_t$ = Total reactant flow rate

1. CHAMBER PRESSURE

The chamber pressure measurements for these test series were taken at various axial stations along the combustor/nozzle length. Only two of these measurements were corrected for use in the data reduction process. The pressure desired was the nozzle entrance station total pressure; however, practical considerations make the direct determination of this pressure impractical. Consequently, other pressures were measured and corrected to

infer this value. In this program two pressures were used in the performance computation, the wall tap nearest the injector face, Pc_1, and a wall tap near the start of contraction just upstream of the combustion chamber throat, Pc_4. The pressure at the "start of contraction" required the smallest amount of correction. Thus, this pressure was used as the most authoritative of the chamber pressure measurements for data reduction. Correction to this pressure was limited to primarily a "static to total" correction for the total gas velocity at that point. The "injector end" pressure was assumed to be a total pressure, but required correction for injector momentum and pressure loss through the combustion process.

The injector end pressure measurement, Pc_1, was measured from a pressure tap mounted in the combustion chamber wall, roughly 2.5 cm downstream of the injector face. The usual "injector end" pressure corrections were applied to this measurement - these being the injector momentum correction, and the combustion pressure loss correction. The total momentum of the injected reactants was assumed to act on the chamber cross section area downstream of the pressure tap. As a result, this pressure was added to the measured pressure value (about 1.4 percent of the measured pressure). The second correction was the "Rayleigh" pressure loss[48] for heat addition in duct flow. This was a function of the chamber contraction ratio and the gamma of the combustion gases. This provided a reduction in the predicted nozzle station stagnation pressure of nearly 6% for this combustor. The gas velocity at the injector face was essentially zero. Consequently, this measured pressure was assumed to be a total pressure, and no static to total correction was made on this measurement.

Chamber pressure number four, Pc_4, was measured at a wall static pressure tap about 48 cm from the injector face, just upstream of the start of throat convergence. Since only a "total to static" pressure correction was required to compute nozzle stagnation pressure, this was very nearly the optimum location for measurement of the C* performance. This "total to static" pressure correction was based on the contraction ratio from the chamber to throat area, and the gamma of the combustion gases. This correction for a typical test slice resulted in a computed nozzle stagnation pressure roughly 7% higher than the measured wall static pressure. Other wall pressure taps upstream of Pc_4, such as Pc_3 and Pc_2, evidenced slightly higher pressure levels. This indicated a continuing temperature rise of the combustion gases, and probably some pressure loss from flow effects. A typical axial pressure distribution during test is shown in Figure G.1.

48 A. H. Shapiro, "The Dynamics and Thermodynamics of Compressible Fluid Flow", Book, Volume I, 1953, Ronald Press.

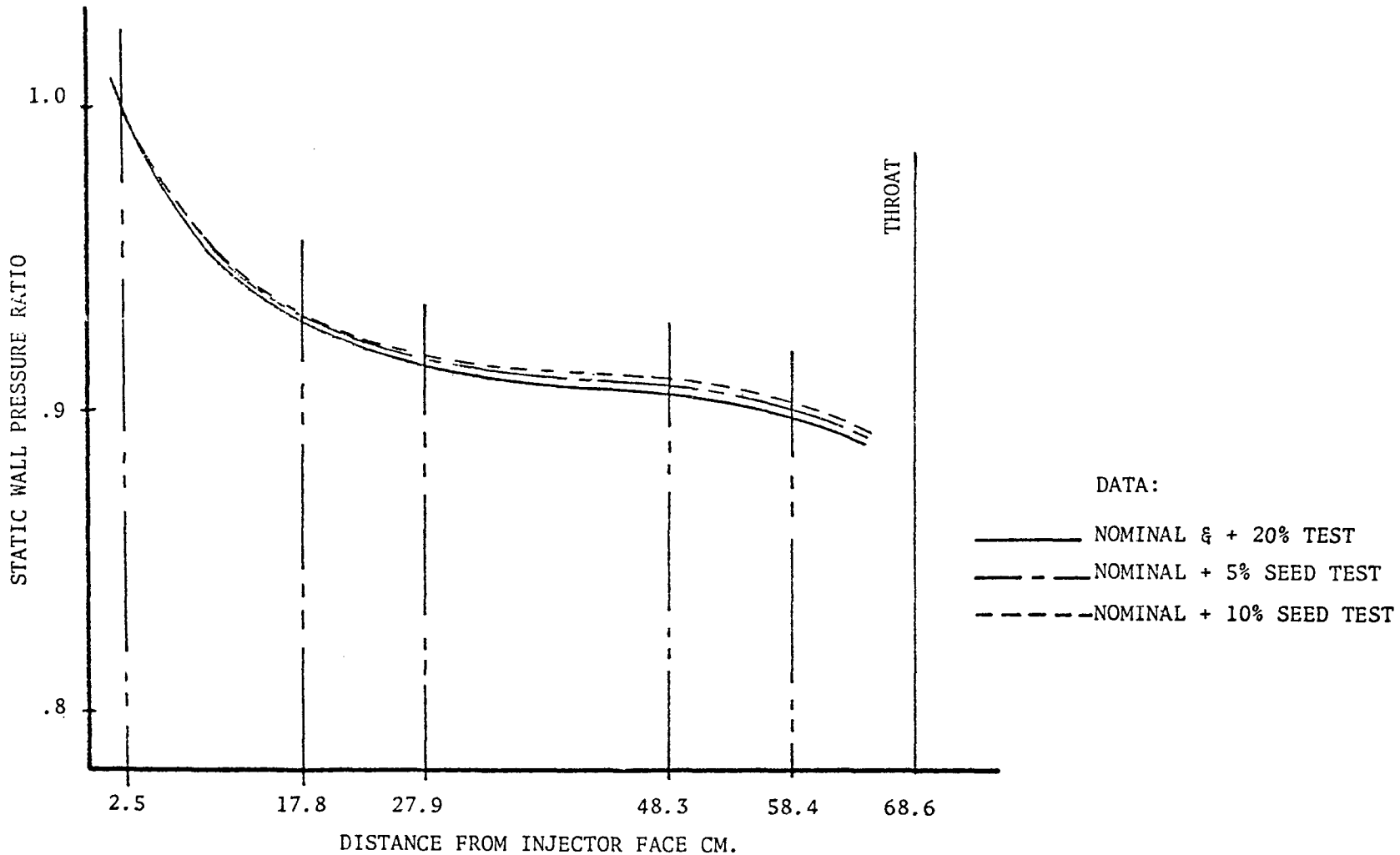

Figure G.1 Combustor Static Pressure Profile.

When both Pc_1 and Pc_4 were corrected to nozzle stagnation values, there appeared to be a fairly consistent bias between the two results. The Pc_1 derived value was approximately 1.0 to 1.5% lower than the reading computed from Pc_4. This level of discrepancy was rather low, but the consistency of the difference indicated that something other than random error was involved. The Pc_4 measurement was the most reliable place to accurately assess combustor performance, and the Pc_3 value, just upstream of the combustor wall, basically verified the higher values reflected by Pc_4. The probable reason for the lower corrected values from Pc_1 was the fact that this tap was actually 2.5 cm downstream from the injector face, and significant gas velocity already existed at this point. This would result in this port measuring a static pressure component rather than the total pressure assumed in making the correction. Low contraction ratio combustors make precise determination of combustion efficiency more difficult, but the values determined from Pc_4 should reflect a good assessment of actual combustion performance.

Reactant mass flow was established by the use of the calibrated cavitating venturis. This technique provided flow control as well as accurate flow determination. Standardized flow computation techniques were used for the room temperature liquids (JP-4 and seed solution), and specialized Rocketdyne developed techniques were used for the liquid oxygen flow measurement. Physical size corrections were applied to the venturi throat to account for thermal effects, and a modified enthalpy relationship[49] was used to establish cavitating flow rates under the various liquid oxygen flow conditions.

The heat rejected to the combustion chamber walls, upstream of the throat section, represented a loss to the computed C* which would not be experienced with a regenerative flight weight chamber. With a regenerative chamber this heat would be added to the fuel prior to injection into the combustion chamber, and would thus be added to the heat released by the reaction. To correct for this effect in the test data, the heat loss to the combustor walls was computed (2.1 MW), and the effect of adding this heat to the combustion products was computed. The actual computation related this heat loss to the total heating value of the fuel flow rate. Typically this correction resulted in roughly a .2 to .3% increase in the computed C* for the heat sink combustor. This correction would not be required if a regeneratively cooled combustor was used.

---

[49] "Thermophysical Properties of Oxygen from the Freezing Liquid Line to 600R for Pressures to 5000 psia," NBS Technical Note 384, issued July, 1971.

The nozzle throat area used for performance computation was corrected from the static geometric area for several effects. The most common correction was for the flow coefficient, to correct for dynamic velocity (vena contracta) and frictional flow restriction. Thermal expansion was another item of significance although in this case the phenomena was really thermal contraction. This was caused by the inner wall nozzle expansion with the cold bulk of the outer wall restraining this expansion, resulting in an inward expansion of the nozzle surface. A permanent change was involved in this expansion since the surface of the throat exceeded the yield stress during the thermal cycle. This effect was known as "thermal ratcheting", and the total change in throat area in this program was approximately 1.7% reduction from the pretest area. A correction was applied during the slice, which uses the temperatures of the throat section, to predict the thermal contraction during the test. This correction was very small - roughly one quarter percent.

The theoretical C*, against which the experimental C* values were compared, was the result of a JANNAF one-dimensional equilibrium computation for the reactants and operating conditions of this test setup. The basic ranges of operating conditions have been computed to establish the family of curves (Figure G.2), and the tabular values have been inputted into an interpolation computer routine for computation of specific points.[50] The effects of mixture ratio, seed flow rate, and chamber pressure were included in these tables.

Table G.1 presents the equations and constants used for the performance calculations and the information required during each test to support the MHD test effort. All the information/equations contained herein were programmed and used to establish the data printed out on the data printout summary sheets. The constants required were supplied where applicable.

A typical data printout is shown in Table G.2 indicating the format that the data are presented by the data reduction program (with all the correlations previously mentioned). Each "slice" is presented on three pages, the first page referencing pretest and fixed data. Page two is the primary performance presentation and most items are self explanatory. The operating conditions presents such items as computed reactant flow rates and densities, while the combustor performance column provides most of the corrected data. These items consist of:

Mixture Ratio - Ratio of oxygen weight flow to fuel (plus SPAN-80 but exclusive of seed solution).

Seed Solution Ratio - Seed solution (cesium carbonate and water), fraction of total input flow rate.

[50] "ICRPG ODE Equilibrium Reference Program, A Computer Program for the Calculation of Chemical Equilibrium Compositions with Applications." ICRPG Performance Standardization Working Group, July 1968.

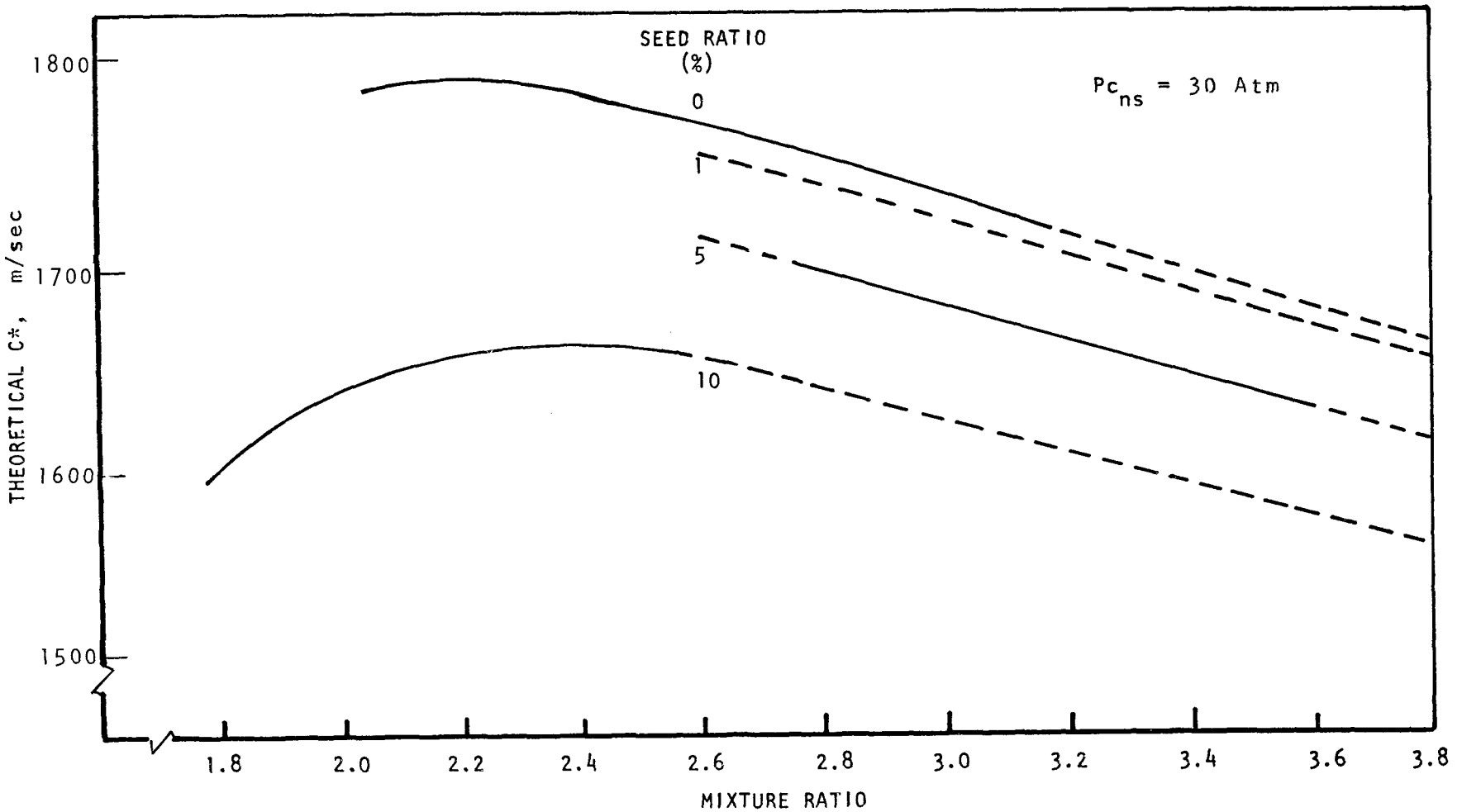

Figure G.2 Gas Generator Theoretical Characteristic Velocity, 7% SPAN-80.

TABLE G.1 30 MW MHD DATA REDUCTION

OPERATING CONDITIONS

1. Combustor Mixture Ratio (O/F) = $\dot{m}_{LO_2}/\dot{m}$ (JP-4 + SPAN-80)
2. Combustor Pressure (Pc_1) = Pc_1 + Pa
3. Combustor Pressure (Pc_4) = Pc_4 + Pa
4. Seed Solution Ratio = $\dot{m}$ (Seed Solution) /$\dot{m}$ (Total)
5. Seed Ratio = 0.723 x Seed Solution Ratio
6. Total Combustor Flow Rate = $\dot{m}$ (Seed Solution) + $\dot{m}$ (LO_2) + $\dot{m}$ (JP-4 + SPAN-80)
7. Throat Area (i) $AC_D\left\{1 - 10 \times 10^{-6}\left[\left(\frac{T_7\,(i) + T_8\,(i)}{2}\right) - 294\right]\right\}[cm^2]$

where

C_D = .9975

A = measured throat area cm^2

T = K

i = time slice

8. Nozzle Stagnation Pressure (1) = A (Pc_1 + Pa)
9. Nozzle Stagnation Pressure (4) = B (Pc_4 + Pa)

where

A = Injector Momentum and Rayleigh Loss Correction

B = Total/Static Pressure Ratio Correction

COMBUSTOR PERFORMANCE

1. Characteristic Velocity (theoretical) = Interpolation using nozzle stagnation pressure, combustor mixture ratio and seed ratio
2. Characteristic Velocity (meas #1) = $\frac{P\ (\text{Noz Stag 1})\ A_T}{\dot{m}\ (\text{total})}$
3. Characteristic Velocity (meas #4) = $\frac{P\ (\text{Noz Stag 4})\ A_T}{\dot{m}\ (\text{total})}$
4. $\eta_{C_1}{}^*$ = C* (meas #1)/C* (theo #1)
5. $\eta_{C_4}{}^*$ = C* (meas #4)/C* (theo #4)

TABLE G.1 30 MW MHD DATA REDUCTION (CONT'D)

ASI OPERATING CONDITIONS

1. ASI #1 Flow Rate = $\dot{m}$ (ASI_1, GO_2) + $\dot{m}$ (ASI_1, CH_4)
2. ASI #1 Mixture Ratio (O/F) = $\dot{m}$ (ASI_1, GO_2) / $\dot{m}$ (ASI_1, CH_4)
3. ASI #1 Temperature = Interpolation
4. ASI #2 Flow Rate = $\dot{m}$ (ASI_2, GO_2) + $\dot{m}$ (ASI_2, CH_4)
5. ASI #2 Mixture Ratio (O/F) = $\dot{m}$ ASI_2, GO_2/$\dot{m}$ (ASI_2, CH_4)

COMBUSTOR THERMAL CHARACTERISTICS

1. Nozzle Stagnation Temperature (theo) = Interpolation
2. Combustor Meter Heat Flux (j) * $= \left(\frac{\dot{m}C_p}{A}\right)_j * \left(\frac{\Delta T_j}{\Delta t}\right)$

   $\left(\frac{\dot{m}C_p}{A}\right)_j$ = constant for each meter j

   $\frac{\Delta T_j}{\Delta t} = \frac{T_j(t_{i+1}) - T_j(t_i)}{t_{i+1} - t_1}$

   i = time slice

   j = heat flux meter 1 through 11
3. Throat Coolant Heat Loss = $k\{\dot{m}$ (comb. cooling)$\}\{\Delta T$ (comb. throat)$\}$

   k = (constant fraction of $\dot{m}$ through throat)(C_p)
4. Nozzle Exit Coolant Heat Loss = h $\dot{m}$ (comb. coolant) ΔT (comb. noz #1)

   h = (fraction of $\dot{m}$ through coolant passage)(Cp)
5. Nozzle Exit Coolant Heat Loss = d $\dot{m}$ (comb. coolant) ΔT (comb. noz #2)

   d = (fraction if $\dot{m}$ through coolant passage)(Cp)
6. Combustor Zone Heat Loss = comb. meter heat flux (j) x zone area
   zone area = constant (j)(T_1 through T_6)
7. Throat Zone Heat Loss = Throat Coolant Heat Loss +

   $(CMHF_7)(ZA_7) + (CMGH_8)(ZA_8) + (CMHF_9)(ZA_9)$**

TABLE G.1 30 MW MHD DATA REDUCTION (CONT'D)

8. Throat Zone Heat Flux = Throat zone heat loss/zone area (Zone Area = ZA7 +ZA8 +ZA9 + throat)

9. Nozzle Exit Zone Heat Loss = Nozzle exit coolant heat loss #1 + #2 $+(CMHF_{10})(ZA_{10})$ $+(CMHF_{11})(ZA_{11})$

10. Nozzle Exit Zone Heat Flux = $\frac{\text{Nozzle Exit Zone Heat Loss}}{\text{ZA10 + ZA11 + EXIT 1 + EXIT 2}}$

11. Combustor Heat Loss (total) = (Combustor zone heat loss + throat zone heat loss + nozzle exit zone heat loss)

* Used for digital data reduction only.

** CMHF = Combustor Meter Heat Flux and ZA = Zone Area

CHANNEL THERMAL CHARACTERISTICS

1. Frame Heat Load (j) = B (j) $\dot{m}$ (channel cooling) ΔT (channel cool j)

   j = 1, 6; B = (Fraction of $\dot{m}$ through an individual frame)(Cp)

2. Total channel heat load = $\dot{m}$ Cp (channel cooling) ΔT (chan H_2O cool)

PRESSURE DROP/TEMPERATURES

Feed System

1. ΔP (LO_2 Injector) = P (LO_2 Injection) - P (Combustor 1)
2. ΔP (LO_2 System) = P (LO_2 Tank) - P (LO_2 Injection)
3. ΔP (LO_2 Valve) = P(LO_2 Main Valve) - P (LO_2 Injection)
4. T (LO_2 Injection) =
5. ΔP (JP-4 Injection) = P (JP-4 Injection) - P (Combustor 1)
6. ΔP (JP-4 System) = P (JP-4 Tank) - P (JP-4 Injection)
7. ΔP (JP-4 Valve) = P (JP-4 Main Valve) - P (JP-4 Injection)
8. T (JP-4 Injection) =
9. ΔP (JP-4 Mixer) = P (JP-4 Mixer Inlet) - P (JP-4 Main Valve)
10. ΔP (Seed System) = P (Seed Tank) - P (JP-4 Injection)
11. ΔP (Seed Mixing/Valve) = P (Seed Valve) - P (JP-4 Main Valve)
12. T (Seed Solution) =

TABLE G.1 30 MW MHD DATA REDUCTION (CONT'D)

Combustor Cooling

1. ΔP (Combustor H_2O System) = P (H_2O Tank) - P (Comb H_2O Inlet)
2. ΔP (Combustor H_2O Cooling) = P (Comb H_2O Inlet) - P (Comb H_2O Exit)
3. ΔT (Combustor Throat) = T (Comb H_2O Inlet) - T (Throat H_2O Exit)
4. ΔT (Combustor Nozzle Exit) = T (Comb H_2O Inlet) - T (Noz H_2O Exit #1)
5. ΔT (Combustor Nozzle Exit) = T (Comb H_2O Inlet) - T (Noz H_2O Exit #2)

Channel Cooling

1. ΔP (Chan H_2O System) = P (H_2O Tank) - P (Chan H_2O Inlet)
2. ΔP (Chan H_2O Cooling) = P (Chan H_2O Inlet) - P (Chan H_2O Exit)
3. ΔT (Chan H_2O Cooling) = T (Chan H_2O Exit) - T (Chan H_2O Inlet)
4. ΔTj (Chan Cool j) (6 req'd) = T (Chan H_2O Exit j) - T (Chan H_2O Inlet)

ASI

1. ΔP (ASI Fuel 1) = P (ASI Fuel Injector 1) - P (ASI 1 Combustor)
2. ΔP (ASI Fuel 2) = P (ASI Fuel Injector 2) - P (ASI 2 Combustor)
3. ΔP (ASI Oxid 1) = P (ASI Oxid Injector 1) - P (ASI 1 Combustor)
4. ΔP (ASI Oxid 2) = P (ASI Oxid Injector 2) - P (ASI 2 Combustor)

Gas Flow Static Pressure Ratios

1. $PR(j) = \dfrac{\text{Wall Pressure (j)}}{\text{Wall Pressure (1)}}$

$j = 1$ thru 16

TABLE G.1 30 MW MHD DATA REDUCTION (CONT'D)

HEAT FLUX METER $\frac{\dot{m}Cp}{A}$ CONSTANTS

Thermocouple	$\frac{\dot{m}Cp}{A}$	$\frac{w}{K\ cm^2}$	Zone Area, cm^2
1	.03061	9.0072	447.4
2	.03061	9.007	536.9
3	.03061	9.007	626.4
4	.03061	9.007	715.9
5	.03061	9.007	706.9
6	.03061	9.007	796.4
7	.03826	11.259	223.8
8	.03826	11.259	223.8
9	.03826	11.259	223.8
10	.03061	2.780	474.2
11	.03061	2.780	403.2
Throat			452.1
Exit 1			211.1
Exit 2			260.1

TABLE G.2 DATA PRINTOUT

SLICE NO. 13 — 30 MEGAWATT MHD DATA REDUCTION — DECK 5R999-1 — PAGE 1

TEST NUMBER	632005.	SLICE TIME	15.259 SEC
TEST DATE	22478.	SLICE DURATION	108. MSEC
ENGINE S/N	20504.	TEST DURATION	2.800 SEC
		REDUCTION TIME	21.40
		REDUCTION DATE	03/14/78

* * * PRE-TEST DATA * * *

BAROMETRIC PRESSURE	IN HG	28.0550
CORRECTED BAROMETRIC PRESSURE	IN HG	28.0900
AMBIENT TEMPERATURE	F	63.0000
COMBUSTION CHAMBER THROAT AREA	IN2	25.4490
COMBUSTION CHAMBER C-SUB-D		0.9975
LOX VENTURI THROAT DIAMETER	IN	0.5827
JP4 VENTURI THROAT DIAMETER	IN	0.3345
SEED SOLUTION VENTURI THROAT DIA.	IN	0.2113
COMBUSTOR COOLANT VENTURI THROAT DIA.	IN	0.9000
CHANNEL COOLANT VENTURI THROAT DIA.	IN	0.0
LOX VENTURI C-SUB-D		0.9870
JP4 VENTURI C-SUB-D		0.9600
SEED SOLUTION VENTURI C-SUB-D		0.9600
COMBUSTOR COOLANT VENTURI C-SUB-D		0.7240
CHANNEL COOLANT VENTURI C-SUB-D		0.0
NO 1 ASI GOX VENTURI INLET DIA.	IN	0.1720
NO 2 ASI GOX VENTURI INLET DIA.	IN	0.1720
NO 1 ASI CH4 VENTURI INLET DIA.	IN	0.1720
NO 2 ASI CH4 VENTURI INLET DIA.	IN	0.1720
NO 1 ASI GOX VENTURI THROAT DIA.	IN	0.0700
NO 2 ASI GOX VENTURI THROAT DIA.	IN	0.0700
NO 1 ASI CH4 VENTURI THROAT DIA.	IN	0.0810
NO 2 ASI CH4 VENTURI THROAT DIA.	IN	0.0810
NO 1 ASI GOX VENTURI C-SUB-D		0.8300
NO 2 ASI GOX VENTURI C-SUB-D		0.8490
NO 1 ASI CH4 VENTURI C-SUB-D		0.8870
NO 2 ASI CH4 VENTURI C-SUB-D		0.8860
COMBUSTOR COOLANT FLOWMETER CONST.	CYC/GAL	0.0
CHANNEL COOLANT FLOWMETER CONST.	CYC/GAL	0.0

TABLE G.2 DATA PRINTOUT (CONT'D)

SLICE NO. 13 — 3C MEGAWATT MHD DATA REDUCTION — DECK 5R999-1 — PAGE 2

TEST NUMBER	032005.	SLICE TIME	15.259 SEC	REDUCTION TIME	21.40
TEST DATE	22478.	SLICE DURATION	108. MSEC	REDUCTION DATE	03/14/78
ENGINE S/N	20504.	TEST DURATION	2.800 SEC		

OPERATING CONDITIONS			COMBUSTOR PERFORMANCE		
AMBIENT PRESSURE	PSIA	13.798	MIXTURE RATIO	O/F	2.9794
LOX DENSITY	LB/FT3	70.866	SEED SOLUTION RATIO	C/F	0.1358
JP4 DENSITY	LB/FT3	48.421	SEED RATIO	O/F	0.0982
SEED SOLUTION DENSITY	LB/FT3	145.47	TOTAL FLOWRATE	LB/SEC	68.743
COMBUSTOR COOLANT DENSITY	LB/FT3	62.394	THROAT AREA	IN2	25.376
CHANNEL COOLANT DENSITY	LB/FT3	62.333	NC 1 INJECTOR END PRESSURE	PSIA	457.78
LOX FLOWRATE	LB/SEC	44.479			
JP4 FLOWRATE	LB/SEC	14.929	NC 1 NOZZLE STAG. PRESSURE	PSIA	438.19
SEED SOLUTION FLOWRATE	LB/SEC	9.335	NC 4 NOZZLE STAG. PRESSURE	PSIA	444.91
COMBUSTOR COOLANT FLOWRATE	LB/SEC	42.868	NC 1 THEORETICAL C-STAR	FT/SEC	5336.2
CHANNEL COOLANT FLOWRATE	LB/SEC	0.0	NC 4 THEORETICAL C-STAR	FT/SEC	5337.2
NC 1 ASI GOX FLOWRATE	LB/SEC	0.0400	NC 1 NOZZLE STAG. C-STAR	FT/SEC	5191.1
NC 2 ASI GOX FLOWRATE	LB/SEC	0.0409	NC 4 NOZZLE STAG. C-STAR	FT/SEC	5270.6
NC 1 ASI CH4 FLOWRATE	LB/SEC	0.0400	NC 1 C-STAR EFFICIENCY	%	97.281
NC 2 ASI CH4 FLOWRATE	LB/SEC	0.0399	NC 4 C-STAR EFFICIENCY	%	98.753

CHAMBER WALL STATIC PRESSURE RATIOS		ASI PERFORMANCE		
NC 1 / NO 1	1.0000	NC 1 MIXTURE RATIO	O/F	0.9995
NC 2 / NO 1	0.9335	NC 2 MIXTURE RATIO	O/F	1.0239
NO 3 / NO 1	0.9190	NC 1 NOZZLE STAG. PRESSURE	PSIA	461.92
NC 4 / NO 1	0.9110	NC 2 NOZZLE STAG. PRESSURE	PSIA	461.29
NO 5 / NO 1	0.9004	NC 1 TOTAL FLOWRATE	LB/SEC	0.0799
NO 6 / NO 1	0.0328	NC 2 TOTAL FLOWRATE	LB/SEC	0.0808
NO 7 / NO 1	0.8823	NC 1 COMBUSTION TEMPERATURE	F	1814.8
NC 8 / NO 1	0.2810	NC 2 COMBUSTION TEMPERATURE	F	1884.5
NC 9 / NO 1	0.4298			
NC 10 / NO 1	0.2338			
NO 11 / NO 1	0.2008	ASI INJECTOR PRESSURE DROPS		
NC 12 / NO 1	0.0434	NC 1 GOX	PSID	5.296
NC 13 / NO 1	0.0368	NC 2 GOX	PSID	3.719
NC 14 / NO 1	0.1299	NC 1 CH4	PSID	2.866
NC 15 / NO 1	0.0942	NC 2 CH4	PSID	2.859
NC 16 / NO 1	0.1178			

TABLE G.2 DATA PRINTOUT (CONT'D)

SLICE NO. 13 — 20 MEGAWATT MHD DATA REDUCTION — DECK 5R999-1 — PAGE 3

TEST NUMBER	632005.	SLICE TIME	15.259 SEC	REDUCTION TIME	21.40
TEST DATE	22478.	SLICE DURATION	108. MSEC	REDUCTION DATE	03/14/78
ENGINE S/N	20504.	TEST DURATION	2.800 SEC		

MAIN FEED SYSTEM		
LOX INJECTOR DELTA PR	PSID	215.20
LOX SYSTEM DELTA PR	PSID	129.83
LOX VALVE DELTA PR	PSID	33.25
LOX INJECTOR TEMP	F	-267.39
JP4 INJECTOR DELTA PR	PSID	313.50
JP4 SYSTEM DELTA PR	PSID	49.31
JP4 VALVE DELTA PR	PSID	16.14
JP4 MIXER DELTA PR	PSID	121.72
JP4 INJECTOR TEMP	F	68.64
SEED SYSTEM DELTA PR	PSID	18.33
SEED MIXING VALVE DELTA PR	PSID	20.40
SEED SOLUTION TEMP	F	66.20
COMBUSTOR COOLING SYSTEM		
SYSTEM DELTA PR	PSID	51.85
COOLING DELTA PR	PSID	490.63
THROAT DELTA TEMP	F	15.86
NO 1 NOZZLE EXIT DELTA TEMP	F	11.22
NO 2 NOZZLE EXIT DELTA TEMP	F	10.24
CHANNEL COOLING SYSTEM		
SYSTEM DELTA PR	PSID	853.20
COOLING DELTA PR	PSID	-62.12
COOLING DELTA TEMP	F	73.32
NO 1 COOLING DELTA TEMP	F	-527.59
NO 2 COOLING DELTA TEMP	F	-528.15
NO 3 COOLING DELTA TEMP	F	73.32
NO 4 COOLING DELTA TEMP	F	73.34
NO 5 COOLING DELTA TEMP	F	73.32
NO 6 COOLING DELTA TEMP	F	-528.18

COMBUSTOR THERMAL CHARACTERISTICS		
NO 1 COMB METER HEAT FLUX	BTU/SEC/IN2	0.301
NO 2 COMB METER HEAT FLUX	BTU/SEC/IN2	0.602
NO 3 COMB METER HEAT FLUX	BTU/SEC/IN2	2.289
NO 4 COMB METER HEAT FLUX	BTU/SEC/IN2	3.178
NO 5 COMB METER HEAT FLUX	BTU/SEC/IN2	3.587
NO 6 COMB METER HEAT FLUX	BTU/SEC/IN2	3.844
NO 7 COMB METER HEAT FLUX	BTU/SEC/IN2	2.753
NO 8 COMB METER HEAT FLUX	BTU/SEC/IN2	0.209
NO 9 COMB METER HEAT FLUX	BTU/SEC/IN2	2.562
NO 10 COMB METER HEAT FLUX	BTU/SEC/IN2	3.212
NO 11 COMB METER HEAT FLUX	BTU/SEC/IN2	2.874
THROAT COOLANT HEAT LOSS	BTU/SEC	284.839
NO 1 NOZ EXIT COOL HEAT LOSS	BTU/SEC	123.175
NO 2 NOZ EXIT COOL HEAT LOSS	BTU/SEC	142.625
COMBUSTOR ZONE HEAT LOSS	BTU/SEC	1513.501
THROAT ZONE HEAT LOSS	BTU/SEC	476.440
THROAT ZONE HEAT FLUX	BTU/SEC/IN2	2.736
NOZ EXIT ZONE HEAT LOSS	BTU/SEC	681.461
NOZ EXIT ZONE HEAT FLUX	BTU/SEC/IN2	3.913
TOTAL COMBUSTOR HEAT LOSS	BTU/SEC	2671.402
NOZZLE STAGNATION TEMP NO 1	F	5737.6
NOZZLE STAGNATION TEMP NO 4	F	5741.5

CHANNEL THERMAL CHARACTERISTICS		
NO 1 FRAME HEAT LOAD	BTU/SEC	0.0
NO 2 FRAME HEAT LOAD	BTU/SEC	0.0
NO 3 FRAME HEAT LOAD	BTU/SEC	0.0
TOTAL CHANNEL HEAT LOAD	BTU/SEC	0.0

Seed Ratio	-	Cesium carbonate fraction of total input flow rate.
Total Flow Rate	-	Total of reactant and non-reactant input flow rate.
Throat Area	-	Corrected throat area during hot fire.
No. 1 Injector End Pressure	-	Measured value at Pc_1 position - corrected only from gage pressure to absolute pressure.
No. 1 Nozzle Stagnation Pressure	-	The corrected, computed value of nozzle stagnation pressure, based on measurements at the Pc_1 location with injector momentum, and Raleigh loss corrections.
No. 4 Nozzle Stagnation Pressure	-	The corrected, computed value for nozzle stagnation pressure based on the Pc_4 measurement corrected for total static pressure relationships.
No. 1 and No. 4 Theoretical C*	-	The theoretical value of C* based on mixture ratio, chamber pressure, and seed solution dilution (the difference is due to chamber pressure differences).
No. 1 and No. 4 Nozzle Stagnation C*	-	The computed and corrected value of demonstrated C* based on the chamber pressure determinations at the Pc_1 and Pc_4 measurement points.
No. 1 and No. 4 C* Efficiency	-	The efficiency value represented by the two previous values.

The chamber wall static pressure ratio values were basically just the measured pressure at each of the listed pressure taps as a function of the value measured at the Pc_1 position. These taps reflected the expansion in the nozzle as well as the pressure progression along the combustor length. The ASI performance values were basically without meaning during an actual data slice, since they represented "locked up" pressure data. The ASI flow rate during mainstage operation was limited to roughly 50 g/sec GN_2 purge flow.

Page three of the printout was primarily concerned with system parameters and heat flux data discussed elsewhere The important value from the performance standpoint on this page was the "combustor zone heat loss and the throat zone heat loss" which were the values used for the performance heat loss correction. This represented the total heat rejection rate for the combustor wall from the injector face to the nozzle throat area.

The nozzle stagnation temperature values shown for Pc_1 and Pc_4 were the theoretical values for the mixture ratio, chamber pressure, and seed solution dilutions. Actual delivered nozzle stagnation temperatures were somewhat lower as a result of combustion efficiency and heat losses.

2. DATA REDUCTION - HIGH FREQUENCY

During the 30 MW MHD combustor program test data was recorded on magnetic FM tape. Three types of data reduction were employed to characterize the existing pressure oscillations in the MHD combustor: (1) "Statos" or expanded pressure-time traces; (2) RMS Power Spectral Density (PSD) plots, and (3) "AMS" or amplitude mean square-time traces.

The "Statos" or expanded pressure-time traces were commonly AC coupled to enable optimum determination of the oscillatory pressure as a function of time. (AMS records were also AC coupled.) Predominant oscillation frequencies were visually observed on the pressure-time trace and their frequency calculated.

The PSD plots consisted of a graphical relationship between a form of power, i.e., psi^2/Hz and the frequency in Hz. Predominant oscillation frequencies were easily identified in the PSD plots.

The AMS record was essentially an integration under the PSD curve between two frequency bounds as a function of time. Predominant oscillation frequencies were not identified using this form of data reduction.

Rocket engines that exhibit "combustion stability" were defined as having no sustained chamber pressure oscillations whose peak-to-peak amplitudes were greater than 10% of the mean combustion chamber pressure. When the amplitude of pressure oscillations occurring during "stable" combustion was desired, the amplitude of the instrument/recorder system noise itself must be taken into account since this contribution may be considerable percent of the total signal. Such system noise was commonly determined after the tape recorder has been turned on and chamber wall coolant flowing, if applicable, and immediately prior to injector reactant flow. Accounting for such system noise was most easily accomplished using the AMS data reduction record but can usually be accomplished without too much difficulty using the Statos expanded pressure-time traces. An additional PSD plot made over a pre-run noise time span would be required to "correct" the PSD plot made over a mainstage combustion time span if an accurate quantitative frequency distribution of oscillation amplitudes was desired.

APPENDIX H

PLANNED FABRICATION PROCESS - DETAILED TASKS

The planned fabrication process detailed tasks are shown in Table H.1 of this appendix. These details cover the detailed fabrication steps from the beginning of the electrode frame component manufacture through the case winding and finishing operations. Also included in the table are the final check out tests on the assembled channel.

TABLE H.1 PLANNED FABRICATION PROCESS/DETAILED TASKS

STEP 1 - FABRICATE ASSEMBLY MANDREL

Tasks:

1. Procure material.
2. Fabricate component parts.
3. Assembly components.
4. Finalize exact outer surface contours.
5. Scribe lines on surfaces to position electrode frames.
6. Apply release coat to surfaces.

STEP 2 - FABRICATE ELECTRODE FRAME COMPONENTS (Including Entrance and Exit Flanges)

1. Machine corner blocks.
2. Fabricate rail subassemblies.
   a. Machine copper rails.
   b. Fabricate Inconel screens.
   c. Braze screens into rails.
   d. Trim screen height even with rail.
3. Machine tube spacer blocks.
4. Fabricate frame anchors.
5. Fabricate pressure taps.
6. Fabricate current taps.
7. Fabricate entrance flange.
8. Fabricate exit flange components.

STEP 3 - ASSEMBLE ELECTRODE FRAME COMPONENTS

Tasks: (For each frame assembly)

1. Position frame corner blocks on mandrel.
2. Trim rail lengths to fit between corner blocks.
3. Tack weld rails to corner blocks.
4. Remove from mandrel and finish braze corner joints.
5. Braze tube spacer blocks to frame.
6. Assembly pressure taps to spacer blocks.
7. Reposition frame on mandrel.
8. Pre-form contoured cooling tubes.
9. Fit cooling tubes to frame.
10. Tack braze tubes to frames.
11. Remove from mandrel and finish braze tubes to frame. Attach frame anchors.

TABLE H.1 PLANNED FABRICATION PROCESS/DETAILED TASKS (CONT'D)

STEP 4 - CHECK OUT FRAME ASSEMBLIES

1. Inspect frame assemblies.
   a. Verify dimensions.
   b. Verify design conformance.
   c. Verify part identification numbers.
2. Check out cooling tubes.
   a. Pressure-leak test each tube.
   b. Run water flow tests each tube.
      (1) Verify pressure drops vs flow rate.
   c. Verify tube to frame braze joint integrity.

STEP 5 - FABRICATE ELECTRODE FRAME ARRAY ON MANDREL (Includes Entrance & Exit Flanges)

Tasks:

1. Dry assemble frames on mandrel.
   a. Verify scribe lines on mandrel surface.
   b. Place exit flange on mandrel.
   c. Inspect fit of flange to mandrel.
   d. Place next electrode frame on mandrel.
   e. Inspect electrode frame geometry:
      (1) Gap between frame and surface of mandrel,
      (2) Spacing between adjacent electrode,
      (3) Angle of inclination between the sides of the frame and the channel axis,
      (4) Perpendicular angle between frame cross rails and the channel axis,
      (5) Relation between frame actual position and the true position established by the mandrel surface scribe lines.
   f. Repeat steps d and e until all frames are placed on mandrel.
   g. Place entrance flange on mandrel.
   h. Inspect fit of flange to mandrel and to adjacent electrode.
2. Inspect frame dry assembly.
   a. Check the location of all cooling tube connections, electrode frame anchors, pressure taps, current taps, flange bolt holes, etc., to verify conformance to design and to prevent any interference of adjacent components with each other.

TABLE H.1 PLANNED FABRICATION PROCESS/DETAILED TASKS (CONT'D)

b. Check the height above the frame external surfaces for all projecting features to verify conformance with the designed thickness distribution of the composite glass-epoxy shell.

3. Mount mandrel with frame array in the winding fixture.
4. Install (emplace) the insulation ceramics between frames.

   a. Clean and air-dry the frame array.
   b. Working one side of the channel at a time (i.e. the side positioned at the top):

      (1) Prepare insulator ceramic mix,
      (2) Fill the gaps between frames with ceramic,
      (3) Air-dry for about 20 min,
      (4) Repeat steps (1), (2), and (3) for other three sides.

   c. Oven dry ceramic for about two hours.
   d. Cool slowly to room temperature.

5. Preparations for applying RTV Hot Gas Barrier.

   a. Install frame anchor rubber boots.
   b. Install tube/wall seal cavity mold cores.
   c. Install cooling tube end seals.
   d. Install electrode frame thermocouples.

6. Apply RTV Hot Gas Barrier.

   NOTE: The RTV material is a self-leveling liquid silicone rubber compound. Consequently, the surface being worked must be in a horizontal plane to prevent excess runoff of the self-leveling liquid before it cures.

   a. Apply RTV to one side of the frame array.
   b. Cure until the RTV does not sag when mandrel is rotated.
   c. Apply RTV to the next side.
   d. Cure to prevent sag.
   e. Repeat steps (c) and (d) until completely coated.
   f. Completely cure the overall RTV Hot Gas Barrier.

TABLE H. 1 PLANNED FABRICATION PROCESS/DETAILED TASKS (CONT'D)

STEP 6 - FABRICATE THE GLASS-EPOXY CASE

Tasks:

1. Fabricate the shell to gas barrier interface layer.
2. Wet-wind the fiberglass-epoxy composite case.
   a. Prepare the fiberglass material.
      (1) filament roving
      (2) woven mat
      (3) cloth fabric
   b. Prepare the epoxy material.
      (1) epoxy resin
      (2) activator - catalyst
   c. Alternately apply epoxy wet layers.
      (1) roving
      (2) mat
      (3) cloth
   d. Build up composite walls to design thickness.
   e. Build up extra thickness region:
      (1) Entrance flange hub,
      (2) Exit flange hub,
      (3) Downstream support mounting pads.
   f. Verify composite case thickness distribution.
3. Cure the composite case at an elevated temperature.
   a. Assemble the curing oven around the winding fixture.

   NOTE: The channel must be continuously and constantly rotated about the longitudinal, horizontal axis from the time that the epoxy resin temperature starts to rise above room temperature until the epoxy resin solidifies and is cooled back down to room temperature. During the elevated temperature cure cycle the viscosity of the epoxy resin decreases significantly (during the exotherm phase the viscosity approaches that of water) and the epoxy resin will drain out of the fiberglass unless constant rotation is maintained.

   b. Raise the channel temperature slowly.
   c. Hold at curing temperature for specified time.
   d. Cool channel slowly to room temperature.
   e. Remove curing oven from winding fixture.

TABLE H. 1 PLANNED FABRICATION PROCESS/DETAILED TASKS (CONT'D)

STEP 7 - CHANNEL FINISHING OPERATIONS

Tasks:

1. External finishing operations.
    a. Remove tube end seals.
    b. Remove tube/wall cavity cores.
    c. Remove excess epoxy flashing.
    d. Sand-blast/abrade tube/wall cavities.
    e. Cast RTV rubber tube/wall seals.
    f. Repair all epoxy voids or defects.
2. Remove assembly mandrel from channel.
3. Internal finishing operations.
    a. Install (emplace) the electrode ceramic.
        (1) Clean and sand-blast/abrade the electrode grooves.
        (2) Emplace the electrode ceramic in the grooves. (Working one wall at a time.)
        (3) Air-dry ceramic for at least 20 min.
        (4) Rotate channel and repeat steps (2) and (3) for each side.
        (5) Oven-dry complete electrode ceramics.
    b. Smooth out insulator and electrode ceramic as required.

STEP 8 - CHECK-OUT TESTS ON CHANNEL

Tasks:

1. Vacuum-leak test channel.
2. Measure channel finished weight.
3. Inspect finished channel:
    a. Measure and record critical dimensions,
    b. Verify configuration conformance to design.

STEP 9 - FABRICATE MANIFOLD COMPONENTS

Tasks:

1. Fabricate metal headers.
2. Procure insulating lines and fittings.
3. Fabricate structural hardware.

TABLE H.1 PLANNED FABRICATION PROCESS/DETAILED TASKS (CONT'D)

STEP 10 - ASSEMBLE MANIFOLDS TO CHANNEL

Tasks:

1. Preassemble lines and fittings.
2. Leak-pressure test lines.
3. Assemble headers and structural hardware around the channel.

   NOTE: The manifolds assembly will be temporarily attached to the channel until installation where the manifolds will be supported by the facility water lines at one end and by the magnet iron at the other end.

4. Assemble all of the channel to manifold coolant lines.

STEP 11 - CHECK OUT TESTS ON SUBSYSTEM

Tasks:

1. Pressure-leak test coolant manifolds, lines, and electrode frame cooling tubes.
2. Inspect finished subsystem.

   a. Measure and record critical dimensions.
   b. Verify configuration conformance to design.

REFERENCES

1. O. K. Sonju and J. Teno, "Study of High Power, High Performance Portable MHD Generator Power Supply Systems," AFAPL-TR-76-87, AD#AO40381, August 1976.

2. "Combustion Stability Specifications and Verification Procedures for Liquid Propellant Rocket Engines," CPIA Publication 247, October 1973.

3. O. K. Sonju, J. Teno, R. Kessler, L. Lontai, and D. E. Meader, "Status Report on the Design Study Analysis and the Design of a 10 MW Compact MHD Generator System," AFAPL-TR-74-47, Part II, June 1974.

4. D. W. Swallom, O. K. Sonju, D. E. Meader, and G. T. Heskey, "MHD Lightweight Channel Development," AFAPL-TR-78-41, June 1978.

5. O. K. Sonju, J. Teno, J. W. Lothrop, and S. W. Petty, "Experimental Research on a 400 kW High Power Density MHD Generator," AFAPL-TR-71-5, May 1971.

6. O. K. Sonju, D. W. Swallom, D. E. Meader, H. Becker, R. V. Burry, A. W. Huebner, and R. F. Cooper, "Development of a Compact, Lightweight High Performance 30 MW MHD Generator System," 17th Symposium on Engineering Aspects of Magnetohydrodynamics, Stanford University, March 1978.

7. G. W. Sutton and A. Sherman, "Engineering Magnetohydrodynamics," McGraw Hill, 1967.

8. O. K. Sonju, "Viscous Magnetohydrodynamic Flows," Stanford University Institute for Plasma Research, SUIPR Report No. 245, 1968.

9. H. C. Garner, "The Development of Turbulent Boundary Layers," ARC of Britain R&M 2133, 1944.

10. J. Teno, T. R. Brogan, S. W. Petty, J. W. Lothrop, and O. K. Sonju, "Research Studies and the Development of MHD Generators and Accelerators," AEDC-TR-70-14, January 1970.

11. Kreith, F., Principles of Heat Transfer, International Textbook Co., 1961.

12. User Information Manual for MITAS (Martin Marietta Thermal Analyzer System); Publication No. 86615000, Rev. A; Cybernet Service Control Data Network; September 1972.

13. Anon., "Flow of Fluids Through Valves, Fittings, and Pipes," Crane Company Technical Paper No. 410, 1976.

14. Coffin, L. F., "Internal Stresses and Fatigue in Metals," G. Rossweiter and W. Grube, Elsevier Publishing Co., 1959.

15. Majors, H., "Comparison of Thermal Fatigue with Mechanical Fatigue Cycling," ASTM STP 165, 1954.

16. Manson, S. S., "The Challenge to Unify Treatment of High Temperature Fatigue," ASTM STP 520, 1973.

17. Dietz, A. G. H., "Composite Engineering Laminates," MIT Press, 1969.

18. Broutman, L. J. (Ed.), "Composite Materials, Vol. 5, " Academic Press, 1974.

19. Timishenko, S., "Strength of Materials - Part I," D. Van Nostrand, 1968.

20. "Chamber Technology for Space Storable Propellants," Fourth Interim Report No. R7985, Rocketdyne, Division of Rockwell International, September 1969.

21. M. D. Schuman and D. G. Behosse, "Standardization Distribution Energy Release (SDER) Computer Program", 13th JANNAF Combustion Meeting, CPIA Publication 281, Volume III, December 1976, pp 79-91 (Also AFRPL-TR-77-1, AFRPL).

22. W. S. Hines, "Turbulant Force Convection Heat Transfer to Liquids at Very High Heat Fluxes and Flow Rates", RR61-14, Rocketdyne, a Division of Rockwell International, 30 November 1961.

23. "Investigation of Thermal Fatique in Non-Tubular Regeneratively Cold Thrust Chambers (FO4611-70-C-0014) Isothermal Fatigue Tests, Task III," No. SR-2112-7001, February 1972.

24. "High Temperature Low Cycle Fatique of Copper Base Alloys in Argon, Part II - Zirconium Copper at 482C, 538C, and 590C, " No. NASA CR-121-260, August 1973.

25. "Correlation of Injector Spray Drop Size Distribution and Injector Variables," Final Report No. R8455, Rocketdyne, Division of Rockwell International, December 1971.

26. J. H. Rupe, "A Correlation Between the Dynamic Properties of a Pair of Impinging Streams and the Uniformity of Mixture Ratio Distribution in the Resulting Spray". Progress Report No. 20-209, JPL, Pasadena, California, 28 March 1956.

27. Oberg, C.L., R.C. Kesselring, C. Warner III, and M.D. Schuman, "Analysis of Combustor Instability in Liquid Propellant Engines With or Without Acoustic Cavities," NAS9-12077, June 1974.

28. 14th NASA F-1 Program Review, May 1964.

29. Dykema, O.W., "An Engineering Approach to Combustion Instability," Second JANNAF Combustion Conference, CPIA No. 105, pp 205-223, May 1966.

30. Oberg, C.L., et al, "Evaluation of Acoustic Cavities for Combustion Stabilization," Seventh JANNAF Combustion Meeting, CPIA No. 204, pp 743-756, February 1971.

31. Oberg, C.L., and T.L. Wong, "Combustion Instability Suppression Devices," Eighth JANNAF Combustion Meeting, CPIA No. 220, pp 781-794, November 1971.

32. Kuluva, N.M., and C.L. Oberg, "Acoustic Liners for Large Engines," Final Report Contract NAS8-21345, (R7792), Rocketdyne, Division of Rockwell International, March 1969.

33. Hines, W.S., "Turbulent Forced Convective Heat Transfer to Liquids at Very High Heat Fluxes and Flow Rates," RR61-14, Rocketdyne, Division of North American Aviation, November 1961.

34. Saas I, E.L. Wilson and R.M. Jones, "Finite Element Stress Analysis of Axisymmetric Solids with Orthotropic, Temperature Dependent Material Properties", TR-0158, (S3316-22)-1, The Aerospace Corporation, San Bernardino, California (September 1967).

35. "25 MW MHD Combustor Design Study Final Report", Report No. R-9967, Rocketdyne, 1976.

36. Chemical Engineers' Handbook, 4th Edition, McGraw-Hill, 1959, Chapter 3, Prediction and Correlation of Physical Properties.

37. Kenics Design Bulletin, Static Mixer Modules, Technology, Processing & Sizing, March 1976.

38. S.J. Chen, "Drop Formation of Low Viscosity Fluids in the Static Mixer Units," KTEK-5, Kenics Corporation, 1972.

39. Middleman, S., "Drop Size Distributions Produced by Turbulent Pipe Flow of Immiscible Fluids through a Static Mixer," Ind. Eng. Chem, Process Research & Development, Vol. 13, No. 1, 1974.

40. C. A. Sleicher, "Maximum Stable Drop Size in Turbulent Flow," AIChE Journal, Vol. 8, No. 4, pp 471-477, 1962.

41. C. A. Sleicher, H. I. Paul, "The Maximum Stable Drop Size in Turbulent Flow: Effect of Pipe Diameter," Chem. Engr. Sci., Vol. 20, pp 57-59, 1965.

42. S. B. Collins, J. G. Knudsen, "Drop Size Distributions Produced by Turbulent Pipe Flow of Immiscible Liquids," AIChE Journal, Vol. 16, No. 6, pp 1072-1080, 1970.

43. J. M. Coulson and J. F. Richardson, Chemical Engineering, Vol. 1, 2nd Ed., Pergamon Press, 1970.

44. "AEDC Test Plan", MLI No. MHD 218-10-1, January 1978.

45. "Interface Control Document", MLI No. MHD 218-9-1, April 1978.

46. Earles, D. R. and M. F. Eddins, Reliability Engineering Data Series Failure Rates, Avco Corporation, April 1962.

47. Nonelectric Reliability Notebook, Hughes Aircraft Company, January 1975.

48. A. H. Shapiro, "The Dynamics and Thermodynamics of Compressible Fluid Flow", Book, Volume I, 1953 Ronald Press.

49. "Thermophysical Properties of Oxygen from the Freezing Liquid Line to 600 R for Pressures to 5000 psia," NBS Technical Note 384, issued July 1971.

50. "ICRPG ODE Equilibrium Reference Program, A Computer Program for the Calculation of Chemical Equilibrium Compositions with Applications". ICRPG Performance Standardization Working Group, July 1968.

LIST OF ABBREVIATIONS, ACRONYMS, AND SYMBOLS

A	Amperes
A_t	Aerodynamic Throat Area
AEDC	Arnold Engineering Development Center
AFAPL	Air Force Aero Propulsion Laboratory
AMS	Amplitude Mean Square
APL	Aero Propulsion Laboratory
ASI	Auxiliary Spark Ignitors
atm	Atmosphere
B	Magnetic Field Strength
C	Velocity of Sound in Combustor
C_s	Velocity of Sound in Acoustic Slots
c^*	Characteristic Velocity
cal	Calorie
CDA	Copper Development Association
cm	Centimeter
cP	Centipoise
CPIA	Chemical Propulsion Information Agency
CRES	Corrosion Resistant Stainless Steel
csc	Copper to Superconductor Ratio
d	Diameter
D	Diameter
$\overline{D}$	Mass-mean Droplet Diameter
D_{30}	Mean Droplet Diameter Based on a Mean Volume Calculated by Dividing Total Volume of Sample by Number of Droplets
D_{32}	Sauter Mean Diameter
D_H	Hydraulic Diameter
dc	Direct Current
deg	Degree
diam	Diameter
E	Modulus of Elasticity
E	Electric Field
EB	Electronbeam
ED	Electrodeposited
ELF	Electroforming
f	Frequency
F	Force
g	Gravitational Constant
g	Grams
G	Mass Flux per Area

GN_2	Gaseous Nitrogen
GO_2	Gaseous Oxygen
GTA	Gas Tungsten Arc
h	Hour
h	Case Thickness
h	Enthalpy
h_c	Convective Heat Transfer Coefficient
h_w	Wall Enthalpy
$h(\ell)$	Local Enthalpy
H	Force
HGFT	Hot Gas Flow Train
HLB	Hydrophilic-lipophilic Balance
HPMS	High Power MHD System
hr	Hour
Hz	Hertz
I	Moment of Inertia
I_{xx}	Moment of Inertia about Principal Central Axis
ICD	Interface Control Document
ICWG	Interface Control Working Group
Jy	Transverse Current Density
JP-4	A Liquid Hydrocarbon Fuel
K	Average Coolant Wall Thickness
K	Kelvin
kg	Kilogram
kV	Kilovolt
kW	Kilowatt
ℓ	Distance from Wall Surface
L	Length
L	Transverse Combustor Length
L*	Combustion Chamber Characteristic Length
L/D	Length to Diameter Ratio
LO_2	Liquid Oxygen
m	Meters
$\dot{m}$	Mass Flow Rate
M	Bending Moment
$\overline{M}$	Edge Moment
Me	Exit Mach Number
M_o	Moment of Inertia
MCA	Magnetic Corporation of America
MHD	Magnetohydrodynamic

MIL-STD	Military Standard
min	Minute
MJ	Megajoules
MLI	Maxwell Laboratories, Inc.
mm	Millimeters
MOV	Main Oxygen Valve
msec	Millisecond
MW_e	Megawatt Electrical
N	Newton
N	Number of Cycles
N_{Nu}	Nusselt Number
N_{Pr}	Prandtl Number
N_{Re}	Reynolds Number
OFHC	Oxygen Free, High Conductivity
p	Pressure
P	Poise
Pc	Main Chamber Pressure
Pns	Nozzle Stagnation Pressure
PcF	Correction Factor for Reactant Viscosity, Surface Tension and Density
pk-pk	Peak to Peak
PSD	Power Spectral Density
PWT	Propulsion Wind Tunnel
q	Heat Flux
Q	Heat Flow
R	Radius
R_T	Radius of the Throat
rad	Radian
RMA	Reliability and Maintainability Analysis
rpm	Revolutions per Minute
RTV	Room Temperature Vulcanizing
SCM	Superconducting Magnet
sec	Second
SF_{tu}	Safety Factor on Ultimate Strength
SF_{ty}	Safety Factor on Yield Strength
SHA	Safety and Hazards Analysis
SSFL	Santa Susana Field Laboratory
t	Wall Thickness
T	Temperature
T	Tesla

U	Velocity
U (ℓ)	Local Velocity
v	Water Velocity
VSC	Vibration Safety Cutoff
w	Width
W*	Critical Weber Number
We	Weber Number
WG/W	Waterglass/Water Volume Ratio
Z	Section Modulus
α	Coefficient of Thermal Expansion
δ	Bending Deflection
ϵ	Strain
ϵ_1	Circumferential Membrane Strain
η_{c^*}	Characteristic Velocity Efficienty
ρ	Density
σ	Bending Stress
σ_1	Circumferential Membrane Stress
σ_2	Axial Stress
θ_w	Nozzle Exit Angle
μ	Micron
ν	Poisson's Ratio

☆U.S.Government Printing Office: 1979 — 657-002/341